# EEG-based investigation of cortical activity during Postural Control

FABIO BAROLLO

Doctor of Philosophy

ASTON UNIVERSITY
REYKJAVIK UNIVERSITY

January 2022

ISBN (electronic version): 978-9935-9620-8-9

ISBN (printed version): 978-9935-9620-9-6

Author’s ORCID: https://orcid.org/0000-0003-3706-9418

# Thesis summary

Aston University, Reykjavik University

**EEG-based investigation of cortical activity during Postural Control**

Fabio Barollo

Doctor of Philosophy

2022

The postural control system regulates the ability to maintain a stable upright stance and to react to changes in the external environment. Although once believed to be dominated by low-level reflexive mechanisms, mounting evidence has highlighted a prominent role of the cortex in this process. Nevertheless, the high-level cortical mechanisms involved in postural control are still largely unexplored. The aim of this thesis is to use electroencephalography, a widely used and non-invasive neuroimaging tool, to shed light on the cortical mechanisms which regulate postural control and allow balance to be preserved in the wake of external disruptions to one's quiet stance.

EEG activity has been initially analysed during a well-established postural task - a sequence of proprioceptive stimulations applied to the calf muscles to induce postural instability – traditionally used to examine the posturographic response. Preliminary results, obtained through a spectral power analysis of the data, highlighted an increased activation in several cortical areas, as well as different activation patterns in the two tested experimental conditions: open and closed eyes.

An improved experimental protocol has then been developed, allowing a more advanced data analysis based on source reconstruction and brain network analysis techniques. Using this new approach, it was possible to characterise with greater detail the topological structure of cortical functional connections during the postural task, as well as to draw a connection between quantitative network metrics and measures of postural performance.

Finally, with the integration of electromyography in the experimental protocol, we were able to gain new insights into the cortico-muscular interactions which direct the muscular response to a postural challenge.

Overall, the findings presented in this thesis provide further evidence of the prominent role played by the cortex in postural control. They also prove how novel EEG-based brain network analysis techniques can be a valid tool in postural research and offer promising perspectives for the integration of quantitative cortical network metrics into clinical evaluation of postural impairment.

*Keywords*: Postural control · Electroencephalography (EEG) · Functional connectivity · Brain network analysis · Proprioceptive vibrations

# Samantekt Ritgerðar

Aston University, Háskólinn í Reykjavík

**Rannsókn á virkni heilabarka við líkamsstöðustjórnun með notkun hágæða heilarafrits**

Fabio Barollo

Doctor of Philosophy

2022

Kerfi stöðustjórnunar er afturvirkt stýrikerfi sem vinnur stöðugt að því að viðhalda uppréttri stöðu líkamans og bregðast við ójafnvægi. Vaxandi þekking á undanförnum árum hefur lýst því að úrvinnsla þessara upplýsinga á sér stað á öllum stigum miðtaugakerfisins, þá sérstaklega barkarsvæði heilahvela. Engu að síður, er nákvæmu hlutverk heilabarkar við stöðustjórnun enn óljóst að mörgu leyti. Tilgangur þessa verkefnis var að rannsaka nánar hlutverk heilabarkar við truflun og áreiti á kerfi stöðustjórnarinnar, með notkun hágæða heilarafrits (EEG).

Við byrjuðum á því að mæla heilarit einstaklinga meðan á þekktri líkamsstöðu-æfingu stóð, til þess að skoða svörun líkamans við röð titringsáreita sem beitt var á kálfavöðvana til að framkalla óstöðugleika. Bráðabirgðaniðurstöður fengnar með PSD-aðferð (power spectral analysis) leiddu í ljós aukna virkni á ákveðnum svæðum í heilaberki og sérstakt viðbragðsmynstur við að framkvæma æfinguna, annars vegar með lokuð augu og hins vegar opin augu.

Rannsókn okkar hélt áfram með nýrri og þróaðari tækni sem gerði okkur kleift að framkvæma fullkomnari greiningaraðferðir til að túlka, greina og skilja merki frá heilaritnu. Með fullkomnari greiningaraðferðum var hægt að lýsa með nákvæmari hætti staðfræðilega uppbyggingu starfrænna tenginga í heilaberki meðan á líkamsstöðu æfingunni stóð, sem og að draga tengsl á milli megindlegra netmælinga og mælinga á líkamsstöðu.

Að lokum bætist við vöðvarafritsmæling við aðferðafræðina, sem gaf okkur innsýn inn í samskipti heilabarka og vöðvana sem stýra vöðviðbrögðum og viðhalda líkamsstöðu við utanaðkomandi áreiti.

Á heildina litið gefa niðurstöðurnar sem settar eru fram í þessari ritgerð enn sterkari vísbendingar um það áberandi hlutverk sem heilabörkurinn gegnir við stjórnun líkamsstöðu. Niðurstöðurnar sanna einnig hvernig ný aðferð á greiningu á tengslaneti heilans sem byggir á heilariti getur verið gilt tæki í líkamsstöðu rannsóknum og er nytsamlegt tól fyrir mælingar á heilakerfisneti í klínískt mat á skerðingu líkamsstöðu.

*Keywords*: Postural control · Electroencephalography (EEG) · Functional connectivity · Brain network analysis · Proprioceptive vibrations

# Acknowledgments

First and foremost, I would like to wholeheartedly thank my supervisors. Paolo, it is hard to express how grateful I am that our paths crossed. Since I first arrived in Iceland as an exchange student, I was immediately captured by the passion and enthusiasms which constantly drives your efforts towards new ambitious goals. It has been truly inspirational to witness and take part in the incredible growth of our department over the years, under your mentorship. Antonio, when you offered me the opportunity to take on the challenge of a joint PhD in the UK, I could not have predicted the extent to which this experience would have enriched me as a young researcher. Thank you for always pushing me to think critically and to never settle for the easy way.

For their invaluable advice and support throughout my research project, I would also like to give a sincere thanks to Ceon Ramon, Hannes Petersen and Mahmoud Hassan. Ceon, thank you for sharing your unmatched knowledge of the human brain with me and for being an example of passionate scientist I can look up to. Hannes, some of my best memories will always be the unmissable summer retreats in Hvalfjörður, discussing science and spending time in great company, surrounded by the breath-taking Icelandic nature. Thank you for providing your guidance on the physiological aspects of this project. Last but not least, I can hardly express my gratitude to Mahmoud, without whom this project would not have been the same. Thank you for your irreplaceable support, and most importantly for being such an inspirational scientist and wonderful person.

I am also truly grateful for all the amazing friends and colleagues whom I met along the way: Kyle, Rún, Marco, Gunnar, Halldór, Sólveig and everyone who shared a part of the journey with me. Above all Isotta, for her friendship and for sharing joys and sorrows of the PhD life from the start to the finish line.

Finally, the biggest thanks go to my friends, my family and my partner, Brad. I could have not done any of this without your unconditional love and support.

# Table of Contents

# List of Abbreviations

| | |
|---|---|
| AP | Anterior-Posterior |
| ASP | Absolute Spectral Power |
| CC | Clustering Coefficient |
| CE | Closed Eyes |
| CMC | Corticomuscular Coherence |
| CNS | Central Nervous System |
| COM | Centre of Mass |
| COP | Centre of Pressure |
| EEG | Electroencephalography |
| (s)EMG | (Surface) Electromyography |
| EOG | Electrooculogram |
| GL | Gastrocnemius Lateralis |
| IMC | Intermuscular Coherence |
| LE | Local Efficiency |
| ML | Medial-Lateral |
| MV | Mean Velocity |
| NNMF | Non-negative Matrix factorisation |
| OE | Open eyes |
| PEP | Perturbation-evoked potential |
| PIVC | Parieto-Insular Vestibular Cortex |
| SPL | Sway Path Length |
| STR | Strength |

# List of Figures

# List of Tables

# 1. General Introduction

Postural control is the phrase used to indicate the complex regulatory system whose aim is the maintenance of a stable human upright stance. The complexity of this task lies in its reliance on a wide range of sensory inputs gathered predominantly through the visual, somatosensory-proprioceptive and vestibular systems. While early research on the topic associated postural control with a reflexive response enacted at the level of the brainstem and spinal cord, extensive recent evidence pointed out the crucial role of the cortex as a hub for the processing of sensory information and the subsequent development of an effective postural control strategy.

Proof of this has emerged from several human and animal studies in which perturbation-evoked cortical activation was captured with various neuroimaging techniques as well as from the observation of postural impairment related to different cortical pathologies (stroke, Parkinson's disease, etc).

Although the centrality of the cortex in postural control has now been well established in literature, the understanding of the underlying cortical mechanisms is still limited (Varghese et al., 2017). The goal of the work presented in this thesis was to use electroencephalography (EEG) and novel analysis tools provided by network neuroscience, to identify and shed light on the interplay between cortical regions that are involved in the high-level coordination of the postural control system, following a mechanical challenge to the participant's upright stance.

Balance perturbation techniques have been used extensively to challenge the upright stance to investigate the elicited postural response. In this work, the disruption of the participants' quiet upright stance was induced by skeletal muscle vibration of the lower limbs, in which a randomized binary vibratory sequence was applied to the gastrocnemius muscles of the calves.

Among the different functional brain imaging techniques which can be used to explore brain activity during postural control, EEG is particularly suited to capture brain network dynamics by virtue of its millisecond-scale time resolution. It also has the advantage of being non-invasive, easy-to-use and relatively cheap. We believe that the adoption of a more comprehensive approach, including the use of EEG-based techniques as an investigative tool, together with traditional posturographic metrics and other electrophysiological signals like electromyography (EMG), can be beneficial in the evaluation of postural control. Indeed, the insight provided can inform us about several aspects of this complex regulatory system, from the way the cortical network configures itself during the execution of a postural task, to how it remodulates itself based on the availability of different sensorial information, to which cortical areas are primarily involved in the process, as well as to which extent the cortex shapes the mechanical response at a muscular level, etc. The gathering of this knowledge has the potential to eventually assist the development of more effective tools for the evaluation of postural performances and the diagnosis of postural decline in elderly people as well as subjects affected by neurological diseases.

The present thesis comprises: an introductory part focused on the theoretical and technical background of postural control analysis (Chapters 1-3); three experimental chapters, structured in the form of scientific publications, presenting the work carried out at Reykjavik University and Aston University (chapters 4-6); and a final discussion chapter (chapter 7).

‘Chapter 2 - Literature review’ provides the essential background on postural control, the historical evolution of this line of research, the associated relevant literature and an overview of the main physiological principles involved. It also provides the theoretical basis of the electrophysiological signals used in the following chapters: EEG and EMG.

‘Chapter 3 – Methodologies’ starts off with an overview of the instrumentation used in the presented studies. It also includes a comprehensive review of the analysis techniques used to process the experimental data: from the more common EEG and EMG preprocessing and analysis methodologies to the novel EEG-based source connectivity analysis. The chapter is concluded with a review of the statistical methods used in the presented studies.

‘Chapter 4 - Postural Control Adaptation and Habituation during Vibratory Proprioceptive Stimulation: An HD-EEG Investigation of Cortical Recruitment and Kinematics’ is the first experimental chapter, where the work done at Reykjavik University is presented. It includes the results of a preliminary HD-EEG investigation during a postural task, performed with instrumentation from Lund University. The chapter has been published in the IEEE TNSRE journal in June 2020 (doi: 10.1109/TNSRE.2020.2988585).

‘Chapter 5 - Cortical pathways during Postural Control: new insights from functional EEG source connectivity’ is the second experimental chapter, comprising an extensive brain network analysis of data collected at Aston University. An extract of this chapter has been published in the IEEE TNSRE journal in January 2022 (doi: 10.1109/TNSRE.2022.3140888).

‘Chapter 6 - Proprioceptive vibratory stimulation modulates cortico-muscular postural response’ is the third experimental chapter, also based on the data collected at Aston University, which focuses on the analysis of the cortico-muscular interactions that take place during the execution of the postural task.

‘Chapter 7 – General discussion and conclusions’ is the final chapter, which recaps the main findings and elements of discussion from the experimental chapters. It also discusses limitations and future developments of the research work.

# 2. Literature Review

## 2.1 Postural Control

Posture is generally described as the alignment of the body with respect to a reference point, and the arrangement of body parts in relation to each other (Smith, 1996). The key concepts that come to mind when talking about posture are those of balance and postural control. Despite having an intuitive understanding of these concepts and their interdependency, there is a lack of universal agreement on the exact definitions of posture, balance and postural control (Wallmann, 2009). Moreover, some confusion is generated by the interchangeable use of terms such as balance and postural control.

Balance has been described as the process that controls posture through a complex interaction of afferent and efferent pathways (Kaufman et al., 1997). Anyway, in physics the concept of balance defines the state of an object in which the resultant of the applied forces is null. The stability of an object depends on its centre of mass (COM, the ideal application point of the gravitational force) and its base of support.

The same concept can be translated from inanimate objects to animals and humans. In humans as well, in fact, if the projection of the COM falls within the area defined by the base of support (area under the feet), it is possible to achieve balance and maintain a stable bipedal upright stance (Fay B Horak and Macpherson, 1996). Nevertheless, humans are characterised by a high COM (two thirds of the body mass is located above the waist) and a small base of support which makes them naturally unstable (Forbes et al., 2018; Hayes, 1982). Therefore, the application of counteracting forces is required to preserve balance. By exerting muscular forces and adapting our posture through joint strategies, we can counteract gravitational forces and prevent falling. The point where the summation of these forces (ground reaction force) is

applied to resist gravity is known as the centre of pressure (COP), whose location reflects the neuromuscular response which is put in place to adjust COM imbalances (Winter et al., 1990). Ultimately, the ability to exert control on our balance constitutes what can be defined as postural control (Pollock et al., 2000).

The ability to maintain an upright posture is indeed an essential component and a crucial aspect of every individual's life (Chiba et al., 2016) as well as a main evolutionary achievement that determined the success of our species. Despite the impact it has on almost every practical task of daily life, most of us do not put much thought or effort in the maintenance of an upright stance. Anyway, while seemingly a basic and almost automatic task that comes naturally and is taken for granted by the majority of people, the physiological mechanisms behind postural control show a high degree of complexity. Indeed, the physiological interplay among all of the components that concur to the postural control system and the way pathologies and age lead to balance impairment have been the subject of research for decades (Loram et al., 2005).

The main explanation of postural control remained unchanged for most of the 1900s, since Sherrington hypothesised, at the beginning of the century, that corrective postural movements were driven by low-level reflexive mechanisms (Sherrington, 1910). The theory that human postural control was dominated by reflexes at the level of muscles and spinal cord was supported by studies on mammals (Creed R. S., 1932; Magnus, 1925). However, following investigations on cats with spinal transection but intact reflexes (short latency responses - SLAT) disproved this idea (Fung and Macpherson, 1999). Criticalities in the translation of animal-based findings to human postural control were also highlighted: namely, regarding the different base of support in bipedal vs. quadrupedal stance and the different height of COM (Loram et al., 2005).

However, given the apparent automaticity of postural control in the maintenance of the upright stance, for many decades the predominant approach in scientific literature remained focused on reflexive and muscular mechanisms of control of the COM: stretch reflex, instantaneous modulation of ankle muscle activity, muscle stiffness control etc. (Fitzpatrick et al., 1996; Fitzpatrick, 2003; V. S. Gurfinkel et al., 1995; Fay B Horak and Macpherson, 1996; Schieppati and Nardone, 1999; Shadmehr and Arbib, 1992; D. A. Winter et al., 1998).

It was not until the end of the century that a more complex approach was proposed: quiet standing, just like any other kind of motor task, was suggested to comprise distinct phases of planning, anticipation and internal models for the execution of postural control (Morasso and Schieppati, 1999).

Finally, more recently, the consensus of the scientific community has shifted to acknowledge that postural control is a complex regulatory feedback process which aims at the maintenance of the upright stance by constantly coordinating small corrective movements for the adjustments of posture and to preserve balance (Fransson, 2005; Patel, 2009). The system relies on a wide range of sensorial feedback for the detection of movement and of one's position in space and is responsible for the engagement of voluntary and reflexive muscle responses. The muscular response is then coordinated at the level of the central nervous system (CNS) (from the medulla to the cerebral cortex) and is informed and enhanced by the information provided by independent receptor systems (Horak and Nashner, 1986; Johansson and Magnusson, 1991; Keshner et al., 1987; Kleiber et al., 1990). The main afferent pathways on which the postural control system relies to gather information are the somatosensory, vestibular and visual systems (Dietz, 1992; Mergner and Rosemeier, 1998). Changes in the conditions of one or more of the receptor systems information, due to physiological impairment

or external challenges, affect the efficiency and shape the strategies put in place by the postural control system to preserve balance. This appears clear in cases of conflicting sensorial information, where, for example, the mismatch between visual and vestibular inputs can negatively impact the control system and lead to unsteadiness, dizziness, motion sickness, and poor balance (Colnat-Coulbois et al., 2011; Lim et al., 2018; Warwick-Evans et al., 1998).

External disturbances of the receptor systems have also been shown to alter the postural response. In particular, the marked increase in body sway and motion amplitude during standing postural tasks caused by the disruption of the somatosensory system highlighted the importance of proprioception in postural control (Kearney and Hunter, 1990; Maki and Ostrovski, 1993; Zarzecki and Asanuma, 1979).

### 2.1.1 Role of the cortex in postural control

The prominent role of the CNS in the postural control system emerged clearly from its involvement in all of the main stages of the process: from the information processing to the development of an adequate response strategy, to the coordination of the motor response. Motor responses, indeed, see the involvement of CNS at many levels from the spinal cord, from the brainstem to the cerebral cortex (Wolpaw, 1994). However, for decades literature has focused on lower level, subcortical reflexive mechanisms, while the role of higher cortical functions in the maintenance of postural stability were not extensively investigated.

Nevertheless, over time, a growing amount of evidence started to gather in favour of the notion of a crucial cortical role in postural control. The initial observations were of anatomical nature: humans and animals suffering from cortical lesions but with intact brainstem showed anomalous postural reaction when challenged with external perturbation (Bard, 1933; Chan et

al., 1979; Diener et al., 1985; Geurts et al., 2005). Moreover, postural responses are characterised by flexible and context-specific muscle synergies which are distributed on the body, and are not present in stretch reflexes (F. B. Horak and Macpherson, 1996).

Next came mounting behavioural evidence to support this thesis. Changes in the cognitive state and attention level during the performance of dual task paradigms (combined cognitive-postural tasks), as well as changes in the sensory-motor conditions, experience, learning and habituation processes, as well as prior warning of an upcoming perturbation are all factors that shape and alter the postural response (for an extensive review see Jacobs and Horak, 2007). Thus, the relationship between alteration of cognitive conditions, mental functions and postural performances are strong indications towards the involvement of the cortex in the development of a postural strategy. Further contributions to the consolidation of the notion of a cortical control of postural responses came from studies that examined falls in aging population and highlighted a strong link between cognitive decline and impaired postural control (Herman et al., 2010; Liu-Ambrose et al., 2013; Muir et al., 2012).

In light of the indications from this amount of indirect evidence, researchers started to look into more direct ways of assessing cortical functions during postural tasks, using neurophysiological and neuroimaging techniques.

Some of the first reported human studies on the topic used EEG to investigate the perception of postural instability and highlighted the presence of neural detectors of postural instability, specifically in the gamma band (Slobounov et al., 2000). They also further supported the idea that postural adjustments for the maintenance of balance are not automatic muscle responses but ‘cortically-controlled intended movements’ (Slobounov et al., 2005). Since then, several other studies have investigated perturbation-induced cortical responses (see Bolton, 2015 and

reference therein for an extensive review). Most of these studies focused on identifying relevant neural markers during evoked-potential EEG studies, the so-called perturbation-evoked potentials (PEP). The most prominent among these is PEP N1, a negative potential peak occurring approximately 100ms after a perturbation and distributed over the central, parietal electrodes, which is thought to be related to general features of event detection (Maki and McIlroy, 2007; Varghese et al., 2017, 2015).

Further investigations included scalp spectral analysis of cortical activity elicited by postural perturbation and time-frequency analysis that tried to associate the predominance of certain frequency rhythms to specific sensorimotor functions (Cavanagh and Frank, 2014; Engel and Fries, 2010; Mierau et al., 2017a; Varghese et al., 2014). However, PEPs have been by far the main focus to unravel the cortical mechanisms of cortically driven balance correction strategies, together with scalp level spectral analysis.

Nevertheless, this line of research presents a number of limiting factors. Firstly, neurophysiological research has been limited by prior assumptions and constraints which led to focus on limited areas of the brain, predominantly the primary motor cortex (Bolton, 2015). In addition, the use of surface EEG, with its limited spatial resolution, does not allow for the identification of precisely where PEPs are generated and therefore the specific role of PEPs components in the generation of the postural reaction (Varghese et al., 2017). Furthermore, there is no consensus on how to interpret the results and therefore the functional role of PEPs, with several studies indicating that the most discussed PEP N1 is the result of distributed cognitive processes that involve several cortical areas (Solis-Escalante et al., 2019a). Therefore, recent reviews on the topic call for further investigations that rely on different

techniques including fMRI-EEG, TMS, fNIRS to reveal the involvement and the specific contribution of the different cortical regions (Varghese et al., 2017).

Moreover, the recent development of network neuroscience and sophisticated functional connectivity analysis techniques shows how cortical functions are better described in terms of brain network, with strong and complex interplay between functionally connected cortical areas (Bassett and Sporns, 2017). They also revealed how most neurological diseases are associated with disruptions and anomalies in the cortical network structure (Sakkalis, 2011). This approach can be beneficial in postural control research as well. The analysis of cortical mechanisms regulating postural control, in fact, can also be better described by examining the whole cortical network and by investigating how this is reweighted in the wake of postural challenges. This is indeed the direction that the more recent studies are following (Cignetti et al., 2018; Handiru et al., 2020; Solis-Escalante et al., 2019a).

Overall, while the cortical role in postural control is now well established and supported by several studies and lines of evidence, the underlying cortical mechanisms and the interactions between cortical functions and regions remain largely unknown.

### 2.1.2 Pathologies affecting the postural control system

Postural control is the central player in charge of human upright posture, but it is most often upon its failure that one becomes aware of its importance. The cases of postural control failure have dual classification. Firstly, it can take the form of a pathological disruption of the afferent sensorial information pathways and/or their central processing, leading to clinical patterns where symptoms of vertigo, dizziness, imbalance and falling are prominent (Petersen et al.,

2014). Secondly, an overstimulation of the system which may provoke a series of symptoms of discomfort known as motion sickness (MS) (Golding, 2016).

Indeed, the reliance of the postural control system on such a wide range of sensorial information makes it susceptible to loss of effectiveness and increased risk of falling when medical conditions or injuries limit the ability to gather sensory information, interrupt the sensory integration process, or damage the neuromuscular systems associated with motor control. Extensive literature reported how a wide range of disorders, pathologies and lesions that affect one or more of the receptor systems result in an impaired postural control system and a subsequent loss of postural stability.

Sudden loss of visual acuity and visual field deficits due to conditions like retinitis pigmentosa and multiple sclerosis limit the possibility to rely on visual inputs for the control of posture and have been related to decreased balance performance (Brandt et al., 1982; Paulus et al., 1984; Ray et al., 2008). Dysfunctions of the vestibular system such as unilateral or bilateral vestibular loss (UVL, BVL) have a shown a direct negative impact on the postural control system as a result of the loss of vestibular information (Quitschal et al., 2014; Sprenger et al., 2017). Moreover, patients who suffered traumatic spinal lesion or polyneuropathies have significantly worse control of the upright posture, and because of the impaired somatosensory input, they need to rely more heavily on visual information (Kristinsdottir et al., 2001). Lesions of the CNS due to trauma or resulting from diseases (e.g., Parkinson's, Huntington's) can also lead to extensive postural control deficits according to the affected area. For example, cerebellar and brainstem lesions can disrupt the ability to coordinate and execute adaptive postural movements (Bastian et al., 1996). Several other causes have been linked to impaired postural performances, from muscular fatigue and deficient muscle force which are common symptoms

of many pathologies, to the use of chemotherapy during childhood in adult cancer survivors (Chabran et al., 2002; Einarsson et al., 2016; Thelen et al., 1996). Finally, aging is widely recognised as one of the prominent factors affecting postural control. The aging process, in fact, is often associated with a decline in all of the sensory receptor functions: visual (Baloh et al., 1993; Lord and Dayhew, 2001; Magnusson and Pyykkö, 1986), proprioceptive (Kristinsdottir et al., 2001; Skinner et al., 1984), vestibular (Kristinsdóttir et al., 1997), as well as an overall cognitive decline, reduced muscle strength (sarCOPenia) and joints mobility (Izquierdo et al., 1999; Nonaka et al., 2002; Thelen et al., 1996).

However, literature has also reported how the extraordinary complexity of the postural control system allows for corrective mechanisms to be put in place when one element of the system is impaired, by a recalibration of the postural strategy and an increased reliance on the intact receptors' information (Horak et al., 1990). It is therefore important to understand the complex interactions of the sensorimotor system and the way integration of inputs from the visual, somatosensory, and vestibular systems works at the CNS and cortical level.

### 2.1.3 Afferent receptor systems

In the following sections the main afferent receptor systems that contribute to postural control will be discussed in more detail. These are the somatosensory, visual and vestibular systems. Despite a certain degree of overlap and redundancy in the information they provide, each one has its own peculiar characteristics and thanks to the cortical integration of the information they provide, they all contribute to form a rich neural picture of our body's position in space, our

posture and the external environment, which are key elements of a successful postural control strategy (Peterka, 2002).

### *2.1.3a Somatosensory receptor system*

The somatosensory system (especially proprioception) plays a crucial role in our body's ability to interpret and interact with the surrounding physical environment and is therefore a key component of postural control. Its contribution consists in providing two main types of information: the sensation of touch, pressure and vibration, and the detection of our limbs' posture and relative position between body segments. Tactile and proprioceptive information is gathered through two types of receptors, mechanoreceptors and proprioceptors, respectively, and then conveyed to the CNS via peripheral nerves to inform the mental representation of external objects, our surroundings and of our own body (Delhaye et al., 2018).

Mechanoreceptors, also known as pressor receptors, and proprioceptors are located at the periphery of the body and are in charge of the translation of mechanical deformations of tissues into neural signals. Both types of receptors are innervated by myelinated afferent nerve fibres which allow high-speed conduction of the signal, in a range from 30 to 100m/s.

Mechanoreceptors are cutaneous receptors which are able to sense the deformation and stretching of the skin. They are spread all over the body, but the highest density can be found at different depths in the skin of hands, lips and feet soles, while they're scarce on legs and back. Those located on the soles of the feet are particularly relevant in postural control; here we can find different specialised mechanoreceptors: some respond to pressure and slow movements (below 5Hz), while others are more responsive to rapid changes and fast

movements. Overall, they are essential to detect shifts in weight distribution and slips (Inglis et al., 2002, 1994). Proprioceptors, on the other hand, are mostly located deeper in the muscles and joints, at the level of tendons and ligaments and are able to detect movement, tension and exerted force. Muscle spindles (bundles of innervated muscle fibres) are the main muscle receptors. They are abundant on the skeletal muscles which perform tiny precise movements, i.e., fingertips. They detect muscle length and react to voluntary or elicited muscle contraction (Basmajian and De Luca, 1985). Golgi tendon organs sense stretching of ligaments and work in accordance with muscle receptors responding to active or passive contractions (Basmajian and De Luca, 1985; Prochazka and Wand, 1980). Finally, joint receptors located on the joint capsules are responsive to pressure and joint movements (Grigg and Greenspan, 1977).

Afferent neural fibres that innervate receptors in neighbouring regions bundle together forming progressively larger fascicles and eventually nerves when they merge with efferent motor fibres. The nerves then approach and ascend the spinal cord and form synaptic connections with neurons of the brainstem, maintaining a somatotypical organisation which allows a structured map of the body (afferents from adjacent body parts remain close, lower body afferents are generally located in the medial section, and upper body ones are in the lateral sections) (Smith and Deacon, 1984).

The somatosensory signals then travel through the dorsal column nuclei (DCN) and the thalamus to reach the cortex. The main recipient of the tactile and proprioceptive information is the primary somatosensory cortex, in the parietal lobe (Delhaye et al., 2018).

### *2.1.3b Visual receptor system*

Visual information originates from light-sensitive photoreceptors in the retina. These receptors are sensitive to movement in the visual field, but also to environmental details like the contrast and brightness of the surroundings. Indeed, a number of factors contribute to a rich visual perception of one's body and the external environment: illumination, visual field size, depth perception, sensitivity to contrast etc. (Amblard et al., 1985; Lord and Dayhew, 2001; Paulus et al., 1984). These elements make the visual system, overall, the main player in spatial orientation (Bronstein, 2016). The importance of vision in postural control has been investigated in several studies which highlighted its role in the perception of self-motion and the awareness of one's body position. Another fundamental function of visual information is the detection of external motion and recognition of oncoming obstacles which allows adequate anticipatory postural measures (Asseman and Gahéry, 2005; Paulus and Brandt, 1993; Paulus et al., 1984). In the execution of postural tasks, vision also aids vestibular sensors in the detection of head position and orientation with respect to the environment and correction of head movement to reduce postural sway (Horak and Nashner, 1986).

### *2.1.3c Vestibular receptor system*

A key actor in postural control and the maintenance of balance is the vestibular system (Fransson et al., 2003; MacDougall et al., 2006). This system relies on the complex of vestibular organs of the inner ear to gather information about the position and motion of the head. The inner ear structure comprises three semicircular canals (labyrinths) aligned to the three planes and otolith organs. The angular acceleration resulting from head movements, generates a displacement of the endolymph fluid inside the semicircular canals, which in turn bends and excites the cilia (fine hair), i.e. the receptors of the inner ear (Oman et al., 1979;

Wilson and Jones, 1979). These act as neuromechanical transductors which convert their mechanical bending in one specific direction into depolarisation waves transmitted through afferent vestibular nerves that innervate the inner ear, thus informing the CNS on the three-dimensional position of the head during angular movement (Wuyts et al., 2007).

Otoliths organs contain little crystals immersed in a jelly medium which act as gravitational sensors and detect linear movement. Linear motion of the head causes the otoliths to move and bend the cilia with the subsequent excitation of the afferent neurons, similar to what happens in the semicircular channels. Semicircular channels are more responsive to frequencies above 0.1 Hz, therefore they are more suitable to detect unexpected rapid motion rather than slow postural oscillations. Otoliths, on the other hand, are specialised in the detection of slow motion (below 0.5Hz) and encode information about the subtle sway which characterises the quiet upright stance. Vestibular information in deeply intertwined with visual information. By stabilising the head position, in fact, it also allows for the stabilisation of the retinal image and thus enhances visual cues during motion (Wilson and Peterson, 1978).

The cortical processing of vestibular information is very peculiar in that, despite a core region having been identified in the parieto-insular vestibular cortex, this is part of a larger, deeply integrated and multisensory network which spans separate temporoparietal areas. This reflects the close interaction between vestibular, visual and somatosensory information.

### 2.1.4 Body mechanisms

As previously mentioned, the human upright stance is naturally unstable, and the maintenance of balance requires constant muscle tonic adjustments and the exertion of forces to counter the gravitational pull (Eyzaguirre and Fidone, 1975; Horak et al., 1997). The forces that prevent

our falling forward under the effect of gravity are generated predominantly by gastrocnemius and soleus, the plantarflexor muscles of the calf, collectively known as *triceps surae*. These muscles pull the body backwards and are balanced by the opposite action of the tibialis anterioris, a dorsiflexor muscle which stabilises and corrects the postural response in a constant dynamic calibration. Biomechanical considerations on the human quiet standing often rely on the inverted pendulum model as a description of the upright posture. According to this representation, the body is simplified into a single rigid segment with one extremity, the feet, fixed to the ground, which can oscillate around the ankle joint (D. Winter et al., 1998). This model, however, neglects the composite geometry of the body, which comprises multiple segments interconnected by joints in several points (V S Gurfinkel et al., 1995).

The mechanics of body motion have been extensively investigated, but the complex interplay between body segments remains challenging to describe (Ishida et al., 1997; Kearney and Hunter, 1990; Keshner et al., 1987; Maki and Ostrovski, 1993; Nashner and McCollum, 1985). On one hand, each segment moves to an extent which is determined by the flexibility of its muscles, joints and tendons, on the other hand, because of the geometrical interconnection between segments, they are mutually affected and move in an interrelated fashion (Carlsöö, 1972).

The problem of postural stability has been tackled in the past by observing the effects of external perturbation on quiet upright stance and by describing the “postural strategies” put in place to counteract the disturbances (Bronstein, 1986; Nashner and McCollum, 1985). Postural strategies have been conceptualised as the set of actions which is executed through muscle synergies and joint torques with the aim to control the COM stability, limb geometry, head and trunk orientation, etc. (Horak et al., 1997). Horak and Nashner (1986) in particular

described two of these strategies known as ankle and hip strategy. Ankle strategy takes place during quiet upright stance or small, slow translation of the support plane and is dominated by a sway in the sagittal plane which involves the plantar- and dorsiflexor muscles (gastrocnemius, soleus, tibilias) as previously described. The hip strategy comes into play during more challenging postural tasks in which COM corrections centred around the ankles are not sufficient. It is a more complex strategy that involves several body muscles including upper body and neck and involves adjustments and sway in the frontal plane. The studies presented in this thesis will focus on quiet and perturbed upright stance, which involve an ankle strategy response and the involvement of calf muscles.

### 2.1.5 Vibratory proprioceptive stimulation

As mentioned earlier, external stimulation of one or more of the afferent systems is a way to challenge the quiet upright stance which is commonly used to study the induced postural reaction. Reported methods of doing this consist in altering the visual conditions, for example by using optokinetic stimulation (Luo et al., 2018; Suarez et al., 2000); applying small currents to the mastoids to create disturbances in the vestibular signal (galvanic vestibular stimulation) (Fransson et al., 2003; Woll et al., 2019); or using vibrations to alter the proprioceptive input (Fransson et al., 2003; Patel et al., 2009).

Disrupting the proprioceptive afferent system is a particularly effective and easy way to cause instability, as faulty proprioceptive information leads to a distorted body perception (Lackner, 1988). Applying vibrations to skeletal muscles or tendons in anatomical areas rich in proprioceptors, such as cervical muscles or the gastrocnemius muscles of the calves, is a convenient way to disrupt the proprioceptive system (Eklund, 1971; Ledin et al., 2003; Malmström et al., 2017; Vuillerme et al., 2002). While cervical stimulation acts by altering the

perception of the head position with respect to the trunk, vibratory stimulation of the calf muscles externally activates muscle spindles, thus generating an illusion of movement and a subsequent reaction in the form of tonic stretch reflexes (Eklund, 2011, 1973; Kavounoudias et al., 1999). Because of the interconnected nature of the body segment, localised stimulation induces a postural response that involves a widespread body realignment and changes in joint angles (Ivanenko et al., 2000; Thompson et al., 2007). The proprioceptive vibration of the skeletal muscles of the calves and the following corrective response result in increased body sway, predominantly in the anterior-posterior plane (Fransson et al., 2000; Ivanenko et al., 1999; Kavounoudias et al., 1998).

Body sway is then recorded by means of posturography. Posturography is a non-invasive clinical methodology widely used for the assessment of postural performances. In clinical practice, it is a common evaluation tool of the ability to maintain balance in subjects that are prone to falls, the elderly, patients affected by vestibular deficits, etc. (Black, 2001; Black and Homer, 1996). It is, indeed, also used in healthy subjects to examine the postural response to externally induced alterations of sensory information (Camicioli and Nutt, 2007). Posturography relies on the use of a force platform (or force plate) which tracks the changes in forces and torques applied by the feet of the participant undergoing postural examination onto the plate and the resulting ground reaction force. More details on this are provided in Section 3.4.

The following paragraphs of this chapter will provide an overview of the physiological and technical background of the electrophysiological signals used in this thesis: EEG and EMG.

## 2.2 EEG

Electroencephalography (EEG) is a well-known, non-invasive technique used in both clinical practice and research to investigate and quantify the electrical activity of the brain. It provides a set of signals that is a measure of changes over time in the distribution of electrical potential on the scalp (Niedermeyer and Lopes da Silva, 2005).

The inventor of EEG was Hans Berger, a German psychiatrist who in 1929 first observed a voltage fluctuation between metal plates placed on the scalp as an effect of spontaneous brain activity (Berger, 1929). This technique found immediate clinical application as a diagnostic tool for a number of neurological diseases, with particular relevance in epilepsy, but also in Alzheimer's and Parkinson's (Ames, 1971; Kamei et al., 2010). Since the 1960s, EEG has also been used to detect changes in brain activity in response to cognitive tasks or external stimuli: the so-called evoked potentials or Event-Related Potentials (ERPs) (Hallez et al., 2007). Over the last few decades, hardware improvements to electrodes and amplification systems, combined with sophisticated signal analysis software packages have enabled the acquisition of EEG signals in a reliable and robust way, with increasing head coverage and higher temporal resolution (Usakli, 2010). The greatly improved quality allows for more advanced applications in different research fields, such as source re-construction for brain network connectivity (Schoffelen and Gross, 2009) and Brain-Machine and Brain-Computer Interface (BMI/BCI) for new generation prosthetics (Bhagat et al., 2016; Lotte et al., 2018). EEG has several benefits when compared with other brain image or signal technologies such as CT, PET or MRI: it is lower cost, non-invasive, and without side effects. Most importantly, it can provide a very high temporal resolution, allowing the analysis of brain activity dynamics on the order of a few milliseconds.

The EEG signal presents itself as a series of continuous oscillating waves that vary in aspect, frequency, amplitude, and spatial distribution. The interpretation of the signal is based on the identification of recurrent patterns. These reflect the cerebral activity during the performance of specific functions, and allow normal, abnormal, or artefactual signal types to be distinguished (Stern and Engel, 2013). These patterns are the result of the persistent activity of waves with constant period and shape and are often referred to as rhythms (Salmelin and Hari, 1994). A recurrent group of two or more wave rhythms clearly distinguishable from the background activity is called complex (e.g., K-complex, sleep spindles). Frequency analysis is the best way to characterise the periodic variation of recorded potentials. EEG rhythms are typically divided into Delta (<3.5Hz), Theta (4-7 Hz) Alpha (8-13Hz), Beta (14-30Hz) and Gamma (>40 Hz) waves. The predominance of a certain kind of brainwaves can be associated

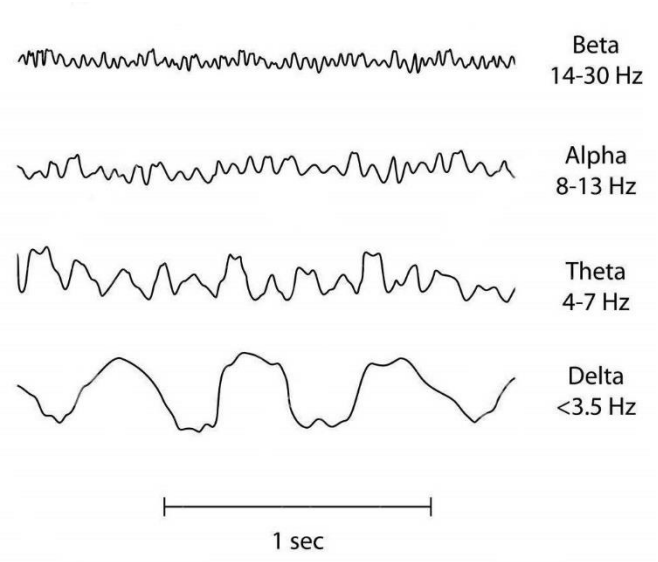


**Figure 2.1.** Examples of brain waves in different frequency bands. Adapted from (Abhang and Gawali, 2015)

with different behavioural states of the subject, such as sleeping phases, meditation, etc. (Birbaumer et al., 1990; Fell et al., 2010).

The area of the scalp from which an EEG signal is collected, i.e., its spatial location, is another factor of great importance in the interpretation. The human brain is divided into two hemispheres and organised into cortical and subcortical structures which are distinguishable both from an anatomical and functional point of view (Fan et al., 2016). Many brain atlases define and map these brain structures at different levels of detail, from a rough parcellation, where only the four major lobes are identified: Frontal, Parietal, Temporal and Occipital (see Figure 2.2), up to dozens of possible structures (Desikan et al., 2006a). Each lobe is associated with different classes of functions, such as speech and motor control (Frontal),

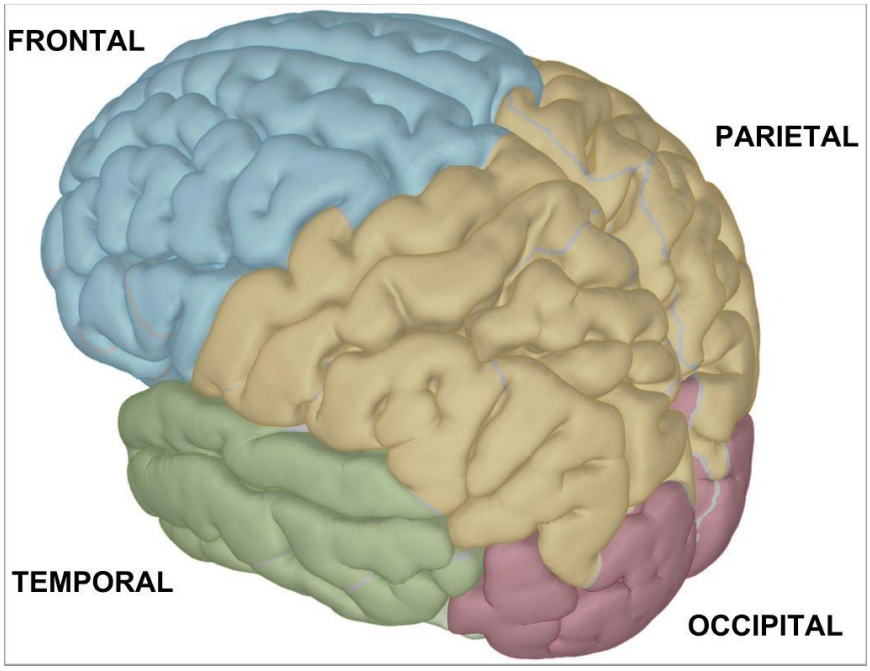


**Figure 2.2.** Cortical lobes.
The four sections (lobes) in which the cerebral cortex can be divided

memory and sound (Temporal), taste and touch (Parietal) and visual information processing (Occipital) (Hudspeth, A. J., Jessell, T. M., Kandel, E. R., Schwartz, J. H., & Siegelbaum, 2013). The EEG signal reflects and correlates in a direct way with these different functionalities of the encephalon and to the alteration in the behavioural state of a subject. For these reasons EEG is a widely used technique in neuroscience, with applications including sleep analysis, epilepsy studies, cognitive science, etc. (Bell and Cuevas, 2012; Campbell, 2009).

### 2.2.1 EEG acquisition system

The EEG signal is picked up by a number of electrodes connected to the scalp at different positions, according to standardised systems of placement and labeling, with the international 10-20 system being one of the most commonly used (Acharya et al., 2016a; Cooper et al., 1974; Jasper, 1958). Electrodes are typically fixed on a wearable cap, available in different sizes for an easier placement, and organised in arrays of 16, 24, 32 and up to 256. The two main types of electrodes currently available are:

**Figure 2.3.** EEG setup.
A 256-channel EEG head-cap. ANT neuro, *eego™ mylab*.
Side and back view.

- Wet electrodes: based on sintered Ag/AgCl or gold sensors, this is the most common and reliable option, used as the clinical standard. It provides a strong signal with low environmental interference but it requires the application of a conductive gel to decrease the impedance at the scalp surface.

- Dry electrodes: a new type of silicone-based, flexible sensors that require no conductive gel, aiming to reduce the time of application while increasing comfort during long term measurements. Currently, their performance is not com-parable with that of wet electrodes, in terms of both signal stability and accuracy (Mathewson et al., 2017; Yu et al., 2016).

Since the scalp potential value at one point can only be measured relatively to that at some other point, every EEG recording system is organised into electrodes pairs, or channels. The pattern in which these channels are associated to a group of electrodes is referred to as montage (Acharya et al., 2016b; Osselton, 1965, 1969). EEG measurements can be acquired using a unipolar or bipolar montage. In a bipolar system the potential is measured between couples of electrodes, while in a unipolar montage every electrode is referred to a common value. In the most basic unipolar configuration, the common-reference montage, one electrode acts as reference and every EEG channel is differentially defined with respect to the potential measured on this electrode. The reference electrode can be located either on the scalp (e.g. Cz electrode) or in areas where electrical activity is supposed to be close to zero such as the earlobe or the mastoid bone. However, it has been shown that no location of the human body can provide a completely neutral potential (Yao, 2001). Therefore, more sophisticated referencing methods are often adopted, where multiple electrodes are used as reference (Mahajan et al., 2017). A few examples of these techniques include: linked ear (LE), where the

reference potential is the average of the two earlobes; Linked mastoid (LM), where the average of two electrodes on the left and right mastoid bones is used; and Average reference (AR), where the signal is referenced to the average computed over all the electrodes (López et al., 2016).

As extensively reported in literature, the choice of the referencing system is a matter of primary importance in EEG studies, since it can significantly bias the recorded signal (Yao et al., 2007). As pointed out in (Yilmaz et al., 2014), the AR system, albeit not qualifiable as the gold standard, can still be considered the best option. This is true especially in situations that are close enough to the ideal conditions of high electrode density and full head coverage (Nunez, 2010), that is, when ahigh number of electrodes (e.g. 256) evenly cover a large portion of the head surface. The ideal situation of full coverage could only be possible with a detached head.

Modern acquisition systems also include an analog-to-digital converter (ADC) for the signal digitalisation, a filter to reduce environmental noise and a multichannel amplifier with shielding for environmental noise.

### 2.2.2 Neural basis of EEG

The question of the physiological origin of the EEG signal was widely disputed from the very first measurements in the 1930s and remained a controversial issue at least until the 1970s (Lopes Da Silva and Storm Van Leeuwen, 1977). The reason for that lies in the complexity of the mechanisms that regulate the action of the neural sources of the signal, at the level of the brain cortex. In fact, the presence of specific patterns and rhythms in EEG signals indicates that neuronal electrical activity is not a random process, unveiling the existence of underlying physiological mechanisms that provide some kind of synchronisation.

The neurone is the primary nerve cell of the central neural system (CNS) and consists of three structures:

- Soma, the main body of the cell, which contains the nucleus
- Dendrides, short branches which carry incoming signals from other neurones to the soma
- Axon, a longer projection, usually partly covered by an insulating fatty layer of myelin, which carries the neural signal from the soma to other neurones.

The total number of neurones in the brain is about $10^{10}$ each one creating 10,000 connections; in just $1mm^3$ of cortex there are 50,000 neurones, for a total 4km of axons. The most common kind of neurones in the brain cortex are the pyramidal neurones, named after the shape of their soma. They are spatially aligned, parallel to each other and perpendicular to the cortical surface.

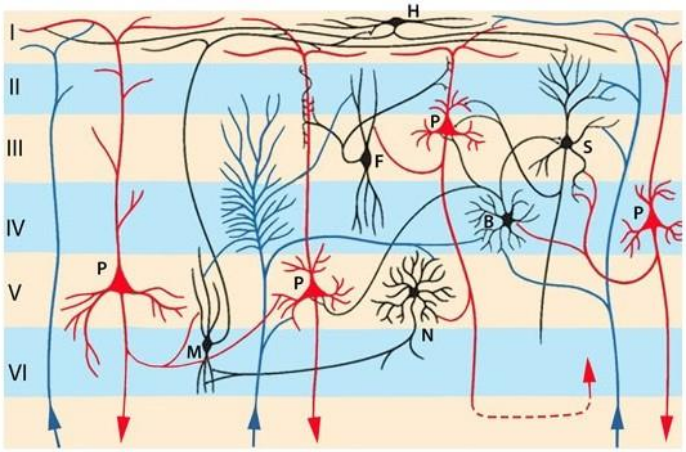


**Figure 2.4.** Pyramidal neurons (marked with P) in the six cortical layers (I-VI). (Standring and Grey, 2008)

The basic neural signal unit is the action potential (AP), a few millisecond long perturbation of the membrane resting potential (-70mV). The flux of Na+ and K+ through the ion gates of the cellular membrane cause a sudden depolarisation (+50mV) and a following hyperpolarisation (-90mV) of this potential. This signal, generated in the axon hillock, travels along the axon towards the synapses (interface between the axon terminals and another neurone's dendrites) where it causes the release of endogenous chemicals: the neurotransmitters. The diffusion of neurotransmitters across the synaptic cleft and in the intracellular space of the postsynaptic neurone, produces a positive or negative ionic current which determines, respectively, an Excitatory Post-Synaptic Potential (EPSP) or an Inhibitory Post-Synaptic Potential (IPSP). PSP effects have a lower amplitude (0.1-10mV) compared to the AP (70-110mV) but last tens to hundreds of milliseconds (Baillet et al., 2001a). It is the spatial and temporal summation of IPSPs and EPSPs that originates the brainwaves detected by the EEG.

In fact, the EEG signal is generated by the collective behaviour of a large number of cortical pyramidal neurones: about 10,000 to 50,000. Their parallel spatial alignment prevents charges from canceling themselves out and the long duration of PSPs makes it more likely for a large number of them to overlap and add together. In this way, the spatial and temporal alignment of the extracellular current flow, from the summed activity of many neurones, creates a dipole that allows the generation of a measurable signal. Volume currents spread from the dipole through the conductive medium of the head tissues. When they reach the scalp they induce the voltage differences that EEG is sensitive to. Not all the cells contribute equally, though. The EEG signal reflects the activity of neurones which are closer to the electrodes, while deeper structures have a smaller contribution. Another aspect that influences the recorded

signal is the orientation of the dipole, radial or tangential to the scalp, according to its position on the irregular surface of the white matter that produces sulci and gyri.

### 2.2.3 Artefactual patterns and identification techniques

Ideal EEG signals would be representative solely of the brain electrical activity; however, the measured signal is inevitably contaminated by a number of different artefacts. Artefacts can be described as anything that is not of cerebral origin, e.g. recorded electrical activities that arise from extracerebral sites. They can be generated by a variety of sources and occur in many different ways: single waveform, burst or series of waveforms that blend with or even overshadow the cortical activity (Tatum et al., 2017). Artefacts can be classified into two main categories: those related to the physiology of the subject and those caused by the acquisition system or the external environment. Table 2.1 lists the most common types of artefacts in EEG recordings (Wendling et al., 2017).

**Table 2.1.** List of common EEG artefacts

| **Physiological artefacts** (subject- related) | **Extra-physiological artefacts** (acquisition system- related) |
|---|---|
| • EOG: eye movement, blink<br>• EMG: muscular tension, movements<br>• EKG: heartbeat<br>• Respiration, tongue movement, etc. | • 50 Hz power line<br>• Electromagnetic interference<br>• Lead wire movements<br>• High electrode impedance, salt bridge, etc. |

The extra-physiological artefacts caused by the acquisition system are usually easy to identify and to troubleshoot by adopting some precautions during the measurement, such as, isolating the subject from external stimuli or shielding the system (using a Faraday cage) to avoid electromagnetic interference with cellphones and other devices (Fathima and Umarani, 2016). The 50 Hz (or 60 Hz in North America) power-line noise is usually tackled with a notch filter to remove that specific undesired frequency component. Channel-specific artefacts are usually due to malfunctioning of the electrodes, caused for example by a sudden detachment (electrode "pop"), a damaged connection with the lead wire, high impedance at the electric interface with the scalp, dry conductive gel, oxidized sensors or bridged electrodes. All these issues can be solved with a careful replacement of the faulty electrodes (Ferree et al., 2001).

The physiologically-generated artefacts are due to the biological properties of many sources on the subject's body that act like electric dipoles. The most evident example of this is given by the eyeballs, which can be represented by a dipole with a positive pole on the cornea and a negative pole on the retina. The dipole rotation due to eyeball movement produces a change in polarisation that results in an extracerebral potential, coherent with the direction and rate of movement, measurable on the scalp. An extra electrode is often applied close to the eye in order to record the electrooculogram (EOG) and recognise its waveform interfering with the EEG (Lopez et al., 2016).

Like the eye, the tongue functions as a dipole with a negative pole on the tip and a positive pole at the base. In this case, the mobility of the tip creates a potential that reflects in a broad portion of the scalp, predominantly in the frontal and temporal area (Tatum et al., 2017).

The heart is another important bioelectrical source in the body and the so-called cardiac dipole is used to describe the wave of depolarisation that spreads through atria and ventricles. Its

spinning in the 3-dimensional plane during a cardiac cycle results in the QRS complex recorded by the electrocardiogram (EKG). In certain patients (infants or people with short, stocky necks) it is possible to clearly identify a timed-locked synchrony between EEG and EKG waveforms.

The preprocessing techniques employed to remove these unwanted components from the recorded scalp EEG signal are described in detail in Chapter 3 – Methodologies.

## 2.3 EMG

The electrical signal generated by muscle activation is called myoelectric signal. Electromyography (EMG) is an electro-diagnostic technique that allows the measurement, evaluation and recording of the electrical signal emanating from muscles.

Muscle activation is controlled by the nervous system in a physiological process that involves the generation of ionic currents flowing through the muscle cells membrane and a consequent change of electric potential in the muscle itself and the surrounding tissues. The resulting time-varying potential signal, which is influenced by the impedance of the soft tissues through which it propagates, can be picked up by electrodes placed on the skin and represents what is called surface EMG (sEMG) (McManus et al., 2020). To avoid the signal attenuation introduced by soft tissues, the electrical activity can also be recorded through invasive intramuscular EMG (needle or fine-wire EMG), but for the purpose of this work, this review will focus on sEMG.

EMG-based procedures have been historically used as a diagnostic tool for the detection of neurological disorders and for the assessment of patients affected by neuromuscular diseases such as muscular dystrophy, inflammatory myopathies, ALS, myasthenia gravis, etc. More

recently though, EMG has also found extensive application in the control of robotic mechanism, smart prosthetics and man-machine interfaces (de la Rosa et al., 2010).

Nevertheless, it is worth pointing out that while intramuscular EMG is commonly used in clinical set-ups especially in clinical neurology, surface EMG, despite its non-invasiveness and ease of use, is predominantly confined to research. A more extensive application of surface EMG in clinical settings is held back by the fact that information is not readily available and a certain degree of knowledge in signal processing is required to extract useful parameters from the signal (Feldner et al., 2019).

An example of sEMG signal is shown in figure 2.5. The amplitude of the signal picked up by skin sensors is rather small, varying between a few μV to around 10mV according to the type of muscle and the intensity of contraction. The signal's useful bandwidth lies between 20-400 Hz, but the dominant frequencies are in the 50-150Hz interval, which accounts for most of the signal's power (Cavalcanti Garcia and Vieira, 2011).

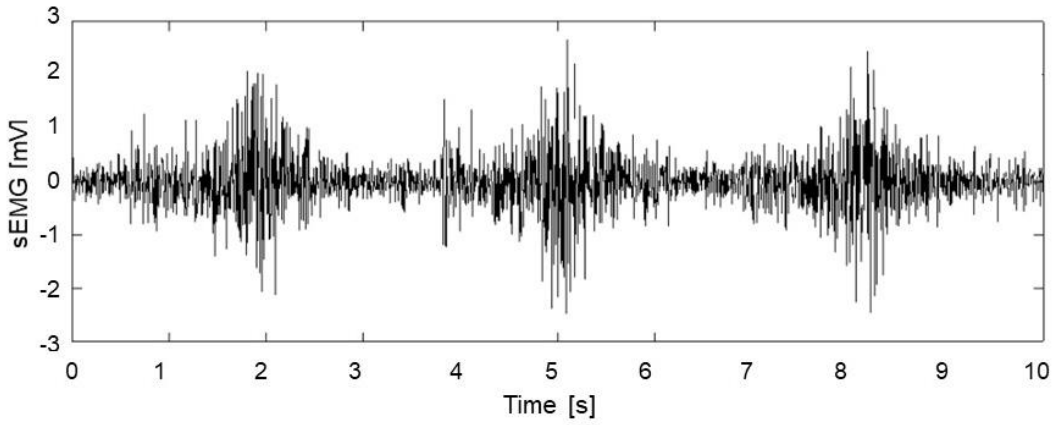


**Figure 2.5.** Example of surface EMG signal.

The literature on the subject has pointed out how the use of surface EMG comes with a number of drawbacks, including: a limited spatial resolution that makes it not suitable to capture high-frequency dynamics; its inability to distinguish the individual activities of two muscles which are in close proximity (electrical cross-talk); a degraded signal quality due to soft tissue attenuation when the recorded muscle is more than 10mm below the skin surface (Pullman et al., 2000). Nevertheless, while some of the published literature emphasises these drawbacks suggesting the ineffectiveness of sEMG as a clinical tool (Klasser and Okeson, 2006; Meekins et al., 2008; Pullman et al., 2000), more recent papers highlighted the diagnostic value and the usefulness of sEMG in a clinical set-up (Bar-On et al., 2013; Mazzoli et al., 2018; Merlo and Campanini, 2019). A recent extensive review on the topic identifies the cause of the relatively limited adoption of sEMG in clinical practice as a lack of ability to translate the technology outside of movement science labs research environment (Campanini et al., 2020). In this context, the European project “Surface EMG for non-invasive assessment of muscles” (SENIAM) set out to improve the translation of sEMG research experience into a clinical environment by providing standard guidelines for proper signal collection and processing (Stegeman, 2007). Indeed, technical improvements to the acquisition systems and more advanced signal analysis techniques, together with its non-invasiveness, resulted in sEMG playing an important and ever-growing role in many fields such as neurorehabilitation, orthopaedic rehabilitation, and sport and ageing sciences. sEMG is in fact proven to be more suitable for movement analysis, where a global measurement of activation is required for one or multiple muscles and multiple, non-invasive assessments are required (McManus et al., 2020). This is attested by the steady increase of peer-reviewed publications on sEMG over the last decades (Campanini et al., 2020).

### 2.3.1 Physiological basis of EMG

To appreciate the importance and usefulness of the information carried by the EMG signal it is necessary to understand how it is generated at the muscular level and the physiological processes involved.

Skeletal muscles represent the most common type of muscle tissue, making up on average between 30 and 40% of the human body weight (depending on gender, age and individual anatomical characteristics) (Janssen et al., 2000) and their main function is to allow movement. They are also known as voluntary muscles as they act under voluntary control, in opposition to smooth muscles of the internal organs and the cardiac muscle. Skeletal muscles encapsulate the skeletal system providing structural support, giving shape to the body, protecting internal organs and stabilizing joints. These muscles are attached to the bones through tendons (connective tissue fibres) and they allow the voluntary movement of limbs and external parts of the body. One of their other prominent functions is the maintenance of posture, which is achieved through constant contraction and tiny adjustments.

Each individual muscle is made up of a bundle of muscle cells, or muscle fibres. Skeletal muscle fibres are striated, and they appear as extremely organised structures consisting of long and tightly packed fibre-like organelles called myofibrils. These organelles contain the contractile proteins (actin and myosin) that are at the base of the muscle fibre's ability to vary its length by stretching and contracting.

Skeletal muscle fibres are innervated by nerve cells called motor neurons. Each motor neuron reaches several muscle fibres, establishing synapsis between its axon terminals and fibres distributed over a relatively wide area of the muscle. Each muscle fibre is innervated by only

one motor neuron and the group of fibres innervated by the same motor neuron is called the motor unit, the elementary functional unit of a muscle. The size of motor units is variable depending on the nature of the muscle and reflects the type of movement and the amount of force that the nervous system wants to produce (Purves et al., 2001).

- Slow motor units (S) are small units where the motor neuron innervates only a few muscle fibres. Their activation threshold is rather low: they exert small amounts of force and allow for fine motor control (grasping, typing, etc.). They are crucial in the maintenance of posture, as they enable sustained muscular contraction. The soleus muscle, with an innervation ratio of 180 muscle fibres comprises mostly S units.

- Fast Fatigable (FF) motor units are bigger units able to produce large forces and sudden changes in body position (running, jumping). The gastrocnemius muscle comprises a mix of S and FF motor units and its innervation ratio is 1000-2000 muscle fibres per motor neuron.

- Fast fatigue-resistant (FR) motor units have an intermediate size, they generate about double the amount of force of the small S units

The presence of different types of motor units within each skeletal muscle gives the nervous system a wide range of control over the muscle.

One of the main characteristics of muscle fibres is their excitability, and motor neurons are responsible for their activation. When an action potential travelling down the motor neuron’s axons reaches the neuromuscular junction, the release of neurotransmitters generates a change in the muscle fibre’s membrane potential with its depolarisation. This action potential

triggers the muscle cell to shorten, inducing a contraction. The summation of the single muscle fibres action potentials makes up the motor unit action potential (MUAP).

MUAPs are characterised by a set of features that includes:

- Duration, usually between 5-15ms
- Amplitude, typically 0.5-2mV
- Phases, the shape of MUAP is generally triphasic (negative-positive-negative)
- Rise time, i.e., the time between the positive peak and the following negative one

Every time the motor unit is activated, a MUAP is generated, and this activation is repeated continuously for as long as the muscle is required to generate force. Repeated activation produces a train of action potentials that can be observed and recorded during slight contractions using needle electrodes inserted into the muscle.

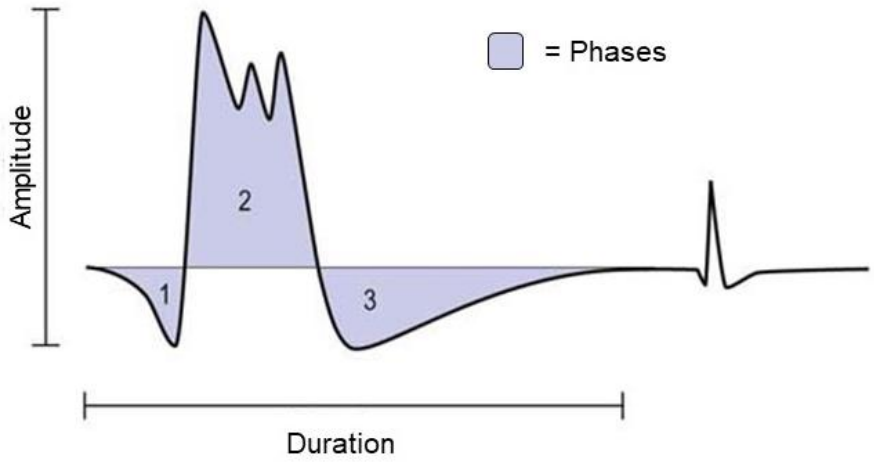


**Figure 2.6.** A single triphasic motor unit action potential (MUAP).
(Adapted from *Basic Electromyography: Analysis of Motor Unit Action Potentials* | *Clinical Gate*)

Figure 2.7 shows what the electrical activation of muscles looks like under different conditions.

A slight contraction of a normal, healthy muscle allows one to observe a train of MUAPs with the distinctive triphasic shape. As the muscle contraction grows progressively stronger, more motor units are recruited. When needed, all the motor units within a muscle can be recruited and produce the so-called maximal voluntary contraction (MVC). This intense level of activation, which can only be sustained for short periods of time, results in the interference pattern depicted in figure where the single MUAPs are no longer recognisable.

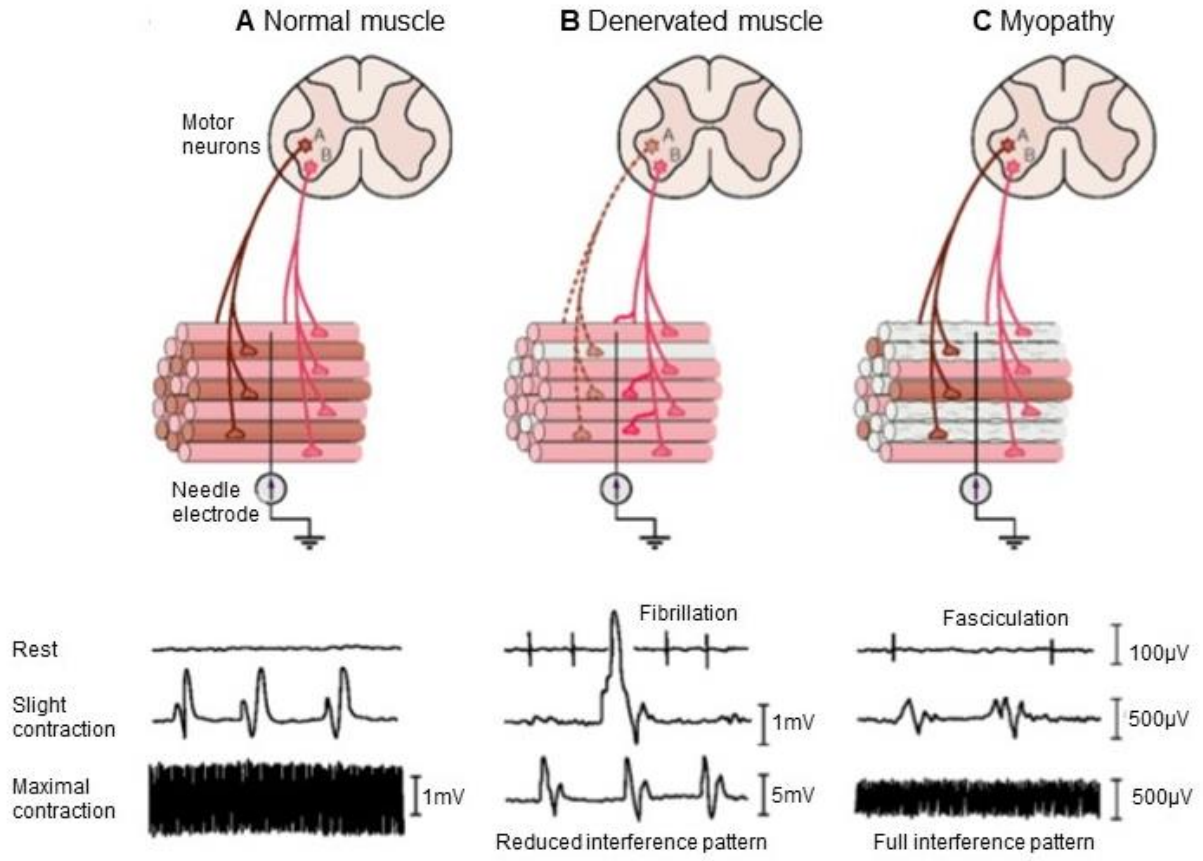


**Figure 2.7.** Examples of muscle activation.

Under the same intensity of contraction, these characteristic EMG patterns change in pathological subjects. Figure 2.7 also reports examples of EMG patterns from denervated muscles and muscles affected by myopathy. The former are characterised by lack of innervation and show a fibrillation pattern in resting state, with recorded action potential even when no voluntary contraction is in place. Slight contractions result in an oddly shaped MUAP, the so-called “giant potential” and their interference pattern is reduced during maximum contraction.

# 3. Methodologies

This chapter describes the devices designed and used during the data collection phase of the studies presented in the thesis. It also provides an overview of the technical and mathematical background on the analysis techniques used to extract information from EEG, EMG and posturography data. More detailed information on the individual studies is provided in Chapters 4, 5 and 6.

## 3.1 Experimental instrumentation

The data presented and discussed in the experimental chapters of this thesis were collected at the Institute of Biomedical and Neural Engineering - Reykjavik University, Iceland (Chapter 4) and at the ALIVE lab – Aston University, Birmingham UK (Chapter 5 and 6).

In both facilities, the experimental equipment consisted of ANTneuro EEG recording devices, a force plate, a stimulation device, and eccentric revolving motors (actuators) which deliver 85Hz vibratory stimuli to the participants' calves. The stimulation sequence consisted of a pseudo-randomised pulse wave (vibration ON/OFF). The stimulus duration and inter-stimulus interval were uniformly distributed between 1s and 6s.

In Reykjavik, data from 30 young healthy participants were recorded using a 256-channel EEG cap connected to four amplifiers (ANTneuro mylab). A closed system developed at Lund University (Sweden) integrated a force plate for posturographic recordings, a control device for the stimulation sequence and actuators (vibrating motors). The ANTneuro amplifiers were connected to this device through a trigger box for the synchronisation of signals.

In Birmingham, a portable ANTneuro mysport system was used to collect both EEG and EMG data on 11 subjects, respectively from a 64-channel cap and 11 bipolar electrodes applied to

the participants' leg muscles. The body sway was recorded using a force plate which was part of a larger motion capture system by Vicon motion systems. For the control of the randomised vibratory stimulation sequence, delivered through vibrators applied to the participants' calves, and its synchronisation with the EEG/EMG and posturographic signal, a custom-made device had to be designed and implemented.

The stimulation controller device comprised a custom-made electrical circuit mounted on a programmable Arduino UNO board, which controlled a pair of actuators. The device, designed to be portable and wearable by the participants, was powered at 18V through 2 rechargeable 9V batteries. The set of batteries provided power to both the Arduino board (9V scaled down to 5V through the internal voltage regulator) and to the actuators.

Two DC motors were used as actuators. The motors were equipped with an eccentric rotating mass (ERM) and encapsulated in a plastic cylinder (diameter: 30mm, length: 62mm). When the motors were powered, the rotation of the ERM produced the vibration. Similar devices, with

**Figure 3.1.** Vibrators used to administer the proprioceptive stimulation. Each plastic cylinder contains a DC motor and an eccentric rotating mass

varying dimensions but same working principle are widely used as pagers, vibration alert notifications on cell phones, haptic feedback on medical instruments, industrial user interfaces, etc. The operational voltage range of the motors was 3V to 15V. To achieve the desired vibratory stimulation frequency, the 18V power supply had to be regulated to feed the ERM motors with a 12.4V input voltage, which provided a rotation speed of 5100 RPM, corresponding to 85 Hz. This was achieved through a LM317 variable voltage regulator and a trimmer potentiometer. The potentiometer was used as a variable resistor to tune the output voltage of the LM317.

To identify the voltage corresponding to the desired vibratory frequency, different values were tested using a signal generator, while an accelerometer was attached to the cylindrical casing of the DC motor to record the spatial displacement due to the increasingly intense vibration. Running a frequency analysis on the displacement signal, it was possible to identify the voltage that induced a peak at 85Hz. As a safety measure, a diode and a capacitor were used in parallel with each motor, in order to filter the noise caused by the DC motors and to protect the Arduino board from reverse voltage spikes caused by the motors acting as inductors.

Figure 3.2 shows a detailed schematic of the electrical circuit. The components (listed in Table 1) were soldered on a prototyping board connected to the Arduino UNO board.

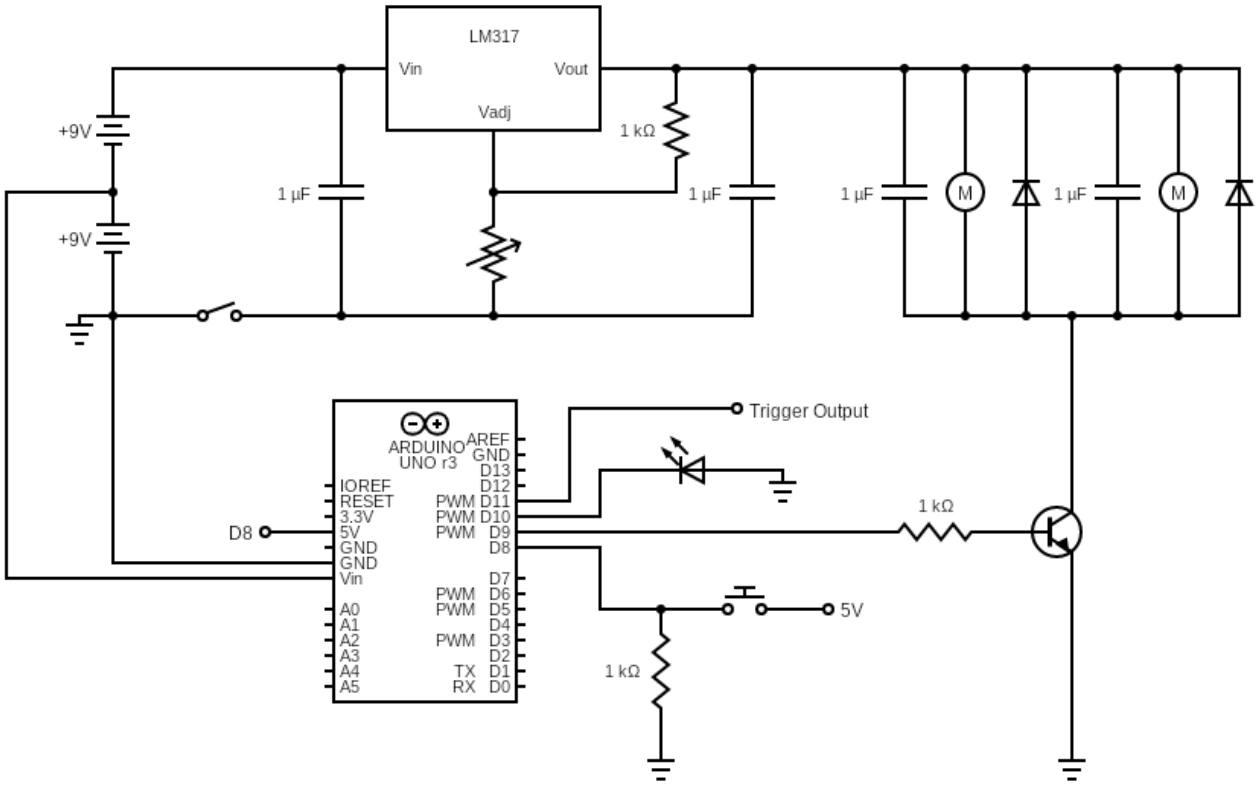


**Figure 3.2.** Schematic of the custom-made control device / trigger box.

**Table 3.1.** List of components for the control device.

| Description | Item number | Quantity |
|---|---|---|
| Arduino Uno REV3 | A000066 | 1 |
| 200mAh NiMH 9V Rechargeable Battery | 199-646 | 2 |
| Voltage Regulator | LM317 | 1 |
| Rocket Switch | 419-744 | 1 |
| SPST Green LED Push Buton Switch | 913-1737 | 1 |
| 1µF Capacitor MLCC 50V | 133-5720 | 4 |
| 1kΩ Resistor 0.25W | 707-7666 | 2 |
| 200Ω Resistor 0.5W | 132-321 | 1 |
| NPN Transistor, 1 A, 40 V | PN2222ATA | 1 |
| Silicon Junction Diode, 1A 400V | 1N4004 | 2 |
| 10kΩ Trimmer Potentiometer, 0.75W | 3006P-1-103 | 1 |
| ERM DC vibrating motor | 253659687604 | 2 |

The script uploaded on the Arduino IC controlled the pseudo-randomised vibratory stimulation sequence and delivered the corresponding trigger signals to the other devices (ANTneuro amplifier and Vicon system). The Arduino's output on pin 9 controls the base terminal of an NPN transistor. The other two terminals of the transistor connected ground to the negative pole of the DC motors (emitter and collector respectively). The NPN transistor operates like a switch: when pin 9 of the Arduino was set to 'HIGH' (5V), it switched on, allowing current to flow to ground through the motors. Thus, by switching the output on pin 9 from 'LOW' to 'HIGH' and vice-versa, it was possible to turn the motors on and off.

To synchronise the vibratory sequence with the recorded signals (EEG/EMG and postural sway) Arduino was programmed to send a 5V TTL trigger signal as an output from pin 11 at the end of each vibration (to the trigger port of the ANTneuro amplifier, and to the Vicon system respectively).

The following lines of code show a portion of the Arduino script. In this example one cycle of vibration is generated. First pin 9 is defined as 'MOTOR' and pin 11 as 'trigger' (lines 1-2). Pin 9 is first set to 'HIGH', enabling the switch and turning the motors on for 2000ms, and then to 'LOW', turning the motors off (lines 3-5). Immediately after, pin 11 is kept on a 'HIGH' status for 2ms to send the trigger signal (lines 6-8). 2ms is the minimum duration for the trigger signal to be read by the force platform and EEG system (having both a sampling frequency of 1000 Hz). Finally, the motors are kept off for 3000ms before moving to the next cycle of vibration (line 9).

```
#1 const int MOTOR = 9;
#2 const int trigger = 11;

#3 digitalWrite(MOTOR,HIGH);
#4 delay(2000);
```

```
#5 digitalWrite(MOTOR,LOW);
#6 digitalWrite(trigger,HIGH);
#7 delay(2);
#8 digitalWrite(trigger,LOW);
#9 delay(3000);
```

Finally, the case that encloses the Arduino board and the electronic circuit was designed with SolidWorks and 3D-printed in Polylactic Acid (PLA) with a Ultimaker3 printer, as shown in Figure 3.3. The box is 9.5cm long, 6cm wide (excluding batteries) and 4cm tall. The 9V batteries are mounted on the sides, together with the rocket switch that powers the device. On one side are three female power connectors for the 3 outputs of the system: 2 motors and 1 trigger cable. On the opposite side the Arduino board connectors are accessible, consisting of a power jack and a USB-B port used to upload scripts on the board microcontroller. On top of the case, a green LED push button could be pressed to start the sequence. The built-in LED would stay on for the whole duration of the stimulation, turning off to signal the end of the trial.

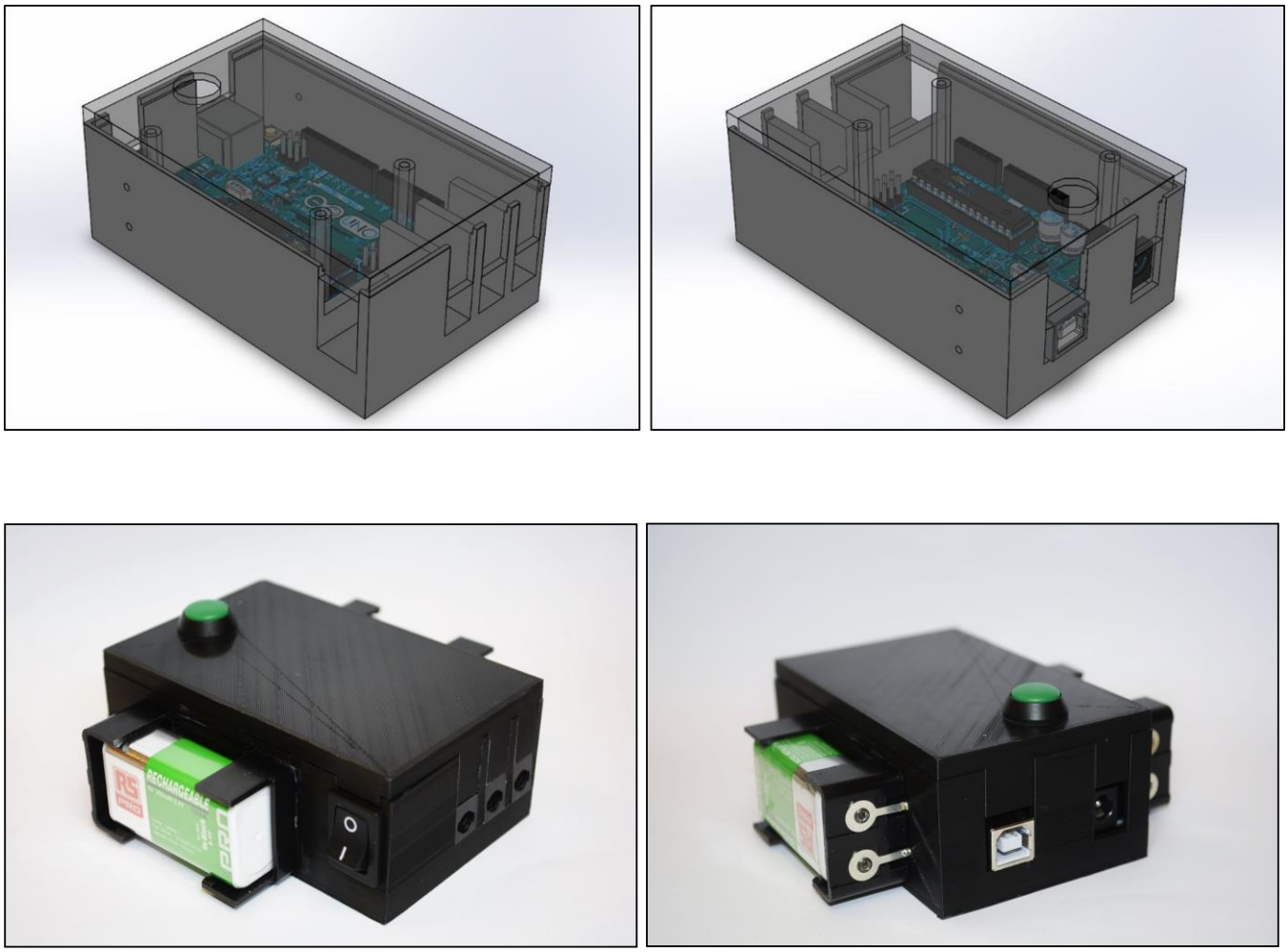


**Figure 3.3.** SolidWorks rendering (top panels) and final 3D-printed version (bottom panels) of the stimulation controller and trigger device. Two 9V batteries mounted on the sides power the device, the left panel shows the rocket switch, the three output connectors (two vibrators and a trigger cable) and the LED start button. On the opposite side (right panel) are the USB-B and external power connectors.

## 3.2 EEG Analysis

### 3.2.1 Preprocessing

As a neuroimaging technique based on the electrophysiological properties of the brain, the aim of EEG is to extract useful information about the electrical activation of specific brain areas during a certain task, cognitive state, or in response to a stimulus. However, the raw voltage signal recorded on the scalp is not easy to decipher without appropriate preprocessing of the data. Common preprocessing steps include filtering the signal in the bandwidth of interest, segmentation of the data, artefact detection and rejection, etc. This process needs to be carried out across each trial, for every participant. Several software packages are available for data preprocessing, for example Matlab EEGLAB toolbox, which offers a set of tools to inspect the data, mark possible artefacts and correct them using a range of techniques, including the commonly used independent or principal component analysis (ICA and PCA respectively). Both techniques perform a statistical transformation of the data, which are decomposed into a set of bases (components). PCA aims to find the set of components that better explains the variability of the data, while ICA aims to identify a set where each component is independent (source separation). Then, both techniques require the selection of a number of components to discard (those related to undesired sources) and the reconstruction of the signal based on the remaining components (Jung et al., 1998; Turnip and Junaidi, 2015). This was the approach used in the first study presented in Chapter 4. However, the identification of data segments (epochs) contaminated by artefacts of different nature can prove to be a cumbersome and time-consuming task, susceptible to arbitrary and subjective evaluations when performed manually, by visual inspection of the data. Specifically, when the use of ICA or PCA is involved in the process, a manual selection of components to retain or discard is

required. This choice, however, could affect the quality of the final data. For example, parts of good signal could be mixed in the rejected components, causing a loss of useful information. To minimise the bias introduced by arbitrary choices, a semi-automated EEG preprocessing approach was adopted in the work presented in Chapter 5. The following pipeline, in particular, was adapted from (Brunet et al., 2011), and the main steps are displayed in Figure 3.6:

- First, the raw data were imported from the ANTneuro recording system. If EEG and EMG had been simultaneously recorded, the EEG channels were isolated and downsampled to 1000Hz.

- Each EEG channel was then filtered between 1-45Hz with a zero-phase band-pass FIR filter, which allowed the extraction of the frequencies of interest while getting rid of the 50Hz power line noise component.

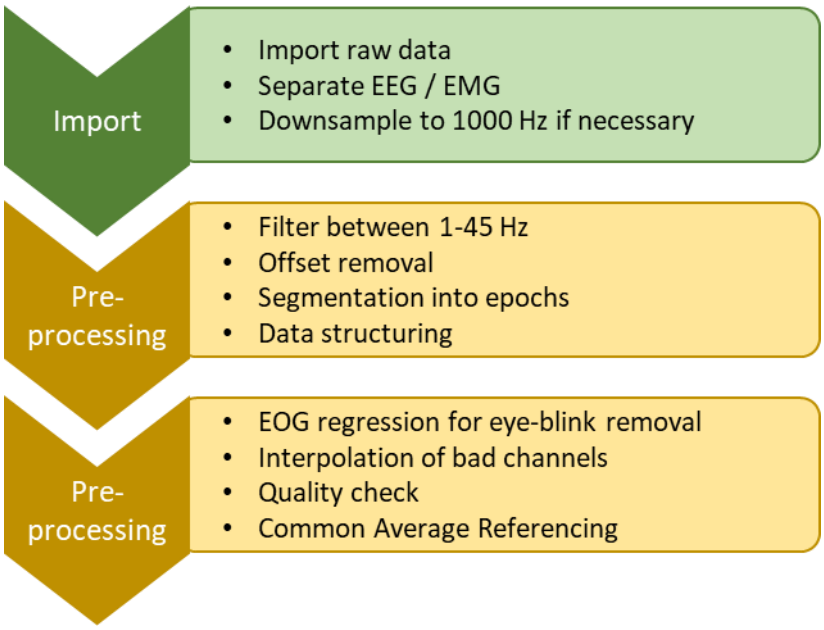


**Figure 3.4.** EEG data import and preprocessing pipeline.

- The signal was then detrended by removing the DC offset component.

- Subsequently, each EEG channel was segmented into epochs according to the experimental design, as discussed in more detail in the following chapters, and organised in orderly data structures.

- To remove eye blink artefacts, an Electrooculography (EOG) regression approach was chosen over ICA (Croft and Barry, 2000; Parra et al., 2005). Eye blink artefacts are characterised by high amplitude (>> 100 $\mu$V) and a characteristic signature which can be clearly observed in the frontal EEG channels but is usually more subtly spread throughout the scalp. For this reason, three frontal channels (Fp1, FpZ, Fp2) were used to perform a regression on the remaining channels, as follows:

$$EEG_i = EEG_i - EOG \cdot \frac{EOG}{EEG_i}$$

The EOG-related artefactual signal is subtracted from each channel $EEG_i$, proportionally in respect to its strength in the specific channel.

- A supervised, automated approach was then used to identify channel epochs affected by artefacts. The classification of bad channels was based on the standard deviation value of the epoch's amplitude. If this exceeded the average std of the remaining channels by a certain factor, the epoch was discarded and then replaced with the interpolated signal obtained from the neighbouring channels (distance < 5cm).

  $if\ std_i > T \cdot std \rightarrow Interpolate\ channel\ i$

  Different factors T were tested and, following a visual inspection of the data, the value of T=1.7 was chosen. It was observed that lower threshold values would have been too conservative, interpolating signals contained within a physiological range of ±80 $\mu$V ,

while higher T values would have let clearly noisy signals pass (Hassan and Wendling, 2018a). The interpolated epochs were then re-filtered in the same bandwidth in order to smooth them out. To avoid edge artefacts the epochs were mirrored before filtering (Cohen, 2014).

- Each epoch in which more than 9 channels (15% of the total) were found to be corrupted and had to be interpolated, was discarded.

- The signal was finally re-referenced to common average

### 3.2.2 Spectral Analysis

A complex physiological signal such as the EEG time series can be described as a sum of sinusoidal waves with different amplitudes and phases. This is valid under the assumption of stationarity of the signal (mean and variance of data distribution do not depend on time), which is accurate for short time windows. The goal of spectral analysis is to extract the frequency content of the EEG signal, enabling the observation of its periodicities and dominant patterns. The Fourier transform (FT) is the mathematical operation that allows the performance of this frequency decomposition of the signal. FT is generally implemented using Fast Fourier Transform (FFT), a widely-used algorithm that allows the computation of Discrete Fourier Transform (DFT) in a quick and computationally efficient way.

Let $x(n)$ be a discrete time series of N samples, acquired with a sampling frequency $Fs$. The original signal can be represented as the weighted sum of basis sinusoidal functions and expressed in the form:

$$\mathrm{x(n)} = \frac{1}{N}\sum_{k=0}^{N-1} X_k e^{j\frac{2\pi}{N}kn} \ , \qquad n = 0.1 \ldots . . N-1$$

Where $X_k$ represent the Fourier coefficients, i.e., the weights associated with each sinusoidal function (expressed in the formula above in the Euler's exponential form). The DFT coefficient can be calculated as:

$$X_k = \sum_{n=0}^{N-1} \mathrm{x(n)} e^{-j\frac{2\pi}{N}kn}$$

The power of each frequency component can then be derived as the squared value of the real part of the corresponding Fourier coefficient. The power reflects the covariance between the original signal and the complex sinusoids at the specific frequency. The power spectral density is obtained by plotting these values against the frequency axis (power per unit frequency, dB/Hz). The upper threshold of the frequency range in which the PSD can be computed is determined by the original sampling frequency, according to the Nyquist theorem, as:

$$F_{max} = {}^{F_s}/_{2}$$

This reflects that to reconstruct a signal without any form of distortion (aliasing), the sampling frequency needs to be at least twice the highest frequency component. The absolute spectral power in a specific band $[f_0 , f_1]$ is defined by integration of PSD in that band.

Because FFT is performed on a finite data set, the algorithm interprets that as one period of a continuous periodic signal which repeats itself in a circular way. Since this is not the case in real applications (where we deal with truncated time series) the two timepoints at the extremities of the EEG time series might not match, causing discontinuities in the signal that

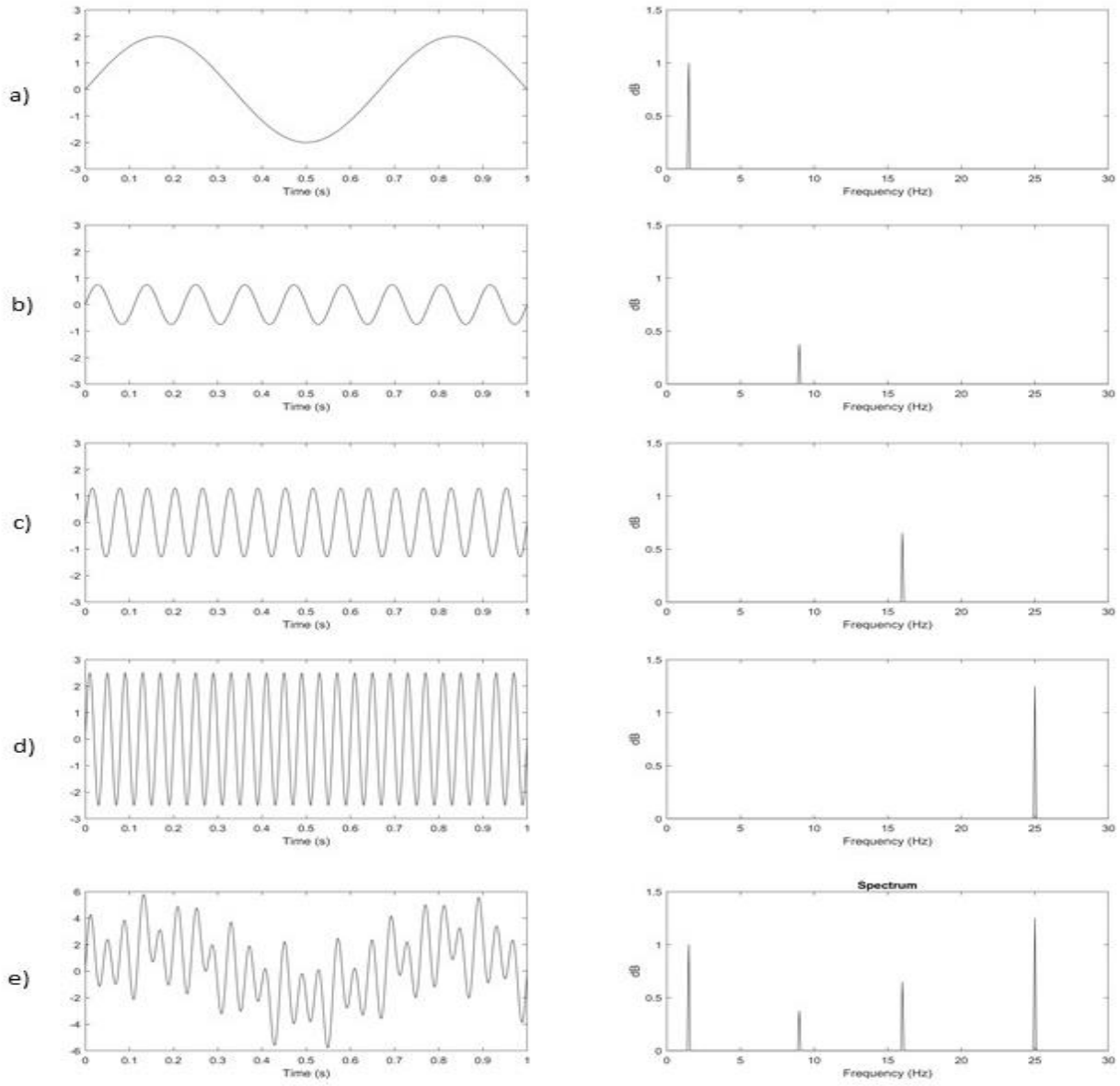


**Figure 3.5.** a) – d): Monofrequency sinusoidal waves at different frequencies (left column) and corresponding power spectrum (right column). e) Linear combination of the sinusoidal waves (left) and corresponding power spectrum (right). It can be observed how the power spectrum of signal e) contains the frequency components of the sinusoids which were combined to generate the signal.

result in an inaccurate spectrum estimate. This problem is known as *spectral leakage*. To minimise this effect, a technique called windowing (or tapering) is used. This consists in multiplying the time series by a finite length window that smoothly modulates the original signal

towards zero at its edges. The Hanning window is one of the many waveforms available to do so and is one of the most commonly used. Nevertheless, the windowing process results in a temporal weighting of the signal, which could attenuate certain signal characteristics, causing loss of information and an altered PSD estimate. In order to improve this, window segments are usually overlapped.

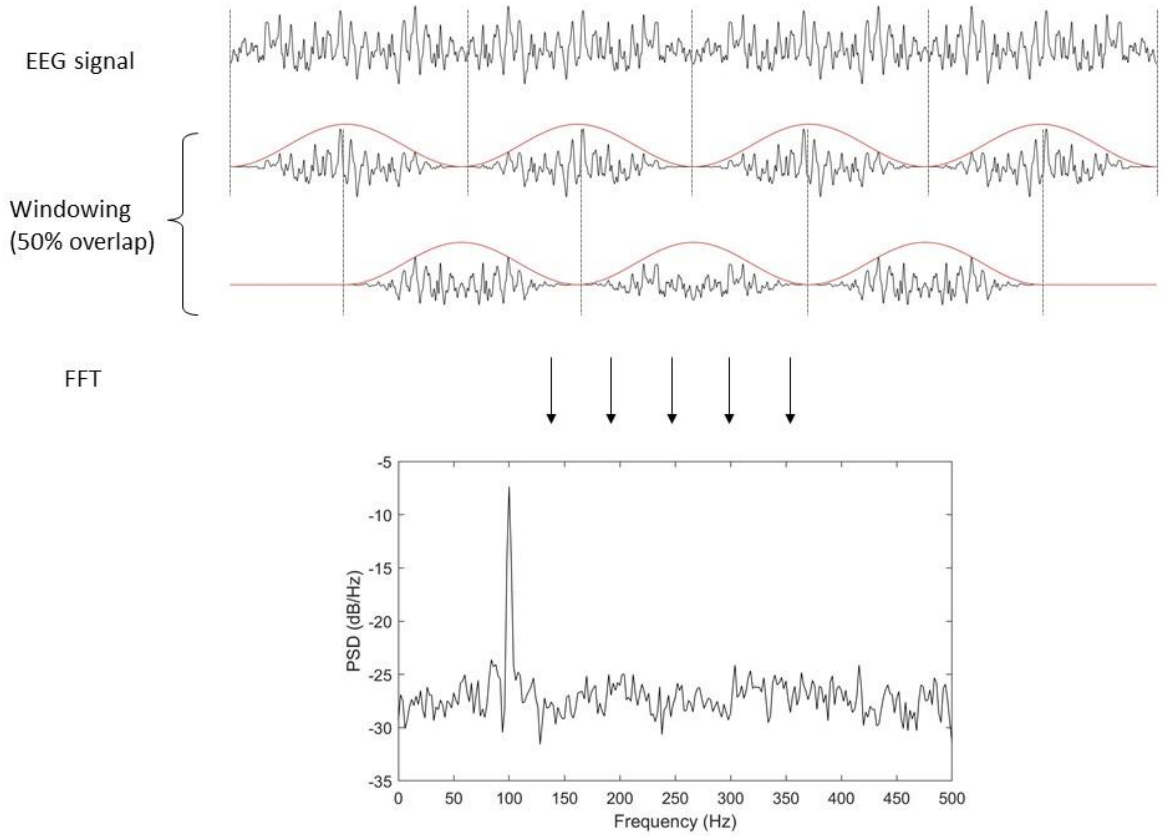


**Figure 3.6.** PSD estimate with Welch´s periodogram method and 50% overlapping Hanning window tapering. First, the original EEG signal is split into overlapping epochs. Then, each epoch is modulated with a Hanning window. Finally, the PSD is estimated for each epoch and averaged to obtain the final estimate.

This approach to PSD estimate is implemented in the Welch's periodogram method (Welch, 1967). First, the original signal is split into overlapping segments (usually 50% overlap), then each segment is windowed and the corresponding DFT is computed. Finally, the individual epochs spectra (periodograms) are averaged to provide the signal's PSD estimate. A schematic representation of Welch´s method is displayed in Figure 3.6.

### 3.2.3 EEG brain network

The brain is a complex system which can be examined using either low or high order statistics. In power spectral analysis the focus is on the activation level of single regions (univariate), but it could be of interest to investigate how couples of regions interact with each other (bivariate) or even explore the multiple joint interactions among several brain areas (multivariate). The latter is the focus of network neuroscience, which employs network analysis techniques to examine the large-scale topological organisation of the brain, rather than focusing on the properties of single regions. This approach provides a more comprehensive way to describe the patterns that allow information to flow throughout the system and highlight how certain conditions, tasks or cognitive states affect these functional organisation patterns of the brain. In the context of postural control, brain network analysis is an extremely relevant approach that can help to shed light on the ways cortical patterns regulate the postural control strategy, how they are affected by proprioceptive vibratory stimulations, how they adapt to prevent falling and how they allow the integration of different levels of sensory information: visual, vestibular, proprioceptive, somatosensory etc., which require the engagement of several distributed cortical regions.

In order to quantitatively assess brain network patterns, the analytical methodologies of graph theory are applied to neurophysiological data. Graph theory allows us to better understand

complex systems by describing them mathematically as graphs. Network neuroscience is a relatively recent field of research (early 2000s) which developed from the application of graph theory to traditional neuroscience and proved to be a powerful tool to quantitatively describe the topological organisation of brain connectivity. Most of the terminology used in brain network analysis was also adopted from graph theory. Here, the brain is rendered through a graph (network) in which nodes represent cortical regions and edges, i.e., the connections among nodes, represent the functional connectivity between two regions.

The two key points for the reconstruction of a brain network are how to define regions (nodes) and how to measure connectivity (edges). This choice depends on the type of neuroimaging technique used. In the case of fMRI nodes can be defined as groups of voxels and connectivity values can be derived by metrics of co-activation of fMRI time-series. When using scalp EEG nodes are usually represented by channels, while edges are linked to some measure of signal synchronisation among pairs of channels.

fMRI is by far the most commonly used imaging technique for brain connectivity analysis, with its main advantage being its excellent spatial resolution and possibility to investigate deep brain structures. However, the application of fMRI to postural control experimental designs is limited by several drawbacks. Most importantly, fMRI requires the subject to lay still for the whole duration of the acquisition, making it impossible to perform natural, realistic balance or motion tasks, thus limiting the possible analysis to motor imagery task, i.e., a mental projection of the real task (Bhatt et al., 2018; Ferraye et al., 2014; Taube et al., 2015). Secondly, the fMRI low temporal resolution does not allow the quick brain dynamics and pattern reconfigurations that happen at the millisecond scale to be captured. Lastly, fMRI is a costly technology. In postural control studies, EEG represents a better alternative, which allows most of these

limitations to be overcome. The flexibility and portability of the instrumentations allows for the performance of more realistic postural tasks, while its high time resolution makes it the ideal tool to investigate dynamic changes in the brain network. EEG instrumentation is also considerably cheaper and widely accessible in both research and clinical set-ups. However, when it comes to scalp EEG-based brain network analysis, there are certain limitations that need to be considered, namely: the low spatial resolution of EEG and the problem of volume conduction effect. The latter in particular poses a major limitation to the reliability of the network reconstruction process. Because of the electrical properties of the different head tissues and the way the electrical signals spreads from the cortical neuronal sources to the surrounding tissues, the signal recorded at each scalp electrode reflects not only the activity of the cortical source directly underneath it, but rather a mix of electrical potentials originated from widespread sources. Therefore, when trying to derive the network structure from scalp EEG signal, there is a chance that the connectivity measured between a pair of channels is in fact the result of signal contamination, rather than a reflection of real functional connection between the two areas. In order to perform a reliable network analysis exploiting the flexibility, high temporal resolution and low cost of EEG while overcoming the discussed limitations, (Hassan and Wendling, 2018a) developed the EEG source connectivity method. The main idea of the proposed approach is to derive the network structure not from the scalp time-series, but from reconstructed cortical time-series (scouts).

The goal is to move from the scalp level (electrodes space) to the cortical level (source space). The electrode space consists of the set of coordinates that identifies the spatial location of each EEG electrode. This can be a standardised 3D map of the EEG cap provided by the manufacturer or subject-specific set of coordinates. The source space represents the brain

cortex, where the signal is generated at a neuronal level. This can be defined using a default MRI-based segmented template or a subject-specific MRI scan. In case of subject-specific MRI scan, the image needs to be segmented to identify different anatomical areas and characterise the electrical properties of each tissue. In this work, a standard template was used since it has been shown that, for healthy adult subjects, there is no significant difference in the final result compared to using a subject-specific head model (Douw et al., 2018). Differences between the two can only be observed in case of older or pathological subjects presenting brain lesions, atrophy, structural alterations, etc. which was not the case for the examined cohort.

Starting from non-invasive scalp recordings, the EEG source connectivity technique estimates functional connectivity networks at the level of brain sources. The process consists of two main steps:

1) Reconstruction of the brain sources
2) Estimation of source connectivity

Therefore, the two main choices to make are: *which algorithm to use to solve the inverse problem* and *which method to use to estimate functional connectivity.*

### 3.2.3a Source reconstruction

The first step of EEG source connectivity is reconstruction of cortical sources. This consists in the solution of an ill-posed inverse problem, where a large number of source time-series *S(t)* is estimated from a limited number of scalp signals *X(t)*, using a current dipole model of the head and appropriate constraints to limit the number of solutions. The current dipole model is used to simulate the way electrical neuronal activity propagates through the head tissues up

to the scalp and the constraints applied to the problem are based on physiological (spatial and temporal) and mathematical properties of the sources, and on regularisation assumptions (Grech et al., 2008; Hallez et al., 2007).

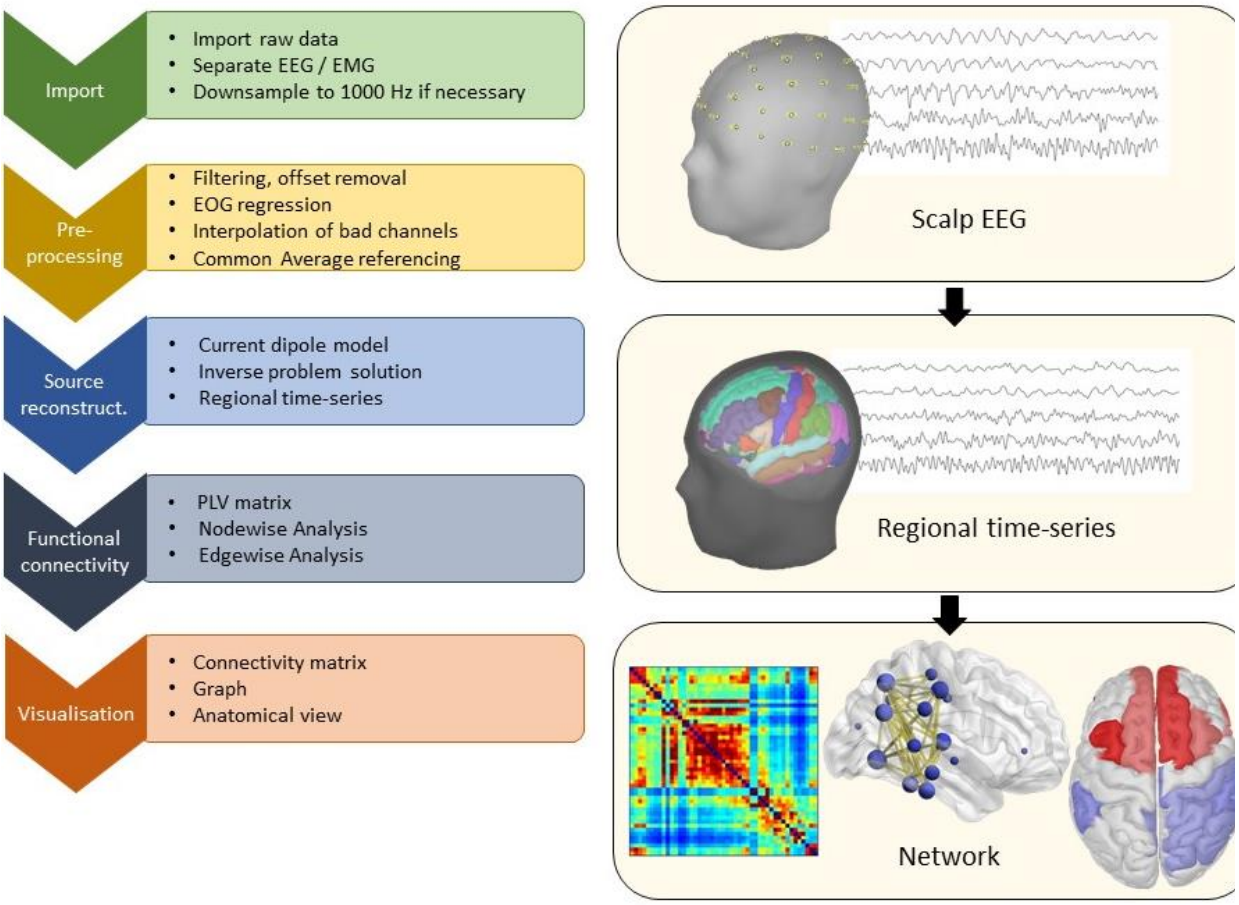


**Figure 3.7.** Schematic representation of the EEG data processing pipeline for brain connectivity analysis. Data are first imported and pre-processed. Then, a head model is used to solve the inverse problem and reconstruct the cortical sources from which the regional time-series are extracted thanks to an anatomical atlas that parcellates the cortex into ROIs. Finally, the network is computed by determining the connectivity among regional time-series and the results are visualised as a connectivity matrix, a graph, or an anatomical map.

Once an equivalent current dipole model has been defined, the scalp EEG signal recorded on *M* channels can be expressed as the linear combination of *P* time-varying current dipole sources as:

$$X(t) = G \cdot S(t) + N(t)$$

*G* is the so-called lead-field matrix (dimension *[M,P]*) , that weighs the contribution of each source towards the recorded signal, *S(t)* is the source time-series matrix and *N(t)* is additive noise. The assumption of linearity of the model comes from the quasi-static approximation, described by Maxwell's equations (Baillet et al., 2001b). The lead-field matrix *G* results from the dipole head-model, which takes into account the anatomical and electrical characteristic of the problem domain (head), modeling the electrical propagation of the current dipole sources located on the cortex through the different head tissues and their resulting projection on the scalp. There are several ways to formulate this model, with varying degrees of anatomical approximation, ranging from a simple sphere to realistic head models. A different number of layers can also be used to describe a corresponding number of tissues (e.g., brain, skull, scalp). Then, different computational techniques are available to solve the set of equations that characterise the model, most notably: the Boundary Element Method (BEM) and Finite Element Method (FEM).

Each model is characterised by:

- The spatial classification of the domain: each voxel of the original MRI image is associated with a specific tissue
- Source localisation: dipolar sources are assigned at the boundary between grey and white matter to mimic the physiology of pyramidal cell neurons

- Electrical characterisation of the different tissues, to account for their different conductivity.

The work presented in Chapter 4 is based on a 3-layer BEM model (Brain, Skull, Scalp) based on a morphological head model template provided by Brainstorm (Tadel et al., 2011).

The objective of the inverse problem is to obtain an estimate $\hat{S}(t)$ of the unknown sources $S(t)$. The problem is ill-posed, as the number of sources to estimate is much larger than the available scalp signals. In order to solve it, we need assumptions on spatial and temporal properties of

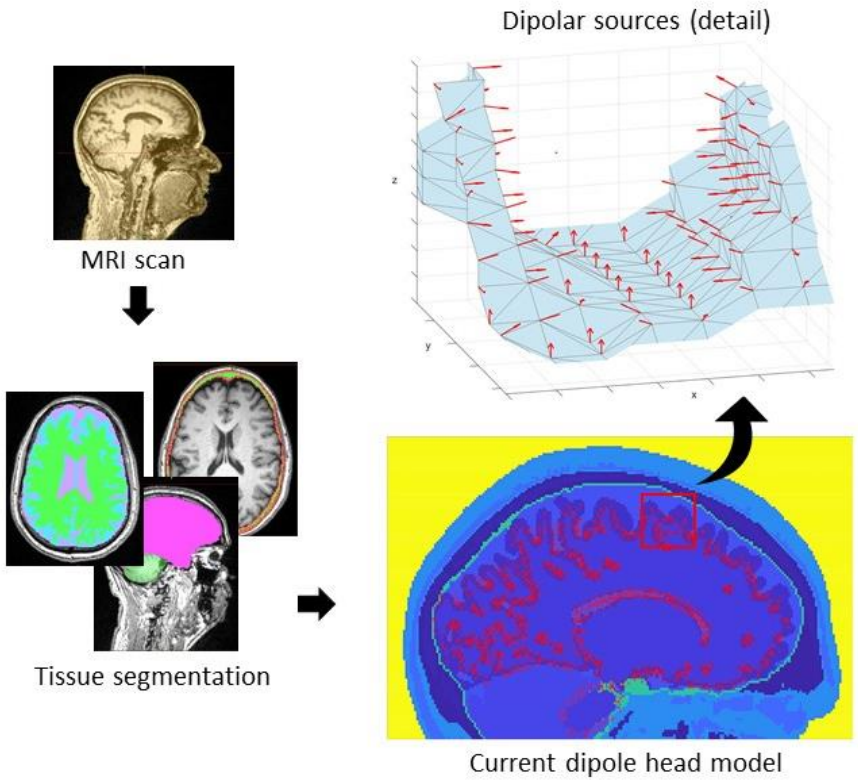


**Figure 3.8.** Schematic representation of the head model used in the source reconstruction process. The original anatomical MRI (or a template) is segmented to identify different head tissues. Each tissue is then associated with its specific conductivity value. Neuronal sources are represented through current dipoles placed at the boundary between grey and white matter, perpendicularly to the cortex surface, as displayed in the zoomed-in cortical sulcus in the top-right detail panel.

the sources and regularisation constraints. In particular, the sources need to describe the physiological properties of the pyramidal cell neurons they are modeling, in terms of their position, dipole orientation, and amplitude of the current they generate. For this reason sources are defined on the mesh that defines the cortical boundary, they are oriented to be normal to the mesh and the dipole current density is defined within a physiological range of 0-40$\mu$V (Malmivuo and Plonsey, 1995). The used model contained 1500 dipolar sources.

Once the model has been properly defined and the lead field matrix G generated, the aim of the inverse problem is to determine the source estimate $\hat{S}(t) = W^T \cdot X(t)$ by computing the inverse solution matrix (or inverse operator) *W*, which contains the spatial filter weights.

Several algorithms are available to solve the inverse problem, the Brainstorm toolbox implements four of the most commonly used:

- wMNE: weighted Minimum Norm Estimated
- SPM: dynamical Statistical Parametric Mapping
- sLORETA: standardised Low Resolution Brain Electromagnetic Tomography
- cMEM: standard Maximum Entropy on the Mean

In the work presented in this thesis, wMNE was used. One of the advantages of using this method is that no spatial a-priori is required, which makes it suitable for this work, where no prior hypothesis existed on the cortical region weights. wMNE is an inverse solution method that addresses the ill-posed nature of the problem (*P>>M*) through regularisation. In particular, it estimates the sources by choosing, among the several possible solutions, the one with the minimum power in a least-square-error sense. The inverse solution matrix and the source estimate are determined as follows.

Given

$$X = G \cdot S + N$$

and defined an inverse operator W such that the source estimate can be written as:

$$\hat{S} = W^T \cdot X$$

wMNE will try to find a solution which is a trade-off between the quality of the fit to the data $\|X - G \cdot \hat{S}\|^2$ and the regularity of the estimate $\lambda^2 \|\hat{S}\|^2$

$$\hat{S}(t) = \underset{S}{\operatorname{argmin}}\{\|Q^{-1/2}(X - GS)\|^2 + \lambda^2 \|R^{-1/2} S\|^2\}$$

Where:

$$Q = cov(N) \quad ; \quad R = cov(S)$$

And $\lambda$ is the Tykhonov regularisation coefficient.

*W* can then be computed as:

$$W = RG^T(GRG^T + \lambda^2 Q)^{-1}$$

In the traditional, unweighted MNE *R = I*. The introduction of a diagonal weighting matrix *R* (with values inversely proportional to the norm of the lead-field matrix *G*), allows compensation for the tendency to favour sources closer to the surface and result in a more accurate source reconstruction. The output of the inverse problem is ultimately the matrix *Ŝ(t)*, which contains the estimate of 1500 source time-series.

A further step towards the network definition is then necessary. Dealing with such a high number of sources at the network level, with one node per source, would not be practical. For this reason, we want to move from the source space to the regional space, made up of a more limited number of regions of interest (ROIs), in which source time-series are clustered together and averaged into regional scouts according to an anatomical atlas. To do so, the first step is the anatomical parcellation of the brain into ROIs according to a reference atlas. In the present work the Desikan-Killiany anatomical atlas was employed (Desikan et al., 2006b). This cortical atlas parcellates the brain into 68 regions based on the morphology of sulci and gyri. By averaging together, the estimated source time series within each regional boundary the regional time series matrix is obtained, thus reducing the complexity from 1500 sources to 68 cortical regions. Once the scouts (ROIs time-series) have been obtained, connectivity can be computed between pairs of signals.

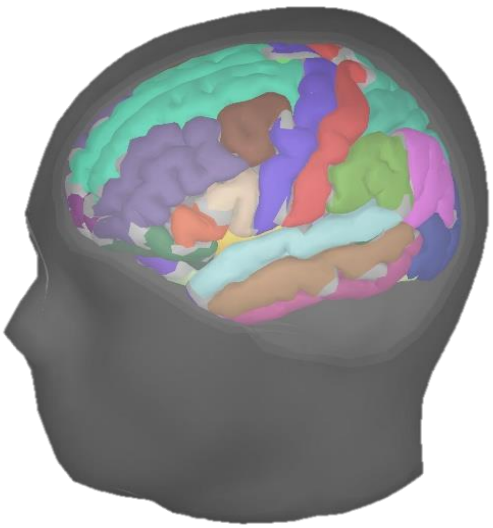

**Figure 3.9.** Desikan-Killiany anatomical atlas for the parcellation of human cortex into 68 regions, based on the anatomy of sulci and gyri.

### 3.2.3b Brain connectivity

Brain connectivity can refer to different aspects of brain organization. Therefore there are several types of measures that provide descriptions of different brain characteristics. Connectivity can be weighted (values distributed within a certain range) or binary (0 or 1). It can be directed (causality) or undirected, and can focus on the physical-anatomical structure of the brain or on the statistical relationships between brain signals from different areas. The three main levels of brain connectivity are:

- Structural: focuses on the physical pathways, by describing the anatomical connections between different areas of the brain (Binary, undirected).
- Functional: focuses on the statistical relationships between distributed cortical areas, i.e., determines metrics of statistical dependence (Weighted, Undirected).
- Effective: allows the determination of the causality of the relationship between two areas. It can combine statistical coupling of the signals with anatomical information on the brain physical structure (Weighted, Directed).

This work is focused on functional connectivity, which is more suitable for whole-brain investigation since it does not require a spatial a-priori.

Several functional connectivity measures are available as a way to determine the statistical coupling of two signals. The most commonly used belong to three families of methods (Wendling et al., 2009):

- Regression (linear or non-linear): e.g., Cross-correlation coefficient ($r^2$) and Nonlinear correlation coefficient ($h^2$) respectively

- Mutual information (*MI*)
- Phase synchronisation: e.g., Phase locking value (*PLV*)

In this work, the latter was used. In particular, the adopted connectivity metrics was the phase locking value (PLV) which, given two signals *x* and *y*, can be described as:

$$PLV_{xy} = \left|\langle e^{i|\varphi_x(t)-\varphi_y(t)|}\rangle\right|$$

Where *φx(t)* and *φy(t)* are the phases of signals x and y computed with the Hilbert transform in a specific frequency band. The PLV value is determined as the phase difference computed for each time-point and averaged over time, expressed as a complex unit-length vector

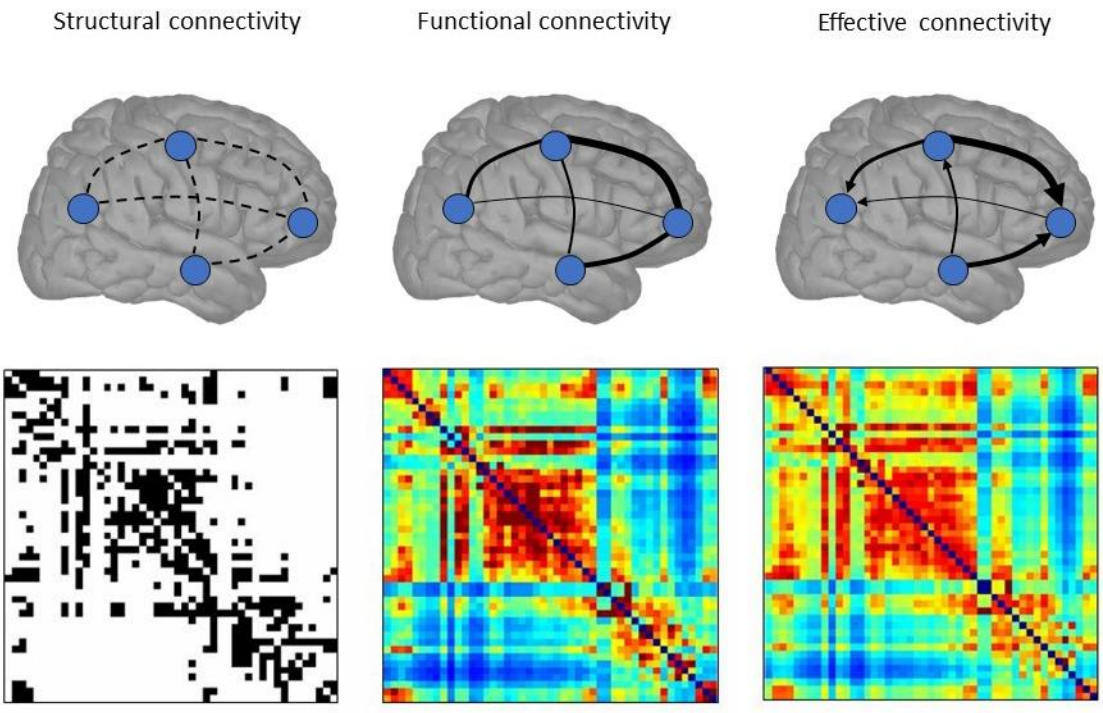


**Figure 3.10.** The three main types of brain connectivity. Structural: characterised by a binary connectivity matrix (0 = no connection, 1 = connection). Functional: weighted connectivity values between pairs of nodes but no directionality. Effective: weighted connectivity values and directed

(Lachaux et al., 1999; Mormann et al., 2000). PLV is a metric of synchronisation of neural activity and can assume values between 0 (independence) and 1 (strong coupling of the signals phases).

Once the PLV values have been computed for each couple of ROIs, they provide an estimated measure of pairwise association between nodes, thereby defining the network itself. PLV values are organized in a symmetric matrix (dimension *[N,N]*, with *N=68*, number of ROIs) which represent the network: each row/column pair *N(i,j)* stores the unique association measure between nodes $N_i$ and $N_j$ . The terms “connectivity matrix”, “adjacency matrix”, “PLV matrix” and “network matrix” can be used interchangeably to indicate this structure.

The computational choices regarding the use of wMNE for source reconstruction and PLV as a connectivity metric is based on previous literature. (Hassan et al., 2017) evaluated the performances of several combinations of inverse solution algorithms and connectivity metrics, using simulated EEG data as well as real intracerebral EEG recordings from epileptic patients. Specifically, dSPM, wMNE, sLORETA and cMEM inverse solution algorithms were tested in combination with: $r^2$, $h^2$, *MI* and *PLV* metrics. It was shown that the combination of wMNE and PLV was the one which allowed to obtain a better match between reconstructed network and real data.

### 3.2.4 Network Analysis

#### *3.2.4a Static Analysis: Nodewise and Edgewise*

The goal of network analysis is to quantitatively describe network properties, both from a local (single nodes) and global (connections) point of view. The term static refers to the fact that this kind of analysis does not take into account the network dynamic over time (how the network

changes over the experimental epochs) but is only focused on determining the network characteristics in a given experimental condition (baseline, task, open/ closed eyes).

Here, we focus on three major properties of the network and the corresponding quantitative measures that describe them, among the many options available on *Brain Network Toolbox* (Rubinov and Sporns, 2010).

| NETWORK PROPERTY | MEASURE |
|---|---|
| Hubness | Strength |
| Integration | Participation coefficient |
| Segregation | Clustering coefficient |

Hubness is a local property associated with individual nodes. A node is considered a hub of the network if it comes with a high number of connections. Hub nodes have a key role within the network topography, their removal would significantly alter the integrity of the network structure itself. On the contrary, nodes with “low hubness”, are peripheral and isolated nodes which are only involved with a low number of connections; therefore, their removal would not significantly alter the overall network topography. The easiest and most intuitive way of quantifying the hubness of a node is by computing its degree, which simply consists in the number of connections (edges) associated to that specific node. If the network’s edges are weighted, the degree can be replaced with a more informative measure: the node’s strength. This is the sum of the weights of all the edges related to that specific node.

One key aspect of the brain functional connectome is the balance between network integration and segregation (Cohen and D'Esposito, 2016). On one hand, the brain needs to organise itself to create efficient structural and functional pathways that enable the integration of a large number of incoming stimuli, the elaboration of this vast amount of information and the planning of the next action. This is particularly true in the execution of a postural control task where visual, proprioceptive, and somatosensory stimuli are processed by the brain to develop and actuate a corrective strategy that counteracts the environmental disturbances in order to preserve the subject's equilibrium and upright stance. On the other hand, the brain must also be capable of segregating different kinds of information into distinct modules for specialised local computations. It has indeed been shown that functional brain networks present a 'modular' topography, which is the tendency to arrange themselves into modules (sub-networks also known as communities) of highly interconnected nodes only sparsely connected to the rest of the network (Kabbara et al., 2020a). In graph theory, two of the measures that better describe this modular structure, highlighting the integration and segregation properties of the network, are the nodes' participation index and clustering index, respectively. The participation index provides a measure of how much a node is connected within its module. The index is 0 if the node is isolated, with its edges distributed uniquely among other nodes of its module. It gets closer to 1 if the node's edges are equally distributed all over the network. The clustering index is the fraction of the node's neighbours that are neighbors of each other. It offers a measure of the density of connections surrounding the node and its tendency to create a cluster.

The extraction of node-related quantitative measures to compare among subjects or experimental conditions in order to highlight patterns of brain network reconfiguration, is

usually referred to as node-wise analysis. Another approach, the so-called edgewise analysis, focuses instead on the connectivity values of the network edges themselves to investigate how the network topography changes over time or following a task. The way these analyses are conducted from a statistical point of view is discussed in section 3.5 of this Chapter.

#### *3.2.4b Dynamic Analysis: sequential modularity and flexibility*

Dynamic network analysis sets out to characterise how the brain network topography evolves over time during the experimental trial. An essential requirement to conduct a dynamic analysis is the computation of networks (connectivity matrices) over several sequential epochs of the original time-series, as depicted in Figure 3.11.

Modularity refers to a characteristic displayed by networks, which allows the identification of special relationships among groups of nodes. Networks can be split up into modules (or communities), which are groups of nodes that are strongly intraconnected and weakly interconnected with the rest of the network (Bassett and Sporns, 2017; Bullmore and Sporns, 2009; Sporns and Betzel, 2016). The identification of such modules allows for the description of the so-called modular brain states, i.e., the main modular structures that characterise a brain network at a certain point in time. This, in turn, is a reflection of the cortical areas which are working in close cooperation at a particular point of a certain task, which provides insight on the kind of cognitive process which is dominating the cortical network at that moment. By applying this principle to dynamic networks computed over several sequential time epochs, it is possible to discriminate between the separate cognitive process that occur during the execution of a task. The potentiality of this approach was shown in (Kabbara et al., 2019), where the sequential modularity algorithm reported here was used to highlight the network related to the different cognitive stages involved in a simple object naming task. From the onset

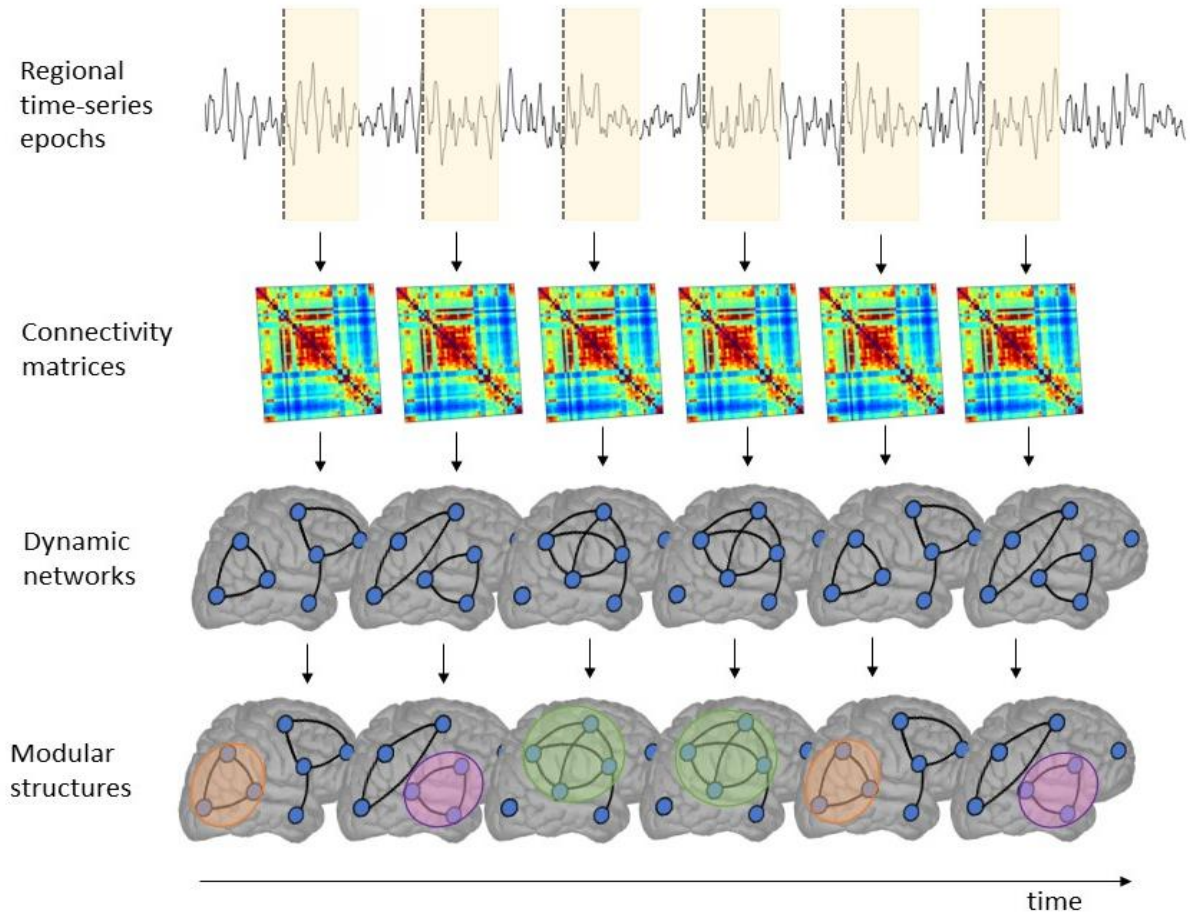


**Figure 3.11.** Schematic representation of the dynamic network analysis process. Connectivity matrices and the associated networks are computed for each epoch of the reconstructed regional time-series. The modular structures within each epoch´s network are then identified.

of the stimulus (presentation of the picture of an object) to the execution of the task (saying the name of the object out loud), the sequential modularity algorithm was able to identify the networks corresponding to all the stages of the cognitive process: visual processing, memory access, categorisation, and articulation.

It was of great interest to translate this approach to postural control tasks investigating the cortical dynamics that regulate the response to an induced perturbation of balance and coordinate the counteraction to prevent falling.

The sequential modularity algorithm, which allows each network to be decomposed into modules, relies on the Louvain method (Blondel et al., 2008) and proposes an iterative approach to overcome the degeneracy problem (repeated calls of modularity algorithms produce different results)(Bassett et al., 2013). The main steps of the algorithm are:

- The Louvain algorithm is called iteratively 200 times
- When first called, Louvain arranges the PLV matrices of each epoch along the diagonal of a single connectivity super-matrix *B* (dimension [#nodes x #epochs, #nodes x #epochs]). All the other values are set to 0 and a fake connectivity of 1 is set on the diagonals that identify the same nodes in different epochs (see figure 3.12).

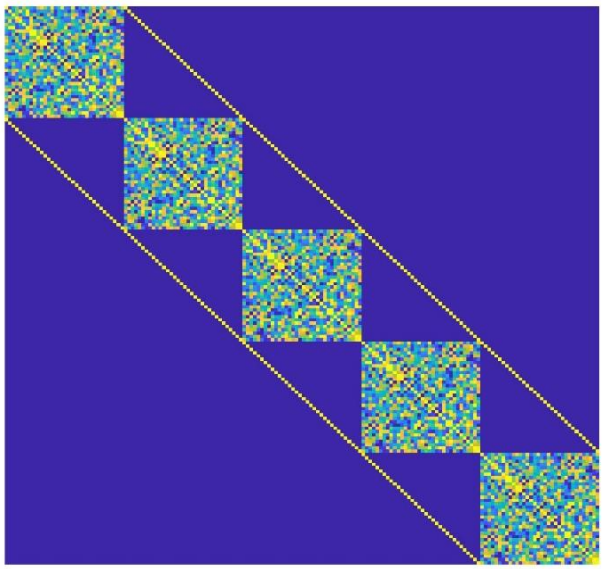

**Figure 3.12.** Organisation of the sequential connectivity matrices during the execution of Louvain algorithm. The connectivity matrices from each epoch are arranged along the diagonal of a super-matrix B. A ‘fake’ connectivity value of 1 is set for the same node across the time epochs.

Louvain is an iterative algorithm itself, which tries to maximise the modularity function *Q*, defined as:

$$Q = \frac{1}{2m}\sum_{ij}\left[A_{ij} - \frac{k_i k_j}{2m}\right]\delta(c_i, c_j)$$

where $A_{ij}$ represents the connectivity value between nodes *i* and *j*, $k_i$ and $k_j$ are their respective strengths and *m* is the sum of all the weighted edges. The terms $c_i$ and $c_j$ are the respective communities of the nodes *i* and *j,* and the delta function is δ = 1 only if the nodes belong to the same community ($c_i = c_j$), it is equal to 0 otherwise. The modularity function *Q* basically provides a ratio between the strength of intra-module connections and the total network connections. The algorithm iterates until *Q* keeps growing, the stop criterion is an increase $< 10^{-10}$ over the previous iteration.

- In the first iteration, each of the [#nodes x #epochs] "nodes" of the super-matrix *B* are considered as an individual unitary module. The modularity value *Q* in this configuration will then be 0. In the following iterative steps neighbouring nodes are progressively clustered together until the modularity value *Q* keeps increasing.
- Each call of the Louvain algorithm could potentially provide a different modular configuration. For this reason, the algorithm is invoked 200 times, generating 200 possible modular configurations.
- To determine the final configuration, the results from the 200 runs are passed to the consensus algorithm. This algorithm creates an association matrix ([#nodes x #nodes]) by computing the number of times each node is assigned to the same module throughout the runs. Then a "null model" of the association matrix is created from a random permutation of the original partitions. The computed association matrix is finally

compared with the null model and only the significant modules are retained (Bassett et al., 2013).

At this point the modular structure of the network has been identified for each epoch. This provides useful information on the dynamic evolution of the network and allows quantitative dynamic parameters such as flexibility to be extracted. The flexibility of a node is defined as the number of times the node changes its affiliation from one module to another over time. This reflects the degree to which certain cortical areas can cooperate and be involved in different cortical pathways. This also indicates how a subject's network is able to reconfigure itself in the wake of an external stimulus or a change of state. Literature has linked the highly flexible dynamic changes in modular organisation with enhanced cognitive and working memory performance, more effective learning strategies and an overall increased ability to adapt to external tasks (Bassett et al., 2011; Braun et al., 2015; Yin et al., 2020). In this study, the flexibility index of the examined cohort was correlated to a metric of postural performance (sample entropy of the body sway) to investigate the possible link between the ability of the cortical network to flexibly reconfigure itself and the level of postural control performance, as well as identify which cortical regions were more involved in the process. This will be discussed in more detail in Chapter 5.

A further step of the sequential modularity analysis consists in determining the similarities among the modular organisation at adjacent time segments and identifying the so-called modular states. The similarity between temporal modular structures is assessed using z-score of Rand coefficient (Kabbara et al., 2020b; Traud et al., 2008). The output is a similarity matrix that, ideally, would show a block pattern along the diagonal, which reflects higher similarity values among adjacent time epochs (see figure 3.13). Similar modular structures are then

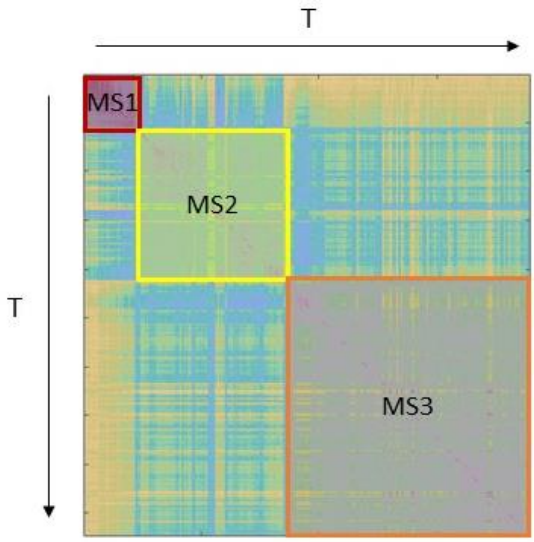


**Figure 3.13.** Example of a similarity matrix, containing the rand coefficient (metric of similarity) between pairs of time epochs (in rows and columns). In this example three modular states were identified among sequential epochs and highlighted along the diagonal of the matrix.

clustered together into modular states (MS) using the consensus modularity, similarly to what is done to identify single epochs modules.

This further step of the sequential modularity was tried on the dataset analysed in Chapter 5 in order to verify whether it was possible to identify modular states that could be associated with the stages of adaptation and habituation of the postural control task, thus providing them with a cortical network characterisation. The analysis, however, was inconclusive as it did not provide any positive result in terms of a meaningful similarity matrix that would allow modular states to be defined. Therefore, this last section of analysis is not included in the work presented in Chapter 5.

## 3.3 EMG Analysis

### 3.3.1 Preprocessing

Surface EMG data for the assessment of electrical activity of the lower limbs muscles were acquired using a common bipolar configuration provided by the ANTneuro mysport system that was also used to simultaneously record the 64-channel EEG signal.

The sEMG recording session followed the SENIAM (Surface ElectroMyography for the Non-Invasive Assessment of Muscles) guidelines for subject preparation and electrode placement. First, the optimal electrode placement location was identified on each muscle of interest, thanks to a simple clinical test described in the SENIAM guidelines. The test consisted in a simple exercise where the muscle of interest was flexed in a specific posture, allowing the lab operator to easily feel the muscle belly and consequently measure the exact electrode position relative to specific anatomical landmarks (e.g., to identify the gastrocnemious muscle's belly the test required a plantar flexion from a prone position with knee extended and the electrode placement location was determined at 1/3 of the line between head of the fibula and heel).

Once the muscle belly was identified, the skin was prepared by shaving the area and cleansing with rubbing alcohol in order to remove as much oil and flaky skin layers that reduce the impedance at the electrode interface. Finally, two Ag/AgCl electrodes were placed at an inter-electrode distance (IDE) of 1-2 cm on the muscle, following the direction of the muscle fibres to increase the selectivity of the recording. A reference electrode was also connected to a non-active bone area (patella).

The preprocessing of the raw sEMG signal was performed in Matlab and included the following steps:

- A zero-phase band-pass Butterworth filter between 20-250 Hz was applied to the data (Roeder 2020)
- Power-line noise removal was performed with a notch filter at 50Hz
- sEMG signal was then rectified using the Hilbert transform (Boonstra and Breakspear, 2012; Murnaghan et al., 2014).
- Finally, the data was segmented into 1s long epochs according to the trigger marking the offset of each vibratory stimulation.

### 3.3.2 Cortico-muscular coherence

The PSD of the EMG signal was then computed from the pre-processed data using the Welch's periodogram method, which has been previously discussed in this chapter in relation to EEG. The PSD of EEG and EMG signals was used to compute the cortico-muscular coherence (CMC).

CMC is a measure of functional connectivity between cortex and muscles (Liu et al., 2019) which highlights the similarity in the frequency content of the two signals and assumes values between 0 (no correlation) and 1 (identical signals). Existing literature indicates the presence of coherent oscillatory patterns between the electrical signal of the motor-somatosensory cortex and that of the contralateral muscles in the beta band (specifically around 20Hz). This would reflect the suggested engagement between cortex and muscles both in terms of cortical drive (cortex to muscle, reflected in the coherence with motor cortex signal) and feedback

afferent pathways (muscles to cortex, reflected in the coherence with somatosensory cortex) (Baker, 2007; Jacobs et al., 2015; Liu et al., 2019).

Given an EEG signal (x) and an EMG signal (y), CMC is a function of frequency which can be derived as follows:

$$C_{xy}(f) = \frac{|P_{xy}(f)|^2}{P_{xx}(f)P_{yy}(f)}$$

Where $P_{xy}$ is the cross-spectral density between the two signals (Fourier transform of the cross-correlation), $P_{xx}$ is the auto-spectral density (i.e., PSD) of the EEG signal and $P_{yy}$ is the PSD of the EMG signal.

The CMC signal was computed in beta band [13-30Hz] between pairs of EEG channels and leg muscles (60 EEG channels x 10 sEMG). Differences in CMC values between baseline and task signals were inspected using a cluster-based permutation test.

## 3.4 Posturography Analysis

Posturography is a non-invasive and widely-used method for the assessment of one's balance. Subjects are asked to stand on a force platform (or force plate) which detects their body sway in a quiet stance condition (static posturography), during the execution of a balance task or following the delivery of external perturbations (dynamic posturography). By detecting the ground reaction forces and torques exerted between the subject's feet and the force platform in their three-dimensional components, it is possible to identify the centre of pressure (COP), i.e., the point of application of the resultant ground reaction force vector. The projection of the COP in the 2D plane of the force platform results in a stabilogram plot which comprises the

anterior-posterior (AP) and medial-lateral (ML) components of the body sway or COP trajectory.

Before plotting the stabilogram, both the AP and ML components of the COP trajectory were filtered with a bi-directional bandpass Butterworth filter between 0.2-20Hz (Zhou et al., 2016a). The signals were then normalised by unit variance, dividing them by their standard deviation (Donker et al., 2007a).

A common metric that can be extracted from the posturography data is the sway path length (SPL). Given a COP trajectory comprising N time-points, SPL can be computed as:

$$SPL = \sum_{i=1}^{N} \sqrt{(AP_{i+1} - AP_i)^2 + (ML_{i+1} - ML_i)^2}$$

By dividing SPL by the total trial time, the sway mean velocity (MV) is obtained. Traditional posturographic measures also include the mean distance from the average COP, and the confidence ellipse area (area of the ellipse that encloses 95% of the COP trajectory points) (Prieto et al., 1996).

In postural control analysis, a relevant feature of the sway signal is the complexity of the signal, which describes the “structural richness” of the data and reflects the postural performance of the subject, being related to his/her ability to dynamically react and adapt to postural perturbations (Busa et al., 2016; Zhou et al., 2016a). An index to quantify complexity is the sample entropy ($S_{EN}$), which expresses the probability that neighbouring points in the time-series will be within a certain range, i.e., how regular (low $S_{EN}$) or complex (high $S_{EN}$) the signal

is. In other words, $S_{EN}$ describes how similar and predictable the point-to-point fluctuations of the signal are. Given a signal comprising N time-points, its sample entropy is defined as:

$$S_{EN} = -\ln \frac{\phi_{m+1}(r)}{\phi_m(r)}$$

Where $\phi_m(r)$ is the probability that points of the time-series at distance m are within the radius of similarity r. Typical recommended values of distance ad similarity radius are m = 2 and r = 15% (Costa et al., 2002a).

## 3.5 Statistical Analysis

The studies presented in the following chapters included single-group repeated measures under pairs of experimental conditions (namely baseline - task and open - closed eyes). Comparisons of summary single values averaged among the cohort such as ASP in a specific channel and frequency band or Node strength were compared using paired t-test, particularly in its non-parametric version (Wilcoxon test) and corrected for multiple comparisons with False discovery rate. Network-related statistics, aimed at comparing structural differences at the edges level, were carried out using a type of cluster-based permutation test specifically developed for network analysis (Zalesky et al., 2010). A spatial cluster-based permutation test was also used to infer significant differences in the CMC signal before and during the postural task. This paragraph will illustrate the principles of the main statistical techniques used in the thesis.

### 3.5.1 Wilcoxon test

The paired Student's t-test is a parametric test which enables pairwise comparisons between two groups of samples extracted from the same population under two experimental conditions (e.g. before and after a treatment). Specifically, the aim of the test is to determine whether there is a statistically significant difference between the means of the two groups, or if the means of the two distributions are equal.

As a parametric test it is based on the assumptions that the data are the result of random sampling and are representative of the population, and that they are (approximately) normally distributed. Further assumptions can also be made on the variance of data: this can be assumed to be equal (homoscedastic) or different between the two groups (heteroscedastic).

The t-test is one of the most commonly used tests for hypothesis testing. Given two groups of data samples, the null hypothesis states that there is no difference between the means of the two distributions.

This can be expressed as:

$$H_0 : \quad \mu_1 - \mu_2 = 0 \ ,$$

where $\mu_1$ and $\mu_2$ are the true population means.

A t-score is determined as:

$$t = \frac{\overline{\mu_1} - \overline{\mu_2}}{\sqrt{\frac{s^2{}_1}{n_1} + \frac{s^2{}_2}{n_2}}}$$

where $\bar{\mu}_1$ and $\bar{\mu}_2$ are the mean values of the two groups, $\boldsymbol{s_1}$ and $\boldsymbol{s_2}$ are their standard deviations, $\boldsymbol{n_1}$ and $\boldsymbol{n_2}$ are the number of samples in each group.

The t-score is compared to the t statistic and a p-value is determined as the probability of observing equal or more extreme realisations of the obtained t-score. If this probability (p-value) is smaller than a set significance level (usually $\alpha = 0.05$) the null hypothesis $H_0$ can be rejected, therefore concluding (with a 95% confidence, for $\alpha = 0.05$) that there is a statistically significant difference in the means of the two distributions from which the groups were sampled.

The Wilcoxon signed rank test is a non-parametric version of the paired t-test, which does not assume the normality of the data (Wilcoxon, 1945). Given two groups of N samples each, the null hypothesis $H_0$ is equivalent to the one formulated for the paired t-test, i.e.: the difference of the means is 0. The steps for the test are as follows:

- For each pair of samples compute the absolute difference $|\mathrm{x_A} - \mathrm{x_B}|$ and the sign $\mathrm{sign}(\mathrm{x_A} - \mathrm{x_B})$
- Differences equal to 0 are removed and the dimension reduced to $N_r$
- The absolute values of paired differences are then ranked from the smallest to the largest
- The rank of negative differences is multiplied by -1. In case of tied differences, the rank is averaged between the two (i.e., if ranks 3 and 4 have the same observed difference, they are both assigned rank 3.5)
- The test statistic W is computed as:

$$W = \sum_{i=1}^{N_r} [sgn(x_A - x_B) * R_i]$$

- where $R_i$ is the rank of the $i^{th}$ pair of samples.
- This value is then compared to the W distributions, which is centred around 0 and is defined for a specific significance value ($\alpha = 0.05$) and sample size $N_r$. If W is lower than a critical value, then the null hypothesis can be rejected.

$$|\mathrm{W}| < \mathrm{W}_{crit(\alpha=0.05,\mathrm{N_r})} \implies \mathrm{H}_0 \text{ rejected}$$

### 3.5.2 Multiple comparison correction

Simultaneously performing repeated statistical tests, testing a hypothesis at a certain significance level, increases the probability of getting significant results simply due to chance and thus incurring a Type I error, where the null hypothesis is erroneously rejected (Shaffer, 1995). This is known as the multiple comparison problem (MCP). To account for this problem several multiple comparison correction methods are available.

The easiest is the Bonferroni correction (Bonferroni, 1935), which simply divides the significance level by the number of comparisons performed. Therefore, if the original $\alpha = 0.05$ and the test is repeated N = 50 times, the corrected significance value will be:

$$\alpha_{Bonferroni} = {}^{\alpha}/_{N} = 0{,}001$$

Bonferroni controls the family-wise error rate (FWER), i.e., the probability of making at least one Type I error at all. However, this correction tends to be too conservative for most real

applications, as it makes rejecting the null hypothesis extremely hard and could lead to a high rate of false negatives (type II errors) and thus missed findings.

A common alternative to Bonferroni is the False Discovery Rate (FDR) correction method. While FWER is the probability of making at least 1 type I error at all, FDR is the expected proportion of Type I errors among the rejected hypotheses. Controlling for FDR is therefore less stringent than Bonferroni and other FWER methods.

The FDR method proposed in (Benjamini and Hochberg, 1995) adjusts uncorrected p-values in a way that limits the number of false positives that are reported as significant, i.e. increasing them.

- p-values are ordered from smallest to largest and ranked
- the largest adjusted p-value is the same as the largest p-value: $p_{FDR,N} = p_N$
- the next largest adjusted p-value is defined as:

$$p_{FDR,N-1} = \min\left(p_{FDR,N} \;,\; p_{N-1} \cdot \frac{\mathrm{N}}{\mathrm{R_{N-1}}}\right)$$

where $\mathrm{R_{N-1}}$ is the rank of the current p-value.

The adjusted p-values can then be compared to the chosen significance level (e.g., $\alpha = 0.05$) to decide whether to reject ($p_{FDR} < \alpha$) or accept ($p_{FDR} > \alpha$) the null hypothesis.

### 3.5.3 Cluster-based permutation test

Cluster based permutation test is a type of statistical testing aimed specifically at tackling the multiple comparison problem in electrophysiological data. It is a non-parametric, iterative test

that uses clustering to introduce biophysically motivated constraints to the data (Maris and Oostenveld, 2007). This test is particularly suitable to infer the differences in electrophysiological signals, which requires a high number of individual tests: one per time-point when comparing data time-series, one per frequency bin when comparing spectral signals or one per channel when comparing two scalp topologies. The MCP is dealt with using clustering, with the base assumption being that if significant physiological differences are present in the data, they tend to be persistent in samples that are adjacent in time (or frequency or space). For the sake of simplicity, the main steps of the cluster-based permutation test are reported here for time-series. The same principle applies also when time-points are replaced by frequency bins or spatially distributed electrodes. The following procedure is detailed in (Maris and Oostenveld, 2007) and is implemented in Matlab in the FieldTrip toolbox (Oostenveld et al., 2011):

- The chosen statistical test (e.g., Wilcoxon) is performed between pairs of samples (from the two experimental conditions) at every single time point, obtaining a large number of sequential t-statistics values.
- A threshold is set (usually T = 0.05) and used to determine clusters of adjacent t-statistics values which are greater than the threshold.
- The t-statistic values are summed within each cluster, and the one with the highest value is retained. This is the cluster-based t-statistic $t_0$
- To evaluate the significance of $t_0$ , an iterative permutation test is then used
- For every iteration (usually N>1000), samples are randomly shuffled between the two groups, creating a random partition

- The clustering procedure is performed on the random partition to extract a t-statistic $t_{\mathrm{i}}$ (i = [1,N])
- The t-statistic values are obtained from random partitions during each iteration to form a distribution
- The original t-statistic $t_0$ is then compared to the randomly generated t-distribution to extract a p-value If the probability of a randomly generated t-statistics to be greater than the observed value $t_0$ is less than 5%, then the null hypothesis can be rejected for the cluster, as a significant difference has been identified.

When this procedure is applied with spatial clustering (as in the statistical analysis of CMC in Chapter 6), the 3D coordinates of the electrodes need to be provided to determine their spatial location and the neighbouring relationship among each other. This way clusters are not determined based on sequential time-points (or frequency bins), but on neighbouring, contiguous groups of electrodes.

### 3.5.4 Network Statistical Analysis

Brain network analysis is based on the representation of the brain as a graph, where regions (nodes) are connected by structural or functional links (edges or connections). Difference in topological properties of the brain network and its organisation can reflect physiological difference between a control group and subjects affected by specific conditions (attention deficit, schizophrenia, depression, etc.), as well as intra-subject differences under different experimental condition. In particular, brain network analysis provides the opportunity to identify changes in functional connection associated with specific tasks, experimental conditions or effects of interest. The statistics involved in Brain network analysis depends on the nature of

the experimental effect of interest and on the type of network analysis performed. The two complementary approaches to network analysis presented in this work are Nodewise and Edgewise, which require independent statistical considerations.

**Nodewise:**

When the interest lies in describing the network's topological organisation at the level of single nodes, measures of topological organisation can be extracted and statistical inference can be done on these quantities. In this case 68 comparison between pairs of values related to the same node under different experimental conditions performed with Wilcoxon t-test. Then the resulting p-values were corrected for multiple comparison with FDR.

**Edgewise:**

When the goal is to investigate differences in the network structure at the level of individual connectivity values, the same hypothesis needs to be tested independently at each and every network edge (edgewise analysis). A main concern in doing so, though, is represented by the huge number of multiple comparisons that need to be performed. Indeed, the statistical process involved in this kind of analysis results in a mass-univariate testing of the hypothesis, which requires a correction for Family-wise errors rate (FWER). Such a great number of comparisons, in fact, poses a problem with regards to the statistical power of the test.

NBS is a statistical method first presented in (Zalesky et al., 2010) which was developed specifically for performing statistical analysis on large networks. It provides a more powerful alternative compared to standard multiple-comparison correction methods such as the False Discovery Rate (FDR) one, which focuses on rejecting the null hypothesis at the level of the single connections while controlling the false discovery rate (rate of false positive connections).

NBS is a nonparametric statistical test, which controls the family-wise error rate (FWER) in the case where the family is made up of the edges that form the network. Its strength in doing so, is that it allows FWER to be controlled while identifying distributed networks spanning multiple connections, rejecting the null hypothesis at the whole network level. Its working principle is analogue to cluster-based permutation tests: the clustering takes place in the network space (sets of connections/edges) and the FWER-corrected p-value associated with each connection results from a permutation testing. The test can be implemented using the NBS Connectome Matlab package.

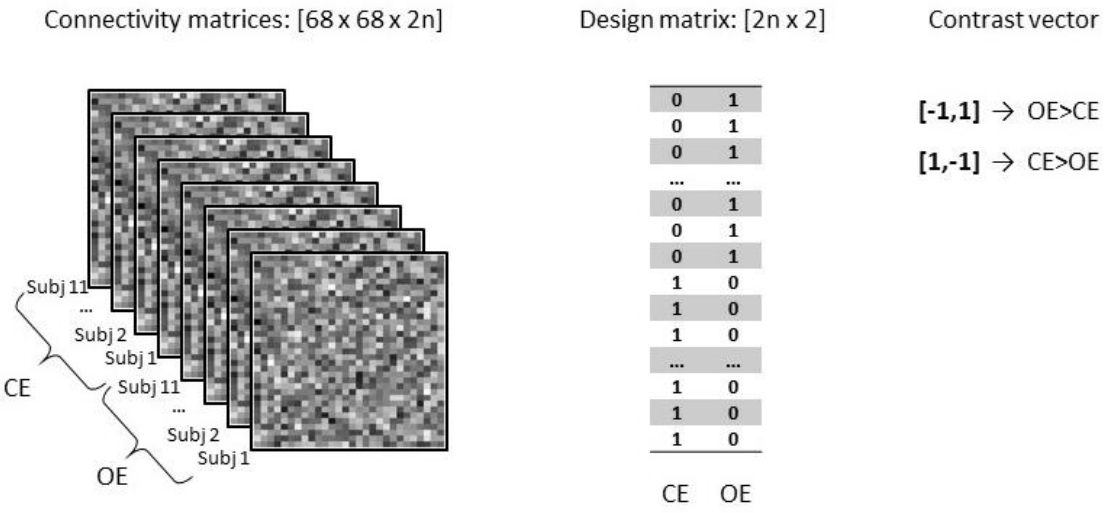


**Figure 3.14.** Schematic representation of the inputs for the NBS algorithm. The connectivity matrices are arranged in a 3D matrix that contains all the repetitions for the two conditions that are being tested. The design matrix specifies the order of the conditions, and the contrast vector determines the type of comparison.

NBS receives as an input the connectivity matrices that represent the graph/ network model, as well as the statistical model that will be fitted to the connections, defined in terms of the General Linear Model (GLM) with a design matrix and a contrast vector, as depicted in Figure 3.14.

The statistical process is as follows:

First, the hypothesis is independently tested on each individual connection, which is associated with a unique test statistic value. Secondly, a subset of edges (for which the null hypothesis could potentially be rejected) is defined by applying a threshold to the test statistic value. Then, a clustering in the topological space allows to identify clusters of connected edges. The assumption at the base of NBS, in fact, is that these clusters well represent the topological configuration associated with the effect of interest, i.e., connections for which the null hypothesis can be rejected are not isolated but arranged in an interconnected configuration. Finally, these steps are repeated several thousands of times, in a permutation testing which is used to compute FWER-connected p-values for each cluster. The basic assumption behind permutation testing is that, in the case of a paired t-test between samples A and B, the random shuffling of samples from A and B will have no effect on the test statistic if the null hypothesis is true. On the other hand, if the null hypothesis is false, this would not be the case. For each permutation, after testing the individual edges and thresholding, the size of the largest identified cluster (set of connected edges) is saved and used to create an empirical null distribution. Based on this distribution, the FWER-corrected p-value of the identified cluster is computed. The output is provided as a set of connections comprising the network which is found to show a significant effect.

# 4. Postural Control Adaptation and Habituation During Proprioceptive stimulation: an HD-EEG investigation of cortical recruitment and kinematics

The content of this Chapter was published in April 2020 in '*IEEE Transactions on Neural Systems and Rehabilitation Engineering'* (Barollo et al., 2020). DOI:10.1109/TNSRE.2020.2988585

**Abstract**— The objective of the present work is to measure postural kinematics and power spectral variation from HD-EEG to assess changes in cortical activity during adaptation and habituation to postural perturbation. To evoke proprioceptive postural perturbation, vibratory stimulation at 85 Hz was applied to the calf muscles of 33 subjects over four 75-second stimulation periods. Stimulation was performed according to a pseudorandom binary sequence. Vibratory impulses were synchronized to high-density electroencephalography (HD-EEG, 256 channels). Changes in absolute spectral power (ASP) were analysed over four frequency bands (Δ: 0.5-3.5 Hz; θ: 3.5-7.5 Hz; α: 7.5-12.5 Hz; β: 12.5-30 Hz). A force platform recorded torque actuated by the feet, and normalised sway path length (SPL) was computed as a construct for postural performance during each period. SPL values indicated improvement in postural performance over the trial periods. Significant variation in absolute power values (ASP) was found in assessing postural adaptation: an increase in θ band ASP in the frontal-central region for closed-eyes trials, an increase in θ and β band ASP in the parietal region for open-eyes trials. In habituation, no significant variations in ASP were observed during closed-eyes trials, whereas an increase in θ, α, and β band ASP was observed with open eyes. Furthermore, open-eyed trials generally yielded a greater number of significant ASP differences across all bands during both adaptation and habituation, suggesting that following cortical activity during postural perturbation may be up-regulated with the availability of visual feedback. These results altogether provide deeper insight into pathological postural control

failure by exploring the dynamic changes in both cortical activity and postural kinematics during adaptation and habituation to proprioceptive postural perturbation.

**Index Terms**— Balance, cerebral cortex, HD-EEG, kinematics, postural control, power spectral density

## 4.1 Introduction

Human posture is a complex and naturally unstable physiological process that requires the continuous integration of compensatory mechanisms to maintain an equilibrium condition of upright stance (Horak, 2006; Shumway-Cook and Horak, 1986). Collectively defined as 'postural control' (Fransson, 2005), this process is dynamically mediated by regulatory feedback elicited from somatosensory, vestibular, and visual systems (Winters and Crago, 2000). Exogenous disruption or nonspecific stimulation of these systems can induce postural sway (Diener et al., 1984; Goh et al., 2017) – the magnitude and latency of which characterise the kinematics of postural control, which can be assessed by changes in force and torque actuated at the support surface of the feet, altogether known as posturography (Cohen, 1961; Galvão et al., 2018; Hu and Woollacott, 1994). Postural control measurement is often employed under conditional balance perturbation, which is typically achieved via visual disturbance or proprioceptive stimulation (Edmunds et al., 2019). Extant research in this regard cites postural control as a fundamental 'learned' motor skill, whose function and efficiency can be systematically improved with routine postural tasks (Galvão et al., 2018) or directed training (Pollock et al., 2000). From these studies, two dimensions of postural learning have been posited: 'adaptation', defined as transient improvements in motor response to upright balance perturbation (Welch and Ting, 2014), and 'habituation', conversely defined by a gradual decrease in response to repeated perturbation (Eccles, 1986).

While the response of sensorimotor systems during postural adaptation and habituation has been well-established in literature (Bolton and Misiaszek, 2012; Honeycutt and Richard Nichols, 2010) interrogating the commensurate role of the cerebral cortex or subcortical central nervous system (CNS) structures is a comparatively recent subject of research. In this regard, literature has extended previous knowledge on subcortical balance maintenance (Magnus, 1926; Sherrington, 1910) to consider the potential governing role of supratentorial information processing in the cerebral cortex (Hülsdünker et al., 2015; Jacobs and Horak, 2007; Mierau et al., 2017b). The neuroimaging method of electroencephalography (EEG) has been cited for its high temporal resolution in measuring cortical activity (Adkin et al., 2008; Goh et al., 2017; Mochizuki et al., 2010). In postural control research, balance perturbation has revealed scalp-level activity changes in frontal-central and frontal-parietal cortical regions, specifically within α (7.5–12.5 Hz) and θ (3.5–7.5 Hz) frequency ranges (Hülsdünker et al., 2015; Sipp et al., 2013). Additional EEG studies report bursts of γ activity (30–80 Hz) during voluntarily anterior-posterior movements (Eccles, 1986). EEG activity in this regard is reported as changes in evoked time-domain event-related potentials (ERP) or as perturbation-evoked responses (PERs), e.g. N1 amplitudes and Contingent Negative Variations (CNV) (Fransson, 2005; Fujiwara et al., 2012; Goh et al., 2017; Jacobs and Horak, 2007).

While recent evidence for the critical role of the cerebral cortex in governing postural adaptation and habituation has been reported (Edmunds et al., 2019), to our knowledge, cortical activity assessment during balance perturbation has never been synchronized with kinematic posturography measurements. In addition, no postural control studies report the use of ‘high-density’, 256-channel EEG (HD-EEG) – a methodology with superior spatial resolution to more conventional 32- or 64-channel systems. Furthermore, power spectral variation analysis from EEG data remains underreported in postural control research, despite its being a conventional

method for EEG signal analysis with proven utility in cognitive and motor task studies (Hülsdünker et al., 2016, 2015). The present study aims to extend current research in this regard with the synchronized assessment of postural kinematics with power spectral variation analyses from HD-EEG to quantify changes in cortical activity during adaptation and habituation to postural perturbations using vibratory proprioceptive stimulation.

## 4.2 Materials and Methods

### 4.2.1 Experimental Set-up

As noted, the present experimental setup aimed at integrating posturography measurement with the assessment of cortical activity by 256-channel HD-EEG during vibratory proprioceptive stimulation. The study was reviewed and approved by the National Bioethics Committee (Vísindasiðanefnd - reference number: VSN-063) and the measurements were performed at the Icelandic Centre for Neurophysiology at Reykjavik University. Thirty-three healthy volunteers (10 females and 23 males, aged 21 to 52) participated in the study. These subjects had no history of vertigo, central nervous disease, or lower extremity injury, and none of the subjects had consumed alcohol within a 24-hour period prior to their measurement. Figure 4.1 illustrates the overall experimental set-up for the present work, as presented at the XV Mediterranean Conference on Medical and Biological Engineering and Computing – MEDICON 2019 (Friðriksdóttir et al., 2020). Participants were instructed to maintain an upright stance during exogenous balance perturbation, evoked by the simultaneous stimulation of vibrators fastened tightly by elastic straps around the widest point of each calf.

The vibrators were designed using revolving DC-motors equipped with a 3.5 gram eccentric weight, which was contained in a cylindrical casing approximately 6 cm in length and 1 cm in

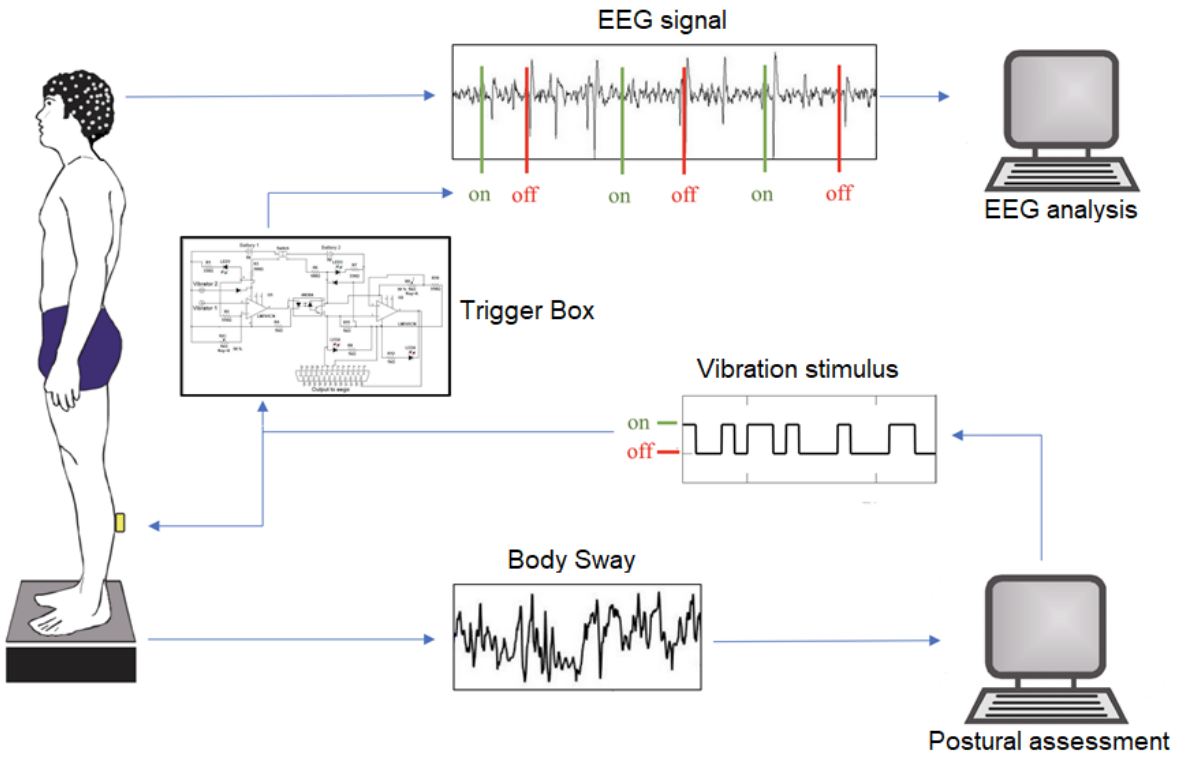


**Figure 4.1.** Experimental setup

diameter. Each stimulation was set to deliver vibrations of 0.1 cm in amplitude, at a frequency of 85 Hz. Stimulation was applied according to a pseudorandom binary sequence schedule (PRBS), where each shift had a random duration of 1 to 6.6 seconds.

### 4.2.2 Posturography measurement

In general, maintaining a normative eased upright stance requires the symmetric distribution of body weight; when challenged, the resultant anterior-posterior or bilateral compensatory motion can be captured using a force platform to record changes in the body's centre of pressure (Carlsöö, 1972; Harro et al., 2016). For the present work, this assessment was achieved using a customised platform system developed at the Department of Solid Mechanics, Lund Institute of Technology in Sweden (Fransson, 2005). Anterior-posterior (ant-post) and lateral (Lat) forces actuated by the feet were recorded at six degrees of freedom with

an accuracy of 0.5 N; these data were sampled at 50 Hz by a custom-made program, Postcon™, on a computer equipped with an analogue-to-digital converter. Participants were instructed to stand on a pressure plate with their arms downwardly relaxed and their feet positioned at an angle of approximately 30 degrees, open to the front, with their heels approximately three centimeters apart. Participants were asked to focus on a fixed marker point in front of them, at about 150 cm distance.

### 4.2.3 HD-EEG data acquisitions

HD-EEG data were acquired using a 256-channel Ag/AgCl wet-electrode cap connected in bipolar configuration to four cascaded 64-channel amplifiers; data collection employed a standardised 10-20 system montage with EEGO software (ANT neuro, Enschede Netherlands). An additional infra-orbital electrode was used to identify any obfuscating electrooculographic (EOG) signals, and EEG data were continuously recorded at a sampling frequency of 1024 Hz. To synchronize EEG acquisition with posturography data, a custom trigger signal box was built to rectify each vibratory stimuli as a 5V TTL timing signal sent to the master amplifier. This trigger system allowed for the generation of vibratory on/off event timestamps at <1ms latency during EEG recordings. As our previous research has identified changes in cortical activity according to the availability of visual feedback, two measurement trials were performed for each subject, beginning with open eyes (OE) and followed by closed eyes (CE). An initial quiet stance (QS) baseline phase (30 seconds) preceded each stimulation phase (300 seconds), resulting in a total duration of 330 seconds for each recording. Each stimulation phase was further subdivided into four 75-second recording periods: P1, P2, P3, and P4.

## 4.3 Data Analysis

### 4.3.1 Assessing postural performances

Force platform data for both OE and CE datasets were analogously segmented into five recording periods (QS, P1, P2, P3, and P4) in order to facilitate the synchronisation of postural sway data with any evoked changes in cortical activity. The normalised Sway Path Length (SPL) was computed to describe the overall postural performance of the subjects during each period.

The centre of pressure (COP) trajectory coincides with the vertical projection on platform plane of the subject's centre of mass and it is widely used in human posture studies to assess body sway (Schubert et al., 2012; Winter, 2009). Torque values were extracted from the collected force platform data and used to derive ant-post and lat displacement during each trial. A graphical representation of the COP trajectory ('statokinesigram') was then obtained by plotting the displacement along the ant-post and lat axes over time, see Figure 4.2. Sway Path Length is one of several posturographic parameters that can be extracted from a postural platform and is one of the most commonly used (Yamamoto et al., 2015). Nevertheless, previous research has established the sensitivity of these indices to different anthropometric characteristics – particularly height and weight, where taller or heavier people appear to be more unstable (Chiari et al., 2002). As such, SPL values were normalised to each subject's height and weight to estimate the COP trajectory on the platform according to the following formula:

$$Stabilogram_k(t) = \frac{\tau}{(0.56 \cdot h_k) \cdot (m_k \cdot 9.81)}$$

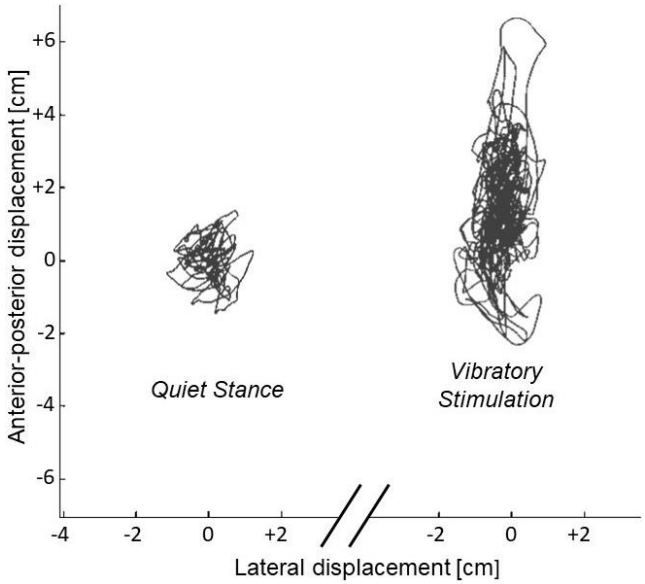


**Figure 4.2.** Statokinesigram showing an example subject's body sway. Left: no stimulation applied. Right: randomized vibratory stimulation applied on the calves to disrupt upright stance. Anterior-posterior and lateral displacements are expressed in cm.

Where k refers to the individual participant, $0.56 \cdot h_k$ is an estimate of the centre of mass's (COM) radial distance to the platform (Davidovits, 2019) and $m_k \cdot 9.81$ is the weight applied to the participant's COM.

### 4.3.2 HD-EEG data preprocessing

Raw HD-EEG data were pre-processed using the EEGLAB Toolbox (Delorme and Makeig, 2004), first with a band-pass filter set between 0.5–80 Hz, followed by a notch filter (49.5–50.5Hz) to remove AC power line interference from each period. Three approaches to artifact rejection were performed: channel interpolation, automatic continuous artifact rejection, and principal component analysis (PCA). All channels were re-referenced to a common average.

To investigate variations in cortical activity between periods, absolute spectral power (ASP) values were obtained using fast Fourier transformation (FFT) analysis at a resolution of 0.977 Hz with a 10% Hanning window. This analysis was performed for four frequency bands: Δ (0.5-

3.5 Hz), θ (3.5-7.5 Hz), α (7.5-12.5 Hz) and β (12.5-30 Hz). This analysis generated ASP values for each frequency band and period, which were extracted and exported for statistical analyses using a customised Matlab GUI (MathWorks, Inc., Natick, 158 Massachusetts, USA). From this analysis, topological maps illustrating OE and CE difference spectra were extracted for each EEG frequency band. In addition, significant changes in mean ASP at each electrode were assessed using paired heteroscedastic t-tests, which yielded topological p-value maps for each EEG waveform (with $p<0.05$ the threshold for significance). False discovery rate (FDR) and Bonferroni significance correction methods were employed and compared to address the statistical problem of multiple comparisons. Channels that resisted these multiple comparison correction methods were specifically marked in significance topologies.

## 4.4 Results

### 4.4.1 SPL data distribution to assess adaptation and habituation periods

When describing time-varying phenomena, a distinction must be made between true adaptation resulting from control dynamic alterations and other time-dependent phenomena, such as fatigue or biomechanical alterations resultant from changes in balance conditions

**Table 4.1.** Normalized Sway Path Length (SPL), means, and standard deviations by experimental epoch and OE/CE condition.

| | QS | | P1 | | P2 | | P3 | | P4 | |
|---|---|---|---|---|---|---|---|---|---|---|
| Eyes | Open | Closed | Open | Closed | Open | Closed | Open | Closed | Open | Closed |
| Mean | 0.3038 | 0.4408 | 1.3624 | 1.8584 | 1.2190 | 1.7276 | 1.2312 | 1.7229 | 1.2574 | 1.6655 |
| SD | 0.0821 | 0.1392 | 0.2810 | 0.5130 | 0.2389 | 0.4447 | 0.2285 | 0.4204 | 0.2422 | 0.4285 |

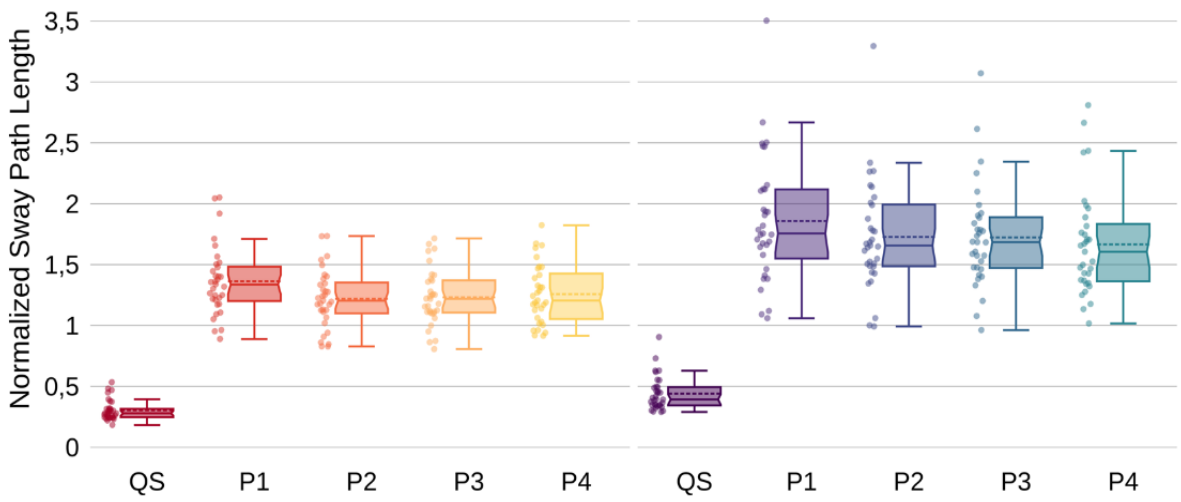


**Figure 4.3.** Normalized Sway Path Length. Left: Open Eyes; Right: Closed Eyes.

(Fransson, 2005). Because of this, we aimed to use SPL results to observe whether postural performance decreased over any of the experimental periods; with both OE and CE conditions, minimum postural sway has been reported to occur at around 150-200 seconds following incident stimuli (Edmunds et al., 2019; Fransson, 2005). Table 4.1 shows the means and standard deviations of the normalised SPL values for the present cohort, across each of the experimental periods and conditions. Figure 4.3 represents the SPL data distribution with box plots to highlight median, mean and outlier values for each period. From these results, SPL did increase in Period 4 (P4) for OE trials but remained comparatively stable over all four periods for CE trials. To avoid any potential obfuscation from fatigue or other time- dependent variations, we therefore used the difference between Period 3 (P3) and Period 1 (P1) ASP values in our assessment of habituation.

### 4.4.2 Absolute power spectra variation from HD-EEG

Figures 4.4 to 4.6 show the results from statistical analyses performed across every channel. Each of the different coloured regions defines a topological map of statistical significance

(p<0.05) corrected for multiple comparisons in accordance with the following conditions: uncorrected paired t-test (yellow), FDR correction (orange), and Bonferroni correction (red). Channels that remained significant following FDR correction are highlighted with a black 'X', while electrodes that resisted Bonferroni correction are indicated by a blue '*'. White regions are considered non-significant (p>0.05). In the second row, topographical maps of changes in ASP are shown solely for areas that presented a statistically significant difference between the examined periods.

**Adaptation:**

As previously mentioned, postural adaptation is shown using normalised ASP differences between P1 and QS, and figures 4.4 and 4.5 depict cortical maps of channels showing significant changes in CE and OE conditions, respectively. These results show an increase in ASP for both conditions, with many more significant regions present from OE trials. Generally,

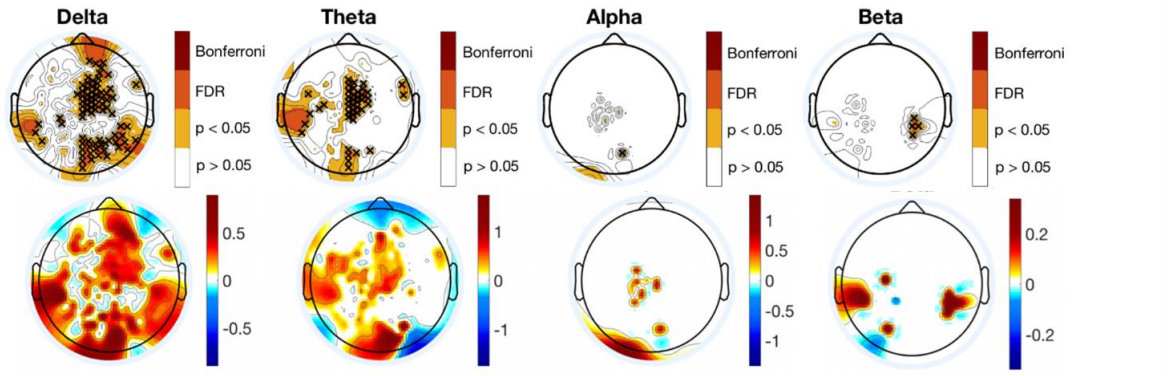


**Figure 4.4.** Adaptation CE. Top row: statistical analysis results. Each colored region identifies topological areas that achieved statistical significance (p<0.05) given the following conditions: uncorrected paired t-test (yellow), FDR correction (orange), and Bonferroni correction (red). Individual electrodes that resisted FDR correction are indicated by a black 'X'. Bottom row: Topographies highlighting the average changes in ASP (between P1 and QS periods) over the whole cohort.

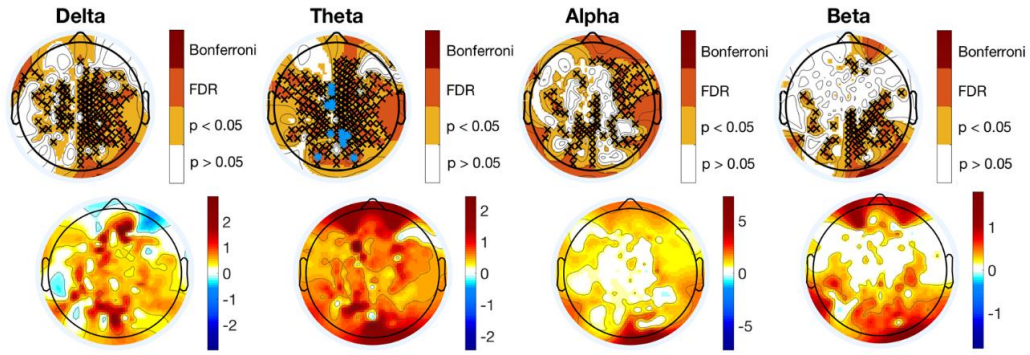


**Figure 4.5.** Adaptation OE. Top row: statistical analysis results. Each colored region identifies topological areas that achieved statistical significance ($p<0.05$) given the following conditions: uncorrected paired t-test (yellow), FDR correction (orange), and Bonferroni correction (red). Individual electrodes that resisted FDR correction are indicated by a black 'X', while electrodes that resisted Bonferroni correction are indicated by a blue '*'. Bottom row: Topographies highlighting the average changes in ASP (between P1 and QS periods) over the whole cohort

ASP in the θ band increased in adaptation – particularly in the frontal-central region ($p<0.05$, FDR corrected) during CE and the parietal region ($p<0.05$, FDR corrected) during OE, where ten electrodes passed the Bonferroni correction test. During OE trials, higher frequency bands (α and β) show significant activity as well. In particular, figure 4.5 shows increased activity in the parietal-occipital region in the β band.

**Habituation:**

Postural habituation is shown using normalised ASP differences between P3 and P1. Figure 4.6 depicts the cortical mapping of grand mean changes in ASP solely in channels shown to have a significant difference between periods ($p<0.05$). White areas are again considered non-significant. The overall results show an increase of ASP in P3 compared to P1 for OE trials, whereas during the CE periods, no significant changes occurred. OE results specifically indicate increased activity in the θ band (temporal region), α band (parietal region), and β band (frontal region).

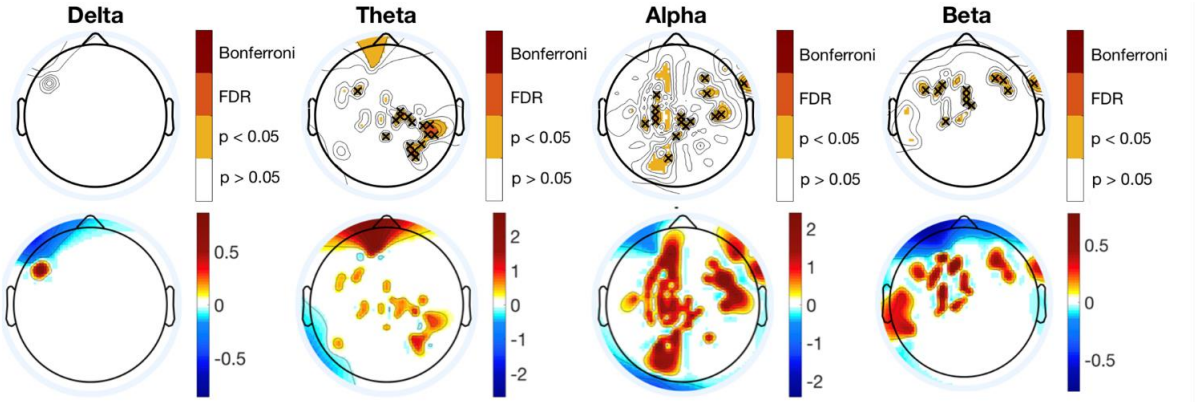


**Figure 4.6.** Habituation OE. Top row: statistical analysis results. Each colored region identifies topological areas that achieved statistical significance ($p<0.05$) given the following conditions: uncorrected paired t-test (yellow), FDR correction (orange), and Bonferroni correction (red). Individual electrodes that resisted FDR correction are indicated by a black 'X'. Bottom row: Topographies highlighting the average changes in ASP (between P3 and P1 periods) over the whole cohort.

## 4.5 Discussion

Power spectral variation analysis from EEG data remains underreported in postural control literature. The present study aimed to extend current research with the synchronized assessment of postural kinematics with power spectral variation analyses from HD-EEG to quantify changes in cortical activity during adaptation and habituation during a postural control task using vibratory proprioceptive stimulation.

Postural sway was recorded to obtain normalised SPL values over five experimental periods, which were then utilised to classify postural adaptation and postural habituation as differences in ASP between specific recording periods. In this regard, adaptation was defined as the difference between P1 and QS periods, in accordance with extant postural perturbation literature (Edmunds et al., 2019; Fransson, 2005; Welch and Ting, 2014). However, normalised

SPL was used to define postural habituation, where P1 ASP values were subtracted from the period with the lowest mean SPL to avoid the influence of time-dependent variations such as fatigue.

There are two main limitations to note from this methodology. Firstly, while it remains possible that the onset of habituation or fatigue may differ subject-to-subject, previous studies have shown that ant-post and lat torque variations during OE and CE trials reach a consistent minimum around 150-200 seconds following incident stimuli, corresponding with P3 in the present work (Edmunds et al., 2019; Fransson, 2005). Nevertheless, further investigation into quantitative indicators for the measurement of cortical habituation is recommended. Another methodological limitation arises from demonstrating the relationship between ASP and SPL. In this regard, we investigated whether there was any linear correlation between ASP and SPL or other metrics derived from COP trajectory, such as the root-mean-square (RMS) of excursion in the ant-post direction. In all of these comparisons, no meaningful correlation was found, suggesting the future importance of considering alternative metrics for postural performance, such as approximate entropy or multiscale entropy, which has shown promise in linking modifications in neural involvement to responses to vibration (Zhou et al., 2016b).

Significant ASP differences were found across the entirety of the cortex in α and θ bands, with the exception of the prefrontal area which yielded minimal significance in the α band. Power in the θ band has been shown to increase in adaptation – particularly in the frontal-central region during CE trials and the parietal area during OE trials (Hülsdünker et al., 2015; Mierau et al., 2017a; Sipp et al., 2013). Here, our results are in accordance with the recent work by (Solis-Escalante et al., 2019a), who showed significant midline ASP differences in both CE and OE conditions as evidenced by the differential modulations of α and low-γ rhythms. This altogether

suggests that central region ASP increases during high-demand postural correction, such as balance maintenance without allowing corrective foot placement, as performed in the present study.

Furthermore, it has been suggested that increase in θ activity in the frontal-central regions is involved in error detection and processing of postural stability during balance control (Adkin et al., 2008; Slobounov et al., 2009). As such, the θ band ASP differences shown here may signify the planning of corrective steps and/or the analysis of falling consequences, as indicated by our previous work on cortical functional dynamics during postural control. Relatedly, significant ASP differences in the α band may reflect an inhibition of error detection within the cingulate cortex due to habituation (Edmunds et al., 2019).

The present results indicate that OE trials reflect a greater number of significant differences in ASP across all bands during both adaptation and habituation. This suggests that following both acute and prolonged proprioceptive perturbation, cortical activity may be up-regulated with the availability of visual feedback. These results generally support our prior hypothesis that the visual recognition of instability may play a critical role in governing cortical processes requisite for postural control (Edmunds et al., 2019). This hypothesis resulted from previous work demonstrating that all-type visual impairment is associated with an increased risk for injurious falling (Saftari and Kwon, 2018; Zetterlund et al., 2019). However, in addition to the impact of vision, it is also important to note that postural control may be driven by brain network interactions rather than isolated changes in cortical activity at specific regions. Our present results support the potential importance of network dynamics, as significant differences in ASP were concurrently measured across many different cortical regions. In this context, we believe that further work investigating the reconfiguration of cortical networks during adaptation and

habituation could reveal new insights about how functionally coordinated brain activity may dictate postural control. Such a model could include source-space or connectivity-based analyses, as we have previously illustrated using lower density EEG (Edmunds et al., 2019). Furthermore, since the examined measures of postural performance (SPL and RMS) were not able to highlight a significant correlation between kinematics and cortical recruitment, a deeper investigation based on different postural parameters would be a fruitful area for further work.

## 4.6 Conclusions

Dynamic posturography is an established method for evaluating postural control. By delivering controlled disruption in the form of calf vibration, we can examine central nervous system (CNS) processing by associating body inertia and changes in upright stance (Johansson et al., 2009). This notion is true for simple upright stance but does not apply to complex postural tasks or pathological conditions, such as compensatory action during motion sickness, postural control failure from unilateral vestibular loss (UVL) (Peterka et al., 2011) or cerebellar stroke (Manor et al., 2010). In these complex postural conditions, incident adaptive and habituative processes are activated within the CNS to ensure the maintenance of upright posture and normative gait. Adding HD-EEG to dynamic posturography measurement enables the commensurate measurement of CNS activity and dynamic postural kinematics during adaptation and habituation to key postural control tasks. This invokes a deeper emphasis on the importance of further investigation into the adaptive and habitual processes implicated in CNS response to disease (i.e. UVL, cerebral and/or cerebellar diseases), which would provide key insight towards the identification of compensatory targets for clinical intervention.

# 5. Cortical pathways during Postural Control: new insights from functional EEG source connectivity

The content of this Chapter was published in January 2022 in '*IEEE Transactions on Neural Systems and Rehabilitation Engineering'* (Barollo et al., 2022). DOI: 10.1109/TNSRE.2022.3140888

**Abstract—** Postural control is a complex feedback system that relies on vast array of sensory inputs in order to maintain a stable upright stance. The brain cortex plays a crucial role in the processing of this information and in the elaboration of a successful adaptive strategy to external stimulation preventing loss of balance and falls. In the present work, the participants postural control system was challenged by disrupting the upright stance via a mechanical skeletal muscle vibration applied to the calves. The EEG source connectivity method was used to investigate the cortical response to the external stimulation and highlight the brain network primarily involved in high-level coordination of the postural control system. The cortical network reconfiguration was assessed during two experimental conditions of eyes open and eyes closed and the network flexibility (i.e. its dynamic reconfiguration over time) was correlated with the sample entropy of the stabilogram sway. The results highlight two different cortical strategies in the alpha band: the predominance of frontal lobe connections during open eyes and the strengthening of temporal-parietal network connections in the absence of visual cues. Furthermore, a high correlation emerges between the flexibility in the regions surrounding the right temporo-parietal junction and the sample entropy of the COP sway, suggesting their centrality in the postural control system. These results open the possibility to employ network-based flexibility metrics as markers of a healthy postural control system, with implications in the diagnosis and treatment of postural impairing diseases.

**Index Terms—** Brain Network Connectivity, EEG, Postural Control

## 5.1 Introduction

Emerging evidence has shown that the human brain is a network whose functions depend on the complex and dynamic interaction of highly specialised and spatially segregated regions (Fornito et al., 2016). Network neuroscience is a fairly new research field that employs graph theory techniques to assess brain functionalities and quantify the reconfiguration of neural pathways in response to tasks, stimuli, drugs administration, and treatments. The overwhelming complexity of the brain, which consists (on the micro-scale) of about $10^{12}$ neurons connected through $10^{15}$ synapsis (Johnston and Wu, 1995), is abstracted (at the macro-scale) into a graph where nodes represent brain regions and edges represent their interconnections. In doing so, network neuroscience provides a powerful set of tools to quantify and investigate the intricate interactions that govern every brain function. Indeed, the insights it provides into the dynamic reconfiguration of connections between cortical regions is fundamental in understanding the deeply integrative functions of the brain, overcoming the limited view of a 'functional localisation', where each segregated region attends to a specific function.

Postural control is a primary example of a complex system, in which the Central Nervous System (CNS) coordinates and elaborates a vast array of signals, from visual cues to spatial orientation information from the vestibular system, to proprioceptive and somatosensory feedback from muscles and sensory organs (Mergner et al., 2003). Furthermore, the body of literature has shown how postural control is deeply related to structural and functional characteristics of the brain (Sullivan et al., 2009). The relationship between postural control and cognitive functions has been extensively documented, highlighting in particular the effect of aging on brain plasticity and the consequent change in high-level strategies of postural

control (Lin et al., 2017; Ozdemir et al., 2016). The complexity of the cortical interactions that govern this process makes network neuroscience methodologies valuable tools, although yet relatively unexplored, to investigate the role of the brain in postural control. Functional connectivity has been previously employed in literature to infer the organisation of the cortex and most of the previous studies based their analysis on MRI data or scalp-level EEG (Thomas Yeo et al., 2011). In this work, on the other hand, we reconstruct brain networks combining non-invasive scalp EEG data with source reconstruction techniques. The approach adopted in the present study allows to evaluate brain networks based on the reconstructed cortical sources, exploiting the high time-resolution of the electroencephalographic signal while overcoming the well-established limitations of scalp-level networks. The purpose of this investigation is to show how scalp-EEG can be used to reconstruct the cortical network mechanisms that come into play during a postural control task in which the participant's quiet stance is disrupted by mechanical skeletal muscle vibrations. The effects of mechanical vibrations on muscle spindles are well documented in postural control literature (Roll et al., 1989; Wierzbicka et al., 1998) and previous studies have employed them to provoke kinematic imbalances in order to assess the subjects postural responses (Fransson et al., 2003; Toosizadeh et al., 2018). The analysis presented in this work includes the evaluation of static properties of the brain network as well as an assessment of its dynamic reconfiguration. Most importantly, this work highlights the relationship between network dynamics and stabilogram characteristics by correlating the dynamic flexibility of the network with the complexity of postural fluctuations. Previous studies showed how variations in the sample entropy of the sway signal, used as a complexity metric, were associated to varying levels of proficiency in the execution of postural task (Zhou et al., 2016c). It is also well assessed how cortical plasticity (reflected in the flexibility of the brain network) is related to an enhanced ability of

reaction to external stimuli (Cai et al., 2014). In this work, we want to investigate whether a correlation between these two metrics exists, and which cortical areas are involved. This study therefore set out to assess the potential for network-based analysis to be beneficial in the development of neurofeedback strategies, targeted at specific nodes (brain regions) of the cortical network and aimed at improving postural performance in subjects with age- or disease-related impairments.

## 5.2 Materials and Methods

Data were collected at Aston University's ALIVE research facility, following approval by the University Research Ethics Committee (ref: #1432). The recruitment of healthy adult volunteers (>18 years old) took place among the campus population. Exclusion criteria included the presence of any neuromuscular or balance disorders, physical limitations preventing a natural upright stance, ongoing medications and consumption of alcohol during the 24 hours prior to the experiment. 11 participants volunteered to take part in the study (age = 24.4 ± 5.8, 5 males and 6 females, all indicating their right leg as the dominant one). The experiment was carried out in one single seating of about 1.5h, including the participant's preparation. A schematic of the experimental set-up is depicted in Figure 5.1. Participants were asked to stand still on a force platform, maintaining a natural upright posture and fixing their gaze on a marker on the wall in front of them, at about 2m distance. After 30s of baseline recording, a randomized sequence of mechanical vibratory stimuli was applied to the participants gastrocnemius muscles of both legs in order to disrupt their stance. The stimulation sequence had a duration of 10 min and consisted of a randomized pulse wave in which both pulse width and inter-stimulus intervals were uniformly distributed between 1 and 6 seconds. The vibration was delivered at 85Hz, via two small eccentric rotating mass DC

motors (ERM) encased in a plastic cylinder and attached to the participants' calves (diameter: 30mm, length: 62mm). This set-up was based on previous works reported in (Fransson et al., 2003; Patel et al., 2009). The session (30 s baseline followed by 10 min stimulation) was repeated twice, with eyes open (OE) and closed (CE), in randomized order. The EEG signals were recorded using a 64-channel wet electrodes cap with a standard 10-20 system montage

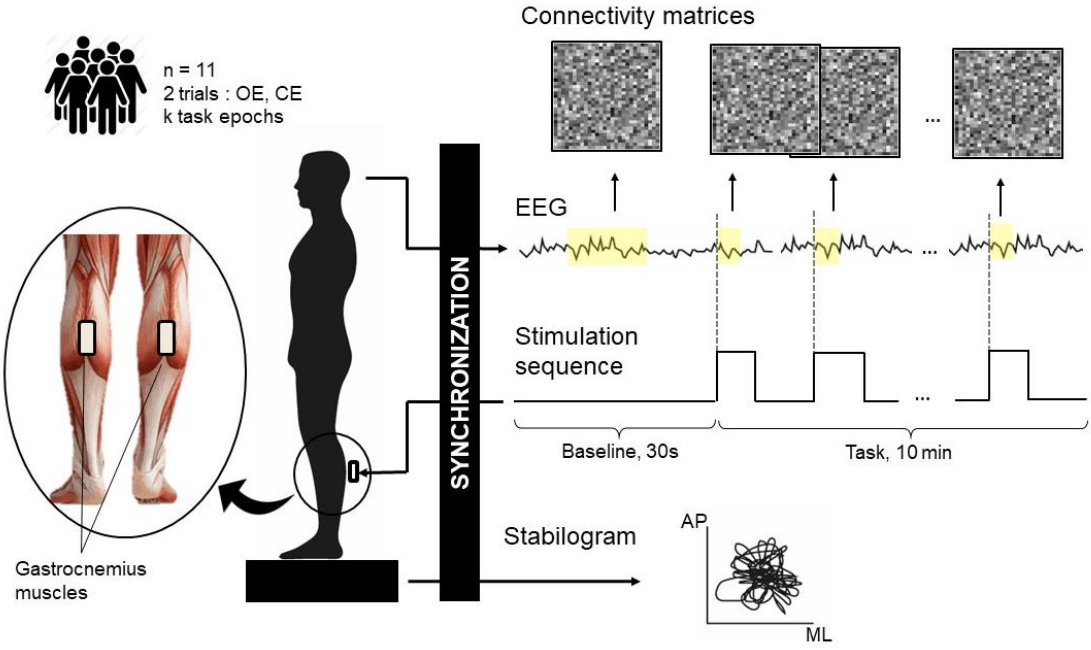


**Figure 5.1.** Experimental set-up.

Schematic representation of the experimental set-up. 11 volunteers made up the analysed cohort, the single experimental session comprised two trials: eyes open (OE) and eyes closed (CE). The participant was asked to stand on a force platform in a quiet, upright stance. After 30 s of resting state (Baseline), a proprioceptive vibratory stimulation sequence was delivered through vibrators applied to the gastrocnemius muscles of the calves. The duration of the pseudo-random binary sequence was 10 min (Task), comprising k vibratory stimulation of variable length uniformly distributed between 1 - 6 s. The acquired EEG data, as well as the stabilogram signal (Anterior-Posterior and Medial-Lateral), were synchronized with triggers at the onset of each vibration. These triggers allowed for the definition of 1 second epochs (highlighted in the figure) from which, after the source reconstruction, network connectivity matrices were extracted.

(*AntNeuro, Enschede - Netherlands*). The recording sampling frequency was $f_S = 1000Hz$. Participants were instructed to keep their facial muscles as relaxed as possible, avoiding teeth grinding and jaw clenching, in order to minimize muscle artefacts in the recorded signal.

Participants stood on an *AMTI OR-6-7* force platform (part of a motion capture system by *Vicon Motion Systems Ltd, Kidlington - UK*) that measured their centre of pressure trajectory (COP) over the course of the experiment, in its anterior-posterior (AP) and medial-lateral (ML) components, at a sampling frequency of $f_S = 1000Hz$. A customised wearable electronic box was developed and built-in order to generate the randomized pulse wave that regulated the calf stimulation and to simultaneously send a series of 5V TTL trigger signals to the EEG amplifier and to the force platform system. The 5V trigger signals were generated at the onset and offset of every vibration and allowed for the synchronisation of EEG and COP data, as well as their segmentation into epochs. The 3D printed box case was secured on a belt so that the participants could wear it around their waist. The device was powered with two rechargeable 9V batteries, while an internal voltage regulator made sure to deliver the appropriate voltage (12.4V) for the two connected ERM motors to deliver an 85Hz vibration (corresponding to a rotational speed of the internal eccentric mass of 5100 RPM).

## 5.3 Data Analysis

### 5.3.1 Preprocessing

The steps followed for the preprocessing of the EEG signal were adapted from a semi-automated pipeline presented in the software Cartool (Brunet et al., 2011) and implemented with custom-made Matlab scripts. The EEG signal was filtered between 1 - 45Hz with a zero-phase band-pass FIR filter; the DC offset was subsequently removed from the whole signal

before segmenting it into epochs. Epochs were defined as 1-second-long signal segments after each onset trigger, corresponding to the 1 second of electric brain signal after the start of each vibration of the sequence. The epoch length of 1 second was chosen in that it is the maximum length that allows to avoid overlapping with the following vibration/rest cycle of the sequence.

Three frontal electrodes (Fp1, FpZ, Fp2) were used to perform an Electrooculography (EOG) regression on the remaining 60-channel data, in order to remove eye blink artefacts (Parra et al., 2005). Channels with poor signal quality were identified within every segmented epoch and replaced with an interpolation of the neighbouring channels signals. The classification of 'bad channels' was performed with a supervised automated approach, based on the standard deviation (std) of the signal. The $i^{th}$ channel was classified as 'bad' if its $std_i$ exceeded the average std (computed among all the channels) times a certain constant threshold value T.

$$if \quad stdi \; > T * std \;\; \Rightarrow \; Interpolate \; channel \; i$$

The outcome of this preprocessing step was visually inspected to evaluate the effectiveness of different T values. The value T = 1.7 was finally chosen, as it proved to be consistent with the choices that would have been made with a purely visually inspected manual rejection. The interpolated channels were filtered between 1-45Hz again to smooth them out. Epochs where more than 15% of the total channels were interpolated (≥ 9 channels) were discarded. Finally, the EEG signal was re-referenced to the common average. Table 5.1 provides an overview of the total number of vibratory stimulations applied to each participant, and the final amount of accepted epochs following the preprocessing of the data. The AP and ML components of the COP trajectory were detrended and filtered between 0.2 - 20Hz with a bi-directional bandpass

**Table 5.1.** Number of vibratory stimuli (k) across subjects during the 10 min task trial in both experimental conditions and number of 1 s epochs following the onset of each vibration that were accepted in the preprocessing phase because free from signal corruption.

(A) Open Eyes

| Subj n. | Stimuli k | Accepted epochs |
|---|---|---|
| 1 | 89 | 89 |
| 2 | 91 | 91 |
| 3 | 89 | 82 |
| 4 | 85 | 85 |
| 5 | 91 | 91 |
| 6 | 89 | 89 |
| 7 | 85 | 84 |
| 8 | 91 | 90 |
| 9 | 68 | 68 |
| 10 | 79 | 64 |
| 11 | 85 | 85 |

(B) Closed Eyes

| Subj n. | Stimuli k | Accepted epochs |
|---|---|---|
| 1 | 89 | 87 |
| 2 | 85 | 61 |
| 3 | 85 | 38 |
| 4 | 87 | 64 |
| 5 | 89 | 89 |
| 6 | 91 | 54 |
| 7 | 89 | 89 |
| 8 | 89 | 57 |
| 9 | 85 | 85 |
| 10 | 89 | 54 |
| 11 | 87 | 56 |

Butterworth filter (Zhou et al., 2016c). The signal was then normalised to unit variance by dividing it for its standard deviation (Donker et al., 2007b).

### 5.3.2 Reconstruction of Functional Brain Networks

Functional brain dynamics were reconstructed using the 'EEG source connectivity' method (Hassan and Wendling, 2018a; Kabbara et al., 2020b). This method was proposed with the aim to overcome the volume conduction and field spread limitations that affect scalp-level networks by performing functional connectivity network analysis at the cortical level. First, this approach requires to reconstruct the cortical sources by solving the inverse problem (Hallez et al., 2007). Given an equivalent current dipole model, the scalp EEG signal recorded on M

channels can be expressed as the linear combination of P time-varying current dipole sources (Baillet et al., 2001a):

$$X(t) = G * S(t) + N(t)$$

Where G is the lead-field matrix of size [M, P], that weighs the contribution of each source towards the recorded signal, S(t) is the matrix containing the sources time series [P, Time-points] and N(t) is the noise covariance matrix. Solving the inverse problem consists in finding an estimate $\hat{S}(t)$ of the source matrix. For this study, a three-layer BME model (brain, skull, scalp) was adopted to define the inverse problem domain. The model's morphology was based on a standard head model template provided by BrainStorm (Tadel et al., 2011). To solve the inverse problem, we used the weighted Minimum Norm Estimate (wMNE) algorithm (Grech et al., 2008; Hincapié et al., 2016). The output consists of 1500 estimated source time-series, localised at the cortical boundary. For the purposes of network analysis, the brain is rendered through a graph in which nodes represent cortical regions. In the present work the Desikan-Killiany anatomical atlas was employed to parse the cortex into 68 regions of interest (ROIs) (Desikan et al., 2006b). By averaging the estimated source time series within each regional boundary, the regional time series matrix is obtained (with dimension [68, Time-points]). Functional connectivity (FC) was computed based on the Phase Locking Value (PLV), a measure of statistical coupling between the cortex-level regional time series. The advantages and limitations of different connectivity metrics have been extensively reviewed in literature (Wendling et al., 2010) and previous research on simulated data showed that the combination of wMNE and PLV has the highest accuracy in terms of similarity with the reference network (Hassan et al., 2017).

Functional connectivity values between each pair of the 68 brain regions were computed for every 1-second epoch in three frequency bands: Alpha (**α**, [8-13] Hz); Beta (**β**, [13-30] Hz); and Gamma (**γ**, [30-45] Hz).

### 5.3.3 Nodewise and Edgewise Static Analysis

The focus of static network analysis is to investigate the global characteristics of the brain network during the execution of the postural control task, without taking into account its dynamic evolution. Therefore, connectivity matrices within each trial (OE and CE) were averaged to obtain a single task-related connectivity matrix for every subject and frequency band. This averaged matrix was then thresholded in order to keep only the top 10% strongest connections, while removing weaker, spurious connections (Hassan et al., 2017; Kabbara et al., 2020b). Many network measures are available to characterise different aspects of the brain connectivity, providing insights on local and global properties of the network structure. First, we analysed local parameters of single nodes of the network, i.e., cortical regions, to characterise their properties and map how their role in the network changes in different experimental conditions (nodewise analysis). Then, we used Network-Based Statistics (NBS), to give a global representation of the network reconfiguration in the two conditions, by focusing on the inter-region connections themselves (edgewise analysis) (Zalesky et al., 2010).

The degree of a node is one of the easiest and most common local network measures; it consists in the number of connections (edges) associated to that specific node. A generalization of this measure is a node's strength, which comes into play when weighted networks are considered and consists in the sum of the weights of the edges related to the node. Degree and Strength are considered measures of hubness, as they describe how central a node is in the network by providing information on the number of connections it is involved

in and their weight. These measures help to determine whether the node is a highly interconnected one (hub) or if it is a marginal, isolated node in the network. The strength parameter was computed for each of the 68 brain regions, in **α**, **β** and **γ** frequency bands and a statistical analysis was carried out to investigate the presence of a significant difference between the two experimental conditions of open eyes and closed eyes. The non-parametric Wilcoxon signed rank test was chosen given the limited sample size (11 repetitions) and the lack of assumption on the normal distribution of the data. The resulting p-values were subsequently corrected for multiple comparisons using the False Discovery Rate (FDR) method. The same analysis was performed on the baseline connectivity matrices obtained from the initial 30 s resting-state epochs, during both conditions (OE and CE). This allowed to verify the presence of differences in nodes strength solely related to the visual input (or lack of thereof), in the absence of vibratory simulation.

Then, for an edgewise analysis of the network, differences in the connectome were investigated using the NBS method. The method was implemented in Matlab using the NBS toolbox (Zalesky et al., 2010). NBS works on the connectivity matrices representing the network in the two testing conditions, organized according to a statistical model specified in terms of the general linear model (GLM). It provides as an output the set of connections comprising the network that is found to show a significant difference in the two conditions, with an associated p-value. The significance level was set at 0.05 (with correction for multiple comparisons using permutation test) and the number of iterations at 5000. The network analysis was performed both on task (during the stimulation) and baseline connectivity matrices.

### 5.3.4 Dynamic Analysis – Flexibility/Complexity correlation

The network dynamic was assessed by computing the flexibility index of each node over the execution of the postural control task. First, the connectivity matrix that identifies the functional network is computed for every 1s epoch following each onset of the binary vibratory sequence throughout the duration of the experiment. Every network of this sequence is decomposed into its dynamic modules, using the community Louvain algorithm (Blondel et al., 2008). Modules represent sets of highly intra-connected regions that are weakly connected with others (Bassett and Sporns, 2017). The flexibility of each node of the network is then computed based on the number of times the affiliation of the node shifts among different modules. Subsequently, a posturographic analysis was performed on the force platform data to extract the sample entropy ($S_{EN}$) from the anterior-posterior (AP) and medial-lateral (ML) components of the centre of pressure (COP) trajectory. This allowed us to quantify the complexity of the postural signal for each participant during the execution of the task. Finally, Pearson's linear correlation coefficient was computed in both experimental conditions (OE and CE) between the flexibility values of each of the 68 nodes and both the SEN values of the AP and ML sway respectively (number of repetitions corresponding to the number of participants). A p-value was also provided together with the Pearson's coefficient by running a Student's t-test for each comparison, testing the null hypothesis of no correlation.

## 5.4 Results

This chapter illustrates the outcome of the functional connectivity analysis. The results of the static analysis are reported in sections 5.4.1 and 5.4.2, which summarize, respectively, the nodewise and edgewise comparisons of the global brain networks during OE and CE tasks.

Paragraph 5.4.3, instead, focuses on the dynamic analysis and reports the results of the correlation analysis performed between the flexibility index of each node and the complexity of the COP sway. The following results refer to the analysis in alpha, as statistically significant results only emerged in this frequency band.

### 5.4.1 Static Analysis – Nodewise

Significant differences in nodes strength values between OE and CE tasks emerged from the nodewise static analysis. The outcome of the strength analysis is displayed in Figure 5.2. The results highlight two main contiguous areas with a different characterization, the frontal regions with higher strength values during OE and the right parieto-temporal regions where higher strength values can be observed during CE.

An increased strength can be observed during the OE task in the network nodes corresponding to the frontal areas of the cortex (Orbitofrontal: left medial , $p = 0.033$; left lateral , $p = 0.036$; right medial, $p = 0.015$; right lateral, $p = 0.015$. Superior-frontal: left, $p = 0.036$; right, $p = 0.015$) as well as the anterior cingulate (left caudal, $p = 0.033$; right rostral, $p = 0.015$). These results present a distinct symmetry between the two hemispheres and a marked percentage increase in strength (>50% increase over the CE task) can be noted especially in the orbitofrontal regions (left lateral, $p = 0.036$; left medial, $p = 0.033$; right lateral, $p = 0.015$; right medial, $p = 0.015$) as well as in the left pars-orbitalis ($p = 0.024$).

On the other hand, network nodes whose strength increased during the CE task, are not symmetrically distributed across the hemisphere but involve predominantly the right one. The corresponding cortical regions in the right hemisphere are focused in the central (post-, $p = 0.031$; para-, $p = 0.036$), parietal (superior, $p = 0.015$; inferior, $p = 0.033$) and temporal

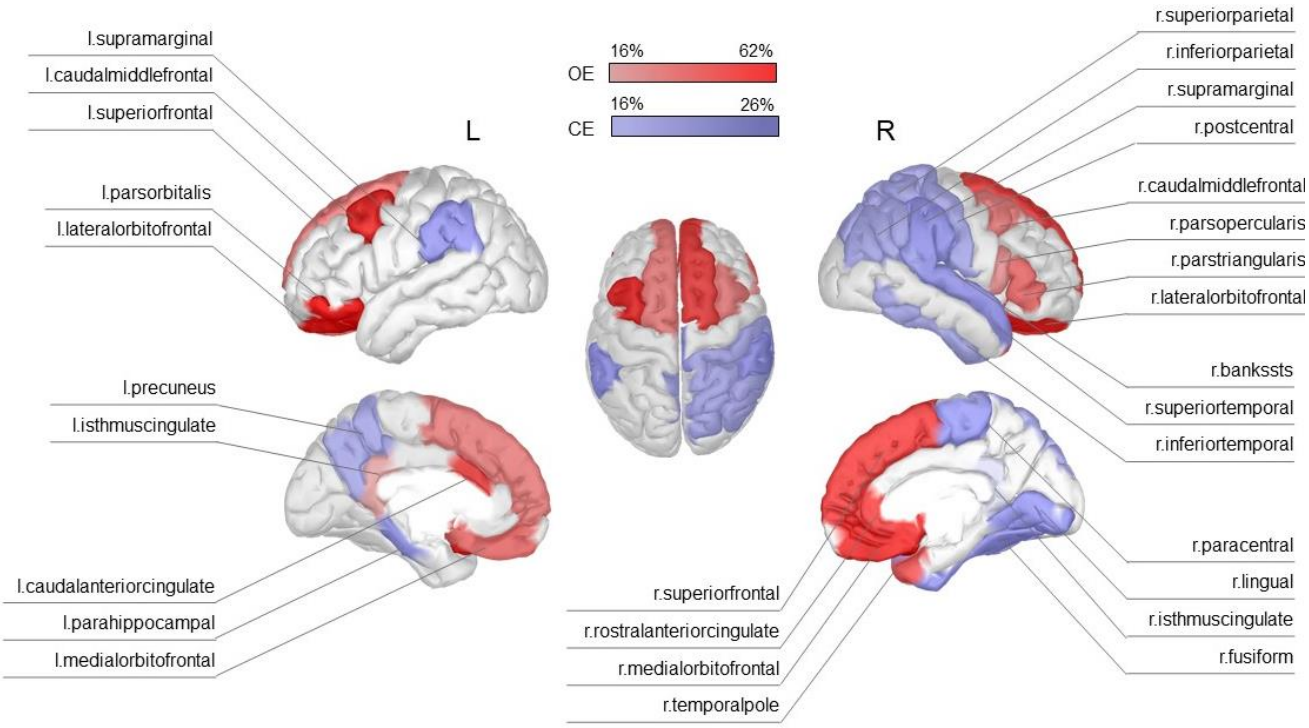


**Figure 5.2.** Nodewise static analysis results.
Percentage variation in each region's strength during the postural task in the two conditions of open (OE) and closed eyes (CE), in the alpha band. The anatomical representation displays the nodes of the network as the corresponding 68 cortical regions, parcellated according to the Desikan-Killiany atlas. The brain is shown from the top as well as in the medial and lateral view of each hemisphere. Regions highlighted in red displayed higher strength values during OE, regions highlighted in blue showed higher strength values in CE. The saturation of the colour denotes the amount of percentage increase, as shown by the colour bar. Only regions with a statistically significant difference in strength are reported (FDR-corrected p-value smaller than 0.05).

(superior, $p = 0.036$; inferior, $p = 0.015$) areas. An increase in the supramarginal region can also be observed in both hemispheres (left, $p = 0.033$; right, $p = 0.033$). Overall, it must be noticed that the percentage increase in strength during CE in these regions is not as pronounced, the maximum value is a 25% increase over the OE task. The baseline analysis, in which strength values extracted from the connectivity matrices related to the quiet stance epochs, in OE and CE conditions, were tested, didn't provide any significant differences. The lack of significant variation in node strength values between OE and CE during the baseline epochs suggest that the significant results emerged from the task analysis in the two

experimental conditions are actually related to the proprioceptive vibratory stimulation. Table 5.2 provides a complete overview of the results for each cortical region, including the mean strength values computed over the participants, their standard deviation, the strength percentage increase values and the associated corrected p-values.

**Table 5.2.** Nodewise static analysis results. List of cortical regions which showed a significant strength increase in open eyes (A) and closed eyes (B), compared to the opposite condition. Also reported are the average strength value across subjects and associated standard deviation, as well as the percentage increase over the opposite condition and relative p-value.

(A) Open Eyes

| | Region Name | Strength value | SD | Strength Increase (%) | p-val |
|---|---|---|---|---|---|
| **Left** | l.parsorbitalis | 3.5 | 1.6 | 62.3 | 0.024 |
| | l.caudalanteriorcingulate | 4.1 | 1.5 | 47.5 | 0.033 |
| | l.medialorbitofrontal | 5.1 | 2.4 | 38.3 | 0.033 |
| | l.lateralorbitofrontal | 3.0 | 1.4 | 56.9 | 0.036 |
| | l.superiorfrontal | 6.6 | 2.3 | 28.9 | 0.036 |
| | l.isthmuscingulate | 7.2 | 4.2 | 15.9 | 0.039 |
| | l.caudalmiddlefrontal | 4.7 | 2.5 | 55.8 | 0.044 |
| **Right** | r.caudalmiddlefrontal | 8.9 | 2.2 | 26.9 | 0.015 |
| | r.lateralorbitofrontal | 5.4 | 1.8 | 58.6 | 0.015 |
| | r.medialorbitofrontal | 5.5 | 2.1 | 56.3 | 0.015 |
| | r.parsopercularis | 8.8 | 1.8 | 26.5 | 0.015 |
| | r.rostralanteriorcingulate | 6.5 | 2.3 | 48.2 | 0.015 |
| | r.superiorfrontal | 7.3 | 2.5 | 45.4 | 0.015 |
| | r.temporalpole | 7.2 | 2.7 | 39.1 | 0.015 |
| | r.parstriangularis | 7.3 | 1.9 | 37.8 | 0.044 |

(B) Closed Eyes

| | Region Name | Strength value | SD | Strength Increase (%) | p-val |
|---|---|---|---|---|---|
| **Left** | l.supramarginal | 24.9 | 3.0 | 22.5 | 0.033 |
| | l.parahippocampal | 26.1 | 3.5 | 21.2 | 0.036 |
| | l.precuneus | 25.6 | 3.7 | 16.1 | 0.036 |
| **Right** | r.bankssts | 25.5 | 3.9 | 16.6 | 0.015 |
| | r.fusiform | 27.3 | 3.4 | 22.4 | 0.015 |
| | r.inferiortemporal | 25.9 | 3.3 | 20.5 | 0.015 |
| | r.isthmuscingulate | 20.1 | 4.8 | 3.9 | 0.015 |
| | r.lingual | 25.9 | 4.5 | 25.5 | 0.015 |
| | r.superiorparietal | 25.1 | 4.6 | 19.1 | 0.015 |
| | r.postcentral | 23.5 | 4.2 | 20.2 | 0.031 |
| | r.inferiorparietal | 21.2 | 4.5 | 16.6 | 0.033 |
| | r.supramarginal | 24.8 | 3.4 | 25.1 | 0.033 |
| | r.paracentral | 25.5 | 3.7 | 22.1 | 0.036 |
| | r.superiortemporal | 21.9 | 4.0 | 24.2 | 0.036 |

### 5.4.2 Static Analysis – Edgewise

The results of the edgewise static analysis are depicted in Figure 5.3. The network reconfiguration in the alpha band between OE and CE tasks, as evaluated by the change in connectivity values, involves 116 edges of the network, all of which showed increased connectivity during the CE task. The resulting network is spatially localised in the posterior areas of the brain, presenting connections across the hemispheres, as well as intra-hemisphere connections on the right side. The significant connections are predominantly temporo-parieto-central, involving mainly the parietal (superior and inferior), the central (post and para) and the temporal (inferior and middle) brain regions.

These results, in terms of cortical regions involved and predominance of the right hemisphere, are in accordance with the nodewise analysis results reported for the CE task in the previous

section. The analysis on the baseline network reconfiguration in the two experimental conditions highlighted 160 significant edges, whose connectivity values increased during CE. The resulting network partly overlaps with the task-related one, especially in the parietal and temporal regions; at the same time, though, it also differentiates itself with regards to its edges distribution. Specifically, it doesn't present a strong right lateralization of intra-hemispheric connections while it displays a higher connection density in the frontal lobe, which was previously unobserved. Nevertheless, the statistical test (NBS) did not highlight any statistically significant difference between the task-related and baseline-related networks. A complete list of the cortical regions involved in both networks, with the corresponding degree value, is available in Table 5.3.

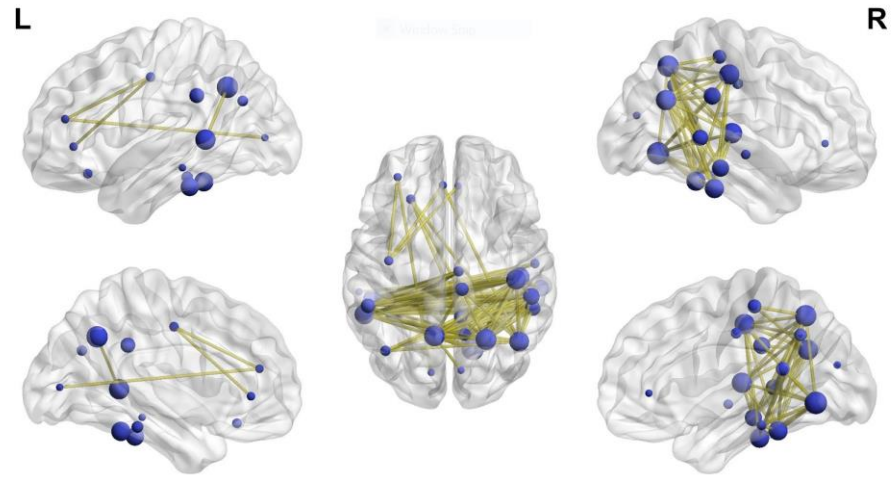


(A) Task

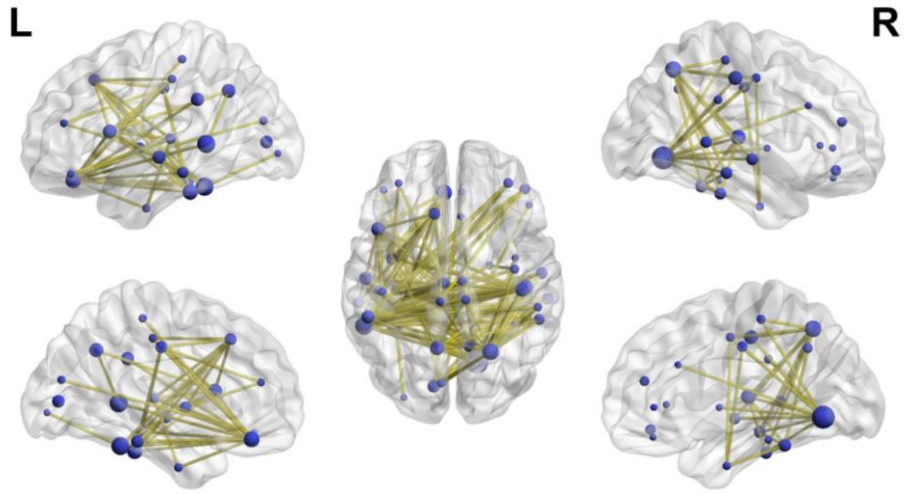


(B) Baseline

**Figure 5.3.** Edgewise static analysis results.

Graphical representation of the network reconfiguration occurring in the alpha frequency band. Cortical regions are represented as nodes of the network, while edges represent the connections between the regions. The size of each node is proportional to its degree, i.e. the number of connections in which it takes part. The figure highlights the differences between the brain network structures in the two experimental conditions (OE and CE), after the respective connectivity matrices were compared and tested to identify edges which underwent a significant change in connectivity value. Figure A depicts the 116 edges that showed a statistically significant difference in connectivity (significance level of NBS set to 0.05) during the task execution, i.e. average of 1s epochs following the onset of each vibratory stimulation. All of them are associated with higher connectivity values during the CE task. In the same way, Figure B shows the 180 edges associated with significantly different level of connectivity during the baseline epoch, i.e. no vibratory stimulation. In this case too, all of the edges are associated with higher connectivity values in the CE condition.

**Table 5.3**. Edgewise static analysis results.

List of cortical regions that are part of the network and corresponding degree.

| | (A) Task | | (B) Baseline | |
|---|---|---|---|---|
| | **Region Name** | **Deg** | **Region Name** | **Deg** |
| **Left** | l.precuneus | 14 | l.bankssts | 17 |
| | l.bankssts | 13 | l.fusiform | 17 |
| | l.fusiform | 12 | l.medialorbitofrontal | 14 |
| | l.inferiortemporal | 11 | l.inferiortemporal | 13 |
| | l.supramarginal | 8 | l.parsopercularis | 11 |
| | l.parahippocampal | 5 | l.precuneus | 11 |
| | l.inferiorparietal | 4 | l.superiortemporal | 10 |
| | l.lateralorbitofrontal | 3 | l.supramarginal | 10 |
| | l.precentral | 3 | l.parahippocampal | 9 |
| | l.rostralanteriorcingulate | 2 | l.pericalcarine | 9 |
| | l.rostralmiddlefrontal | 2 | l.insula | 8 |
| | l.middletemporal | 1 | l.posteriorcingulate | 8 |
| | l.pericalcarine | 1 | l.superiorfrontal | 8 |
| | | | l.middletemporal | 7 |
| | | | l.transversetemporal | 6 |
| | | | l.cuneus | 3 |
| | | | l.entorhinal | 3 |
| | | | l.paracentral | 3 |
| | | | l.postcentral | 3 |
| | | | l.parsorbitalis | 2 |
| **Right** | r.lingual | 15 | r.lingual | 24 |
| | r.superiorparietal | 14 | r.superiorparietal | 15 |
| | r.inferiorparietal | 13 | r.transversetemporal | 12 |
| | r.postcentral | 13 | r.postcentral | 11 |
| | r.transversetemporal | 13 | r.fusiform | 9 |
| | r.fusiform | 12 | r.inferiortemporal | 8 |
| | r.inferiortemporal | 12 | r.middletemporal | 8 |
| | r.middletemporal | 10 | r.superiortemporal | 8 |
| | r.supramarginal | 10 | r.bankssts | 7 |
| | r.bankssts | 9 | r.parsorbitalis | 6 |
| | r.isthmuscingulate | 7 | r.posteriorcingulate | 6 |
| | r.paracentral | 7 | r.precuneus | 5 |
| | r.precuneus | 6 | r.rostralmiddlefrontal | 5 |
| | r.posteriorcingulate | 4 | r.paracentral | 4 |
| | r.parahippocampal | 3 | r.precentral | 4 |
| | r.superiortemporal | 3 | r.entorhinal | 3 |
| | r.cuneus | 1 | r.supramarginal | 3 |
| | r.rostralanteriorcingulate | 1 | r.parahippocampal | 2 |
| | | | r.caudalanteriorcingulate | 1 |
| | | | r.insula | 1 |
| | | | r.medialorbitofrontal | 1 |
| | | | r.parstriangularis | 1 |
| | | | r.rostralanteriorcingulate | 1 |

### 5.4.3 Dynamic Analysis – Flexibility/Complexity correlation

In the dynamic analysis we tested the correlation, in the alpha frequency band, between node flexibility and $S_{EN}$ values of the COP sway (in the OE and CE experimental conditions and in the AP and ML sway components). Significant Pearson's correlation $\boldsymbol{\rho}$ values emerged between the flexibility of nodes in OE condition and the corresponding AP stabilogram sway.

In this case, significant correlation values were found in the postcentral, supramarginal and inferior parietal areas as well as in the temporal-occipital regions and the cingulate cortex of the right hemisphere (see figure 5.4). Specifically, high Pearson coefficients ($\boldsymbol{\rho}$>0.70) could be observed in areas of the cingulate cortex (isthmus cingulate $\boldsymbol{\rho}$ = 0.80, p= 0.003 and posterior cingulate $\boldsymbol{\rho}$ = 0.69, p=0.019) as well as in the temporal-occipital cortex (middle temporal gyrus $\boldsymbol{\rho}$ = 0.81 p=0.002 and cuneus $\boldsymbol{\rho}$ =0.7 p=0.018).

Table 5.4 reports the Pearson coefficient and corresponding p-value for each significant region.

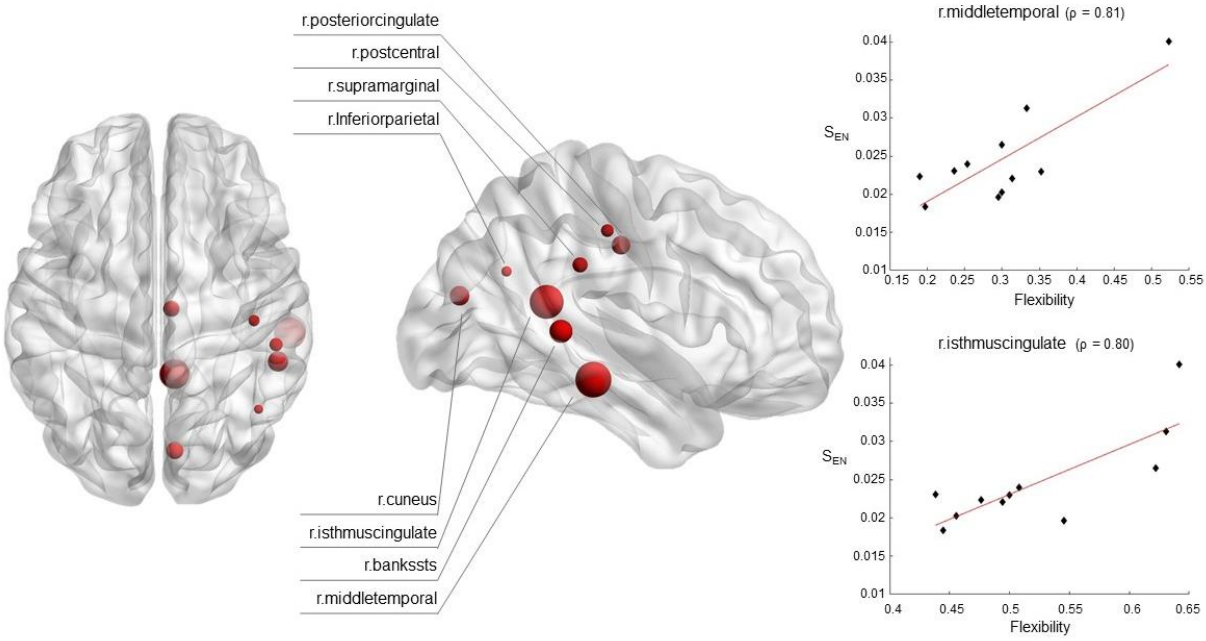


**Figure 5.4.** Results of the correlation analysis between network flexibility during OE task and sample entropy of the AP component of the postural sway.

The highlighted regions correspond to the nodes of the network whose flexibility correlated with the corresponding SEN of the posturographic signal in a statistically significant way ($p<0.05$). Each of these regions is represented with a node whose size is proportional to the associated Pearson's correlation coefficient ($\boldsymbol{\rho}$). The figure also shows the correlation scatter plots (including regression lines) related to the two regions with highest Pearson coefficients; flexibility values are in the x-axis while the sample entropy index is in the y-axis.

**Table 5.4.** Flexibility-complexity correlation results.

List of cortical regions associated with a significant Pearson's correlation coefficient.

| | Region Name | Pearson's ρ | p-val |
|---|---|---|---|
| **Right** | r.supramarginal | 0.66 | 0.026 |
| | r.posteriorcingulate | 0.69 | 0.019 |
| | r.postcentral | 0.65 | 0.032 |
| | r.middletemporal | 0.81 | 0.002 |
| | r.isthmuscingulate | 0.80 | 0.003 |
| | r.inferiorparietal | 0.63 | 0.039 |
| | r.cuneus | 0.70 | 0.018 |
| | r.bankssts | 0.72 | 0.012 |

## 5.5 Discussion

Postural control is the phrase used to indicate the complex regulatory system whose aim is to maintain a stable upright stance. The complexity of this task lies in its reliance from a wide range of sensory inputs gathered predominantly through the visual, somatosensory, proprioceptive and vestibular systems. While early research on the topic associated postural control with a reflex response enacted at the level of the brainstem and spinal cord (Sherrington, 1910), extensive recent evidence pointed out the crucial role of the cortex as a hub for the processing of sensory information and the subsequent development of an effective postural control strategy (Bolton, 2015).

Balance perturbations techniques have been extensively used to challenge the upright stance in order to investigate the elicited postural response. In the present work the disruption of the participants quiet upright stance was induced by skeletal muscle vibration of the lower limbs, in which a randomized binary vibratory sequence was applied to the gastrocnemius muscles of the calves.

The characteristics of the cortical network structure in the two experimental conditions of open and closed eyes, as well as the dynamic reconfiguration of the network in relationship with the posturographic data, were investigated using 68 regional time-series obtained from reconstructed cortical sources, averaged according to an anatomical atlas as presented in the methodology section of this work. To our knowledge, the use of EEG source connectivity to characterise functional networks involved in postural control has been scarcely used in previous works, since most of the previous studies on the topic relied on scalp-level EEG data (Mierau et al., 2017b). The scalp-level approach, though, presents limitations (most notably

distortions introduced by the volume conduction effect) that have been extensively highlighted and discussed in literature (Schoffelen and Gross, 2009). The results which emerged from this investigation, consistently highlighted the presence of statistically significant cortical network structures in the alpha band ($\alpha$: [8-13] Hz). This is in line with results from previous literature which showed the role of alpha band connectivity in cortical processes related to postural control tasks (Mierau et al., 2017b; Peterson and Ferris, 2019). Cortical effects were also previously reported in beta band during balance tasks (Palmer et al., 2021; Peterson and Ferris, 2019). It is worth noting, though, that the majority of previous literature focuses on cortical activation in terms of spectral and power-based analyses, while the novel methodology proposed in this work involves functional connectivity which relies on phase metrics (PLV) and therefore focuses on the cortical signals' phase synchrony rather than their amplitude.

### 5.5.1 Discussion of nodewise OE results

The results of the nodewise analysis, in which we compared the node strength in the two experimental conditions, display two clear and well-defined clusters of regions. The OE condition is marked by an increased node strength in the orbito-frontal, superior-frontal and anterior cingulate regions of the cortex, which characterises them as central hubs of this brain network. Previous research has shown how the frontal lobe plays a role in the allocation of attentional resources during motor performances (Fujita et al., 2016). In particular, the caudal and middle-frontal regions comprise the Frontal Eye Field (FEF), which is related to visual field perception and awareness and the maintenance of attention to peripheral locations (Schall, 2008). FEF is also part of the Dorsal attention Network, which has been shown to be a centre of top-down control of visual attention (Japee et al., 2015). Moreover, besides being involved in spatial attention, it has been suggested that offline motor planning is one of the core function

of this network, i.e. the representation of abstract kinematic movement, which would indicate the evolution of this network from a role of pure motor control to a much wider range of cognitive functions (Ptak et al., 2017). This motor attention frontal area interplays with the orbitofrontal cortex (lateral- and medial-orbitofrontal regions) which is a heterogeneous region acting as a centre for sensory integration (Kringelbach, 2005) as well as with the anterior cingulate cortex (caudal- and rostral- anterior cingulate regions), which has been traditionally related to decision-making and has been shown to play a role in the recognition of unstable posture (Lavin et al., 2013; Slobounov et al., 2009). These findings suggest that the reaction to a challenged upright stance, during the OE condition, engages an attention-related network in the alpha band located predominantly in the frontal lobe, with the visual information playing a predominant role in the integration of the postural control feedback system. They also highlight the reliance on visual cues in the detection of postural instability and the subsequent development of a corrective strategy. These results also accord with and corroborates the observations of previous studies which showed how certain cognitive functions, namely attention, interact with motor function and postural control (Doumas et al., 2008; Fujita et al., 2016; Rapp et al., 2006).

### 5.5.2 Discussion of nodewise and edgewise CE results

Observing the results of the nodewise analysis for the CE condition, on the other hand, it clearly emerges a predominance of the parietal and temporal lobes. Another noticeable feature of these results is the asymmetry of the network nodes involved, which are primarily localised in the right hemisphere. The increased hubness of these nodes in the network organisation associated with a postural response in the absence of visual cues is also supported by a qualitative inspection of the task edgewise analysis, which however didn't provide statistically

significant differences when compared the baseline network. The analysis conducted on the network connections in the two experimental conditions, highlights the strengthening of inter-hemisphere connections among parietal and temporal regions as well as a dense network of intra-hemisphere connections in the right side of the brain, during the CE condition. These results are backed by a strict network-based statistical analysis that confirms the significance of the displayed connections. The emerging network clearly highlights the involvement of the parietal lobe. The Anterior parietal cortex (APC) is the main recipient of proprioceptive signals. While commonly identified as a whole with the primary somatosensory cortex, APC actually comprises of four areas distinctively defined by their cytoarchitecture. It has been shown how two of these areas in particular (Brodmann's 3a and 2) are the primary target for proprioceptive information regarding muscle fibres lengthening, joints position, etc. (Delhaye et al., 2018). The Posterior parietal cortex (PPC) is a hub of multisensory integration, being responsive to visual, auditory and vestibular solicitations which is also involved in motor planning functions. The superior and inferior parietal lobules are in fact centres of interpretation of sensory information involving body image and spatial perception. Previous studies reported how parietal lesions are linked to disturbances in motor behaviour resulting from the failure to gather contralesional space information by limb movement (Karnath, 1997). The network connections between parietal cortex and temporal regions (in particular superior temporal) suggests an involvement of what has been identified as the vestibular cortex. In order to properly identify the nature of a perceived motion, distinguishing between motion of the surrounding environment from self-motion, and resolve discrepancies in the visual signal, the brain relies on the integration of vestibular signals from the inner ear's sensors. The broad range of interactions that the vestibular system has with other sensory systems is reflected in its distributed cortical network. The exact localisation of this network has been amply investigated

and discussed in literature, both in human and non-human primates (Ventre-Dominey, 2014). The network that emerges from the edgewise results, with a significant strengthening of the superior-temporal region and of the areas surrounding the posterior end of the lateral sulcus (Sylvian fissure) reflects what is commonly defined as the parieto-insular vestibular cortex (PIVC). This area has been hypothesized to be involved in a vestibular cortical pathway that spreads from the temporal parietal junction (TPJ) to the retro-insular cortex (RI) and is active in the integration of visual and vestibular information for a self-referential processing that informs about self-location in space (Ventre-Dominey, 2014). More recent literature further investigated the anatomical and functional characteristics of this area, identifying two main components to the vestibular cortex: PIVC and Posterior-insular cortex (PIC) (Frank and Greenlee, 2018). Both areas are involved in the processing of vestibular cues, but they differ in the way they respond to visual stimulation. It has been shown that PIC processes visual clues related to self-motion while PIVC's activity is inhibited in the presence of visual signals, to avoid visual-vestibular conflict. Despite the limits of the adopted brain parcellation that doesn't allow to discriminate between these two subregions, this functional dynamic suggests that, giving the lack of visual cues during the CE task, the presented results reflect the activation of PIVC.

Overall, these findings characterise a cortical network that operates in alpha band and manifests itself in the coordination of a reaction to a mechanical postural challenge in the absence of visual information. The network reconfiguration in the two experimental conditions, in the wake of the postural challenge, was evident in the characteristics of single nodes, namely in their different characterizations as central hubs of the network, as pointed out by the comparison with the baseline nodewise results. These results highlight how in order to counterbalance the disruption of the upright stance and prevent falling, the postural control

system heavily relies on the elaboration of proprioceptive and vestibular information. The asymmetry of the network further suggests the significant involvement of the vestibular cortex, which is characterised by a right hemispheric dominance in right -handed people (the entirety of the analysed cohort) (Brandt and Dieterich, 2015). Moreover, the highly demanding postural task characterised by the lack of visual cues and the consequent challenge presented by the necessity to rely solely on proprioceptive and vestibular information, might explain the predominance of strongly interconnected regions in the right-hemisphere, i.e. the contralateral somatosensory areas to the non-dominant leg (all the participants have in fact identified the right leg as their dominant one). This interpretation is in accord with previous research which linked postural fatigue and absence of visual information with enhanced reliance on somatosensory information from foot and ankle for the control of upright stance (Hlavackova and Vuillerme, 2012). A qualitative inspection of the network resulting from the task edgewise analysis seems to confirm this interpretation, showing significant connections among the same network hubs emerging from the nodewise analysis in the parieto-temporal, vestibular cortex. Nevertheless, at the wider level of network structure, the brain reconfiguration in OE and CE, following the proprioceptive stimulation, was not statistically different from the resting state network before the stimulation. The baseline analysis indicates that the observed differences are most likely related to the presence of visual cues (or lack of thereof). This observation, which requires further investigation, suggests the predominance in the network of those cortical pathways related to the processing of visual information which seem to ‘overshadows’ the effects on the network reconfiguration of vestibular and proprioceptive related strategies to counteract the postural disruption.

### 5.5.3 Flexibility - Complexity correlation

The flexibility of a node is determined by how often its modular affiliation changes over the course of the experiment. Since modules are clusters of highly interconnected nodes often associated with specialised functions, the flexibility of a given node points at the ability of the corresponding brain region to be involved into multiple functions (Kabbara et al., 2019). Prominently among other brain network properties, flexibility has been widely used in literature as a biomarker to capture neuroplasticity differences across individuals and its correlation with cognitive performance has been documented during memory and attention training as well as motor tasks (Bassett et al., 2011; Chapman et al., 2015; Gallen et al., 2016; Reddy et al., 2018).

Previous literature has also highlighted how healthy physiological processes such as postural control are characterised by a complex dynamic and complexity in the fluctuations of the COP signal has been commonly used to investigate the effectiveness of the postural control system (Costa et al., 2002b; Lipsitz and Goldberger, 1992; Manor and Lipsitz, 2013). At the same time, it has been shown how age- or disease-related impairments, associated with worsening postural performance translate into a loss of complexity of the posturographic signal. Thus, if on the one hand, highly flexible networks are associated with greater brain plasticity and the ability to develop adaptive strategies to counteract external disruptive stimuli, on the other hand, more complex COP fluctuations (characterised by higher $S_{EN}$ values) reflect an enhanced automaticity of the postural control system (Donker et al., 2007b). Therefore, the aim of our analysis was to investigate the possible relationship between these two markers of a healthy dynamic postural system, by correlating the flexibility value of each brain region with the sample entropy of the COP trajectory. Brain regions whose flexibility strongly correlates

with the posturographic signal complexity, are likely to play an active role in the cortical functioning of the postural control system.

The correlation between cognitive decline and balance, especially in relationship with the incidence of falls has been extensively discussed in literature (Ambrose et al., 2013; Bolton, 2015; Karim et al., 2014; Muir et al., 2012; Ozdemir et al., 2016). This highlights the necessity of developing targeted therapies to mitigate fall risk as well as the opportunity for the design of neurofeedback strategies aimed at improving postural performances in ageing population or cognitively impaired subjects. In order to do this, it is first necessary to identify the specific cortical regions to target and markers that can be correlated with postural performance. Observing the results, it can be noticed that the regions that displayed a significant correlation with the complexity of the anterior-posterior COP fluctuation encompass predominantly parts of the cingulate, parietal and temporal cortices. The results once again highlight the role of cortical centres of proprioceptive and vestibular processing, with the involvement of APC/PPC and the regions surrounding the lateral sulcus (PIVC). The inferior parietal cortex, whose role in spatial perception and body image neural representation has been previously discussed, appears involved as well. Of particular interest though, is the high correlation that emerged in the cingulate cortex and in the middle temporal and cuneus areas. The posterior cingulate cortex (PCC) has been associated with the main function of visuospatial orientation, and of integrating neural representation of self-location and body ownership acting as a mediator in the interplay between different cortical areas in the parietal and medial temporal regions (Guterstam et al., 2015). Moreover, previous research has shown the PCC's centrality as a node within the default mode network (DMN) and highlighted its high metabolic activity and dense structural connectivity with widespread brain regions which characterise it as a central cortical hub (Leech et al., 2012). Furthermore, it has been suggested that PCC plays an active

role in cognition, as indicated by its reduced metabolism in Alzheimer's disease and ageing patients. While the functions of this cortical regions are still being investigated, there is clear evidence of its involvement in cognition control through signaling of environmental changes (Leech and Sharp, 2014). It appears clear then, how the flexibility of such a deeply interconnected processing hub of the cortex is necessary in order to effectively react to environmental challenges, such as a motor perturbation of equilibrium represents. The results also offer an indication of the likely involvement of certain visual pathways, especially considering the correlation observed between the posturographic signal complexity and the flexibility of cuneus and middle temporal regions. Cuneus is a region of the occipital lobe which is most known for its involvement in basic visual processing and for its role as a mediator in the exchange of visual information between the primary visual cortex (V1) and extrastriate cortices such as the middle temporal visual area (MT/V5) (Vanni et al., 2001). The involvement of the middle temporal gyrus further points towards a possible role of the MT/V5, a functional area of the extrastriate visual cortex located at the boundary with the occipital lobe (Kolster et al., 2010). This area is part of the visual cortex and in particular it is involved in the dorsal visuospatial pathway, also referred to as 'motion' pathway (Gilaie-Dotan et al., 2013). MT is in fact a motion-sensitive cortical region involved in a range of functions including directing attention in the visual environment, integration of local motion signals and kinematic recognition. Its critical role in motion perception has been extensively documented, showing how lesion to MT/V5 adversely affects motion perception (Billino et al., 2009; Vaina et al., 2001). Both cuneus and middle temporal regions play a complex role of mediators in visual processing pathways and project to a number of satellite cortical areas in charge of complementary cognitive functions especially related to motion detection. These characteristics might explain why a more flexible dynamic behaviour in these regions, i.e. their

ability to shift affiliation between different network modules, is reflected in an overall more successful postural strategy, as highlighted by the high correlation values with the SEN of the COP trajectory.

Nevertheless, a note of caution is due in this interpretation, especially concerning the role of the MT/V5 area, as it may be somewhat limited by the anatomical atlas used. In fact, recent tractography-based parcellation of the middle temporal gyrus identified four distinct subregions based on anatomical connectivity, each one being associated with unique functions in a wide range that includes sound recognition, semantic retrieval, language processing and decoding gaze direction (Xu et al., 2015). The aspect of auditory influence on postural control, in particular, has been discussed in previous works and its effects at a cortical network level requires a more in depth investigation (Anton et al., 2020; Petersen et al., 1995). Therefore, the 68-region cortical anatomical atlas employed in this study does not provide the required detail of parcellation that would allow us to positively identify, within the broader middle temporal gyrus region, the specific area involved as the MT/V5 and thus infer with certainty on its direct involvement in the postural control system. Furthermore, it is worth noting that no significant differences in network reorganisation emerged when comparing baseline with task epochs. This might be due to the limited sample size of the current work. A further investigation involving a larger cohort is required to validate the observations presented here, as well as testing the flexibility and complexity metrics in a control study against ageing and impaired subjects.

## 5.6 Conclusions

The goal of this work was to use the tools provided by network neuroscience to identify and shed light on the interplay between cortical regions that are predominantly involved in the high-level coordination of the postural control system, following a mechanical challenge to the participant's upright stance. Indeed, network neuroscience provides a valuable set of analysis tools that can complement the body of postural control literature, providing further insight into the mechanisms that govern brain functions.

The results show differences in the properties of cortical networks, both in individual regions and in the overall connectome structure, during the postural task execution, between the experimental conditions of open and closed eyes. While differences in individual nodes strength are backed by statistical significance, differences in the network connections only provide a qualitative support to the results and require further investigation on a larger cohort. Overall, the results highlight the proprioceptive, vestibular and visual pathways of cortical response that we would expect as a result of the mechanical skeletal muscle perturbation that was applied. In particular, they revealed the different cortical strategies put in place during open and closed eyes task, with a reliance on visual frontal pathways in the former case and vestibular and proprioceptive temporal-parietal pathways in the latter. Moreover, the assessment of the flexibility of cortical regions provides valuable insights on the subject's ability to dynamically reconfigure the modular structure of their cortical network over time, in response to external stimuli or tasks. At the same time, complexity of the posturographic signal has been recognized as a hallmark of a healthy postural control system's ability to respond and adapt to external perturbations and cognitive stressors, reflecting the presence of a "highly adaptable

network of neuro-muscular connections" (Busa and van Emmerik, 2016; Manor and Lipsitz, 2013).

Overall, the fact that high flexibility emerges in the reported regions of the temporal, parietal and cingulate cortex is coherent with their involvement in highly integrative functions characterised by complex interconnections of visual, proprioceptive and vestibular processes. It is interesting to observe how clearly the flexibility index of these regions correlates with a well-established index of postural performance, easily obtainable through posturographic analysis of the body sway. This suggests the possibility of employing the flexibility of those network nodes as a marker to denote a healthy and effective postural control system. Furthermore, in addition to being a neurological diagnostic tool to detect early signs of postural functions decline, it could be of interest in the development of neurofeedback strategies aimed at improving postural performances by enhancing the flexibility of those cortical areas via targeted cognitive training or local stimulation technique

# 6. Proprioceptive vibratory stimulation modulates cortico-muscular postural response

**Abstract—** For decades, postural control has been believed to be dominated by reflexive mechanisms, but more recent evidence characterises it as an articulate system which relies on multisensory integration (vestibular, visual, proprioceptive) and cortical coordination to preserve balance in the wake of external disruptions to the quiet stance. Corrective strategies to stabilise the body's centre of mass and prevent falls are planned at the central nervous system level and executed through the modulation of muscular activity, especially in the lower legs muscles: gastrocnemius, soleus and tibialis. In this study, we use localised proprioceptive vibratory stimulation to induce a perturbation of the subjects' quiet stance. By integrating traditional force plate data with electrophysiological signals (EEG and EMG), we use cortico-muscular and inter-muscular coherence to investigate how brain and muscles interact to shape an effective response to a postural challenge. Our results show how the cortical drive is enhanced in beta [13-30]Hz and gamma [30-45]Hz bands, specifically for the soleus and gastrocnemius muscles, during the task execution. We also reveal a remodulation of the lower legs muscle network, with a distributed strengthening of muscle activity coupling.

**Keywords—** postural control; electroencephalography (EEG); electromyography (EMG); cortico-muscular coherence (CMC); inter-muscular coherence (IMC); proprioceptive stimulation

## 6.1 Introduction

Since the earliest studies at the beginning of the 20th century, human postural control has been believed to be the result of low-level reflexive mechanisms and tonic muscle contractions (Magnus, 1925). This paradigm held for decades, until it was challenged by novel anatomical and behavioural observations. Mounting experimental evidence eventually formed a consensus around a new theory that considers postural control as an articulated system which relies on multisensory integration and higher-level coordination. Indeed, the seemingly effortless act of maintaining balance in a quiet upright stance has been shown to require the active planning of corrective strategies in order to adapt to changes in the surrounding environment, external perturbations and altered sensorial conditions (Fransson, 2005; Patel, 2009). Vestibular, visual, and somatosensory/proprioceptive systems have been shown to play a key role in providing the central nervous system (CNS) with the sensory feedback required to constantly monitor the postural condition (Forbes et al., 2018; F. B. Horak and Macpherson, 1996). The integration of this sensory information at the cortical level is the basis for the development of a corrective strategy. The postural corrective strategy is then executed through cortical modulation of muscle contractions over time, with the aim to adjust the body's centre of mass, thus reducing instability, and ultimately preventing falls. The muscles that are primarily involved in postural control are those of the lower legs (tibialis, soleus and gastrocnemius), which take part in the so-called 'ankle strategy' and help to stabilise the body's position (Horak and Nashner, 1986).

Traditionally, human postural control has been investigated by posturographic means, i.e., by analysing the fluctuations of the centre of pressure (COP) over time during different balance tasks. In this study, we set out to use electroencephalography (EEG) and electromyography

(EMG) to gain a better understanding of the physiological mechanisms shaping human postural control. In particular, we want to explore the relationship between cortical and muscular activity and the way the brain and muscles coordinate to effectively respond to a postural challenge.

Here, the participant's upright stance is disrupted by a randomised sequence of proprioceptive skeletomuscular vibrations applied to the calves. Mechanical vibrations applied to muscles and tendons are a widely-used method to alter the proprioceptive afferent system (Ledin et al., 2003; Malmström et al., 2017; Patel et al., 2009). The application of an external vibration induces the muscle spindles to synchronise to the vibratory stimulation, finally resulting in an increase of the motor unit firing rate (Burke and Schiller, 1976; Hagbarth et al., 1976; Homma et al., 1972). Specifically, the altered proprioceptive feedback tricks the CNS with the illusion of movement and muscles fibres being stretched, resuting in a tonic reflexive response that shortens the muscle fibres while tilting the body in the direction of the vibration (Čapičíková et al., 2006).

To better understand how the efferent cortical drive responds to this kind of postural challenge and to investigate the muscular response, we used two tools: cortico-muscular coherence (CMC) and inter-muscular coherence (IMC) (Boonstra, 2013).

CMC is a common approach to assess the level of interplay between neural signals and muscle activity. It is considered to reflect predominantly the descending efferent corticospinal pathway that carries the neural signal from the pyramidal neurons of the cortex to the spinal motor neurons and eventually controls the muscle fibres activity (Liu et al., 2019). In addition, more recent literature also suggested a role of the ascending afferent system in shaping the CMC, with the proprioceptive signal stemming from muscle receptors and travelling to the

somatosensory cortex (Witham et al., 2011). This is supported by observations of beta band (13-30Hz) synchronisation in the motor and somatosensory cortices (Witham et al., 2007; Witham and Baker, 2007). Consistently, beta band activity has been shown to be a signature of enhanced proprioceptive feedback integration for the maintenance of the ongoing sensorimotor state -or status quo-, which here relates well to the attempt of preserving balance in the wake of a disturbance (Baker, 2007; Engel and Fries, 2010).

IMC is a helpful tool to shed light on the motor control that the CNS exerts through muscles. In particular, it has been hypothesised that the CNS works by flexibly controlling combinations of muscular groups, resulting in so-called muscle synergies (Todorov, 2004; Tresch and Jarc, 2009). The degree to which groups of muscle work together towards a specific task can be observed in the oscillatory patterns of their electrical activity, which reflect common oscillatory inputs from the CNS as well as afferent pathways (Boonstra, 2013). Graph analysis techniques, usually employed in neural network scenarios, proved to be an innovative tool to improve IMC analysis by providing an intuitive representation of the muscular response organisation, in the form of a 'muscle network' (Hassan and Wendling, 2018b; Rubinov and Sporns, 2010). In other words, IMC offers a way to evaluate the functional connectivity between muscles (nodes of the network), allowing the investigation of muscle activity modulation across tasks and experimental conditions, thus highlighting muscle synergies (Boonstra et al., 2015; Kerkman et al., 2020).

In this study, we want to verify whether the postural challenge induced by localised proprioceptive vibrations leads to a shift towards high-level postural control strategy, with enhanced interplay between cortico-muscular signals and a modulation of muscular activity coupling.

## 6.2 Materials and methods

The data presented in this chapter were collected in the same recording sessions as the previous study presented in Chapter 5. EEG, EMG and posturography signals (COP) were captured in a single-group, repeated-measure experimental design.

Experimental data were acquired on 11 young healthy volunteers at Aston University's ALIVE Lab, under the approval of the University Research Ethics Committee (ref: #1432). All participants were recruited among the student population (age = 24.4 ± 5.8, 5 males and 6 females). Criteria for participants' recruitment included a minimum age of 18, no neuromuscular or balance disorders, no physical impediments to the maintenance of a prolonged upright stance and no medications or alcohol consumption during the previous 24 hours.

The first part of the experimental session consisted in participant preparation. The bellies of the soleus (SOL), gastrocnemius lateralis (GL) and tibialis anterior (TA) muscles were identified following the SENIAM guidelines (Stegeman, 2007). Starting from a prone position, participants were asked to perform simple exercises to contract the muscles of interest, as the experimenter measured the distance between predefined anatomical landmarks and marked the position of the muscle bellies on both legs. The skin area around the identified locations was then shaved and cleaned with alcohol wet wipes. Finally, for the recording of surface electromyographic signal, two bipolar Ag/AgCl electrodes were applied to each muscle following the presumed direction of the underlying muscle fibres (*Arbo Solid Gel, KendallTM, CovidienTM* 30 mm x 24 mm, centre-to-centre distance 24 mm). A reference electrode was also applied to the medial malleolus.

A 64-channel EEG cap was adjusted on the participant's head (*AntNeuro, Enschede – Netherlands*) and electroconductive gel was applied to reduce the impedance between the scalp and the Ag/AgCl wet electrodes of the cap, arranged according to a standard 10-20 system montage. Different cap sizes were used to ensure optimal fit and anatomical measures guided the cap placement (CPz electrode centred according to nasion-inion and left-right lobe midline).

The EEG cap was connected to a portable amplifier (EEGOmysport, AntNeuro, Enschede – Netherlands) which the participant carried inside a small backpack. The EMG bipolar electrodes were also connected to the same amplifier through a series of cascaded bipolar adaptors (XS-271.A, XS270.B, XS-270.C)

Finally, two vibrators were secured on the participant's calves and connected to a custom-made actuator box attached to a belt and worn around the waist. The vibrators consisted of two eccentric rotating mass DC motors encapsulated in plastic cylinders (diameter: 30mm, length: 62mm), which delivered an 85Hz vibration. The actuator box, in addition to controlling the vibratory stimulation sequence, also acted as a trigger box connected to the amplifier and the force plate, enabling the synchronisation of the recorded signals with the stimulation epochs.

Participants were finally asked to stand still on a force plate (AMTI OR-6-7, Vicon Motion Systems Ltd, UK), in a natural upright posture, with arms relaxed along the body and facing straight ahead, gazing at a marker on the wall at about 2-meter distance. Each session comprised two identical trials, performed respectively with open and closed eyes (OE, CE), in randomised order and with a 5-minute pause in between.

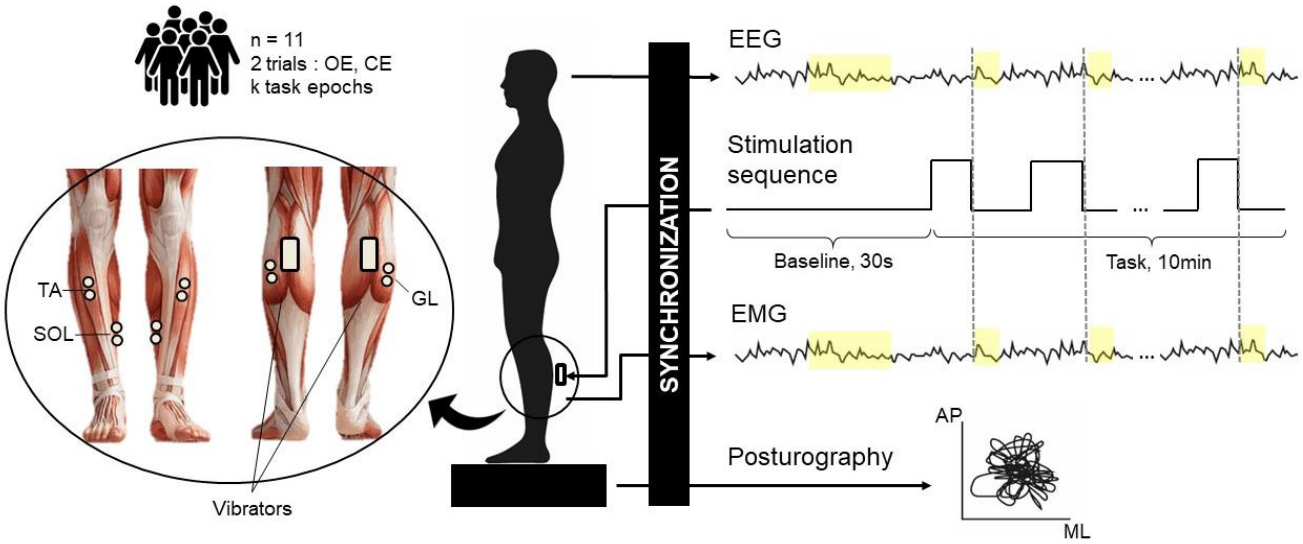


**Figure 6.1.** Schematic representation of the experimental set-up.
The participant was asked to stand on a force platform in a quiet, upright stance. After 30 s of resting state (Baseline), a proprioceptive vibratory stimulation sequence was delivered through vibrators applied to the gastrocnemius muscles of the calves for 10min. The 64-channel EEG data, the EMG signals acquired on the TA, SOL and GL muscles, and the posturographic signal, were synchronized with triggers at the offset of each vibration. These triggers allowed for the definition of 1 second task epochs (highlighted in the figure), which were then concatenated into four quartiles.

Each trial started with 30s of baseline recording during an unperturbed quiet stance. Subsequently, the participant's posture was disrupted by means of proprioceptive stimulation of the skeletal muscles of the calves. The stimulation was delivered for a total duration of 10min, in a randomised binary sequence of vibration and resting periods, with duration uniformly distributed between 1-6s.

## 6.3 Data analysis

### 6.3.1 Preprocessing

The EEG signal was acquired at a sampling frequency of 1000Hz and subsequently preprocessed using custom-made scripts in Matlab ®R2019a (The Mathworks, Inc., Natick,

MA). The preprocessing followed the semi-automated pipeline proposed in CARTOOL (Brunet et al., 2011) and illustrated in the previous chapter (section 5.3.1). First, the signal was filtered with a zero-phase band pass FIR filter between 1-45Hz and the DC offset was removed. The signal was then segmented into epochs of 1s duration, according to the triggers which marked the offset of each vibration period. An EOG regression based on three frontal electrodes (Fp1, FpZ, Fp2) was performed to remove eye blink artefacts from the segmented epochs (Parra et al., 2005). For each epoch, the 'bad channels' were identified as those whose standard deviation (SD) exceeded the average std of a factor greater than 1.7 and replaced with an interpolation of the adjacent channels. Epochs in which more than 15% of the channels were classified as 'bad channels' were discarded. The signal was finally re-referenced to the common average.

The EMG signal was also preprocessed using custom-made Matlab scripts. First, the signal was filtered between 20-250Hz with a zero-phase band-pass Butterworth filter (Roeder et al., 2020) and the 50Hz power line noise was removed with a notch filter. Then, the signal was rectified using a Hilbert transform (Boonstra and Breakspear, 2012). Finally, the acquired signal was segmented into 1s epochs, in the same way as the EEG signal, i.e., according to the triggers which denoted the end of each vibration period, in order to ensure data free from vibration-induced artefacts..

The COP trajectory recorded through the force plate was first detrended and filtered between 0.2-20Hz with a Butterworth filter (Zhou et al., 2016a). Then, the signal was normalised to unit variance (Donker et al., 2007a) and segmented into epochs in the same fashion as the synchronised EEG and EMG signals.

Finally, the central 20s of the initial resting state recording were used to define the baseline epoch, while task epochs of each signal were concatenated into quartiles: Q1, Q2, Q3, Q4.

### 6.3.2 Posturography metrics

The average distance (DIST) and mean velocity (MV) of the COP were extracted from the posturographic data for baseline, Q1 and Q4.

Given the anterior-posterior (AP) and medial lateral (ML) components of the COP sway signal, over a time period of length T, comprising N time points, the average displacement of the COP from the centre of the stabilogram is defined as:

$$DIST = \frac{\sum_{n=1}^{N} \sqrt{AP_n^2 + ML_n^2}}{N}$$

The average velocity of the COP sway is defined as:

$$MV = \frac{\sum_{n=1}^{N} \sqrt{(AP_{n+1} - AP_n)^2 + (ML_{n+1} - ML_n)^2}}{T}$$

A Wilcoxon signed-ranked test was performed to check for statistically significant variations in these metrics, between baseline and Q1, and between Q1 and Q4. The computed p-values were then corrected for multiple comparisons with FDR (correction over 2 metrics and 2 tests).

### 6.3.3 Cortico-muscular Coherence

The magnitude-squared coherence spectrum between EEG and EMG signals was computed to quantify the similarity of their frequency and phase content. For every subject, CMC was computed in beta band [13-30] Hz, for all the possible pairs of EMG and EEG channels (6 and

60, respectively), in baseline, Q1 and Q4, for the two experimental conditions (OE and CE). The coherence signal was computed as follows:

$$C_{xy}(f) = \frac{|P_{xy}(f)|^2}{P_{xx}(f)P_{yy}(f)}$$

Where $P_{xy}$ is the cross-spectral density between the two signals (Fourier transform of the cross-correlation), $P_{xx}$ is the power spectral density (PSD) of the EEG signal and $P_{yy}$ is the PSD of the EMG signal. The PSD was estimated via Welch's periodogram method (Welch, 1967), segmenting the epochs using non-overlapping Hamming windows with duration of one second (Jacobs et al., 2015). To verify the presence of statistically significant changes in the coherence spectra following the administration of the proprioceptive vibratory stimulation, a cluster-based permutation test was performed between the coherence spectra computed during the resting state period (baseline) and during the first quartile of the postural task (Q1). To investigate potential changes in cortico-muscular strategies over the course of the trial, as a result of habituation processes, a cluster-based permutation test was also performed between the first and last quartile of the task trial (Q1 and Q4, respectively).

The cluster-based permutation test was performed in the channel and frequency dimensions, with the aim to identify clusters of neighbouring EEG electrodes whose coherence with a specific muscle showed a statistically significant difference during the execution of the postural task compared to the resting state. The test was carried out in Fieldtrip (Oostenveld et al., 2011) using 2000 permutations and comparisons were run in the beta and gamma frequency ranges. The cluster-based permutation test is a widely-used statistical tool particularly well-suited for the analysis of time-frequency series, in that it does not require assumptions about the data distribution, it allows physiologically plausible constrains to be factored in (by

clustering significant effects within neighbouring channels, frequency bins, or time points), and it deals with the multiple comparison problem without diminishing the statistical power as much as more conservative correction methods.

Finally, the average CMC spectra in the two compared periods (baseline/Q1 or Q1/Q4) were computed across the identified clusters of EEG electrodes and plotted with the respective standard deviation (SD).

### 6.3.4 Intermuscular Connectivity

IMC was also computed among EMG channels as a measure to estimate the degree to which the activity of couples of muscles is coordinated. This allowed the participant's lower leg muscles to be represented as a network in which each muscle represents a node (n=6). The number of edges of the network is determined by the number of possible pairs (k=2) of muscles as:

$$C_{n,k} = \frac{n!}{k!\,(n-k)!} = 15$$

The PSD of the EMG signal was estimated on overlapping 1s windows using Welch's method (75% overlap) and the magnitude-squared coherence was computed between [0-40] Hz (Boonstra et al., 2015). This process was repeated for each of the 15 pairs of muscles in baseline, Q1 and Q4, in both experimental conditions. To isolate the contribution of different frequency components, a non-negative matrix factorisation (NNMF) approach was used. A NNMF iterative algorithm (5000 iterations) decomposed the coherence spectra into 5 frequency components and a set of associated weights. NNMF is a dimension-reduction

technique that guarantees the non-negativity of the extracted components. Given the matrix of coherence spectra X, the algorithm returns two matrices W and H such that:

$$X = W \cdot H$$

and the norm of the difference $X - WH$ is minimised. The 5 columns of W contain the extracted frequency components, while the 5 rows of H contain the weights associated with the linear combination of the components. The original matrix X was created by concatenating coherence spectra of each participant, for each muscle pair, in each experimental condition. This ensured that the NNMF process resulted in the same frequency components, allowing for statistical comparison among subjects and trials.

The weight matrix H was then reshaped for every subject into 5 $[n \times n]$ connectivity matrices, one for each frequency component, with n being the number of muscles. The connectivity matrices so obtained were then used to perform a node-wise and edge-wise analysis on the lower leg muscle network.

For the node-wise analysis, 3 network metrics were extracted from each adjacency matrix, for each of the 6 nodes of the network: clustering coefficient (CC), local efficiency (LE) and strength (STR). For every muscle, differences in network metrics between baseline and Q1, and between Q1 and Q4 were tested with a two-tailed Wilcoxon signed-rank test. A false discovery rate (FDR) correction was applied on the resulting p-values to correct for multiple comparisons (procedure applied over 30 multiple comparisons, resulting from nodes/muscles times frequency components).

The edge-wise analysis consisted in a statistical comparison among connectivity matrices, to highlight significant changes in connectivity values in specific edges of the network. Differences were tested with a two-tailed Wilcoxon signed-rank test; p-values were corrected for multiple comparisons using FDR (procedure applied over 75 multiple comparisons, resulting from edges/muscle pairs times frequency components).

## 6.4 Results

### 6.4.1 Posturography results

The posturography results are reported in table 6.1 and illustrated in figure 6.2. The box plots show the distribution of DIST and MV values in baseline, Q1 and Q4, in the two experimental conditions (OE and CE). In both conditions, a significant increase in DIST and MV can be observed between baseline and Q1, with the associated p-values ($p<0.05$) reported in the figure. No significant variation in posturography metrics can be observed between the first and last quartile of the postural task, except for a slight increase in COP mean distance during the open-eyes trial.

**Table 6.1.** Posturography results.
The average values of COP mean distance (DIST) and mean velocity (MV) are reported in the table, with their standard deviation interval, for baseline, Q1 and Q4, in the two experimental conditions (CE and OE).

| | CE | | | OE | | |
|---|---|---|---|---|---|---|
| | **Base** | **Q1** | **Q4** | **Base** | **Q1** | **Q4** |
| **DIST** | 0.735 ± 0.317 | 1.546±0.432 | 1.443±0.132 | 0.882±0.429 | 1.310±0.257 | 1.499±0.292 |
| **MV** | 4.132±2.3414 | 8.236±3.807 | 7.537 ±1.873 | 6.415±7.429 | 9.183±7.383 | 10.036±7.746 |

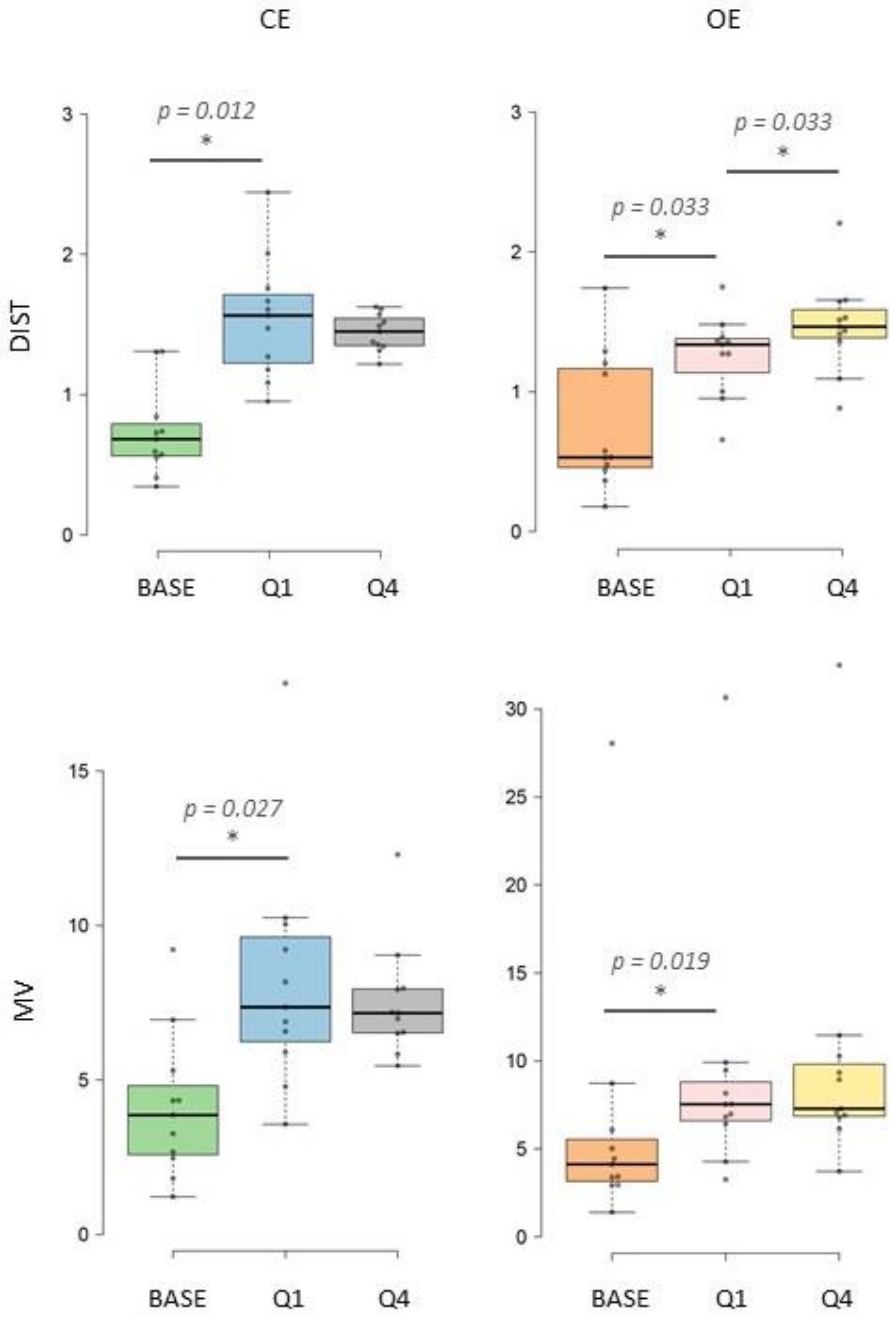


**Figure 6.2.** Posturography results. The box plots depict the distribution of 11 sample points for the posturography metrics: DIST (first row) and MV (second row), in baseline, first and last quartile (BASE, Q1 and Q4 respectively). Results during the closed-eyes trial are reported in the left column, results during open-eyes trial are reported in the right column. Centre lines show the medians; box limits indicate the 25th and 75th percentiles, sample points are represented by dots. Significant differences between BASE and Q1, or between Q1 and Q4 are indicated by a star. Significant p-values ($p<0.05$) are also reported.

### 6.4.2 CMC results

Figures 6.3 - 6.5 provide an overview of the results of the cluster -based permutation tests performed on cortico-muscular coherence spectra.

Three muscles showed a significant increase in CMC in beta band during the first quartile of the CE trial compared to baseline, as observed in Fig 6.3. The coherence between the left TA and a cluster of 14 central-occipital electrodes resulted significantly higher in Q1, in the frequency bin centreed at 21.48Hz ($p = 0.0235$). The SOL muscles of both legs also showed a significant increase in Q1. Specifically, CMC between the left SOL and a cluster of 15 central electrodes was found to be significantly higher at 20.51Hz ($p = 0.015$). For the right SOL, significant differences were found on two adjacent frequency bins at [19.53 – 20.51] Hz, involving two overlapping clusters of central electrodes ($p = 0.01$). During the OE trial, the only significant result emerged in the beta band, for the right TA muscle, as shown in figure 6.4. The CMC spectra in Q1 and baseline, computed between the right TA and a cluster of 9 occipital electrodes, mostly overlaps throughout the beta band. However, in the 25.39 Hz frequency bin, a significant decrease in CMC during Q1 was detected ($p = 0.013$). The cluster-based permutation test performed in the gamma band [30-40] Hz, highlighted only one significant comparison, during the CE trial, as shown in figure 6.5. The CMC of the left GL muscle was found to significantly increase in Q1 compared to baseline in two adjacent frequency bins: [41.02 -42] Hz ($p = 0.005$). As shown by the topographies the results involve two overlapping clusters of central electrodes.

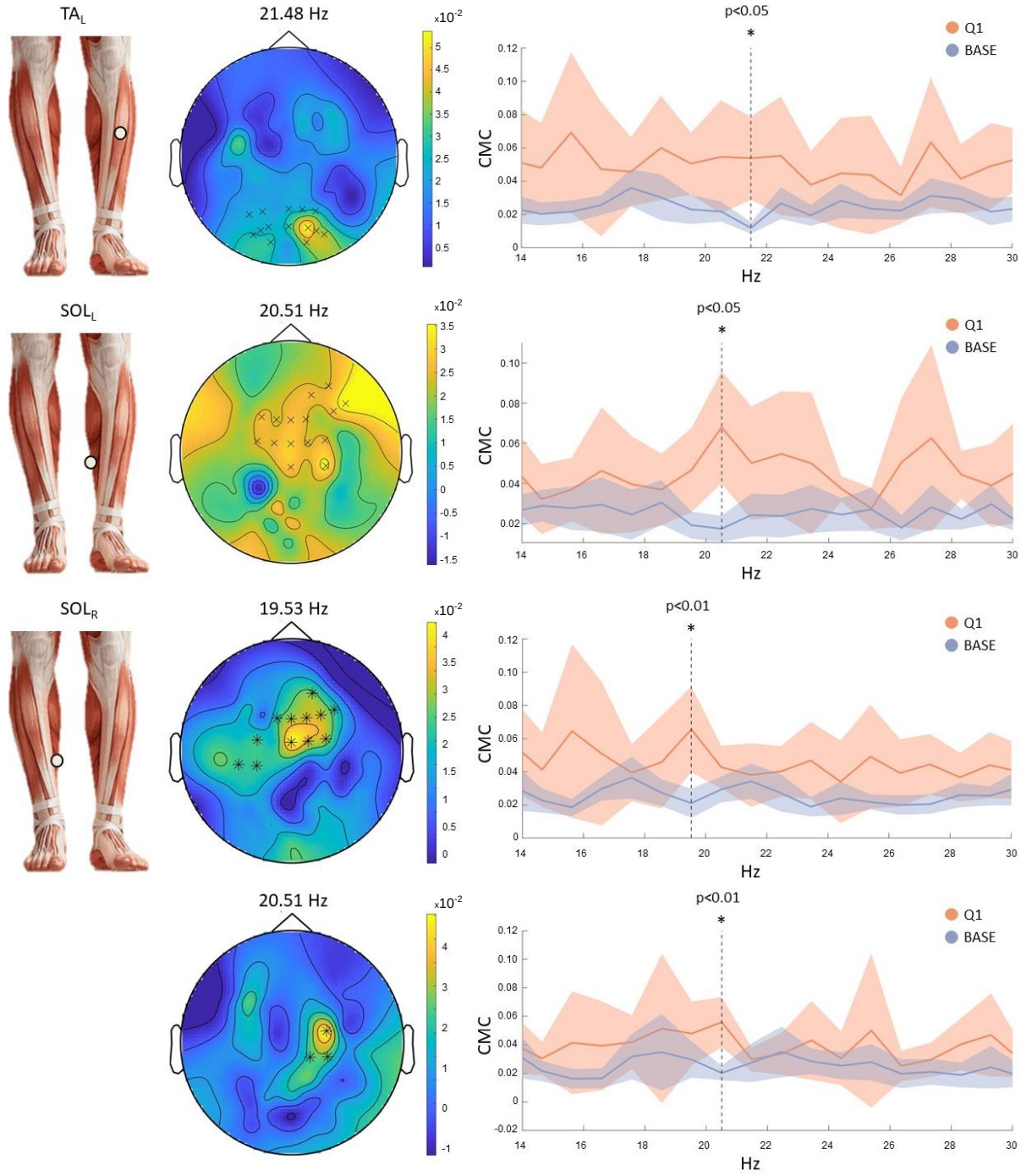


**Figure 6.3.** CMC results - Beta, Closed eyes.

Each row depicts a pair of muscle and EEG electrodes cluster, whose CMC signal showed a significant difference between BASE and Q1 in one or multiple (consecutive) frequency bins. The first column shows the muscle electrode position on the participant's lower legs. The second column depicts the location of the electrode clusters on the scalp, overlayed to the topographical distribution of CMC differences (BASE vs. Q1) in the specific frequency bin. If the p-value associated with the cluster is p<0.05, electrodes are marked with an 'X'; if p <0.01, electrodes are marked with a '*'. The third column shows the CMC signals, averaged across the cluster's electrodes, in Q1 and baseline, over the whole beta frequency band. The coloured area denotes the SD interval and a dashed line marks the frequency bin who resulted in a significant CMC difference.

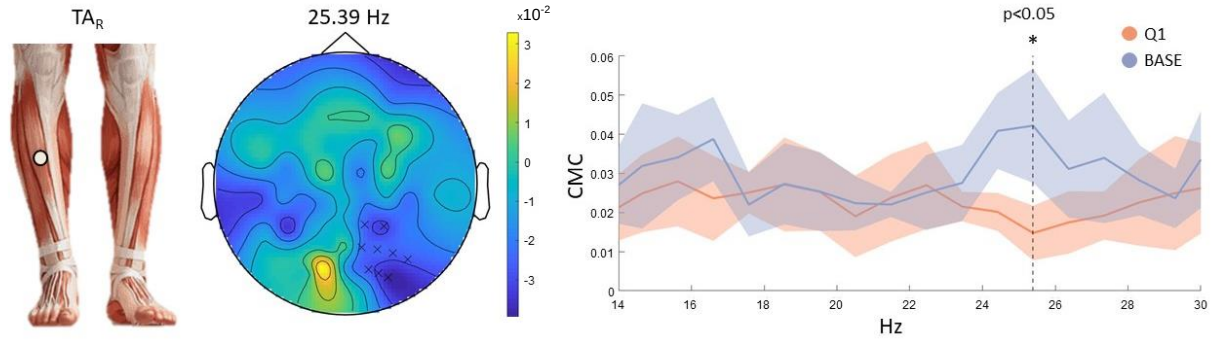


**Figure 6.4.** Beta, Open eyes.

The figure shows the CMC results for the right TA muscle (first column), whose CMC signal with the cluster of electrodes depicted in the topography (second column) showed a significant difference between BASE and Q1 at 25.39Hz. The first column shows the muscle electrode position on the participant's lower legs. The second column depicts the location of the electrode clusters on the scalp, overlayed to the topographical distribution of CMC differences (BASE vs. Q1) in the specific frequency bin. If the p-value associated with the cluster is p<0.05, electrodes are marked with an 'X'; if p <0.01, electrodes are marked with a '*'. The third column shows the CMC signals, averaged across the cluster's electrodes, in Q1 and baseline, over the whole beta frequency band. The coloured area denotes the SD interval and a dashed line marks the frequency bin who resulted in a significant CMC difference.

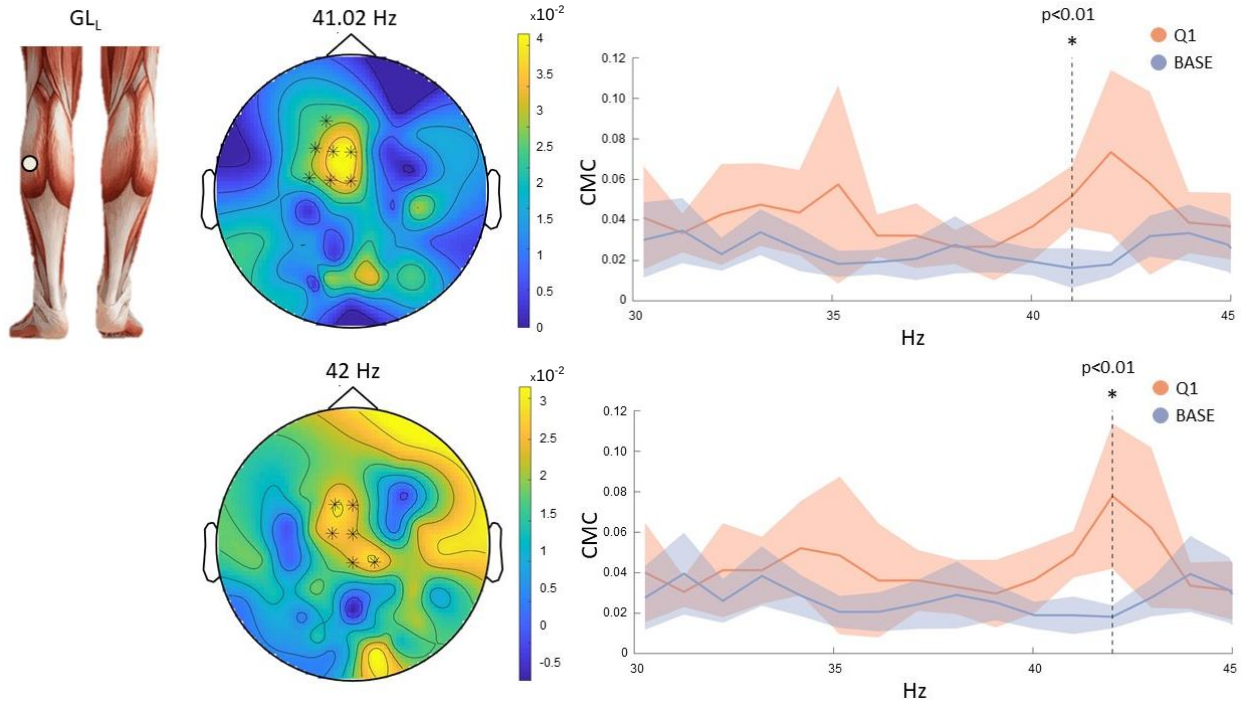


**Figure 6.5.** Gamma, Closed eyes.

The figure shows the CMC results for the left GL muscle (first column), whose CMC signal with the cluster of electrodes depicted in the topographies (second column) showed a significant difference between BASE and Q1 at 41.02Hz and 42Hz (first and second row respectively). The first column shows the muscle electrode position on the participant's lower legs. The second column depicts the location of the electrode clusters on the scalp, overlayed to the topographical distribution of CMC differences (BASE vs. Q1) in the specific frequency bin. If the p-value associated with the cluster is p<0.05, electrodes are marked with an 'X'; if p <0.01, electrodes are marked with a '*'. The third column shows the CMC signals, averaged across the cluster's electrodes, in Q1 and baseline, over the whole beta frequency band. The colored area denotes the SD interval and a dashed line marks the frequency bin who resulted in a significant CMC difference.

### 6.4.3 IMC results

#### Edgewise

The results of the IMC edgewise analysis are summarised in figures 6.6 and 6.7, for the closed eyes and open eyes trials respectively.

Each row of the figures reports the network edgewise results associated with one of the five frequency components obtained through the NNMF of the inter-muscular coherence spectra. The frequency components are reported in the first column. The second and third columns report the adjacency matrices computed in baseline and Q1, respectively, averaged across subjects. These 6x6 matrices contain the connectivity values across pairs of muscles. The fourth column depicts the muscle network itself, where each of the 6 nodes corresponds to a muscle. For the sake of visual interpretation, the network is superimposed on the silhouette of a participant's lower legs (with the participant standing facing the reader). The networks reported in the fourth column result from the statistical analysis that was conducted on the edges. They highlight edges which showed a significant variation ($p<0.05$) between baseline and Q1. In particular, increased connectivity values in Q1 are marked with green lines, while decreased connectivity values are marked in red. The edge thickness is proportional to the percent variation.

The first frequency component is dominated by very low frequencies around 0 Hz and because of its amplitude and scale, it is more likely to reflect an artefactual pattern rather than a physiological mechanism. The second component is the smallest in amplitude but is widespread across the whole frequency band analysed, with greater values in the beta and early gamma band. The last three components have comparable amplitudes and are

characterised by clearer frequency bands. The third one peaks around 5Hz and 15 Hz. The fourth component is dominated by a 2 Hz contribution, while the fifth one is centreed around 10 Hz.

The results of both experimental conditions show, in the first two frequency components, a generalised decrease in network connectivity in Q1. Specifically, the reduced connection weights are appreciable across all muscles, both infra- and intra- leg (see Figure 6.6 and 6.7, first and second rows). In the remaining three frequency components, on the other hand, the results show a generalised increment of connectivity across the network in Q1 compared to baseline. Consistently across OE and CE trials, the connection weights between muscles belonging to the same leg do not change between baseline and Q1, while the connections weights between bilateral muscles increases steadily across the three components.

No significant differences resulted from the comparison of the muscle networks obtained during Q1 and those obtained during Q4.

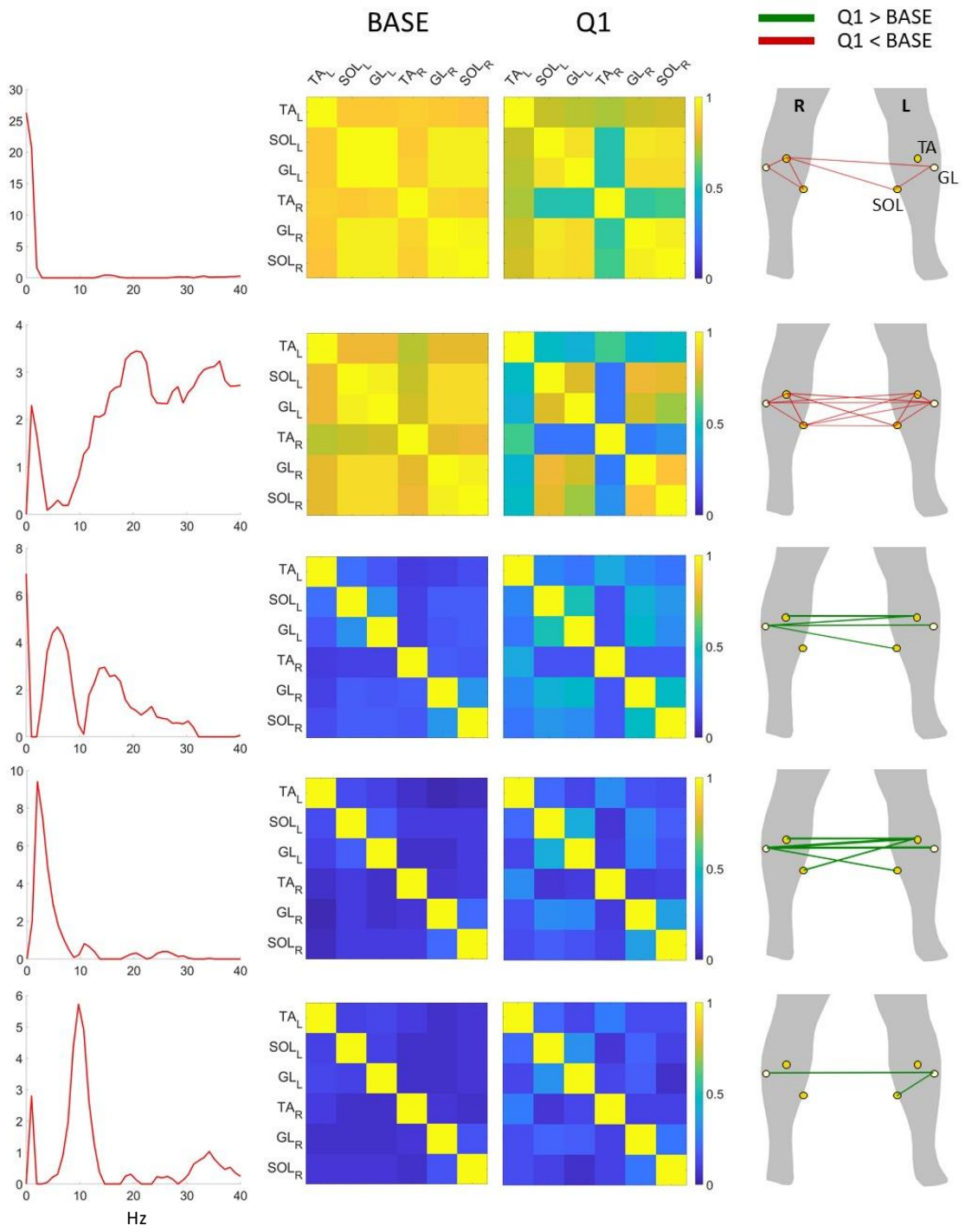


**Figure 6.6.** IMC edgewise results - Closed eyes.

Each row corresponds to one of the five frequency components resulting from the NNMF of the coherence spectra. The first column shows the frequency components themselves, defined between [0-40] Hz. The second and third columns display the adjacency matrices, averaged across subjects, during baseline and Q1 respectively. The fourth column depicts the muscle network resulting from the statistical analysis, which highlights edges that showed a significant variation in connectivity values between baseline and Q1 ($p<0.05$, FDR corrected). Specifically, green edges indicate increased connectivity in Q1 compared to baseline, while red edges indicate decreased connectivity. The thickness of the network edges is proportional to the percent of variation.

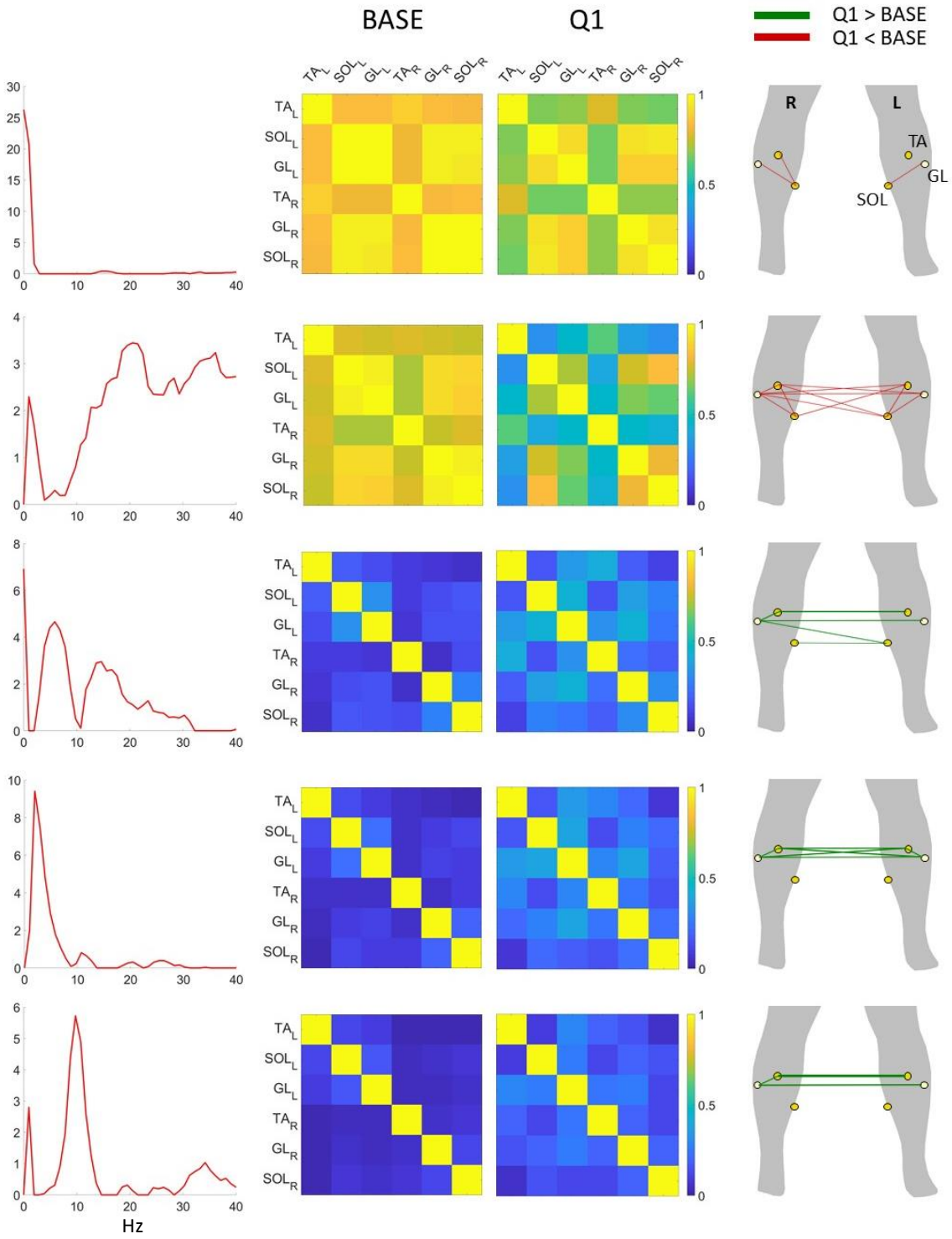


**Figure 6.7.** IMC Edgewise - Open eyes.

Each row corresponds to one of the five frequency components resulting from the NNMF of the coherence spectra. The first column shows the frequency components themselves, defined between [0-40] Hz. The second and third columns display the adjacency matrices, averaged across subjects, during baseline and Q1 respectively. The fourth column depicts the muscle network resulting from the statistical analysis, which highlights edges that showed a significant variation in connectivity values between baseline and Q1 ($p<0.05$, FDR corrected). Specifically, green edges indicate increased connectivity in Q1 compared to baseline, while red edges indicate decreased connectivity. The thickness of the network edges is proportional to the percent of variation.

**Nodewise**

The nodewise results are reported in figures 6.8 and 6.9, for the closed eyes and open eyes trials, respectively. Each row corresponds to the results for a specific frequency component, depicted in the first row. Columns 2, 3 and 4 show the significant variations, at a node level, in three network metrics: clustering coefficient (CC), local efficiency (LE) and strength (STR). Green nodes represent an increase in the specific network metric value, while red nodes indicate a decrease. The size of the node is proportional to the percent variation.

Trials in the two experimental conditions (open and closed eyes) show similar patterns. The first two frequency components are associated with a slight but generalised decline in all the three metrics measured in Q1 compared to those measured at the baseline. The remaining three frequency components, on the other hand, see a consistent increase of CC, LE and STR. In particular, at low frequencies (~2Hz), which is represented by the fourth components, a substantial increase in CC and LE can be observed for the TA and GL muscles of both legs in Q1 compared to baseline. Increased values can then be observed over all the network metrics for the GL muscles in the fifth components (with peaks at 1Hz and 10Hz). Moreover, although all significant, the changes observed for the last three components are more substantial than those observed for the first two components, especially around 2-10 Hz, for the TA and the GL.

No significant differences resulted from the comparison of the network metrics obtained during Q1 and those obtained during Q4.

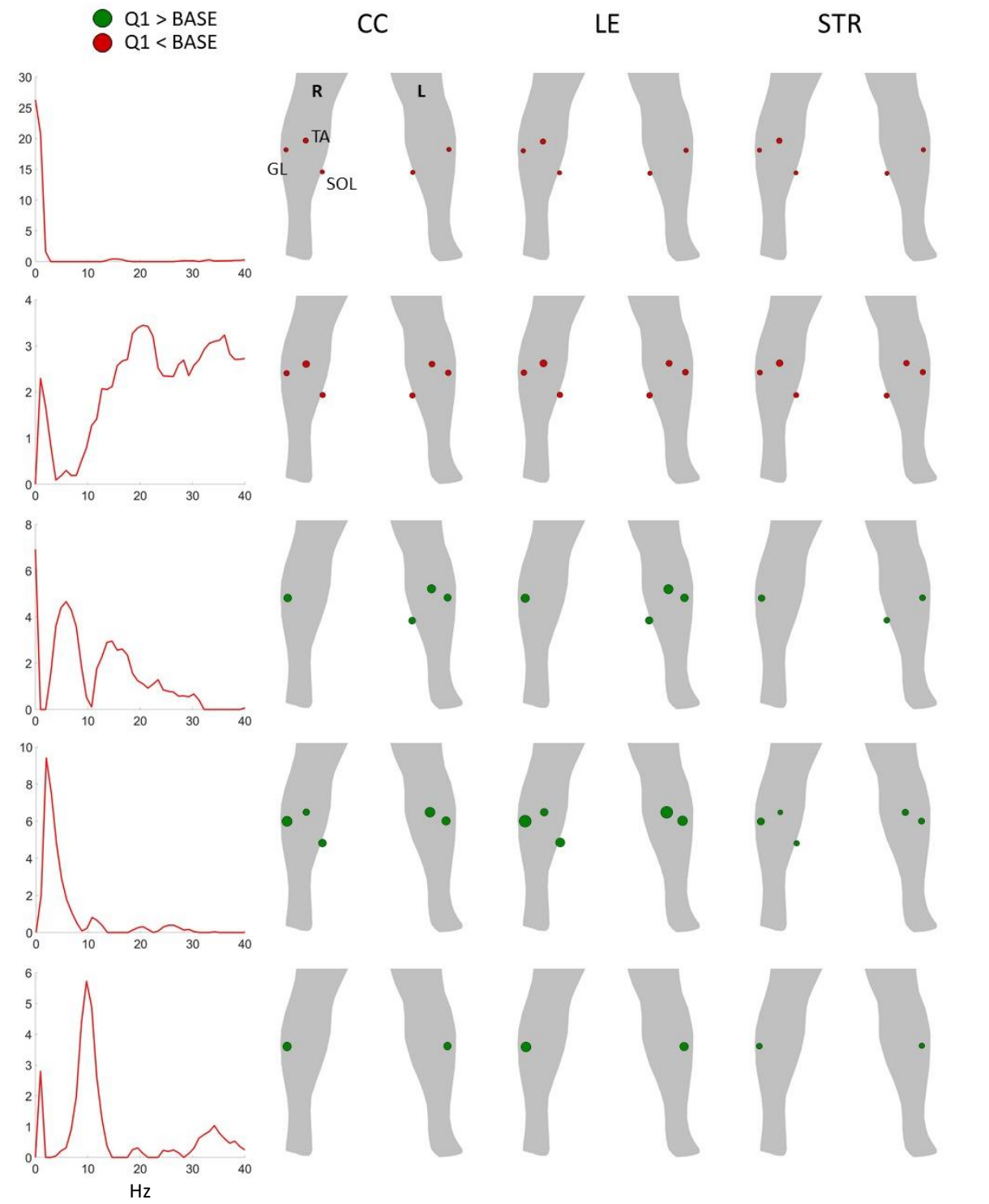


**Figure 6.8.** IMC nodewise results - Closed eyes.

Each row corresponds to one of the five frequency components resulting from the NNMF of the coherence spectra. The first column shows the frequency components themselves, defined between [0-40] Hz. The second, third and fourth columns show, respectively, the significant changes ($p<0.05$, FDR corrected) for clustering coefficient (CC), local efficiency (LE) and strength (STR), between baseline and Q1. Specifically, green nodes denote an increased value for the corresponding muscle in Q1 compared to the baseline value. Red nodes denote a decreased value. The size of the nodes is proportional to the percent of variation.

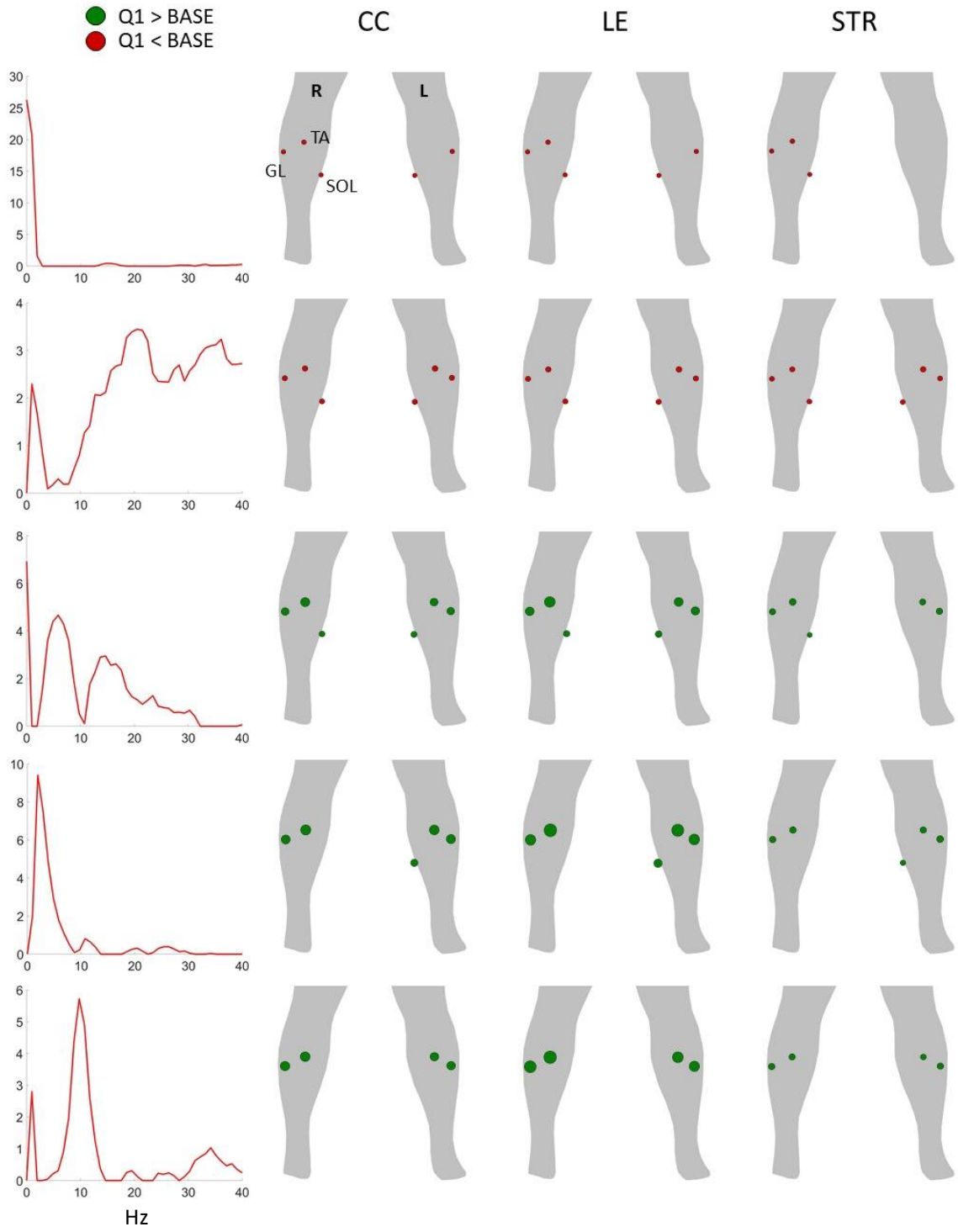


**Figure 6.9.** IMC nodewise results - Open eyes.

Each row corresponds to one of the five frequency components resulting from the NNMF of the coherence spectra. The first column shows the frequency components themselves, defined between [0-40] Hz. The second, third and fourth columns show, respectively, the significant changes ($p<0.05$, FDR corrected) for clustering coefficient (CC), local efficiency (LE) and strength (STR), between baseline and Q1. Specifically, green nodes denote an increased value for the corresponding muscle in Q1 compared to the baseline value. Red nodes denote a decreased value. The size of the nodes is proportional to the percent of variation.

## 6.5 Discussion

In line with expectations, the analysis of the COP sway confirmed the disruptive effect that proprioceptive vibration of the calves has on the participants' quiet stance. In both experimental conditions, the administration of the localised vibratory sequence resulted in an increased COP DIST and MV, which together reveal a decreased ability to maintain balance during Q1 compared to the resting state (BASE) (Palmieri-Smith et al., 2002). Interestingly, no significant difference was observed in the posturographic response between the initial and final phases of the trial (Q1 and Q4). With the exception of a slight but statistically significant increase of DIST during the OE task, the last quartile showed negligible postural variation when compared to Q1. These data, therefore, cannot support the presence of the phenomenon that has been termed 'habituation' in previous literature, and describes an adjustment in motor control strategies following the prolonged or repeated exposure to external perturbations or changing of environment (Fransson, 2005).

This seems to be further confirmed by the results of cortico-muscular and inter-muscular coherence, where no significant difference emerged in any of the considered metrics between Q1 and Q4.

Cortico-muscular coherence is a technique traditionally used to analyse the cortical drive to the muscles, i.e. the descending neural signal that modulates muscle activation (Halliday et al., 1995). Studies on the phase lags of CMC signals showed their consistency with the conduction time between motor cortex and muscles, reinforcing the idea that CMC reflects the drive that cortical processes exert on motor neurons (Gross et al., 2000; Negro and Farina, 2011). Previous literature also established beta and low gamma bands (13-30 Hz and 30-

45Hz, respectively) as the primary frequency range where neuromuscular coupling effects can be observed, showing how different types of muscle movements modulate the speed of cortico-muscular oscillations (Gwin and Ferris, 2012; Liu et al., 2019; Reyes et al., 2017).

The investigation conducted in this study focused on those muscles (GL and SOL) which are mostly involved in the postural stabilisation mechanism defined as 'ankle strategy', the primary one used to reposition the centre of gravity either during quiet stance or in response to external perturbations (Gatev et al., 1999; Winter, 1995). Being a dorsiflexor, the TA was also included to fully characterise the muscle response to the vibratory stimulation. The most significant results were observed during the CE trial. As depicted in figure 6.3, the results display a consistent increase in CMC, spread throughout the beta band, for the SOL muscles after the administration of the proprioceptive vibration, compared to resting state. A statistically significant difference in CMC, identified by the cluster-based permutation test in the frequency bins around 20Hz, is consistent with what was reported in previous literature (Baker, 2007). The same pattern can be observed for GL in the gamma band (see fig 6.5) (Gwin and Ferris, 2012). While beta-band CMC has been traditionally associated with static force output, gamma-band CMC has been reported during strong contractions and dynamic force (Gwin and Ferris, 2012). In addition, it has been shown how superficial extensor muscles, such as GL, are characterised by higher contraction frequency than deep extensors such as SOL (Honma and Seki, 1964).

The results of SOL and GL support the fact that the response to a disruptive proprioceptive vibration evokes an enhanced cortico-muscular coupling, particularly observable in correspondence with more challenging tasks such as the CE trial. The lack of visual input, a key afferent in the postural control system, seems to make a greater degree of high-level

control necessary, as reflected by the increased CMC which suggest a lower degree of automaticity in the execution of the task (Peterson and Ferris, 2019).

From a statistical standpoint, the observed results are particularly significant ($p<0.01$) in the GL and SOL muscles of the dominant leg (right). On the other hand, the results for the TA muscle in beta (OE and CE) present a higher p-val ($p<0.05$) and a criticality in the location of the associated electrode clusters in the scalp topography. Indeed, while the electrode clusters identified in the CMC results of SOL in beta band and GL in gamma band are located in the central area of the scalp topography, which is spatially coherent with the underlying motor cortical area (primary and supplementary motor cortex) where the cortical drive is originated, the TA results show an occipital-region cluster whose electrodes are unlikely to pick up electrical activity from the motor cortex (Melnik et al., 2017; Sreeja et al., 2017). For these reasons, it is possible that the TA results do not actually correspond to a cortico-muscular coupling effect, but instead represent some other type of not fully understood synchronisation mechanism.

The results of the IMC analysis provide further insight into the postural mechanisms that take place to counteract the imbalance caused by the proprioceptive vibration. Here, the IMC signals computed between pairs of muscles were decomposed into 5 frequency components, and the sets of weights associated with each component were used as a metric of connectivity in determining the networks of lower leg muscles. By comparing the resting state network topography with that recorded during execution of the postural task, we evaluated how the network reconfigured itself to shape a more effective postural strategy. The network topography highlights the groups of muscles whose activity is synchronized, showing the muscles involvement in common muscle synergies (Boonstra, 2013).

Looking at the results reported in figure 6.6 and 6.7 it can be noticed that the adjacency matrices associated with the first two frequency components identified by the NNMF, present high (~1) and most likely non-physiological connectivity values in both baseline and Q1 (Boonstra et al., 2015). The distribution over the frequency band of these two components (the first dominated by ~0Hz and the second spread all over the band) further points to their artefactual nature.

Consistent with the previous results, significant differences in connectivity values and network metrics emerged among baseline and Q1. However, in this case, significant changes were observed during the OE trial as well as during the CE one (figure 6.6 and 6.7). In particular, higher connectivity values were observed during the execution of the postural task, as well as increased network metrics. The increased connectivity observed in the third frequency component supports the previously reported CMC-based results by confirming, even from a muscular network perspective, a stronger cortical drive expressed in terms of enhanced muscular synergies, IMC in the 16-40 Hz range is in fact thought to have a cortical origin (Nandi 2019). Because IMC does not reflect only cortical drive to the muscles, but also common afferent inputs (Boonstra 2013), the increased connectivity observed in the 6-15 Hz range (fifth component) and in the 0-5 Hz one (fourth component) could also reflect an increased inflow of subcortical inputs too (Nandi et al., 2019).

The fact that not only cortical, but also afferent inputs are enhanced during the task execution, thus contributing to shape the postural response, is in line with the well-known fact that vibrations applied to the muscle bellies induce a stimulation of the muscle spindles (Burke et al., 1976b). Therefore, these proprioceptive structures are likely to be more sensitive

immediately after the stimulation, increase the sensory input inflow and provide a larger contribution to the modulation of muscle activation, as suggested by our results.

In addition, the nodewise analysis highlights a strong increase in the clustering coefficient and local efficiency of the tibialis and gastrocnemius muscles in the low frequencies, around 2Hz (third frequency component, see figures 6.8 and 6.9). CC and LE are related network metrics which characterise the density of the network around a certain node by quantifying, respectively, the tendency of a node to form a cluster and the density of connections within the cluster (inverse of the shortest path length). A strengthening of the network at this low frequency (<5Hz) is consistent with results reported in previous IMC studies during balance tasks (Boonstra et al., 2008, 2015; Peterson and Ferris, 2019).

In the present discussion, a note of caution must be introduced concerning a number of factors which limit the ability to provide a univocal interpretation of the presented results. From a methodological point of view, both CMC and IMC techniques present some limitations, specifically the arbitrariness in the choice of the number of frequency components to use in the IMC analysis, as well as the intrinsic limitations in NNMF procedures themselves. As far as the results interpretation is concerned, the underlying mechanisms of CMC and IMC are still debated and not fully understood (Boonstra, 2013). Furthermore, these techniques have been traditionally used in motor tasks involving voluntary movements and steady-state contractions such as grip, but not as extensively in balance or postural control tasks (Omlor et al., 2007; Ushiyama et al., 2017; Watanabe et al., 2020). The literature on the topic also lacks an extensive review of the factors affecting CMC and IMC, which explains the variability observed across experimental designs, individuals etc. Finally, the current data are based on a limited cohort of young, healthy individuals. It will be of great interest to conduct further

investigation on different subpopulations (such as ageing individuals) to compare the cortico-muscular recalibration strategies in the wake of the same postural challenge.

## 6.6 Conclusions

Our results show how proprioceptive mechanical vibratory stimulation of the calves causes a disruption of the quiet upright stance, which is met with the execution of a postural responsive mechanism to prevent falling. Cortico-muscular coherence analyses revealed how the stimulation of the proprioceptive system increased the higher-level modulation required to maintain balance. This is true especially during more challenging postural tasks (e.g., eyes closed), where increased CMC levels are likely to reflect the presence of more cortical modulation and more direct cortical control of muscular activation. This is observable in the GL and SOL muscles (particularly those of the dominant leg), which are known to shape the primary mechanical postural responses of the ankle strategy.

The stimulation of the proprioceptive system via means of focal vibrations led to a clear change in the control strategies adopted to shape the postural response. Not only the cortical drive modulating the recruitment of muscle synergies increased, but also the subcortical, or spinal, control of muscle groups increased, which is likely to be explained by the increased sensitivity of muscle spindle induced by the stimulation itself.

More interestingly, no changes were observed in the recruiting mechanism over the course of the task. The previously proposed concept of habituation is therefore not supported by the conducted analyses, where the same muscle networks were observed across frequency components over Q1 and Q4.

Some methodological limitations and the lack of extensive supporting literature make the interpretation of the results challenging. However, it will be beneficial to further this work by performing a comparative assessment on groups of subjects with impaired postural control, with the aim of identifying how the postural response differs in these subjects in terms of cortico-muscular synergies.

# 7. General Discussion and Conclusions

This Chapter provides an overarching analysis of the key findings presented in this thesis, as well as the main discussion points raised in the three experimental chapters (Chapters 4, 5 and 6). The limitations of the presented studies are also discussed here, as well as lessons learned and recommendations for future developments of this line of postural research.

## 7.1 General Discussion

### 7.1.1 Study 1

As described in Chapter 4, our investigation started by adapting a well-established experimental set-up in which the quiet upright stance of the participant is disrupted by means of muskoloskeletal proprioceptive vibrations (Edmunds et al., 2019; Fransson, 2005; Patel et al., 2009). The original equipment, developed at Lund University (Sweden), comprised a force plate and a stimulation device which controlled two vibrating cylinders for the administration of the proprioceptive stimulation. The set-up was then integrated with a HD-EEG acquisition system by *AntNeuro mylab* and a trigger box for the synchronisation of posturographic and EEG signals.

The aim of this first study was to investigate the spectral power variations in the EEG signal over the course of a postural control task, thus expanding the limited existing literature on the topic. In particular, the focus was on the identification of cortical correlates of the concepts of adaptation and habituation, which were presented in previous literature based on posturography-oriented studies (Fransson, 2005). For this reason, the trial (30s of quiet stance followed by 300s of stimulation) was split into five periods (Baseline, P1, P2, P3, P4) and ASP was compared between baseline and P1, denoted as adaptation, and P1 and P3, denoted as habituation. The choice of the third task period as the focus of investigation for habituation

dynamics was made based on posturographic data, specifically the SPL of the COP sway, which showed the lowest value in that period.

Indeed, the EEG-based analysis conducted on the collected data, highlighted significant variations in ASP in the so-defined phases of adaptation and habituation, during the experimental conditions of open and closed eyes. In particualr, the alpha and theta frequency bands showed a statistically significant ASP increase across widespread regions of the scalp. In accordance with previous studies (Hülsdünker et al., 2015; Solis-Escalante et al., 2019b), different topographical patterns were observed in the theta band adaptation phase when comparing the CE and OE trials: increased ASP values involved frontal-central regions in the former condition and parietal regions in the latter. The modulation of theta activity, particularly in the frontal-central regions, could be related to the planning of a corrective strategy, as suggested by previous literature that linked it to mechanisms of error detection and processing of postural stability (Adkin et al., 2008; Slobounov et al., 2009). Conversely, the observed variation in alpha activity during the habituation phase could relate to the inhibition of the error detection process in the cingulate cortex (Edmunds et al., 2019).

Altogether, this preliminary EEG-based investigation supported the idea of an increased cortical engagement during the execution of a postural task and suggested an important role of visual feedback in the up-regulation of cortical activity in the wake of a postural challenge. Most importantly, it provided renewed confidence in the possibility of using EEG data to shed light on the underlying cortical mechanisms regulating postural control.

However, some noteworthy limitations also emerged from the discussion of this study's outcome. Firstly, the arbitrariness in the definition of adaptation and habituation phases called for the identification of better quantitative indicators to investigate and describe the insurgence,

following prolonged and repeated exposure to the proprioceptive stimulus, of cortical processes to be associated with a phenomenon of habituation that shapes the long-term postural response. Secondly, the difficulty in the interpretation of spatially widespread scalp-based EEG results suggested the necessity to find alternative analysis methodologies, which can allow a better description of the activation patterns that characterise the postural response at a cortical level, while also highlighting the interplay between different cortical areas. Finally, the failure to identify a meaningful correlation between ASP and SPL suggested the need for further investigation into different metrics, more effectively descriptive of the cortical and kinematic responses, respectively, which would allow to identify markers that link cortical and postural performances.

### 7.1.2 Study 2

Discussing and learning from the limitations that affect this first study, we gained valuable insight into defining the following steps in the research project. The observations mentioned above were in fact tackled in the second study, which involved a substantial change of approach in the data analysis, as presented in Chapter 5.

New EEG data were collected from a cohort of volunteers at Aston University (UK). Here, the established experimental protocol, involving proprioceptive vibratory stimulations of the calf muscles for the disruption of the participant posture, was replicated with some improvements. First, the design of a custom-made, portable stimulation device and trigger box, allowed greater control of and flexibility with the stimulation sequence and its duration. The trial was extended to 30s of resting state followed by 10min of stimulation and the order of OE and CE trials was randomised. Then, the EEG signal was synchronised with data from a force platform

as well as with EMG data from the GL, SOL and TA muscles (which were later used for further analysis in the third study presented in Chapter 6).

In order to find adequate answers to the issues raised by the first study, a new approach was adopted for the data analysis. Source reconstruction and graph theory techniques were combined into a novel investigation methodology, EEG source connectivity (Hassan and Wendling, 2018b; Kabbara et al., 2020b), which focused on the way brain regions interact and shape the postural response at a cortical network level. In particular, we wanted to gain insight into the modular reconfiguration of the brain activity that takes place during a postural task under different experimental conditions, test the possibility to determine the insurgence of habituation mechanisms based on an associated and distinctive brain network state, and verify a possible correlation between posturographic and cortical performance metrics. To do this, we adapted methodologies originally developed for cognitive science studies. In common tasks such as “object naming”, a picture is presented to the subject, who is asked to pronounce the name of the presented object. This simple task involves the sequential activation of different cortical networks, each one in charge of a specific function (visual processing, memory access, decision making, verbalisation) (Kabbara et al., 2019). In order to investigate the brain network states associated with the execution of a postural control task, we split the acquired signal into epochs and obtained several snapshots of the brain network configuration over the course of the trial. This way, we could look at the dynamic evolution of the brain activity as represented by the brain network remodulation. Using classification algorithms based on network similarities, similar networks in adjacent epochs were then clustered together to identify a limited number of significantly different modular states that appear over the course of the task. Each modular state can then be associated with a specific cognitive process. In our case, the signal was segmented into 1s epochs according to the trigger signal that marked the start of

each vibratory stimulation. This was done for the sake of consistency, in order to have epochs of the same length, with 1s being the maximum available length to avoid overlapping with the following vibratory stimulus. The vibration and resting cycles of the stimulation sequence were randomised following a uniform distribution between 1-6s.

Consistent with previous studies, our investigation highlighted the centrality of alpha band functional brain networks during the execution of the postural task (Mierau et al., 2017a; Peterson and Ferris, 2019). Specifically, the network analysis (both nodewise and edgewise) of the cortical activity during the vibration-induced balance perturbation compared to the quiet stance, highlighted two well-defined clusters of cortical regions in the two experimental conditions. Indeed, two different alpha-band cortical pathways emerged for the OE and CE tasks, pointing at different postural strategies put in place according to the availability of visual feedback.

The brain network involved in the execution of the OE task was characterised by central hub nodes in the orbito-frontal, superior-frontal and cingulate regions of the cortex. As previously discussed, the activation and strengthening of the interplay between these cortical regions in the alpha band suggests a strategy that engages primarily a motor attention network which largely overlaps with the dorsal attention network and particularly the frontal eye field regions, in charge of visual field perception, sustained attention to peripheral locations and allocation of attentional resources during motor performances (Fujita et al., 2016; Japee et al., 2015; Schall, 2008). These motor attention regions appear to be in close relationship with the orbito-frontal cortex, which is thought to be a heterogeneous hub of sensory integration and the cingulate cortex, previously associated with recognition of unstable posture (Kringelbach, 2005; Lavin et al., 2013; Slobounov et al., 2009).

On the other hand, during the CE trial, i.e., when the visual stimulus is absent, stronger functional connections are observed among parietal and temporal cortical regions, with a predominant involvement of the right hemisphere. Overall, the network structure highlighted a cortical organisation which engaged areas of the parietal cortex traditionally characterised as receptor of proprioceptive stimuli (anterior parietal cortex) as well as a hub of multisensory integration (posterior parietal cortex) (Delhaye et al., 2018). Integration and interpretation of sensory inputs inform spatial perception and image of the body in space. Notably, a primary role seems to emerge for the regions of the Sylvain fissure, previously identified as parieto-insular vestibular cortex (PIVC) (Ventre-Dominey, 2014). Altogether, this network configuration and the analysis of both nodes and edges properties point towards a primary reliance on the vestibular and proprioceptive systems in the absence of visual feedback. This is reflected by the centrality of the PIVC regions in the network and the strengthening of their widespread connections across parietal and temporal regions in charge of proprioceptive and somatosensory integration. Moreover, the asymmetry of the network further suggests an important role of the vestibular system, which is characterised, in right-handed subjects, by right-hemispheric dominance (Brandt and Dieterich, 2015).

Promising results also emerged from the analysis of dynamic properties of the network nodes, in particular how the flexibility index of certain cortical regions correlates with $S_{EN}$ of the COP sway. Flexibility is a metric that is computed over sequential task epochs and expresses a dynamic property of the network, i.e., the extent to which each node switches modular affiliation over time, signalling the level of network plasticity and ability to reconfigure its topology in order to put in place more effective cognitive strategies (Kabbara et al., 2019). The sample entropy of the COP sway, especially in the AP direction, is a measure of postural stability which relates to the complexity of the oscillatory motion and has been previously used to evaluate postural

performances in healthy and impaired subjects (Zhou et al., 2016c). Higher $S_{EN}$ values reflect more complex fluctuations of the COP signal, a trademark of an effective postural control system, which describes the complex dynamics of the physiological systems involved.

The network nodes in which significant flexibility- $S_{EN}$ correlation emerged, correspond to areas of the cingulate, parietal and temporal cortices. We hypothesise that the nodes whose degree of engagement in the network topology dynamic reconfiguration over the course of the task correlates with the complexity level of the posturographic signal, are those which are more directly involved in the cortical strategy overseeing postural control. The ability of these key areas to flexibly integrate their respective cortical functions with different modules would be an indicator of the ability of the subject to develop an effective response to the postural challenge, which is reflected in the complexity of the COP fluctuations. Therefore, once again, the results seem to trace a crucial role for the cortical areas related to proprioception and vestibular processing, specifically the parietal cortex and the regions of the PIVC. Furthermore, the posterior cingulate (PCC) and middle temporal regions showed particularly high connectivity values. PCC is a highly interconnected processing hub which is engaged in visuospatial orientation and self-location processes (Guterstam et al., 2015; Leech et al., 2012) as well as in signalling environmental changes (Leech and Sharp, 2014). The middle temporal region results could suggest an involvement of MT/V5 area, part of the extrastriate visual cortex and involved with the dorsal visuospatial pathway, or ‘motion pathway’ (Kolster et al., 2010; Vanni et al., 2001).

Overall, the study provided useful insight into the way cortical regions interact to shape a response to the postural challenge under different experimental conditions. It also allowed the identification of specific cortical areas which are, as expected, more directly involved in

postural control, namely: somatosensory/proprioceptive, vestibular and visual. The dynamic analysis, with the possibility to correlate node flexibility (in particular in the parieto-temporal and cingulate regions) with the sample entropy of anterior-posterior COP sway, provided a promising outcome with a view to establish EEG-based analysis as a valid complementary tool to integrate posturography-based assessment of postural performances.

Nevertheless, some aspects emerged from this investigation provide new elements of consideration that are worth a more in-depth evaluation in the continuation of this line of research, in order to solidify and validate the presented observations. First, the presented results are mostly based on the comparison of task epoch networks, reflecting the cortical configuration during the execution of the postural task under the two conditions of open and closed eyes. At the present time, we failed to identify statistically significant network differences in a direct comparison between resting state (baseline epochs) and task, in each condition. Secondly, the dynamic analysis was not able to identify different and clearly defined modular states over the course of the task execution, that is: a clear change in the cortical strategy of postural control over time (which could be associated with the concepts of adaptation and habituation). This might be due to the small sample size or shortcomings of the experimental design, which possibly limit the power of the EEG source connectivity analysis, originally developed for cognitive tasks and here adapted to a postural task characterised by external mechanical perturbations. Further discussion on this point, including ideas for future improvements, will be discussed later in this chapter.

Additionally, the important role of visual cues emerged clearly from the presented results, in the cortical regions dominating the networks as well as in the clear difference in network topology between OE and CE tasks. While matching the expectations and validating the

observations of previous power-based analysis, this aspect is worth further investigations in that the predominance of visual-processing-related networks (during the OE trial) could overshadow other cognitive processes. Furthermore, the fact that dynamic correlation analysis highlighted significant flexibility-$S_{EN}$ correlation values only during the OE task merits further investigation.

Finally, in the current investigation we did not formulate any a priori assumption in terms of frequency band, inspecting the presence of significant networks in the alpha, beta and gamma bands. However, only the alpha band carried significant results in terms of network analysis. While previous studies point out cortical activation in the alpha (as well as theta) bands (Mierau et al., 2017a; Peterson and Ferris, 2019), a significant body of literature seems to draw a connection between balance tasks and beta band activity (Palmer et al., 2021; Peterson and Ferris, 2019). It is still worth noting, anyway, that the great majority of previous literature on the topic focuses on forms of spectral power analysis, power spectral density, spectral/corticomuscular coherence, etc. This approach is complementary but different from the functional correlation brain network analysis carried out in chapter 5 of this thesis, which characterises connectivity in terms of phase synchrony. PLV-based network connectivity focuses, in fact, not on the amplitude but on the phase synchrony among cortical sources. As such, the documented modulation in beta spectral power does not necessarily imply an increased functional connectivity among brain regions in the same band. This is, however, an interesting point of discussion that will benefit from an expansion of the currently scarce literature.

### 7.1.3 Study 3

The analysis of beta band cortical dynamics was, however, taken into account in the third study, presented in Chapter 6. Specifically, the focus of this study was an investigation of the neuromuscular coupling effects in postural control by means of electrophysiological signals recorded during the execution of the task.

In order to gain a full picture of the role of the cortex in the postural control system it is important to shed light on the way cortical activity drives the muscular response to balance perturbations, with particular focus on the lower leg muscles.

Previous literature has established how the postural control system, rather than continuously modulating the contraction of each individual muscle, operates by putting in place 'strategies' which involve the simultaneous activation of groups of muscles (Horak and Nashner, 1986; Nashner and McCollum, 1985). That results in what have been described as 'muscle synergies', in which the co-activation of muscular groups aims to stabilise the body's COM and maintain balance (Horak et al., 1997; Nashner and McCollum, 1985).

It has been shown how, during perturbed and unperturbed standing, the predominant strategy is the so-called ankle strategy during which soleus and gastrocnemius, plantar-flexors muscles of the calves, are activated (Blenkinsop et al., 2017). For this reason, our investigation of the cortical modulation of muscle contraction during the postural task focused on SOL and GL, as well as on TA, which is the primary dorsiflexor of the ankle.

The posturography data were used to assess the average distance and mean velocity of the COP during the resting state and the execution of the task. The reported increase in both DIST and MV following the administration of the local vibratory stimulation, supported its disruptive

effects on the subject's ability to maintain a balanced upright stance (Palmieri-Smith et al., 2002).

The analysis of cortical modulation of muscle activity was twofold: CMC was employed to assess the coupling between scalp EEG and surface EMG signals, while IMC was used to assess the synergies between the muscles of interest and to reconstruct a muscular network topology. A noteworthy result is that, once again, significant variations in both CMC magnitude and IMC network topology only emerged when comparing resting state with the first quartile of the task trial (in both experimental conditions), while no differences were observed over different phases of the task trial, namely, first and last quartile. This seems to further indicate the absence of a modulation of the cortical response over time and therefore a habituation process.

The CMC analysis was carried out in beta and gamma bands, which have been shown to be the frequencies predominantly characterised as a signature of cortico-muscular coupling (Gwin and Ferris, 2012; Liu et al., 2019). For each of the six considered muscles (right and left SOL, GL, TA), a cluster-based permutation test in the frequency and spatial domain allowed the identification of groups of neighbouring scalp electrodes whose CMC spectrum significantly varied, in specific frequency bins, between resting state and task epochs.

The results highlight a highly significant ($p<0.01$) enhancement of cortico-muscular coupling following the vibratory stimulation, happening between electrode clusters in the central area of the scalp topography (compatible with the underlying location of the motor cortex) and the GL and SOL muscles. This was observed during the CE trial in the beta band (around 20Hz) for SOL and in the gamma band (around 41Hz) for GL. The frequency bins identified as significant are consistent with previous literature (Baker, 2007; Gwin and Ferris, 2012), but it also

emerges that the CMC enhancement during the postural task is consistent over the whole frequency band. This clearly indicates how the disruption of the quiet stance evokes the necessity to resort to a postural strategy which relies more heavily on high-level, cortical control, as indicated by the increased synchrony in neural and muscular signals. In other words, these results seem to confirm how the enactment of an effective muscular response to the postural challenge induced by mechanical vibrations cannot rely solely on low-level reflexive mechanisms, especially in the case of more challenging tasks, such as CE, with the lack of visual cues.

As far as the CMC analysis of TA is concerned, the results involve a cluster of electrodes in the occipital region of the scalp topography, which is hardly relatable to the activity of the motor cortex. This observation, together with the lower significance level ($p<0.05$) and the contrasting CMC spectrum patterns (increased magnitude in Q1 compared to resting state during CE, and decreasing during OE), are worth further investigation but lead to the reasonable conclusion that TA results are influenced by artefactual patterns which do not actually describe the cortical drive of this muscle.

Inter-muscular coherence analysis provides a valuable and complementary insight into the cortico-muscular response to the postural challenge. Despite not involving EEG signals in the analysis, IMC offers a picture of the synchronisation patterns happening between couples of muscles, therefore indirectly shedding light on those ‘muscle synergies’ resulting from the simultaneous recruitment of muscular groups, which is coordinated at a central, cortical level (Boonstra, 2013). The inter-muscular relationships, as described by co-activation patterns, are rendered in the form of a network, where IMC values represent the connections among pairs of muscles, i.e., the nodes of the network. This analysis, once again, proves the flexibility and

effectiveness of graph theory tools in the investigation, quantification and rendering of large-scale relationships occurring among interacting electrophysiological signals.

IMC analysis was conducted, following the methodology reported in (Boonstra, 2013), by splitting the IMC frequency domain [0-40Hz] into 5 frequency components through NNMF. This is done in light of the lack of a strong frequency a-priori, unlike the one that exists for beta and gamma bands in the analysis involving EEG.

Out of the five frequency components identified, two seem to relate to non-physiological patterns, one being dominated by ~0Hz component and the other being of low magnitude and distributed across the whole band. Furthermore, their associated adjacency matrices (both during resting state and task) display unusually high connectivity values, close to 1.

The analysis was carried out both in terms of global network topology (edgewise) and individual nodes properties (nodewise). Specifically, the metrics of clustering coefficient, local efficiency and strength were tested as widely adopted indicators of significant network properties. Both analyses confirmed a significant remodulation of the muscular strategy during the execution of the postural task compared to resting state. In particular, generalised increased connectivity values were observed across the relevant frequency components, as well an increase in all node metrics, following the proprioceptive perturbation, in both OE and CE conditions.

Looking at the frequency values dominating the relevant components, and referring to previous IMC literature, it can be argued that the presented results reflect an increased synchrony in muscular activity which can be related to both high- and low-level processes. In fact, if the enhanced IMC in the [16-40] Hz range (present in our third frequency component) is likely a reflexion of higher cortical drive, the increased values registered at lower frequencies, [0-5]Hz

and [6-15]Hz (fourth and fifth component, respectively) seem to be partially or exclusively related to the inflow of subcortical inputs (Nandi et al., 2019). The coupling level recorded by IMC following the proprioceptive stimulation can reflect both an efferent, cortically driven, synchronised muscle activation (at higher frequencies) and a low-level (spinal) modulation of muscular activity.

While this could reflect a composite postural strategy that enacts both reflexive and cortical control mechanisms in order to shape a muscular response which preserves balance, it is also possible that the administration of localised mechanical solicitation on the lower leg muscles resulted in an increased influx of proprioceptive inputs (Burke et al., 1976a). The stimulation of muscle spindles induced by the vibratory sequence could in fact lead to a modulation of muscular activity that reflects as an enhanced proprioceptive, afferent component in the IMC signal.

In conclusion, while providing interesting insight into the cortico-muscular interactions which shape the postural response, it is evident that several elements limit the ability to provide a univocal physiological interpretation of the presented results. CMC and IMC techniques are gaining increasing interest as valid tools for the analysis of interactions of complex physiological signals. Anyway, their application to postural studies is still relatively novel: their variability across experimental designs results, at the moment, in a lack of consensus around results interpretation (Boonstra, 2013). This comes down predominantly to the fact that the two signals reflect and are influenced by both afferent and efferent pathways, making it challenging to distinguish cortical drive from proprioceptive signal. Furthermore, it is worth pointing out that the present results are based on a limited cohort of young healthy subjects, and the

experimental design presents some limitations that will need to be addressed in the development of this line of research, as discussed in the following section.

## 7.2 Recommendations for future developments

In the work presented in this thesis, the postural challenge to the participant's quiet stance was achieved via mechanical proprioceptive stimulation. This consisted in a randomised binary sequence of vibrations administered locally on the calf muscles through revolving DC motors. 85Hz vibration bouts were alternated with resting periods, both having a uniformly distributed duration between 1 and 6s. This common and effective way to induce postural instability has been extensively used in previous literature (Edmunds et al., 2019; Fransson, 2005; Patel et al., 2009). As a result of the stimulation pattern, the analyses of cortical and cortico-muscular responses to the perturbation relied on segmented epochs of the data defined according to triggers which marked the onset and offset of the vibration bouts. Specifically, onset triggers were used in the second study (Chapter 5) to define the start of epochs from which to extract the cortical networks, while offset triggers were used in the third study (Chapter 6) to the define the start of EEG and EMG epochs involved in the neuromuscular coupling analysis. In both cases, the maximum epoch length to avoid overlapping with the following stimulation cycle was 1s. This resulted in the definition of sequential but not adjacent, nor overlapping, epochs, which is sub-optimal in terms of EEG brain connectivity analysis. This methodology was in fact originally developed for cognitive tasks, which allow a continuous segmentation of the data via running overlapping windows. In addition, the direct application of the stimulation on the calf muscles presents two main problems with regards to the inclusion of EMG data in the analysis. Firstly, task epochs used for the analysis had to be defined at the end of each vibration period, since the mechanical vibration introduces high-amplitude artefacts which significantly corrupt

the EMG signal especially in the muscles spatially closer to the stimulation area (GL and SOL). Secondly, this kind of proprioceptive stimulation acts by exciting the muscle spindles which in turn cause an increase in the motor units firing rate, resulting in an induced stretching of the muscle fibres. Therefore, even after the end of the vibration bouts, it is reasonable to suppose that the repeated stimulation and the excitation of proprioceptive receptors, might alter the overall muscle electrical activity, thus possibly skewing the physiological interpretation of the postural response at a muscular level.

For these reasons, the use of different types of stimulation should be considered in future studies. This would broaden the picture of how cortical mechanisms regulate postural control under different disruptive circumstances and, most importantly, would allow the discussed limitations of the current study design to be overcome. The benefits would be twofold: on one hand, by allowing a continuous segmentation of the recorded signal, the effectiveness of dynamic sequential modularity algorithms could be improved, enabling the identification of better-defined modular brain states over the course of the trial. On the other hand, different kinds of stimulation would reduce the interference with the electromyographic signal, allowing a more accurate representation of the muscular response.

The development of an alternative experimental protocol in future studies, can rely on the equipment recently put in use at the Reykjavik University research facilities. This comprises a mechanical platform integrated with force plate and a VR system (Virtualis VR, France) as shown in Figure 7.1. The use of immersive VR technology has been gaining traction over the past few years in a vast number of experimental fields, including perturbation evoked potentials (Varghese et al., 2017; Yelshyna et al., 2016), postural control and motion sickness studies (Fransson et al., 2019; Recenti et al., 2021). The device in use at Reykjavik University, allows

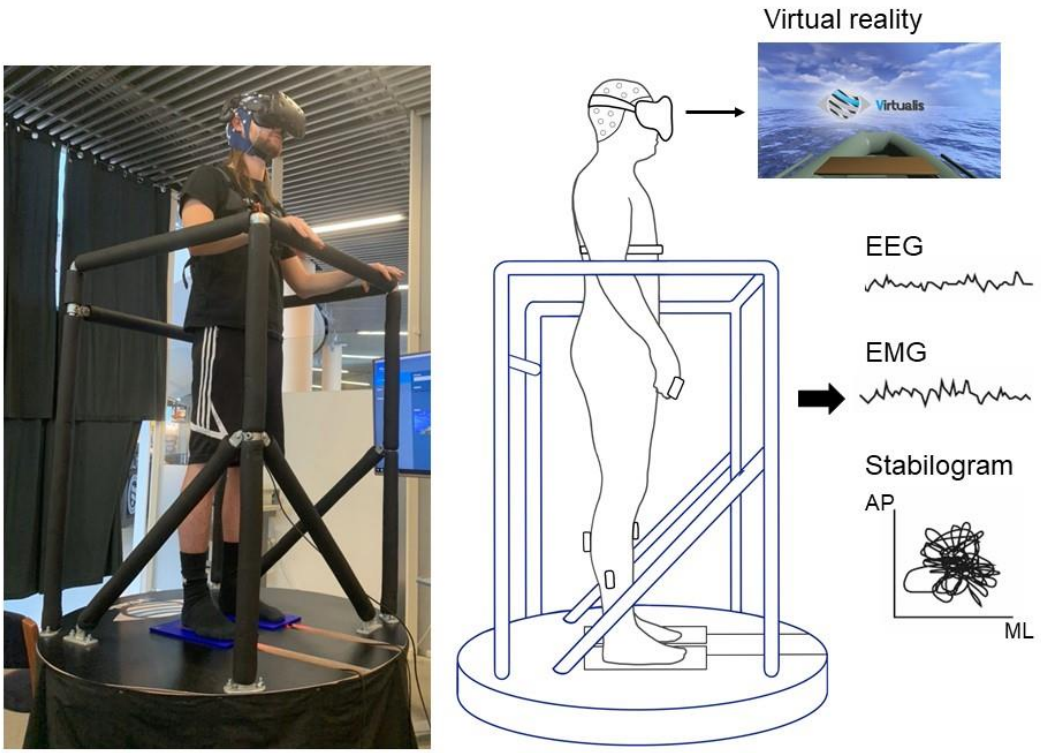


**Figure 7.1.** Schematic of possible future setup.
A force plate is installed on a mechanical platform, capable of tilting and rotating. A safety scaffolding allows the participant to stand on the raised moving platform while wearing a VR headset with customisable virtual environments. A portable amplifier allows EEG and EMG signals to be recorded during the execution of the postural task. Figure adapted from (Recenti et. al, 2021)

fast tailored movements of the support platform in several directions coupled with synchronised movements of the virtual environment. Furthermore, it allows the integration of several portable electrophysiological signal acquisition devices, as tested in a recent study (Recenti et al., 2021).

The flexibility of the mechanical platform together with the customisable VR software, could potentially enable a number of alternative ways to induce postural imbalance. It would allow, for example, the design of scenarios in which the visual field within the virtual environment is shifted of a few degrees in one direction, while the base of the force platform is mechanically

rotated in the opposite direction, similar to what has already been tested in previous literature (Peterson and Ferris, 2019). It could also provide a visual input that induces the illusion of self-motion in the participants. The repeated exposure to this kind of mismatch between physical and visual motion has been shown to induce a sensory (visual-vestibular) conflict which results in postural instability (Akizuki et al., 2005).

The adjustments of the mechanisms of processing and integration of sensory information at a cortical level could then be examined in terms of source EEG network connectivity over the course of the trial in a continuous manner, allowing the identification of possible changes in cortical strategies in terms of reconfigurations of modular states. Moreover, the coupling of cortical and muscular activity could be investigated in a more reliable way, since the stimulation modality would not interfere with the muscular response. The new experimental paradigm would also allow the modulation of the intensity of the stimulation (frequency, amplitude, speed and direction of the platform and visual field motion) to observe the remodulation of cortical and muscular strategy during different levels of postural challenge.

Finally, the recruitment of a larger and more diverse cohort of subjects, would allow an in-depth, stratified analysis in terms of age and gender, as well as a comparison of the cortical postural control strategies between healthy volunteers and subjects affected by postural impairment. The recruitment of older subjects in particular would greatly improve our understanding of the relationship between cognitive decline, postural performance decline and changes in cortical strategies.

## 7.3 Conclusions

The key findings emerging from the work presented in this thesis unveil different postural control strategies, in terms of cortical network topology and properties, highlighting the synergies between specific cortical areas and their associated functions. In particular, our findings show how the processing and integration of sensory information changes under different experimental conditions, namely with or without the availability of visual cues, by recruiting distinct cortical pathways. Indeed, we now have further proof of the centrality of vestibular, visual and somatosensory/proprioceptive processes, as well as a clearer view of the way they interact, and powerful tools to quantify their contribution to the system. The adoption of a novel methodology which integrates source reconstruction techniques, functional connectivity analysis and graph theory tools, provided a rich picture of the cortical mechanisms regulating postural control, while also overcoming many of the shortcomings that hinder scalp-EEG-based power analyses. Encouraging results were also achieved in the attempt to identify neural markers which can relate to postural performance and integrate more traditional kinematic and posturographic metrics used to describe it. Moreover, cortico-muscular and inter-muscular coherence analyses, once again supported by graph theory tools, provided further evidence of the enhanced neuromuscular coupling that occurs when facing a postural challenge.

Overall, the present work provides promising results which unequivocally confirm the crucial involvement of cortical mechanisms in the postural control system and offers solid bases for further developments of the line of research that has been established. Relying on the knowledge and analytical know-how gathered during this project, and thanks to the discussed improvements to the experimental setup, future studies will be able to provide a significant

contribution in this incresingly relevant research area. Indeed, the importance of understanding high level mechanisms that contribute to effective postural control strategies lies in the eventual practical implications. This knowledge could be the basis on which aimed training and therapeutic strategies can be developed. Research in this direction can assess the validity of EEG as a non-invasive and easily accessible tool for the evaluation of postural performances leading to an early detection of decline and the put in place of preventive strategies. The identification of neural markers and the characterisation of the role of individual cortical region within the brain network could pave the way, for example, to the development of specific stimulation procedure (e.g., TMS) (Banea et al., 2021; Bolognini and Miniussi, 2018), while a deeper understanding of the cortical-level connection between cognitive and postural functions could help the development of focused training methodologies aimed at preventing cognitive decline while also preventing the loss of postural performance in ageing people (balance training, re-adaptation of sensory strategies, etc.) (Bronstein and Pavlou, 2013).

In conclusion, the relevance and potential impact of the practical applications stemming from this line of postural research is clear when considering the major healthcare concerns represented by fall-related injuries in an ageing society. This is evident when looking at the figures which document the rising individual and societal costs resulting from falls, which are the second leading cause of injury deaths worldwide according to the World Health Organisation, with age-related postural impairment being the primary risk factor (Carroll et al., 2015; WHO, 2021).

# References


Acharya, J.N., Hani, A.J., Cheek, J., Thirumala, P., Tsuchida, T.N., 2016a. American Clinical Neurophysiology Society Guideline 2: Guidelines for Standard Electrode Position Nomenclature. Neurodiagn. J. https://doi.org/10.1080/21646821.2016.1245558

Acharya, J.N., Hani, A.J., Thirumala, P., Tsuchida, T.N., 2016b. American Clinical Neurophysiology Society Guideline 3: A Proposal for Standard Montages to Be Used in Clinical EEG. Neurodiagn. J. 56, 253–260. https://doi.org/10.1080/21646821.2016.1245559

Adkin, A.L., Campbell, A.D., Chua, R., Carpenter, M.G., 2008. The influence of postural threat on the cortical response to unpredictable and predictable postural perturbations. Neurosci. Lett. https://doi.org/10.1016/j.neulet.2008.02.018

Akizuki, H., Uno, A., Arai, K., Morioka, S., Ohyama, S., Nishiike, S., Tamura, K., Takeda, N., 2005. Effects of immersion in virtual reality on postural control. Neurosci. Lett. 379, 23–26. https://doi.org/10.1016/J.NEULET.2004.12.041

Amblard, B., Crémieux, J., Marchand, A.R., Carblanc, A., 1985. Lateral orientation and stabilization of human stance: static versus dynamic visual cues. Exp. Brain Res. 1985 611 61, 21–37. https://doi.org/10.1007/BF00235617

Ambrose, A.F., Paul, G., Hausdorff, J.M., 2013. Risk factors for falls among older adults: A review of the literature. Maturitas. https://doi.org/10.1016/j.maturitas.2013.02.009

Ames, F.R., 1971. “self-induction” in photosensitive epilepsy. Brain. https://doi.org/10.1093/brain/94.4.781

Anton, K., Ernst, A., Basta, D., 2020. Auditory influence on postural control during stance tasks in different acoustic conditions. J. Vestib. Res. Equilib. Orientat. 29, 287–294. https://doi.org/10.3233/VES-190674

Asseman, F., Gahéry, Y., 2005. Effect of head position and visual condition on balance control in inverted stance. Neurosci. Lett. 375, 134–137. https://doi.org/10.1016/J.NEULET.2004.10.085

Baillet, S., Mosher, J.C., Leahy, R.M., 2001a. Electromagnetic brain mapping. IEEE Signal

Process. Mag. 18, 14–30. https://doi.org/10.1109/79.962275

Baillet, S., Mosher, J.C., Leahy, R.M., 2001b. Electromagnetic brain mapping. IEEE Signal Process. Mag. https://doi.org/10.1109/79.962275

Baker, S.N., 2007. Oscillatory interactions between sensorimotor cortex and the periphery. Curr. Opin. Neurobiol. https://doi.org/10.1016/j.conb.2008.01.007

Baloh, R., KM, J., TM, S., 1993. The effect of aging on visual-vestibuloocular responses. Exp. brain Res. 95, 509–516. https://doi.org/10.1007/BF00227144

Banea, O.C., Bandeira dos Santos, L.G., Marcu, S., Stefánnson, S.B., Wassermann, E.M., Ívarsson, E., Jónasson, V.D., Aubonnet, R., Jónasson, A.D., Magnúsdóttir, B.B., Haraldsson, M., Gargiulo, P., 2021. Network signatures of rTMS treatment in patients with schizophrenia and auditory verbal hallucination during an auditory-motor task using HD-EEG. Schizophr. Res. https://doi.org/10.1016/J.SCHRES.2021.06.002

Bar-On, L., Aertbeliën, E., Wambacq, H., Severijns, D., Lambrecht, K., Dan, B., Huenaerts, C., Bruyninckx, H., Janssens, L., Van Gestel, L., Jaspers, E., Molenaers, G., Desloovere, K., 2013. A clinical measurement to quantify spasticity in children with cerebral palsy by integration of multidimensional signals. Gait Posture 38, 141–147. https://doi.org/10.1016/j.gaitpost.2012.11.003

Bard, P., 1933. STUDIES ON THE CEREBRAL CORTEX: I. LOCALIZED CONTROL OF PLACING AND HOPPING REACTIONS IN THE CAT AND THEIR NORMAL MANAGEMENT BY SMALL CORTICAL REMNANTS. Arch. Neurol. Psychiatry 30, 40–74. https://doi.org/10.1001/ARCHNEURPSYC.1933.02240130048003

Barollo, F., Frioriksdóttir, R., Edmunds, K.J., Karlsson, G.H., Svansson, H.A., Hassan, M., Fratini, A., Petersen, H., Gargiulo, P., 2020. Postural Control Adaptation and Habituation during Vibratory Proprioceptive Stimulation: An HD-EEG Investigation of Cortical Recruitment and Kinematics. IEEE Trans. Neural Syst. Rehabil. Eng. 28, 1381–1388. https://doi.org/10.1109/TNSRE.2020.2988585

Barollo, F., Hassan, M., Petersen, H., Rigoni, I., Ramon, C., Gargiulo, P., Fratini, A., 2022. Cortical pathways during Postural Control: new insights from functional EEG source connectivity. IEEE Trans. Neural Syst. Rehabil. Eng. 1–1.

https://doi.org/10.1109/TNSRE.2022.3140888

Basmajian, J. V., De Luca, C.J., 1985. Muscles alive : their functions revealed by electromyography 561.

Bassett, D.S., Porter, M.A., Wymbs, N.F., Grafton, S.T., Carlson, J.M., Mucha, P.J., 2013. Robust detection of dynamic community structure in networks. Chaos 23. https://doi.org/10.1063/1.4790830

Bassett, D.S., Sporns, O., 2017. Network neuroscience. Nat. Neurosci. https://doi.org/10.1038/nn.4502

Bassett, D.S., Wymbs, N.F., Porter, M.A., Mucha, P.J., Carlson, J.M., Grafton, S.T., 2011. Dynamic reconfiguration of human brain networks during learning. Proc. Natl. Acad. Sci. U. S. A. https://doi.org/10.1073/pnas.1018985108

Bastian, A., TA, M., JG, K., WT, T., 1996. Cerebellar ataxia: abnormal control of interaction torques across multiple joints. J. Neurophysiol. 76, 492–509. https://doi.org/10.1152/JN.1996.76.1.492

Bell, M.A., Cuevas, K., 2012. Using EEG to Study Cognitive Development: Issues and Practices. J. Cogn. Dev. https://doi.org/10.1080/15248372.2012.691143

Benjamini, Y., Hochberg, Y., 1995. Controlling the False Discovery Rate: A Practical and Powerful Approach to Multiple Testing. J. R. Stat. Soc. 57, 289–300. https://doi.org/10.2307/2346101

Berger, H., 1929. Über das Elektrenkephalogramm des Menschen. Arch. Psychiatr. Nervenkr. 87, 527–570. https://doi.org/10.1007/BF01797193

Bhagat, N.A., Venkatakrishnan, A., Abibullaev, B., Artz, E.J., Yozbatiran, N., Blank, A.A., French, J., Karmonik, C., Grossman, R.G., O'Malley, M.K., Francisco, G.E., Contreras-Vidal, J.L., 2016. Design and optimization of an EEG-based brain machine interface (BMI) to an upper-limb exoskeleton for stroke survivors. Front. Neurosci. https://doi.org/10.3389/fnins.2016.00122

Bhatt, T., Patel, P., Dusane, S., DelDonno, S.R., Langenecker, S.A., 2018. Neural mechanisms involved in mental imagery of slip-perturbation while walking: A preliminary fMRI study. Front. Behav. Neurosci. 12, 203. https://doi.org/10.3389/fnbeh.2018.00203

Billino, J., Braun, D.I., Böhm, K.D., Bremmer, F., Gegenfurtner, K.R., 2009. Cortical networks for motion processing: Effects of focal brain lesions on perception of different motion types. Neuropsychologia. https://doi.org/10.1016/j.neuropsychologia.2009.04.005

Birbaumer, N., Elbert, T., Canavan, A.G., Rockstroh, B., 1990. Slow potentials of the cerebral cortex and behavior. Physiol. Rev. 70, 1–41. https://doi.org/10.1152/physrev.1990.70.1.1

Black, F., 2001. What can posturography tell us about vestibular function? Ann. N. Y. Acad. Sci. 942, 446–464. https://doi.org/10.1111/J.1749-6632.2001.TB03765.X

Black, F., Homer, L., 1996. Platform posturography. Arch. Otolaryngol. Head. Neck Surg. 122, 1273–1274. https://doi.org/10.1001/ARCHOTOL.1996.01890230115021

Blenkinsop, G.M., Pain, M.T.G., Hiley, M.J., 2017. Balance control strategies during perturbed and unperturbed balance in standing and handstand. R. Soc. Open Sci. 4. https://doi.org/10.1098/rsos.161018

Blondel, V.D., Guillaume, J.L., Lambiotte, R., Lefebvre, E., 2008. Fast unfolding of communities in large networks. J. Stat. Mech. Theory Exp. https://doi.org/10.1088/1742-5468/2008/10/P10008

Bolognini, N., Miniussi, C., 2018. Noninvasive brain stimulation of the parietal lobe for improving neurologic, neuropsychologic, and neuropsychiatric deficits. Handb. Clin. Neurol. 151, 427–446. https://doi.org/10.1016/B978-0-444-63622-5.00022-X

Bolton, D.A.E., 2015. The role of the cerebral cortex in postural responses to externally induced perturbations. Neurosci. Biobehav. Rev. https://doi.org/10.1016/j.neubiorev.2015.08.014

Bolton, D.A.E., Misiaszek, J.E., 2012. Compensatory balance reactions during forward and backward walking on a treadmill. Gait Posture. https://doi.org/10.1016/j.gaitpost.2011.12.002

Bonferroni, C.E., 1935. Il Calcolo delle Assicurazioni su Gruppi di Teste, in: Studi in Onore Del Professore Salvatore Ortu Carboni. pp. 13–60.

Boonstra, T., Roerdink, M., Daffertshofer, A., van Vugt, B., van Werven, G., Beek, P., 2008. Low-alcohol doses reduce common 10- to 15-Hz input to bilateral leg muscles during quiet standing. J. Neurophysiol. 100, 2158–2164. https://doi.org/10.1152/JN.90474.2008

Boonstra, T.W., 2013. The potential of corticomuscular and intermuscular coherence for research on human motor control. Front. Hum. Neurosci. 7, 1–2. https://doi.org/10.3389/FNHUM.2013.00855

Boonstra, T.W., Breakspear, M., 2012. Neural mechanisms of intermuscular coherence: implications for the rectification of surface electromyography. J. Neurophysiol. 107, 796–807. https://doi.org/10.1152/jn.00066.2011

Boonstra, T.W., Danna-Dos-Santos, A., Xie, H.B., Roerdink, M., Stins, J.F., Breakspear, M., 2015. Muscle networks: Connectivity analysis of EMG activity during postural control. Sci. Rep. 5, 1–14. https://doi.org/10.1038/srep17830

Brandt, T., Dieterich, M., 2015. Does the vestibular system determine the lateralization of brain functions? J. Neurol. https://doi.org/10.1007/s00415-014-7548-8

Brandt, T., Esser, J., Büchele, W., Krafczyk, S., 1982. “Visuo-Spinal Ataxia” Caused by Disorders of Eye Movements 425–430. https://doi.org/10.1007/978-94-009-8000-6_45

Braun, U., Schäfer, A., Walter, H., Erk, S., Romanczuk-Seiferth, N., Haddad, L., Schweiger, J.I., Grimm, O., Heinz, A., Tost, H., Meyer-Lindenberg, A., Bassett, D.S., 2015. Dynamic reconfiguration of frontal brain networks during executive cognition in humans. Proc. Natl. Acad. Sci. U. S. A. 112, 11678–11683. https://doi.org/10.1073/pnas.1422487112

Bronstein, A.M., 2016. Multisensory integration in balance control. Handb. Clin. Neurol. 137, 57–66. https://doi.org/10.1016/B978-0-444-63437-5.00004-2

Bronstein, A.M., 1986. Suppression of visually evoked postural responses. Exp. Brain Res. 63, 655–658. https://doi.org/10.1007/BF00237488

Bronstein, A.M., Pavlou, M., 2013. Balance. Handb. Clin. Neurol. 110, 189–208. https://doi.org/10.1016/B978-0-444-52901-5.00016-2

Brunet, D., Murray, M.M., Michel, C.M., 2011. Spatiotemporal analysis of multichannel EEG: CARTOOL. Comput. Intell. Neurosci. https://doi.org/10.1155/2011/813870

Bullmore, E., Sporns, O., 2009. Complex brain networks: Graph theoretical analysis of structural and functional systems. Nat. Rev. Neurosci. 10, 186–198. https://doi.org/10.1038/nrn2575

Burke, D., Hagbarth, K.E., Lofstedt, L., Wallin, B.G., 1976a. The responses of human muscle spindle endings to vibration during isometric contraction. J. Physiol. 261, 695–711. https://doi.org/10.1113/jphysiol.1976.sp011581

Burke, D., Hagbarth, K.E., Löfstedt, L., Wallin, B.G., 1976b. The responses of human muscle spindle endings to vibration during non-contracting muscles. J. Physiol. 261, 695–711. https://doi.org/10.1113/jphysiol.1976.sp011581

Burke, D., Schiller, H.H., 1976. Discharge pattern of single motor units in the tonic vibration reflex of human triceps surae. J. Neurol. Neurosurg. Psychiatry 39, 729–741. https://doi.org/10.1136/jnnp.39.8.729

Busa, M.A., Jones, S.L., Hamill, J., van Emmerik, R.E.A., 2016. Multiscale entropy identifies differences in complexity in postural control in women with multiple sclerosis. Gait Posture 45, 7–11. https://doi.org/10.1016/j.gaitpost.2015.12.007

Busa, M.A., van Emmerik, R.E.A., 2016. Multiscale entropy: A tool for understanding the complexity of postural control. J. Sport Heal. Sci. 5, 44–51. https://doi.org/10.1016/j.jshs.2016.01.018

Cai, L., Chan, J.S.Y., Yan, J.H., Peng, K., 2014. Brain plasticity and motor practice in cognitive aging. Front. Aging Neurosci. https://doi.org/10.3389/fnagi.2014.00031

Camicioli, R., Nutt, J.G., 2007. Gait and Balance. Textb. Clin. Neurol. Third Ed. 327–342. https://doi.org/10.1016/B978-141603618-0.10018-9

Campanini, I., Disselhorst-Klug, C., Rymer, W.Z., Merletti, R., 2020. Surface EMG in Clinical Assessment and Neurorehabilitation: Barriers Limiting Its Use. Front. Neurol. 11. https://doi.org/10.3389/fneur.2020.00934

Campbell, I.G., 2009. EEG recording and analysis for sleep research. Curr. Protoc. Neurosci. https://doi.org/10.1002/0471142301.ns1002s49

Čapičíková, N., Rocchi, L., Hlavačka, F., Chiari, L., Cappello, A., 2006. Human Postural Response to Lower Leg Muscle Vibration of Different Duration. Physiol. Res 55, 129–134.

Carlsöö, S., 1972. How man moves: kinesiological studies and methods,. Heinemann.

Carroll, N. V., Slattum, P.W., Cox, F.M., 2015. The Cost of Falls Among the Community-

Dwelling Elderly. https://doi.org/10.18553/jmcp.2005.11.4.307 11, 307–316. https://doi.org/10.18553/JMCP.2005.11.4.307

Cavalcanti Garcia, M.A., Vieira, T.M.M., 2011. Surface electromyography: Why, when and how to use it. Rev. Andaluza Med. del Deport.

Cavanagh, J.F., Frank, M.J., 2014. Frontal theta as a mechanism for cognitive control. Trends Cogn. Sci. 18, 414–421. https://doi.org/10.1016/J.TICS.2014.04.012

Chabran, E., B, M., A, F., 2002. Effects of postural muscle fatigue on the relation between segmental posture and movement. J. Electromyogr. Kinesiol. 12, 67–79. https://doi.org/10.1016/S1050-6411(01)00027-X

Chan, C.W.Y., Jones, G.M., Kearney, R.E., Watt, D.G.D., 1979. The 'late' electromyographic response to limb displacement in man. I. Evidence for supraspinal contribution. Electroencephalogr. Clin. Neurophysiol. 46, 173–181. https://doi.org/10.1016/0013-4694(79)90066-X

Chapman, S.B., Aslan, S., Spence, J.S., Hart, J.J., Bartz, E.K., Didehbani, N., Keebler, M.W., Gardner, C.M., Strain, J.F., Defina, L.F., Lu, H., 2015. Neural mechanisms of brain plasticity with complex cognitive training in healthy seniors. Cereb. Cortex. https://doi.org/10.1093/cercor/bht234

Chiari, L., Rocchi, L., Cappello, A., 2002. Stabilometric parameters are affected by anthropometry and foot placement. Clin. Biomech. https://doi.org/10.1016/S0268-0033(02)00107-9

Chiba, Takakusaki, J, O., A, Y., N, H., 2016. Human upright posture control models based on multisensory inputs; in fast and slow dynamics. Neurosci. Res. 104, 96–104. https://doi.org/10.1016/J.NEURES.2015.12.002

Cignetti, M, V., LM, D., MH, G., N, G., Y, C., P, P., C, A., 2018. Brain network connectivity associated with anticipatory postural control in children and adults. Cortex. 108, 210–221. https://doi.org/10.1016/J.CORTEX.2018.08.013

Cohen, J.R., D'Esposito, M., 2016. The segregation and integration of distinct brain networks and their relationship to cognition. J. Neurosci. 36, 12083–12094. https://doi.org/10.1523/JNEUROSCI.2965-15.2016

Cohen, L.A., 1961. Role of eye and neck proprioceptive mechanisms in body orientation and motor coordination. J. Neurophysiol. https://doi.org/10.1152/jn.1961.24.1.1

Cohen, M.X., 2014. Analyzing Neural Time Series Data. MIT Press; 1 edition.

Colnat-Coulbois, S., Gauchard, G.C., Maillard, L., Barroche, G., Vespignani, H., Auque, J., Perrin, P.P., 2011. Management of postural sensory conflict and dynamic balance control in late-stage Parkinson's disease. Neuroscience 193, 363–369. https://doi.org/10.1016/j.neuroscience.2011.04.043

Cooper, R., Osselton, J.W., Shaw, J.C., 1974. Fundamentals of EEG Technology, EEG technology. https://doi.org/10.1016/B978-0-407-16001-9.50001-8

Costa, M., Goldberger, A.L., Peng, C.K., 2002a. Multiscale Entropy Analysis of Complex Physiologic Time Series. Phys. Rev. Lett. https://doi.org/10.1103/PhysRevLett.89.068102

Costa, M., Goldberger, A.L., Peng, C.K., 2002b. Multiscale Entropy Analysis of Complex Physiologic Time Series. Phys. Rev. Lett. 89, 6–9. https://doi.org/10.1103/PhysRevLett.89.068102

Creed R. S., 1932. Reflex activity of the spinal cord. Clarendon Press.

Croft, R.J., Barry, R.J., 2000. EOG correction: Which regression should we use? Psychophysiology 37, 123–125. https://doi.org/10.1017/S0048577200001633

Davidovits, P., 2019. Static Forces, in: Physics in Biology and Medicine. Elsevier, pp. 1–20. https://doi.org/10.1016/b978-0-12-813716-1.00001-x

de la Rosa, R., Alonso, A., Carrera, A., Durán, R., Fernández, P., 2010. Man-machine interface system for neuromuscular training and evaluation based on EMG and MMG signals. Sensors 10, 11100–11125. https://doi.org/10.3390/s101211100

Delhaye, B.P., Long, K.H., Bensmaia, S.J., 2018. Neural Basis of Touch and Proprioception in Primate Cortex. Compr. Physiol. https://doi.org/10.1002/cphy.c170033

Delorme, A., Makeig, S., 2004. EEGLAB: An open source toolbox for analysis of single-trial EEG dynamics including independent component analysis. J. Neurosci. Methods. https://doi.org/10.1016/j.jneumeth.2003.10.009

Desikan, R.S., Ségonne, F., Fischl, B., Quinn, B.T., Dickerson, B.C., Blacker, D., Buckner, R.L., Dale, A.M., Maguire, R.P., Hyman, B.T., Albert, M.S., Killiany, R.J., 2006a. An automated labeling system for subdividing the human cerebral cortex on MRI scans into gyral based regions of interest. Neuroimage 31, 968–980. https://doi.org/10.1016/j.neuroimage.2006.01.021

Desikan, R.S., Ségonne, F., Fischl, B., Quinn, B.T., Dickerson, B.C., Blacker, D., Buckner, R.L., Dale, A.M., Maguire, R.P., Hyman, B.T., Albert, M.S., Killiany, R.J., 2006b. An automated labeling system for subdividing the human cerebral cortex on MRI scans into gyral based regions of interest. Neuroimage 31, 968–980. https://doi.org/10.1016/j.neuroimage.2006.01.021

Diener, H.C., Dichgans, J., Bootz, F., Bacher, M., 1984. Early stabilization of human posture after a sudden disturbance: influence of rate and amplitude of displacement. Exp. Brain Res. https://doi.org/10.1007/BF00237448

Diener, H, A., J, D., B, G., 1985. Medium- and long-latency responses to displacements of the ankle joint in patients with spinal and central lesions. Electroencephalogr. Clin. Neurophysiol. 60, 407–416. https://doi.org/10.1016/0013-4694(85)91014-4

Dietz, 1992. Human neuronal control of automatic functional movements: interaction between central programs and afferent input. Physiol. Rev. 72, 33–70. https://doi.org/10.1152/PHYSREV.1992.72.1.33

Donker, S.F., Roerdink, M., Greven, A.J., Beek, P.J., 2007a. Regularity of center-of-pressure trajectories depends on the amount of attention invested in postural control. Exp. Brain Res. 181, 1–11. https://doi.org/10.1007/s00221-007-0905-4

Donker, S.F., Roerdink, M., Greven, A.J., Beek, P.J., 2007b. Regularity of center-of-pressure trajectories depends on the amount of attention invested in postural control. Exp. Brain Res. https://doi.org/10.1007/s00221-007-0905-4

Doumas, M., Smolders, C., Krampe, R.T., 2008. Task prioritization in aging: Effects of sensory information on concurrent posture and memory performance. Exp. Brain Res. https://doi.org/10.1007/s00221-008-1302-3

Douw, L., Nieboer, D., Stam, C.J., Tewarie, P., Hillebrand, A., 2018. Consistency of

magnetoencephalographic functional connectivity and network reconstruction using a template versus native MRI for co-registration. Hum. Brain Mapp. 39, 104–119. https://doi.org/10.1002/hbm.23827

Eccles, J.C., 1986. Learning in the motor system. Prog. Brain Res. 64, 3–18. https://doi.org/10.1016/S0079-6123(08)63395-6

Edmunds, K.J., Petersen, H., Hassan, M., Yassine, S., Olivieri, A., Barollo, F., Friðriksdóttir, R., Edmunds, P., Gíslason, M.K., Fratini, A., Gargiulo, P., 2019. Cortical recruitment and functional dynamics in postural control adaptation and habituation during vibratory proprioceptive stimulation. J. Neural Eng. https://doi.org/10.1088/1741-2552/ab0678

Einarsson, E.-J., Patel, M., Petersen, H., Wiebe, T., Fransson, P.-A., Magnusson, M., Moëll, C., 2016. Decreased postural control in adult survivors of childhood cancer treated with chemotherapy. Sci. Reports 2016 61 6, 1–10. https://doi.org/10.1038/srep36784

Eklund, G., 2011. General Features of Vibration-Induced Effects on Balance. https://mc.manuscriptcentral.com/ujms 77, 112–124. https://doi.org/10.1517/03009734000000016

Eklund, G., 1973. Further studies of vibration-induced effects on balance - PubMed. Ups J Med Sci 78, 65–72.

Eklund, G., 1971. Some physical properties of muscle vibrators used to elicit tonic proprioceptive reflexes in man - PubMed. Acta Soc Med Ups 76.

Engel, A.K., Fries, P., 2010. Beta-band oscillations-signalling the status quo? Curr. Opin. Neurobiol. https://doi.org/10.1016/j.conb.2010.02.015

Eyzaguirre, C., Fidone, S.J., 1975. Physiology of the nervous system : an introductory text 418.

Fan, L., Li, H., Zhuo, J., Zhang, Y., Wang, J., Chen, L., Yang, Z., Chu, C., Xie, S., Laird, A.R., Fox, P.T., Eickhoff, S.B., Yu, C., Jiang, T., 2016. The Human Brainnetome Atlas: A New Brain Atlas Based on Connectional Architecture. Cereb. Cortex 26, 3508–26. https://doi.org/10.1093/cercor/bhw157

Fathima, N., Umarani, K., 2016. Reduction of Noise in EEG Signal using Faraday's Cage and Wavelets Transform: A comparative Study, International Journal of Engineering Science and Computing.

Feldner, H.A., Howell, D., Kelly, V.E., McCoy, S.W., Steele, K.M., 2019. “Look, Your Muscles Are Firing!”: A Qualitative Study of Clinician Perspectives on the Use of Surface Electromyography in Neurorehabilitation. Arch. Phys. Med. Rehabil. 100, 663–675. https://doi.org/10.1016/j.apmr.2018.09.120

Fell, J., Axmacher, N., Haupt, S., 2010. From alpha to gamma: Electrophysiological correlates of meditation-related states of consciousness. Med. Hypotheses. https://doi.org/10.1016/j.mehy.2010.02.025

Ferraye, M.U., DebÛ, B., Heil, L., Carpenter, M., Bloem, B.R., Toni, I., 2014. Using motor imagery to study the neural substrates of dynamic balance. PLoS One 9, e91183. https://doi.org/10.1371/journal.pone.0091183

Ferree, T.C., Luu, P., Russell, G.S., Tucker, D.M., 2001. Scalp electrode impedance, infection risk, and EEG data quality. Clin. Neurophysiol. 112, 536–44.

Fitzpatrick, R., Burke, D., Gandevia, S., 1996. Loop gain of reflexes controlling human standing measured with the use of postural and vestibular disturbances. J. Neurophysiol. 76, 3994–4008. https://doi.org/10.1152/JN.1996.76.6.3994

Fitzpatrick, R.C., 2003. More pulsating movement. J. Physiol. 551, 4. https://doi.org/10.1113/JPHYSIOL.2003.044792

Forbes, P.A., Chen, A., Blouin, J.S., 2018. Sensorimotor control of standing balance. Handb. Clin. Neurol. 159, 61–83. https://doi.org/10.1016/B978-0-444-63916-5.00004-5

Fornito, A., Zalesky, A., Bullmore, E.T., 2016. Fundamentals of Brain Network Analysis, Fundamentals of Brain Network Analysis. Elsevier Inc. https://doi.org/10.1016/C2012-0-06036-X

Frank, S.M., Greenlee, M.W., 2018. The parieto-insular vestibular cortex in humans: More than a single area? J. Neurophysiol. https://doi.org/10.1152/jn.00907.2017

Fransson, P.-A., 2005. Analysis of adaptation in human postural control. Lund Univ. Sweden. Lund University.

Fransson, P.-A., Patel, M., Jensen, H., Lundberg, M., Tjernström, F., Magnusson, M., Ekvall Hansson, E., 2019. Postural instability in an immersive Virtual Reality adapts with repetition and includes directional and gender specific effects. Sci. Reports 2019 91 9, 1–

10. https://doi.org/10.1038/s41598-019-39104-6

Fransson, P., Johansson, R., Hafström, A., Magnusson, M., 2000. Methods for evaluation of postural control adaptation. Gait Posture 12, 14–24. https://doi.org/10.1016/S0966-6362(00)00052-7

Fransson, P.A., Hafström, A., Karlberg, M., Magnusson, M., Tjäder, A., Johansson, R., 2003. Postural Control Adaptation during Galvanic Vestibular and Vibratory Proprioceptive Stimulation. IEEE Trans. Biomed. Eng. 50, 1310–1319. https://doi.org/10.1109/TBME.2003.819851

Friðriksdóttir, R., Karlsson, G.H., Svansson, H., Barollo, F., Edmunds, K.J., Petersen, H., Gargiulo, P., 2020. Brain Processing During Postural Control – A Study Case, in: IFMBE Proceedings. Springer, pp. 1147–1154. https://doi.org/10.1007/978-3-030-31635-8_139

Fujita, H., Kasubuchi, K., Wakata, S., Hiyamizu, M., Morioka, S., 2016. Role of the Frontal Cortex in Standing Postural Sway Tasks while Dual-Tasking: A Functional Near-Infrared Spectroscopy Study Examining Working Memory Capacity. Biomed Res. Int. https://doi.org/10.1155/2016/7053867

Fujiwara, K., Maekawa, M., Kiyota, N., Yaguchi, C., 2012. Adaptation changes in dynamic postural control and contingent negative variation during backward disturbance by transient floor translation in the elderly. J. Physiol. Anthropol. https://doi.org/10.1186/1880-6805-31-12

Fung, J., Macpherson, J.M., 1999. Attributes of quiet stance in the chronic spinal cat. J. Neurophysiol. 82, 3056–3065. https://doi.org/10.1152/jn.1999.82.6.3056

Gallen, C.L., Baniqued, P.L., Chapman, S.B., Aslan, S., Keebler, M., Didehbani, N., D'Esposito, M., 2016. Modular brain network organization predicts response to cognitive training in older adults. PLoS One. https://doi.org/10.1371/journal.pone.0169015

Galvão, T.S., Magalhães Júnior, E.S., Orsini Neves, M.A., de Sá Ferreira, A., 2018. Lower-limb muscle strength, static and dynamic postural stabilities, risk of falling and fear of falling in polio survivors and healthy subjects. Physiother. Theory Pract. https://doi.org/10.1080/09593985.2018.1512178

Gatev, P., Thomas, S., Kepple, T., Hallett, M., 1999. Feedforward ankle strategy of balance

during quiet stance in adults. J. Physiol. 514, 915–928. https://doi.org/10.1111/j.1469-7793.1999.915ad.x

Geurts, M, de H., IJ, van N., J, D., 2005. A review of standing balance recovery from stroke. Gait Posture 22, 267–281. https://doi.org/10.1016/J.GAITPOST.2004.10.002

Gilaie-Dotan, S., Saygin, A.P., Lorenzi, L.J., Egan, R., Rees, G., Behrmann, M., 2013. The role of human ventral visual cortex in motion perception. Brain. https://doi.org/10.1093/brain/awt214

Goh, K.L., Morris, S., Lee, W.L., Ring, A., Tan, T., 2017. Postural and cortical responses following visual occlusion in standing and sitting tasks. Exp. Brain Res. https://doi.org/10.1007/s00221-017-4887-6

Golding, J.F., 2016. Motion sickness. Handb. Clin. Neurol. 137, 371–390. https://doi.org/10.1016/B978-0-444-63437-5.00027-3

Grech, R., Cassar, T., Muscat, J., Camilleri, K.P., Fabri, S.G., Zervakis, M., Xanthopoulos, P., Sakkalis, V., Vanrumste, B., 2008. Review on solving the inverse problem in EEG source analysis. J. Neuroeng. Rehabil. https://doi.org/10.1186/1743-0003-5-25

Grigg, P., Greenspan, B., 1977. Response of primate joint afferent neurons to mechanical stimulation of knee joint. J. Neurophysiol. 40, 1–8. https://doi.org/10.1152/JN.1977.40.1.1

Gross, J., Tass, P., Salenius, S., Hari, R., Freund, H., Schnitzler, A., 2000. Cortico-muscular synchronization during isometric muscle contraction in humans as revealed by magnetoencephalography. J. Physiol. 527 Pt 3, 623–631. https://doi.org/10.1111/J.1469-7793.2000.00623.X

Gurfinkel, V S, Ivanenko, Y.P., Levik, Y.S., 1995. The influence of head rotation on human upright posture during balanced bilateral vibration - PubMed. Neuroreport 7.

Gurfinkel, V. S., Ivanenko, Y.P., Levik, Y.S., Babakova, I.A., 1995. Kinesthetic reference for human orthograde posture. Neuroscience 68, 229–243. https://doi.org/10.1016/0306-4522(95)00136-7

Guterstam, A., Björnsdotter, M., Gentile, G., Ehrsson, H.H., 2015. Posterior cingulate cortex integrates the senses of self-location and body ownership. Curr. Biol. https://doi.org/10.1016/j.cub.2015.03.059

Gwin, J.T., Ferris, D.P., 2012. Beta- and gamma-range human lower limb corticomuscular coherence. Front. Hum. Neurosci. 0, 258. https://doi.org/10.3389/FNHUM.2012.00258

Hagbarth, K.E., Hellsing, G., Löfstedt, L., 1976. TVR and vibration-induced timing of motor impulses in the human jaw elevator muscles. J. Neurol. Neurosurg. Psychiatry 39, 719. https://doi.org/10.1136/JNNP.39.8.719

Hallez, H., Vanrumste, B., Grech, R., Muscat, J., De Clercq, W., Vergult, A., D'Asseler, Y., Camilleri, K.P., Fabri, S.G., Van Huffel, S., Lemahieu, I., 2007. Review on solving the forward problem in EEG source analysis. J. Neuroeng. Rehabil. 4, 46. https://doi.org/10.1186/1743-0003-4-46

Halliday, D.M., Rosenberg, J.R., Amjad, A.M., Breeze, P., Conway, B.A., Farmer, S.F., 1995. A framework for the analysis of mixed time series/point process data-theory and application to the study of physiological tremor, single motor unit discharges and electromyograms. Prog. Biophys. Mol. Biol. 64, 237–278.

Handiru, Alivar, A., Hoxha, A., Saleh, S., Suviseshamuthu, E.S., Yue, G., Allexandre, D., 2020. Graph-theoretical Analysis of EEG Functional Connectivity during Balance Perturbation in Traumatic Brain Injury. bioRxiv 2020.10.08.332353. https://doi.org/10.1101/2020.10.08.332353

Harro, C.C., Marquis, A., Piper, N., Burdis, C., 2016. Reliability and Validity of Force Platform Measures of Balance Impairment in Individuals With Parkinson Disease. Phys. Ther. https://doi.org/10.2522/ptj.20160099

Hassan, M., Merlet, I., Mheich, A., Kabbara, A., Biraben, A., Nica, A., Wendling, F., 2017. Identification of Interictal Epileptic Networks from Dense-EEG. Brain Topogr. 30, 60–76. https://doi.org/10.1007/s10548-016-0517-z

Hassan, M., Wendling, F., 2018a. Electroencephalography Source Connectivity: Aiming for High Resolution of Brain Networks in Time and Space. IEEE Signal Process. Mag. 35, 81–96. https://doi.org/10.1109/MSP.2017.2777518

Hassan, M., Wendling, F., 2018b. Electroencephalography Source Connectivity. IEEE Signal Process. Mag. 81–96. https://doi.org/10.1109/MSP.2017.2777518

Hayes, K.C., 1982. Biomechanics of Postural Control. Exerc. Sport Sci. Rev. 10, 363–391.

Herman, T., Mirelman, A., Giladi, N., Schweiger, A., Hausdorff, J.M., 2010. Executive Control Deficits as a Prodrome to Falls in Healthy Older Adults: A Prospective Study Linking Thinking, Walking, and Falling. Journals Gerontol. Ser. A 65A, 1086–1092. https://doi.org/10.1093/GERONA/GLQ077

Hincapié, A.S., Kujala, J., Mattout, J., Daligault, S., Delpuech, C., Mery, D., Cosmelli, D., Jerbi, K., 2016. MEG connectivity and power detections with minimum norm estimates require different regularization parameters. Comput. Intell. Neurosci. 2016. https://doi.org/10.1155/2016/3979547

Hlavackova, P., Vuillerme, N., 2012. Do somatosensory conditions from the foot and ankle affect postural responses to plantar-flexor muscles fatigue during bipedal quiet stance? Gait Posture. https://doi.org/10.1016/j.gaitpost.2011.10.361

Homma, S., Kanda, K., Watanabe, S., 1972. Preferred spike intervals in the vibration reflex. Jpn. J. Physiol. 22, 421–432.

Honeycutt, C.F., Richard Nichols, T., 2010. Disruption of cutaneous feedback alters magnitude but not direction of muscle responses to postural perturbations in the decerebrate cat. Exp. Brain Res. https://doi.org/10.1007/s00221-010-2281-8

Honma, S., Seki, Y., 1964. Muscle spindles in phasic and tonic muscle. Tohoku J. Exp. Med. 83, 391–397. https://doi.org/10.1620/tjem.83.391

Horak, F., Nashner, L., Diener, H., 1990. Postural strategies associated with somatosensory and vestibular loss. Exp. brain Res. 82, 167–177. https://doi.org/10.1007/BF00230848

Horak, F.B., 2006. Postural orientation and equilibrium: What do we need to know about neural control of balance to prevent falls?, in: Age and Ageing. https://doi.org/10.1093/ageing/afl077

Horak, Fay B, Macpherson, J.M., 1996. 7 . Postural orientation and equilibrium, in: Rowell LB, S.J. (Ed.), Handbook of Physiology, Exercise: Regulation and Integration of Multiple Systems. Oxford University Press, New York, pp. 255–92.

Horak, F. B., Macpherson, J.M., 1996. Postural Orientation and Equilibrium. B. Rowell, J. T. Sheperd (Eds.), Handb. Physiol. Section 12, 255–292.

Horak, F.B., Nashner, L.M., 1986. Central programming of postural movements: Adaptation to

altered support-surface configurations. J. Neurophysiol. 55, 1369–1381. https://doi.org/10.1152/jn.1986.55.6.1369

Horak, F.B., Sharon, S.M., Shumway-Cook, A., 1997. Postural Pertubations: New Insights for Treatment of Balance Disorders. Phys. Ther. 77, 517–533.

Hu, M.H., Woollacott, M.H., 1994. Multisensory training of standing balance in older adults: I. Postural stability and one-leg stance balance. Journals Gerontol. https://doi.org/10.1093/geronj/49.2.M52

Hudspeth, A. J., Jessell, T. M., Kandel, E. R., Schwartz, J. H., & Siegelbaum, S.A. (Eds. ., 2013. Principles Of Neural Science, The McGraw-Hill Companies. https://doi.org/10.1007/s13398-014-0173-7.2

Hülsdünker, T., Mierau, A., Neeb, C., Kleinöder, H., Strüder, H.K., 2015. Cortical processes associated with continuous balance control as revealed by EEG spectral power. Neurosci. Lett. 592, 1–5. https://doi.org/10.1016/j.neulet.2015.02.049

Hülsdünker, T., Mierau, A., Strüder, H.K., 2016. Higher balance task demands are associated with an increase in individual alpha peak frequency. Front. Hum. Neurosci. https://doi.org/10.3389/fnhum.2015.00695

Inglis, J., Kennedy, P., Wells, C., Chua, R., 2002. The role of cutaneous receptors in the foot. Adv. Exp. Med. Biol. 508, 111–117. https://doi.org/10.1007/978-1-4615-0713-0_14

Inglis, J.T., Horak, F.B., Shupert, C.L., Jones-Rycewicz, C., 1994. The importance of somatosensory information in triggering and scaling automatic postural responses in humans. Exp. Brain Res. 101, 159–164. https://doi.org/10.1007/BF00243226

Ishida, A., Imai, S., Fukuoka, Y., 1997. Analysis of the posture control system under fixed and sway-referenced support conditions. IEEE Trans. Biomed. Eng. 44, 331–336. https://doi.org/10.1109/10.568908

Ivanenko, Y., Solopova, I., Levik, Y., 2000. The direction of postural instability affects postural reactions to ankle muscle vibration in humans. Neurosci. Lett. 292, 103–106. https://doi.org/10.1016/S0304-3940(00)01438-5

Ivanenko, Y., Talis, V., Kazennikov, O., 1999. Support stability influences postural responses to muscle vibration in humans. Eur. J. Neurosci. 11, 647–654.

https://doi.org/10.1046/J.1460-9568.1999.00471.X

Izquierdo, M., Ibañez, J., Gorostiaga, E., Garrues, M., Zúñiga, A., Antón, A., Larrión, J., Häkkinen, K., 1999. Maximal strength and power characteristics in isometric and dynamic actions of the upper and lower extremities in middle-aged and older men. Acta Physiol. Scand. 167, 57–68. https://doi.org/10.1046/J.1365-201X.1999.00590.X

Jacobs, J. V., Horak, F.B., 2007. Cortical control of postural responses, in: Journal of Neural Transmission. Springer, pp. 1339–1348. https://doi.org/10.1007/s00702-007-0657-0

Jacobs, J. V., Wu, G., Kelly, K.M., 2015. Evidence for beta corticomuscular coherence during human standing balance: Effects of stance width, vision, and support surface. Neuroscience. https://doi.org/10.1016/j.neuroscience.2015.04.009

Janssen, I., Heymsfield, S.B., Wang, Z.M., Ross, R., 2000. Skeletal muscle mass and distribution in 468 men and women aged 18-88 yr. J. Appl. Physiol. 89, 81–88. https://doi.org/10.1152/jappl.2000.89.1.81

Japee, S., Holiday, K., Satyshur, M.D., Mukai, I., Ungerleider, L.G., 2015. A role of right middle frontal gyrus in reorienting of attention: A case study. Front. Syst. Neurosci. https://doi.org/10.3389/fnsys.2015.00023

Jasper, H.H., 1958. The Tenn Twenty Electrode System of The International Federation, Electroencephalography and Clinical Neurophysiology. https://doi.org/10.1016/0013-4694(58)90053-1

Johansson, R., Fransson, P.A., Magnusson, M., 2009. Optimal coordination and control of posture and movements. J. Physiol. Paris. https://doi.org/10.1016/j.jphysparis.2009.08.013

Johansson, R., Magnusson, M., 1991. Human postural dynamics. Crit. Rev. Biomed. Eng.

Johnston, Wu, 1995. Foundations of cellular neurophysiology, MIT Press.

Jung, T.P., Humphries, C., Lee, T.W., Makeig, S., McKeown, M.J., Iragui, V., Sejnowski, T.J., 1998. Removing electroencephalographic artifacts: Comparison between ICA and PCA, in: Neural Networks for Signal Processing - Proceedings of the IEEE Workshop. IEEE, pp. 63–72. https://doi.org/10.1109/nnsp.1998.710633

Kabbara, A., Khalil, M., O'neill, G., Dujardin, K., El Traboulsi, Y., Wendling, F., Hassan, M., 2019. Detecting modular brain states in rest and task. Netw. Neurosci. https://doi.org/10.1162/netn_a_00090

Kabbara, A., Paban, V., Hassan, M., 2020a. The dynamic modular fingerprints of the human brain at rest.

Kabbara, A., Paban, V., Hassan, M., 2020b. The dynamic modular fingerprints of the human brain at rest. bioRxiv 2020.05.30.125385. https://doi.org/10.1101/2020.05.30.125385

Kamei, S., Morita, A., Serizawa, K., Mizutani, T., Hirayanagi, K., 2010. Quantitative EEG Analysis of Executive Dysfunction in Parkinson Disease. J. Clin. Neurophysiol. 27, 193–197. https://doi.org/10.1097/WNP.0b013e3181dd4fdb

Karim, H.T., Sparto, P.J., Aizenstein, H.J., Furman, J.M., Huppert, T.J., Erickson, K.I., Loughlin, P.J., 2014. Functional MR imaging of a simulated balance task. Brain Res. 1555, 20–27. https://doi.org/10.1016/j.brainres.2014.01.033

Karnath, H.O., 1997. Spatial orientation and the representation of space with parietal lobe lesions, in: Philosophical Transactions of the Royal Society B: Biological Sciences. https://doi.org/10.1098/rstb.1997.0127

Kaufman, Nasher, Allison, 1997. Balance is a critical parameter in orthopedic rehabilitation, Orthopaedic Physical Therapy Clinics of North America. Orthop. Phys. Ther. Clin. North Am. 6, 43–77.

Kavounoudias, A., Gilhodes, J., Roll, R., Roll, J., 1999. From balance regulation to body orientation: two goals for muscle proprioceptive information processing? Exp. brain Res. 124, 80–88. https://doi.org/10.1007/S002210050602

Kavounoudias, A., Roll, R., Roll, J., 1998. The plantar sole is a "dynamometric map" for human balance control. Neuroreport 9, 3247–3252. https://doi.org/10.1097/00001756-199810050-00021

Kearney, Hunter, 1990. System Identification of Human Joint Dynamics. Crit. Rev. Biomed. Eng.

Kerkman, J.N., Bekius, A., Boonstra, T.W., Daffertshofer, A., Dominici, N., 2020. Muscle Synergies and Coherence Networks Reflect Different Modes of Coordination During

Walking. Front. Physiol. 0, 751. https://doi.org/10.3389/FPHYS.2020.00751

Keshner, E.A., Allum, J.H.J., Pfaltz, C.R., 1987. Postural coactivation and adaptation in the sway stabilizing responses of normals and patients with bilateral vestibular deficit. Exp. Brain Res. 1987 691 69, 77–92. https://doi.org/10.1007/BF00247031

Klasser, G.D., Okeson, J.P., 2006. The clinical usefulness of surface electromyography in the diagnosis and treatment of temporomandibular disorders. J. Am. Dent. Assoc. 137, 763–771. https://doi.org/10.14219/jada.archive.2006.0288

Kleiber, GA, H., V, D., 1990. Body sway stabilization in human posture. Acta Otolaryngol. 110, 168–174. https://doi.org/10.3109/00016489009122533

Kolster, H., Peeters, R., Orban, G.A., 2010. The retinotopic organization of the human middle temporal area MT/V5 and its cortical neighbors. J. Neurosci. https://doi.org/10.1523/JNEUROSCI.2069-10.2010

Kringelbach, M.L., 2005. The human orbitofrontal cortex: Linking reward to hedonic experience. Nat. Rev. Neurosci. https://doi.org/10.1038/nrn1747

Kristinsdóttir, E., Jarnlo, G., Magnusson, M., 1997. Aberrations in postural control, vibration sensation and some vestibular findings in healthy 64-92-year-old subjects. undefined.

Kristinsdottir, E.K., PA, F., M, M., 2001. Changes in postural control in healthy elderly subjects are related to vibration sensation, vision and vestibular asymmetry. Acta Otolaryngol. 121, 700–706. https://doi.org/10.1080/00016480152583647

Lachaux, J.P., Rodriguez, E., Martinerie, J., Varela, F.J., 1999. Measuring phase synchrony in brain signals. Hum. Brain Mapp. 8, 194–208. https://doi.org/10.1002/(SICI)1097-0193(1999)8:4<194::AID-HBM4>3.0.CO;2-C

Lackner, J., 1988. Some proprioceptive influences on the perceptual representation of body shape and orientation. Brain 111 ( Pt 2, 281–297. https://doi.org/10.1093/BRAIN/111.2.281

Lavin, C., Melis, C., Mikulan, E., Gelormini, C., Huepe, D., Ibañez, A., 2013. The anterior cingulate cortex: an integrative hub for human socially-driven interactions. Front. Neurosci. https://doi.org/10.3389/fnins.2013.00064

Ledin, T., Hafström, A., Fransson, P., Magnusson, M., 2003. Influence of neck proprioception on vibration-induced postural sway. Acta Otolaryngol. 123, 594–599. https://doi.org/10.1080/00016480310001835

Leech, R., Braga, R., Sharp, D.J., 2012. Echoes of the brain within the posterior cingulate cortex. J. Neurosci. https://doi.org/10.1523/JNEUROSCI.3689-11.2012

Leech, R., Sharp, D.J., 2014. The role of the posterior cingulate cortex in cognition and disease. Brain. https://doi.org/10.1093/brain/awt162

Lim, Kim, J.S., Lee, H.W., Kim, S.H., 2018. Postural instability induced by visual motion stimuli in patients with vestibular migraine. Front. Neurol. 9, 433. https://doi.org/10.3389/fneur.2018.00433

Lin, C.C., Barker, J.W., Sparto, P.J., Furman, J.M., Huppert, T.J., 2017. Functional near-infrared spectroscopy (fNIRS) brain imaging of multi-sensory integration during computerized dynamic posturography in middle-aged and older adults. Exp. Brain Res. 235, 1247–1256. https://doi.org/10.1007/s00221-017-4893-8

Lipsitz, L.A., Goldberger, A.L., 1992. Loss of 'Complexity' and Aging: Potential Applications of Fractals and Chaos Theory to Senescence. JAMA J. Am. Med. Assoc. https://doi.org/10.1001/jama.1992.03480130122036

Liu-Ambrose, T., Nagamatsu, L.S., Hsu, C.L., Bolandzadeh, N., 2013. Emerging concept: 'central benefit model' of exercise in falls prevention. Br. J. Sports Med. 47, 115–117. https://doi.org/10.1136/BJSPORTS-2011-090725

Liu, J., Sheng, Y., Liu, H., 2019. Corticomuscular coherence and its applications: A review. Front. Hum. Neurosci. https://doi.org/10.3389/fnhum.2019.00100

Lopes Da Silva, F.H., Storm Van Leeuwen, W., 1977. The cortical source of the alpha rhythm. Neurosci. Lett. 6, 237–41.

Lopez, A., Ferrero, F.J., Valledor, M., Campo, J.C., Postolache, O., 2016. A study on electrode placement in EOG systems for medical applications, in: 2016 IEEE International Symposium on Medical Measurements and Applications (MeMeA). IEEE, pp. 1–5. https://doi.org/10.1109/MeMeA.2016.7533703

López, S., Gross, A., Yang, S., Golmohammadi, M., Obeid, I., Picone, J., 2016. AN ANALYSIS

OF TWO COMMON REFERENCE POINTS FOR EEGS. ... IEEE Signal Process. Med. Biol. Symp. (SPMB). IEEE Signal Process. Med. Biol. Symp. 2016. https://doi.org/10.1109/SPMB.2016.7846854

Loram, I.D., Maganaris, C.N., Lakie, M., 2005. Human postural sway results from frequent, ballistic bias impulses by soleus and gastrocnemius. J. Physiol. 564, 295–311. https://doi.org/10.1113/jphysiol.2004.076307

Lord, S., Dayhew, J., 2001. Visual risk factors for falls in older people. J. Am. Geriatr. Soc. 49, 508–515. https://doi.org/10.1046/J.1532-5415.2001.49107.X

Lotte, F., Bougrain, L., Cichocki, A., Clerc, M., Congedo, M., Rakotomamonjy, A., Yger, F., 2018. A review of classification algorithms for EEG-based brain-computer interfaces: A 10 year update. J. Neural Eng. https://doi.org/10.1088/1741-2552/aab2f2

Luo, H., Wang, X., Fan, M., Deng, L., Jian, C., Wei, M., Luo, J., 2018. The Effect of Visual Stimuli on Stability and Complexity of Postural Control. Front. Neurol. 9, 48. https://doi.org/10.3389/FNEUR.2018.00048

MacDougall, H., Moore, S., Curthoys, I., Black, F., 2006. Modeling postural instability with Galvanic vestibular stimulation. Exp. brain Res. 172, 208–220. https://doi.org/10.1007/S00221-005-0329-Y

Magnus, R., 1926. Some results of studies in the physiology of posture. Lancet.

Magnus, R., 1925. The Croonian Lecture: animal posture. Proc. R. Soc. B 98, 339–353.

Magnusson, M., Pyykkö, I., 1986. Velocity and asymmetry of optokinetic nystagmus in the evaluation of vestibular lesions. Acta Otolaryngol. 102, 65–74. https://doi.org/10.3109/00016488609108648

Mahajan, Y., Peter, V., Sharma, M., 2017. Effect of EEG referencing methods on auditory mismatch negativity. Front. Neurosci. 11, 1–11. https://doi.org/10.3389/fnins.2017.00560

Maki, B., Ostrovski, G., 1993. Scaling of postural responses to transient and continuous perturbations. Gait Posture 1, 93–104. https://doi.org/10.1016/0966-6362(93)90020-2

Maki, B.E., McIlroy, W.E., 2007. Cognitive demands and cortical control of human balance-recovery reactions. J. Neural Transm. 114, 1279–1296. https://doi.org/10.1007/s00702-

007-0764-y

Malmivuo, J., Plonsey, R., 1995. BioelectromagnetismPrinciples and Applications of Bioelectric and Biomagnetic Fields. Oxford University Press. https://doi.org/10.1093/acprof:oso/9780195058239.001.0001

Malmström, E., Fransson, P., Jaxmar Bruinen, T., Facic, S., Tjernström, F., 2017. Disturbed cervical proprioception affects perception of spatial orientation while in motion. Exp. brain Res. 235, 2755–2766. https://doi.org/10.1007/S00221-017-4993-5

Manor, B., Hu, K., Zhao, P., Selim, M., Alsop, D., Novak, P., Lipsitz, L., Novak, V., 2010. Altered control of postural sway following cerebral infarction: A cross-sectional analysis. Neurology. https://doi.org/10.1212/WNL.0b013e3181cef647

Manor, B., Lipsitz, L.A., 2013. Physiologic complexity and aging: Implications for physical function and rehabilitation. Prog. Neuro-Psychopharmacology Biol. Psychiatry. https://doi.org/10.1016/j.pnpbp.2012.08.020

Maris, E., Oostenveld, R., 2007. Nonparametric statistical testing of EEG- and MEG-data. J. Neurosci. Methods 164, 177–190. https://doi.org/10.1016/j.jneumeth.2007.03.024

Mathewson, K.E., Harrison, T.J.L., Kizuk, S.A.D., 2017. High and dry? Comparing active dry EEG electrodes to active and passive wet electrodes. Psychophysiology 54, 74–82. https://doi.org/10.1111/psyp.12536

Mazzoli, D., Giannotti, E., Manca, M., Longhi, M., Prati, P., Cosma, M., Ferraresi, G., Morelli, M., Zerbinati, P., Masiero, S., Merlo, A., 2018. Electromyographic activity of the vastus intermedius muscle in patients with stiff-knee gait after stroke. A retrospective observational study. Gait Posture 60, 273–278. https://doi.org/10.1016/j.gaitpost.2017.07.002

McManus, L., De Vito, G., Lowery, M.M., 2020. Analysis and Biophysics of Surface EMG for Physiotherapists and Kinesiologists: Toward a Common Language With Rehabilitation Engineers. Front. Neurol. 11, 576729. https://doi.org/10.3389/fneur.2020.576729

Meekins, G.D., So, Y., Quan, D., Vavricek, J., 2008. American Association of Neuromuscular & Electrodiagnostic Medicine evidenced-based review: Use of surface electromyography in the diagnosis and study of neuromuscular disorders. Muscle and Nerve 38, 1219–1224.

https://doi.org/10.1002/mus.21055

Melnik, A., Hairston, W.D., Ferris, D.P., König, P., 2017. EEG correlates of sensorimotor processing: independent components involved in sensory and motor processing. Sci. Rep. 7. https://doi.org/10.1038/S41598-017-04757-8

Mergner, Rosemeier, 1998. Interaction of vestibular, somatosensory and visual signals for postural control and motion perception under terrestrial and microgravity conditions--a conceptual model. Brain Res. Brain Res. Rev. 28, 118–135. https://doi.org/10.1016/S0165-0173(98)00032-0

Mergner, T., Maurer, C., Peterka, R.J., 2003. A multisensory posture control model of human upright stance, in: Progress in Brain Research. Elsevier, pp. 189–201. https://doi.org/10.1016/S0079-6123(03)42014-1

Merlo, A., Campanini, I., 2019. ☆Impact of instrumental analysis of stiff knee gait on treatment appropriateness and associated costs in stroke patients. Gait Posture 72, 195–201. https://doi.org/10.1016/j.gaitpost.2019.06.009

Mierau, A., Klimesch, W., Lefebvre, J., 2017a. State-dependent alpha peak frequency shifts: Experimental evidence, potential mechanisms and functional implications. Neuroscience. https://doi.org/10.1016/j.neuroscience.2017.07.037

Mierau, A., Pester, B., Hülsdünker, T., Schiecke, K., Strüder, H.K., Witte, H., 2017b. Cortical Correlates of Human Balance Control. Brain Topogr. https://doi.org/10.1007/s10548-017-0567-x

Mochizuki, G., Boe, S., Marlin, A., McIlroy, W.E., 2010. Perturbation-evoked cortical activity reflects both the context and consequence of postural instability. Neuroscience. https://doi.org/10.1016/j.neuroscience.2010.07.008

Morasso, P.G., Schieppati, M., 1999. Can muscle stiffness alone stabilize upright standing? J. Neurophysiol. 82, 1622–1626. https://doi.org/10.1152/jn.1999.82.3.1622

Mormann, F., Lehnertz, K., David, P., E. Elger, C., 2000. Mean phase coherence as a measure for phase synchronization and its application to the EEG of epilepsy patients. Phys. D Nonlinear Phenom. 144, 358–369. https://doi.org/10.1016/S0167-2789(00)00087-7

Muir, S.W., Gopaul, K., Montero Odasso, M.M., 2012. The role of cognitive impairment in fall

risk among older adults: A systematic review and meta-analysis. Age Ageing. https://doi.org/10.1093/ageing/afs012

Murnaghan, C.D., Squair, J.W., Chua, R., Inglis, J.T., Carpenter, M.G., 2014. Cortical contributions to control of posture during unrestricted and restricted stance. J. Neurophysiol. 111, 1920–1926. https://doi.org/10.1152/jn.00853.2012

Nandi, T., Hortobágyi, T., van Keeken, H.G., Salem, G.J., Lamoth, C.J.C., 2019. Standing task difficulty related increase in agonist-agonist and agonist-antagonist common inputs are driven by corticospinal and subcortical inputs respectively. Sci. Rep. 9, 1–12. https://doi.org/10.1038/s41598-019-39197-z

Nashner, L.M., McCollum, G., 1985. The organization of human postural movements: A formal basis and experimental synthesis. Behav. Brain Sci. 8, 135–150. https://doi.org/10.1017/S0140525X00020008

Negro, F., Farina, D., 2011. Linear transmission of cortical oscillations to the neural drive to muscles is mediated by common projections to populations of motoneurons in humans. J. Physiol. 589, 629. https://doi.org/10.1113/JPHYSIOL.2010.202473

Niedermeyer, E., Lopes da Silva, F., 2005. Electroencephalography : basic principles, clinical applications, and related fields, 5th ed. ed. Lippincott Williams & Wilkins, Philadelphia ; London.

Nonaka, H., Mita, K., Watakabe, M., Akataki, K., N, S., Okuwa, T., Yabe, K., 2002. Age-related changes in the interactive mobility of the hip and knee joints: a geometrical analysis. Gait Posture 15, 236–243. https://doi.org/10.1016/S0966-6362(01)00191-6

Nunez, P.L., 2010. REST: a good idea but not the gold standard. Clin. Neurophysiol. 121, 2177–80. https://doi.org/10.1016/j.clinph.2010.04.029

Oman, C., Frishkopf, L., Goldstein, M., 1979. Cupula motion in the semicircular canal of the skate, Raja erinacea. An experimental investigation. Acta Otolaryngol. 87, 528–538. https://doi.org/10.3109/00016487909126461

Omlor, W., Patino, L., Hepp-Reymond, M.C., Kristeva, R., 2007. Gamma-range corticomuscular coherence during dynamic force output. Neuroimage 34, 1191–1198. https://doi.org/10.1016/j.neuroimage.2006.10.018

Oostenveld, R., Fries, P., Maris, E., Schoffelen, J.M., 2011. FieldTrip: Open source software for advanced analysis of MEG, EEG, and invasive electrophysiological data. Comput. Intell. Neurosci. 2011. https://doi.org/10.1155/2011/156869

Osselton, J.., 1965. Acquisition of EEG data by bipolar unipolar and average reference methods: a theoretical comparison. Electroencephalogr. Clin. Neurophysiol. 19, 527–528. https://doi.org/10.1016/0013-4694(65)90195-1

Osselton, J.W., 1969. Bipolar, Unipolar and Average Reference Recording Methods II: Mainly Practical Considerations. Am. J. EEG Technol. 9, 117–133. https://doi.org/10.1080/00029238.1969.11080747

Ozdemir, R.A., Contreras-Vidal, J.L., Lee, B.C., Paloski, W.H., 2016. Cortical activity modulations underlying age-related performance differences during posture–cognition dual tasking. Exp. Brain Res. 234, 3321–3334. https://doi.org/10.1007/s00221-016-4730-5

Palmer, J.A., Payne, A.M., Ting, L.H., Borich, M.R., 2021. Prefrontal-motor and somatosensory-motor cortical network interactions during reactive balance are associated with distinct aspects of balance behavior in older adults. bioRxiv 2021.01.30.428951. https://doi.org/10.1101/2021.01.30.428951

Palmieri-Smith, R.M., Ingersoll, C.D., Stone, M.B., Krause, B.A., 2002. Center-of-Pressure Parameters Used in the Assessment of Postural Control. J. Sport Rehabil. 11, 51–66.

Parra, L.C., Spence, C.D., Gerson, A.D., Sajda, P., 2005. Recipes for the linear analysis of EEG. Neuroimage 28, 326–341. https://doi.org/10.1016/j.neuroimage.2005.05.032

Patel, M., 2009. Postural control and adaptation to threats to balance stability.

Patel, M., Fransson, P.A., Magnusson, M., 2009. Effects of ageing on adaptation during vibratory stimulation of the calf and neck muscles. Gerontology 55, 82–91. https://doi.org/10.1159/000188114

Paulus, W., Brandt, T., 1993. The role of visual motion in the stabilization of body posture - PubMed. Rev Oculomot Res.

Paulus, W.M., A, S., T, B., 1984. Visual stabilization of posture. Physiological stimulus characteristics and clinical aspects. Brain 107 ( Pt 4, 1143–1163.

https://doi.org/10.1093/BRAIN/107.4.1143

Peterka, R.J., 2002. Sensorimotor integration in human postural control. J. Neurophysiol. 88, 1097–1118. https://doi.org/10.1152/jn.2002.88.3.1097

Peterka, R.J., Statler, K.D., Wrisley, D.M., Horak, F.B., 2011. Postural compensation for unilateral vestibular loss. Front. Neurol. https://doi.org/10.3389/fneur.2011.00057

Petersen, H., Magnusson, M., Johansson, R., Akesson, M., Fransson, P.A., 1995. Acoustic cues and postural control. Scand. J. Rehabil. Med.

Petersen, H., Patel, M., Ingason, E.F., Einarsson, E.J., Haraldsson, Á., Fransson, P.-A., 2014. Long-Term Effects from Bacterial Meningitis in Childhood and Adolescence on Postural Control. PLoS One 9, e112016. https://doi.org/10.1371/JOURNAL.PONE.0112016

Peterson, S.M., Ferris, D.P., 2019. Group-level cortical and muscular connectivity during perturbations to walking and standing balance. Neuroimage 198, 93–103. https://doi.org/10.1016/j.neuroimage.2019.05.038

Pollock, A.S., Durward, B.R., Rowe, P.J., Paul, J.P., 2000. What is balance? Clin. Rehabil. 14, 402–406. https://doi.org/10.1191/0269215500cr342oa

Prieto, T.E., Myklebust, J.B., Hoffmann, R.G., Lovett, E.G., Myklebust, B.M., 1996. Measures of postural steadiness: Differences between healthy young and elderly adults. IEEE Trans. Biomed. Eng. 43, 956–966. https://doi.org/10.1109/10.532130

Prochazka, A., Wand, P., 1980. Tendon organ discharge during voluntary movements in cats. J. Physiol. 303, 385. https://doi.org/10.1113/JPHYSIOL.1980.SP013293

Ptak, R., Schnider, A., Fellrath, J., 2017. The Dorsal Frontoparietal Network: A Core System for Emulated Action. Trends Cogn. Sci. https://doi.org/10.1016/j.tics.2017.05.002

Pullman, S.L., Goodin, D.S., Marquinez, A.I., Tabbal, S., Rubin, M., 2000. Clinical utility of surface EMG: Report of the therapeutics and technology assessment subcommittee of the American Academy of Neurology. Neurology 55, 171–177. https://doi.org/10.1212/WNL.55.2.171

Purves, D., Augustine, G.J., Fitzpatrick, D., Katz, L.C., LaMantia, A.-S., McNamara, J.O., Williams, S.M., 2001. The Motor Unit.

Quitschal, R., JY, F., MM, G., HH, C., 2014. Evaluation of postural control in unilateral vestibular hypofunction. Braz. J. Otorhinolaryngol. 80, 339–345. https://doi.org/10.1016/J.BJORL.2014.05.015

Rapp, M.A., Krampe, R.T., Baltes, P.B., 2006. Adaptive task prioritization in aging: Selective resource allocation to postural control is preserved in Alzheimer disease. Am. J. Geriatr. Psychiatry. https://doi.org/10.1097/01.JGP.0000192490.43179.e7

Ray, C.T., M, H., R, C., RC, M., SL, W., 2008. The impact of vision loss on postural stability and balance strategies in individuals with profound vision loss. Gait Posture 28, 58–61. https://doi.org/10.1016/J.GAITPOST.2007.09.010

Recenti, M., Ricciardi, C., Aubonnet, R., Picone, I., Jacob, D., Svansson, H.Á.R., Agnarsdóttir, S., Karlsson, G.H., Baeringsdóttir, V., Petersen, H., Gargiulo, P., 2021. Toward Predicting Motion Sickness Using Virtual Reality and a Moving Platform Assessing Brain, Muscles, and Heart Signals. Front. Bioeng. Biotechnol. 0, 132. https://doi.org/10.3389/FBIOE.2021.635661

Reddy, P.G., Mattar, M.G., Murphy, A.C., Wymbs, N.F., Grafton, S.T., Satterthwaite, T.D., Bassett, D.S., 2018. Brain state flexibility accompanies motor-skill acquisition. Neuroimage. https://doi.org/10.1016/j.neuroimage.2017.12.093

Reyes, A., Laine, C.M., Kutch, J.J., Valero-Cuevas, F.J., 2017. Beta Band Corticomuscular Drive Reflects Muscle Coordination Strategies. Front. Comput. Neurosci. 0, 17. https://doi.org/10.3389/FNCOM.2017.00017

Roeder, L., Boonstra, T.W., Kerr, G.K., 2020. Corticomuscular control of walking in older people and people with Parkinson's disease. Sci. Rep. 10. https://doi.org/10.1038/s41598-020-59810-w

Roll, J.P., Vedel, J.P., Ribot, E., 1989. Alteration of proprioceptive messages induced by tendon vibration in man: a microneurographic study. Exp. Brain Res. 76, 213–222. https://doi.org/10.1007/BF00253639

Rubinov, M., Sporns, O., 2010. Complex network measures of brain connectivity: Uses and interpretations. Neuroimage 52, 1059–1069. https://doi.org/10.1016/j.neuroimage.2009.10.003

Saftari, L.N., Kwon, O.S., 2018. Ageing vision and falls: A review. J. Physiol. Anthropol. https://doi.org/10.1186/s40101-018-0170-1

Sakkalis, 2011. Review of advanced techniques for the estimation of brain connectivity measured with EEG/MEG. Comput. Biol. Med. 41, 1110–1117. https://doi.org/10.1016/J.COMPBIOMED.2011.06.020

Salmelin, R., Hari, R., 1994. Spatiotemporal characteristics of sensorimotor neuromagnetic rhythms related to thumb movement. Neuroscience 60, 537–550. https://doi.org/10.1016/0306-4522(94)90263-1

Schall, J.D., 2008. Frontal Eye Fields, in: Encyclopedia of Neuroscience. Springer Berlin Heidelberg, pp. 1635–1638. https://doi.org/10.1007/978-3-540-29678-2_1861

Schieppati, M., Nardone, A., 1999. Group II spindle afferent fibers in humans: their possible role in the reflex control of stance. Prog. Brain Res. 123, 461–472. https://doi.org/10.1016/S0079-6123(08)62882-4

Schoffelen, J.M., Gross, J., 2009. Source connectivity analysis with MEG and EEG. Hum. Brain Mapp. https://doi.org/10.1002/hbm.20745

Schubert, P., Kirchner, M., Schmidtbleicher, D., Haas, C.T., 2012. About the structure of posturography: Sampling duration, parametrization, focus of attention (part I). J. Biomed. Sci. Eng. https://doi.org/10.4236/jbise.2012.59062

Shadmehr, R., Arbib, M.A., 1992. A mathematical analysis of the force-stiffness characteristics of muscles in control of a single joint system. Biol. Cybern. 1992 666 66, 463–477. https://doi.org/10.1007/BF00204111

Shaffer, J.P., 1995. Multiple hypothesis testing. Annu. Rev. Psychol. 46, 561–584. https://doi.org/10.1146/annurev.ps.46.020195.003021

Sherrington, C.S., 1910. Flexion-reflex of the limb, crossed extension-reflex, and reflex stepping and standing. J. Physiol. 40, 28–121. https://doi.org/10.1113/jphysiol.1910.sp001362

Shumway-Cook, A., Horak, F.B., 1986. Assessing the influence of sensory interaction on balance. Suggestion from the field. Phys. Ther. https://doi.org/10.1093/ptj/66.10.1548

Sipp, A.R., Gwin, J.T., Makeig, S., Ferris, D.P., 2013. Loss of balance during balance beam walking elicits a multifocal theta band electrocortical response. J. Neurophysiol. https://doi.org/10.1152/jn.00744.2012

Skinner, H.B., Barack, R.L., Cook, S.D., 1984. Age-related decline in proprioception. Clin Orthop Relat Res 184.

Slobounov, R, T., E, S., M, R., W, R., 2000. Human oscillatory brain activity within gamma band (30-50 Hz) induced by visual recognition of non-stable postures. Brain Res. Cogn. Brain Res. 9, 177–192. https://doi.org/10.1016/S0926-6410(99)00055-5

Slobounov, S., Cao, C., Jaiswal, N., Newell, K.M., 2009. Neural basis of postural instability identified by VTC and EEG. Exp. Brain Res. https://doi.org/10.1007/s00221-009-1956-5

Slobounov, S., Hallett, M., Stanhope, S., Shibasaki, H., 2005. Role of cerebral cortex in human postural control: An EEG study. Clin. Neurophysiol. https://doi.org/10.1016/j.clinph.2004.09.007

Smith, L., 1996. Brunnstrom's clinical kinesiology., 5th ed. /. ed. F.A. Davis Company, Philadelphia.

Smith, M., Deacon, P., 1984. Topographical anatomy of the posterior columns of the spinal cord in man. The long ascending fibres. Brain 107 ( Pt 3, 671–698. https://doi.org/10.1093/BRAIN/107.3.671

Solis-Escalante, T., van der Cruijsen, J., de Kam, D., van Kordelaar, J., Weerdesteyn, V., Schouten, A.C., 2019a. Cortical dynamics during preparation and execution of reactive balance responses with distinct postural demands. Neuroimage 188, 557–571. https://doi.org/10.1016/j.neuroimage.2018.12.045

Solis-Escalante, T., van der Cruijsen, J., de Kam, D., van Kordelaar, J., Weerdesteyn, V., Schouten, A.C., 2019b. Cortical dynamics during preparation and execution of reactive balance responses with distinct postural demands. Neuroimage 188, 557–571. https://doi.org/10.1016/j.neuroimage.2018.12.045

Sporns, O., Betzel, R.F., 2016. Modular brain networks. Annu. Rev. Psychol. 67, 613–640. https://doi.org/10.1146/annurev-psych-122414-033634

Sprenger, A., Wojak, J.F., Jandl, N.M., Helmchen, C., 2017. Postural Control in Bilateral

Vestibular Failure: Its Relation to Visual, Proprioceptive, Vestibular, and Cognitive Input. Front. Neurol. 8, 1. https://doi.org/10.3389/FNEUR.2017.00444

Sreeja, S.R., Rabha, J., Samanta, D., Mitra, P., Sarma, M., 2017. Classification of motor imagery based EEG signals using sparsity approach. Lect. Notes Comput. Sci. (including Subser. Lect. Notes Artif. Intell. Lect. Notes Bioinformatics) 10688 LNCS, 47–59. https://doi.org/10.1007/978-3-319-72038-8_5

Stegeman, D.F., 2007. Standards for suface electromyography: The European project Surface EMG for non-invasive assessment of muscles (SENIAM).

Stern, J.M., Engel, J., 2013. Atlas of EEG patterns. Wolters Kluwer/Lippincott Williams & Wilkins Health.

Suarez, H., Muse, P., Suarez, A., Arocena, M., 2000. Postural behaviour responses to visual stimulation in patients with vestibular disorders. Acta Otolaryngol. 120, 168–172. https://doi.org/10.1080/000164800750000847

Sullivan, E. V., Rose, J., Rohlfing, T., Pfefferbaum, A., 2009. Postural sway reduction in aging men and women: Relation to brain structure, cognitive status, and stabilizing factors. Neurobiol. Aging 30, 793–807. https://doi.org/10.1016/j.neurobiolaging.2007.08.021

Tadel, F., Baillet, S., Mosher, J.C., Pantazis, D., Leahy, R.M., 2011. Brainstorm: a user-friendly application for MEG/EEG analysis. Comput. Intell. Neurosci. 2011, 879716. https://doi.org/10.1155/2011/879716

Tatum, W.O., Reinsberger, C., Dworetzky, B.A., 2017. Artifacts of Recording and Common Errors in Interpretation. Oxford University Press. https://doi.org/10.1093/med/9780190228484.003.0011

Taube, W., Mouthon, M., Leukel, C., Hoogewoud, H.M., Annoni, J.M., Keller, M., 2015. Brain activity during observation and motor imagery of different balance tasks: An fMRI study. Cortex 64, 102–114. https://doi.org/10.1016/j.cortex.2014.09.022

Thelen, D., AB, S., NB, A., JA, A.-M., 1996. Effects of age on rapid ankle torque development. J. Gerontol. A. Biol. Sci. Med. Sci. 51, M226-32. https://doi.org/10.1093/GERONA/51A.5.M226

Thomas Yeo, B.T., Krienen, F.M., Sepulcre, J., Sabuncu, M.R., Lashkari, D., Hollinshead, M.,

Roffman, J.L., Smoller, J.W., Zöllei, L., Polimeni, J.R., Fisch, B., Liu, H., Buckner, R.L., 2011. The organization of the human cerebral cortex estimated by intrinsic functional connectivity. J. Neurophysiol. 106, 1125–1165. https://doi.org/10.1152/jn.00338.2011

Thompson, C., Bélanger, M., Fung, J., 2007. Effects of bilateral Achilles tendon vibration on postural orientation and balance during standing. Clin. Neurophysiol. 118, 2456–2467. https://doi.org/10.1016/J.CLINPH.2007.08.013

Todorov, E., 2004. Optimality principles in sensorimotor control. Nat. Neurosci. 2004 79 7, 907–915. https://doi.org/10.1038/nn1309

Toosizadeh, N., Ehsani, H., Miramonte, M., Mohler, J., 2018. Proprioceptive impairments in high fall risk older adults: The effect of mechanical calf vibration on postural balance. Biomed. Eng. Online 17. https://doi.org/10.1186/s12938-018-0482-8

Traud, A.L., Kelsic, E.D., Mucha, P.J., Porter, M.A., 2008. Comparing community structure to characteristics in online collegiate social networks. SIAM Rev. https://doi.org/10.1137/080734315

Tresch, M., Jarc, A., 2009. The case for and against muscle synergies. Curr. Opin. Neurobiol. 19, 601–607. https://doi.org/10.1016/J.CONB.2009.09.002

Turnip, A., Junaidi, E., 2015. Removal artifacts from EEG signal using independent component analysis and principal component analysis, in: Proceedings of 2014 2nd International Conference on Technology, Informatics, Management, Engineering and Environment, TIME-E 2014. Institute of Electrical and Electronics Engineers Inc., pp. 296–302. https://doi.org/10.1109/TIME-E.2014.7011635

Usakli, A.B., 2010. Improvement of EEG signal acquisition: an electrical aspect for state of the art of front end. Comput. Intell. Neurosci. 2010, 630649. https://doi.org/10.1155/2010/630649

Ushiyama, J., Yamada, J., Liu, M., Ushiba, J., 2017. Individual difference in β-band corticomuscular coherence and its relation to force steadiness during isometric voluntary ankle dorsiflexion in healthy humans. Clin. Neurophysiol. 128, 303–311. https://doi.org/10.1016/j.clinph.2016.11.025

Vaina, L.M., Cowey, A., Eskew, R.T., LeMay, M., Kemper, T., 2001. Regional cerebral of global

motion perception evidence from unilateral cerebral brain damage. Brain. https://doi.org/10.1093/brain/124.2.310

Vanni, S., Tanskanen, T., Seppä, M., Uutela, K., Hari, R., 2001. Coinciding early activation of the human primary visual cortex and anteromedial cuneus. Proc. Natl. Acad. Sci. U. S. A. https://doi.org/10.1073/pnas.041600898

Varghese, A, M., KB, B., WR, S., G, M., WE, M., 2014. Frequency characteristics of cortical activity associated with perturbations to upright stability. Neurosci. Lett. 578, 33–38. https://doi.org/10.1016/J.NEULET.2014.06.017

Varghese, J.P., Beyer, K.B., Williams, L., Miyasike-daSilva, V., McIlroy, W.E., 2015. Standing still: Is there a role for the cortex? Neurosci. Lett. 590, 18–23. https://doi.org/10.1016/j.neulet.2015.01.055

Varghese, J.P., McIlroy, R.E., Barnett-Cowan, M., 2017. Perturbation-evoked potentials: Significance and application in balance control research. Neurosci. Biobehav. Rev. 83, 267–280. https://doi.org/10.1016/j.neubiorev.2017.10.022

Ventre-Dominey, J., 2014. Vestibular function in the temporal and parietal cortex: Distinct velocity and inertial processing pathways. Front. Integr. Neurosci. https://doi.org/10.3389/fnint.2014.00053

Vuillerme, N., Danion, F., Forestier, N., Nougier, V., 2002. Postural sway under muscle vibration and muscle fatigue in humans. Neurosci. Lett. 333, 131–135. https://doi.org/10.1016/S0304-3940(02)00999-0

Wallmann, H.W., 2009. The basics of balance and falls. Home Heal. Care Manag. Pract. 21, 436–439. https://doi.org/10.1177/1084822309337189

Warwick-Evans, L.A., Symons, N., Fitch, T., Burrows, L., 1998. Evaluating sensory conflict and postural instability. Theories of motion sickness. Brain Res. Bull. 47, 465–469. https://doi.org/10.1016/S0361-9230(98)00090-2

Watanabe, T., Nojima, I., Mima, T., Sugiura, H., Kirimoto, H., 2020. Magnification of visual feedback modulates corticomuscular and intermuscular coherences differently in young and elderly adults. Neuroimage. https://doi.org/10.1016/j.neuroimage.2020.117089

Welch, P.D., 1967. The Use of Fast Fourier Transform for the Estimation of Power Spectra: A

Method Based on Time Averaging Over Short, Modified Periodograms. IEEE Trans. Audio Electroacoust. 15, 70–73. https://doi.org/10.1109/TAU.1967.1161901

Welch, T.D.J., Ting, L.H., 2014. Mechanisms of motor adaptation in reactive balance control. PLoS One. https://doi.org/10.1371/journal.pone.0096440

Wendling, F., Ansari-Asl, K., Bartolomei, F., Senhadji, L., 2009. From EEG signals to brain connectivity: A model-based evaluation of interdependence measures. J. Neurosci. Methods 183, 9–18. https://doi.org/10.1016/j.jneumeth.2009.04.021

Wendling, F., Chauvel, P., Biraben, A., Bartolomei, F., 2010. From intracerebral EEG signals to brain connectivity:Identification of epileptogenic networks in partial epilepsy. Front. Syst. Neurosci. 4. https://doi.org/10.3389/fnsys.2010.00154

Wendling, F., Congendo, M., Lopes da Silva, F.H., 2017. EEG Analysis. Oxford University Press. https://doi.org/10.1093/med/9780190228484.003.0044

WHO, 2021. Falls [WWW Document]. https://www.who.int/news-room/fact-sheets/detail/falls. URL https://www.who.int/news-room/fact-sheets/detail/falls (accessed 10.21.21).

Wierzbicka, M.M., Gilhodes, J.C., Roll, J.P., 1998. Vibration-induced postural posteffects. J. Neurophysiol. 79, 143–150. https://doi.org/10.1152/jn.1998.79.1.143

Wilcoxon, F., 1945. Individual Comparisons by Ranking Methods. Biometrics Bull. 1, 80–83.

Wilson, V., Peterson, B., 1978. Peripheral and central substrates of vestibulospinal reflexes. Physiol. Rev. 58, 80–105. https://doi.org/10.1152/PHYSREV.1978.58.1.80

Wilson, V.J., Jones, G.M., 1979. Mammalian Vestibular Physiology 365.

Winter, D., Patla, A., Prince, F., Ishac, M., Gielo-Perczak, K., 1998. Stiffness control of balance in quiet standing. J. Neurophysiol. 80, 1211–1221. https://doi.org/10.1152/JN.1998.80.3.1211

Winter, D.A.., 1995. Human balance and posture control during standing and walking. Gait Posture 3, 193–214. https://doi.org/10.1016/0014-5793(86)80927-9

Winter, D.A., 2009. Biomechanics and Motor Control of Human Movement: Fourth Edition, Biomechanics and Motor Control of Human Movement: Fourth Edition. https://doi.org/10.1002/9780470549148

Winter, D.A., Patla, A.E., Prince, F., Ishac, M., Gielo-Perczak, K., 1998. Stiffness Control of Balance in Quiet Standing. J. Neurophysiol. 80, 1211–1221. https://doi.org/10.1152/jn.1998.80.3.1211

Winter, Patla, Frank, 1990. Assessment of balance control in humans. Med. Prog. Technol. 16, 31–51.

Winters, J.M., Crago, P.E. (Eds.), 2000. Biomechanics and Neural Control of Posture and Movement, 1st ed. Springer-Verlag New York. https://doi.org/10.1007/978-1-4612-2104-3

Witham, C.L., Baker, S.N., 2007. Network oscillations and intrinsic spiking rhythmicity do not covary in monkey sensorimotor areas. J. Physiol. 580, 801–814. https://doi.org/10.1113/jphysiol.2006.124503

Witham, C.L., Riddle, C.N., Baker, M.R., Baker, S.N., 2011. Contributions of descending and ascending pathways to corticomuscular coherence in humans. J. Physiol. 589, 3789–3800. https://doi.org/10.1113/jphysiol.2011.211045

Witham, C.L., Wang, M., Baker, S.N., 2007. Cells in somatosensory areas show synchrony with beta oscillations in monkey motor cortex. Eur. J. Neurosci. 26, 2677–2686. https://doi.org/10.1111/j.1460-9568.2007.05890.x

Woll, J., Sprenger, A., Helmchen, C., 2019. Postural control during galvanic vestibular stimulation in patients with persistent perceptual-postural dizziness. J. Neurol. 266, 1236–1249. https://doi.org/10.1007/S00415-019-09255-7

Wolpaw, J.R., 1994. Aquisition and maintenance of the simplest motor skill: Investigation of cns mechanisms. Med. Sci. Sports Exerc.

Wuyts, F., Furman, J., Vanspauwen, R., Van de Heyning, P., 2007. Vestibular function testing. Curr. Opin. Neurol. 20, 19–24. https://doi.org/10.1097/WCO.0B013E3280140808

Xu, J., Wang, J., Fan, L., Li, H., Zhang, W., Hu, Q., Jiang, T., 2015. Tractography-based Parcellation of the Human Middle Temporal Gyrus. Sci. Rep. https://doi.org/10.1038/srep18883

Yamamoto, T., Smith, C.E., Suzuki, Y., Kiyono, K., Tanahashi, T., Sakoda, S., Morasso, P., Nomura, T., 2015. Universal and individual characteristics of postural sway during quiet

standing in healthy young adults. Physiol. Rep. https://doi.org/10.14814/phy2.12329

Yao, D., 2001. A method to standardize a reference of scalp EEG recordings to a point at infinity. Physiol. Meas. https://doi.org/10.1088/0967-3334/22/4/305

Yao, D., Wang, L., Arendt-Nielsen, L., N Chen, A.C., 2007. The effect of reference choices on the spatio-temporal analysis of brain evoked potentials: The use of infinite reference. Comput. Biol. Med. 37, 1529–1538. https://doi.org/10.1016/j.compbiomed.2007.02.002

Yelshyna, D., Gago, M.F., Bicho, E., Fernandes, V., Gago, N.F., Costa, L., Silva, H., Rodrigues, M.L., Rocha, L., Sousa, N., 2016. Compensatory postural adjustments in Parkinson's disease assessed via a virtual reality environment. Behav. Brain Res. 296, 384–392. https://doi.org/10.1016/j.bbr.2015.08.017

Yilmaz, G., Ungan, P., Sebik, Oäÿ., UginÄ• ius, P., TÃ¼rker, K.S., 2014. Interference of tonic muscle activity on the EEG: a single motor unit study. Front. Hum. Neurosci. 8, 1–10. https://doi.org/10.3389/fnhum.2014.00504

Yin, W., Li, T., Hung, S.C., Zhang, H., Wang, L., Shen, D., Zhu, H., Mucha, P.J., Cohen, J.R., Lin, W., 2020. The emergence of a functionally flexible brain during early infancy. Proc. Natl. Acad. Sci. U. S. A. 117, 23904–23913. https://doi.org/10.1073/pnas.2002645117

Yu, Y.H., Chen, S.H., Chang, C.L., Lin, C.T., Hairston, W.D., Mrozek, R.A., 2016. New flexible silicone-based EEG dry sensor material compositions exhibiting improvements in lifespan, conductivity, and reliability. Sensors (Switzerland) 16. https://doi.org/10.3390/s16111826

Zalesky, A., Fornito, A., Bullmore, E.T., 2010. Network-based statistic: Identifying differences in brain networks. Neuroimage 53, 1197–1207. https://doi.org/10.1016/j.neuroimage.2010.06.041

Zarzecki, P., Asanuma, H., 1979. Proprioceptive Influences on Somatosensory and Motor Cortex. Prog. Brain Res. 50, 113–119. https://doi.org/10.1016/S0079-6123(08)60812-2

Zetterlund, C., Lundqvist, L.O., Richter, H.O., 2019. Visual, musculoskeletal and balance symptoms in individuals with visual impairment. Clin. Exp. Optom. 102, 63–69. https://doi.org/10.1111/cxo.12806

Zhou, J., Lipsitz, L., Habtemariam, D., Manor, B., 2016a. Sub-sensory vibratory noise

augments the physiologic complexity of postural control in older adults. J. Neuroeng. Rehabil. 13, 1–8. https://doi.org/10.1186/s12984-016-0152-7

Zhou, J., Lipsitz, L., Habtemariam, D., Manor, B., 2016b. Sub-sensory vibratory noise augments the physiologic complexity of postural control in older adults. J. Neuroeng. Rehabil. https://doi.org/10.1186/s12984-016-0152-7

Zhou, J., Lipsitz, L., Habtemariam, D., Manor, B., 2016c. Sub-sensory vibratory noise augments the physiologic complexity of postural control in older adults. J. Neuroeng. Rehabil. 13, 44. https://doi.org/10.1186/s12984-016-0152-7